https://orcid.org/0000-0002-5178-5907

VILNIUS UNIVERSITY
CENTER FOR PHYSICAL SCIENCES AND TECHNOLOGY

Raimonda Bogužaitė

Development of an Electrochemical Sensor Based on Polypyrrole and Modification of its Properties

DOCTORAL DISSERTATION

Natural Sciences,
Chemistry (N 003)

VILNIUS 2024

This dissertation was written between 2019 and 2023 at the State Research Institute Center for Physical Sciences and Technology.

Academic Supervisor:
Dr. Vilma Ratautaitė (State Research Institute Center for Physical Sciences and Technology, Natural Sciences, Chemistry, N 003) (since 12 Jun 2020)
Prof. Habil. Dr. Arūnas Ramanavičius (State Research Institute Center for Physical Sciences and Technology, Natural Sciences, Chemistry, N 003) (from 01 Oct 2019 to 11 Jun 2020)

Chairman:
Habil. Dr. Rimantas Ramanauskas (State Research Institute Center for Physical Sciences and Technology, Natural Sciences, Chemistry, N 003).
Members:
Dr. Renata Butkutė (State Research Institute Center for Physical Sciences and Technology (FTMC), Natural Sciences, Material Engineering, T 008);
Prof. Habil. Dr. Audrius Maruška (Vytautas Magnus University (VDU), Natural Sciences, Chemistry, N 003);
Dr. Krzysztof Noworyta (Institute of Physical Chemistry, Poland, Natural Sciences, Chemistry, N 003);
Assoc. Prof. Dr. Jolanta Sereikaitė (Vilnius Gediminas Technical University (VILNIUS TECH), Natural Sciences, Chemical Engineering, T 005).

This doctoral dissertation will be defended in a public meeting of the Dissertation Defence Panel at 11:00 on the 20th of September 2024 at Meeting Room A101 of the State Research Institute Center for Physical Sciences and Technology.

Address: Saulėtekio 3, Vilnius, Lithuania Tel. +37052648884; e-mail: office@ftmc.lt

The text of this dissertation can be accessed at the libraries of the State Research Institute Center for Physical Sciences and Technology and Vilnius University, as well as on the website of Vilnius University: www.vu.lt.

VILNIAUS UNIVERSITETAS
FIZINIŲ IR TECHNOLOGIJOS MOKSLŲ CENTRAS

Raimonda Bogužaitė

Elektrocheminio jutiklio kūrimas polipirolo pagrindu ir jo savybių modifikavimas

DAKTARO DISERTACIJA

Gamtos mokslai,
Chemija (N 003)

VILNIUS 2024

Disertacija rengta 2019–2023 metais Valstybiniame mokslinių tyrimų institute Fizinių ir technologijos mokslų centre.

Mokslinis vadovas:
Dr. Vilma Ratautaitė (Fizinių ir technologijos mokslų centras, gamtos mokslai, chemija, N 003) (nuo 2020 06 12)
Prof. habil. dr. Arūnas Ramanavičius (Fizinių ir technologijos mokslų centras, gamtos mokslai, chemija, N 003) (nuo 2019 10 01 iki 2020 06 11)

Gynimo taryba:
Pirmininkas:
Habil. dr. Rimantas Ramanauskas (Valstybinis mokslinių tyrimų institutas Fizinių ir technologijos mokslų centras, gamtos mokslai, Chemija – N 003).
Nariai:
Dr. Renata Butkutė (Valstybinis mokslinių tyrimų institutas Fizinių ir technologijos mokslų centras (FTMC), gamtos mokslai, Medžiagų inžinerija – T 008).
Prof. habil. dr. Audrius Maruška (Vytauto Didžiojo universitetas (VDU), gamtos mokslai, Chemija – N 003).
Dr. Krzysztof Noworyta (Lenkija, Institute of Physical Chemistry, gamtos mokslai, Chemija – N 003).
Doc. dr. Jolanta Sereikaitė (Vilniaus Gedimino technikos universitetas (VILNIUS TECH), gamtos mokslai, Chemijos inžinerija – T 005).

Disertacija ginama viešame Gynimo tarybos posėdyje 2024 m. rugsėjo 20 d., 11 val. Valstybinio mokslinių tyrimų instituto Fizinių ir technologijos mokslų centro A101 konferencijų salėje.

Adresas: Saulėtekio al. 3, Vilnius, Lietuva tel. +37052648884; el. paštas: office@ftmc.lt.

Disertaciją galima peržiūrėti Fizinių ir technologijos mokslų centro bei Vilniaus universiteto bibliotekose ir VU interneto svetainėje: www.vu.lt.

ABBREVIATIONS

AFM	–	Atomic force microscopy
AA	–	Azure A
ITO	–	Indium tin oxide electrode
LOD	–	Limit of detection
LR	–	Linear range
MB	–	Methylene blue
MIP	–	Molecularly imprinted polymer
MIP-Ppy	–	Molecularly imprinted polypyrrole
MIT	–	Molecularly imprinted technology
NIP	–	Non-imprinted polymer
NIP-Ppy	–	Non-imprinted polypyrrole
PMB	–	Polymethylene blue
Ppy	–	Polypyrrole
Ppy-MB	–	Polypyrrole – methylene blue
Ppy-PAA	–	Polypyrrole – poly(azure A)
Ppy-PMB	–	Polypyrrole – poly(methylene blue)
Ppy-PTH	–	Polypyrrole – polythionine
Pt	–	Platinum electrode
PT	–	Phenothiazine
SARS-CoV-2	–	Severe acute respiratory syndrome Coronavirus-2
SEM	–	Scanning electron microscopy
TH	–	Thionine

TABLE OF CONTENTS

INTRODUCTION

Electrochemical sensors play a role in various industries and applications because they can detect and quantify specific chemical compounds. In environmental monitoring, healthcare and medical applications, industrial processes and safety, as well as some other applications, electrochemical sensors are used. They are essential for the rapid, precise, and selective detection of target analytes.

The market for electrochemical sensors is expanding rapidly due to technological advancements, increased environmental regulations, and growing healthcare needs. The global biosensors market size was estimated at US$ 28.44 billion in 2023, and it is expected to hit US$ 58.44 billion by 2033 with a registered compound annual growth rate (CAGR) of 7.9% from 2024 to 2033 [1].

The literature offers a wide variety of electrochemical sensor designs. However, such difficulties as insufficient repeatability, the stability of sensors, poor detection limits, more sustainable solutions, the integration of sensors into practical, user-friendly devices, and the legal regulation still slow down the market entry of sensors.

The morphological and physical properties of conducting polymers have led to numerous potential industrial applications and sensor designs. Polypyrrole (Ppy) is a polymer often used to design electrochemical sensors because it combines electrical conductivity, electrochemical activity, stability, selectivity, and adaptability. Due to its special characteristics, sensors that can detect a variety of analytes, such as gases, ions, biomolecules, and environmental contaminants, have been developed.

This study aims to evaluate polypyrrole modification possibilities to develop an electrochemical sensor. For this aim, the polypyrrole layer was modified with phenothiazine derivatives or molecular imprints.

Objectives

- To polymerize the pyrrole layer modified with phenothiazine derivatives and other additives on the glass electrode coated with a thin layer of indium tin oxide (ITO);
- To determine the most suitable conditions for creating a more stable pyrrole layer on the ITO electrode for the application in a sensor design;
- To polymerize the pyrrole layer on a platinum electrode and apply it to the creation of a sensor based on molecular polymer imprint technology;

- To evaluate the resulting structures and their use;
- To apply an integrated Cottrell equation for assessing the molecularly imprinted polypyrrole (MIP-Ppy) and molecularly not imprinted polypyrrole (NIP-Ppy).

Scientific Novelty

- In particular, three phenothiazine derivatives (methylene blue (MB), azure A (AA), and thionine (TH)) were used to develop an electrochromic sensor design. This study sought to demonstrate that polysaccharides could be applied in layer modification and positively affect the properties of the sensor design. At that time, such a combination was less common in the literature.
- At the beginning of the COVID-19 pandemic which emerged in late 2019 in China, it was of importance to update the research, by adapting it to the current affairs of those days. Expeditiously conducted experiments were undertaken in response to the government policy to achieve control of the pandemic as soon as possible. The scientific team of the *Center for Physical Sciences and Technology* (FTMC), Department of Nanotechnology was one of the first to publish how the molecularly imprinted polymer (MIP) technology was used in developing a polypyrrole sensor to detect the SARS-CoV-2 spike (SARS-CoV-2-S) glycoprotein.
- The MIP-based polypyrrole sensor design for MB recognition was developed to fill the gap in methylene blue detection methods.

Statements to be Defended

- Three phenothiazine (PT) derivatives – methylene blue, azure A, and thionine – can be used to improve the electrochromic sensor properties.
- Polysaccharides in the polymerization mixture contribute to a positive change in the properties of the layer which is used to create sensor design – heparin is a suitable material to improve layer adhesion.
- The molecularly imprinted polypyrrole (MIP-Ppy)-based layer can be designed as a sensor for the determination of SARS-CoV-2 spike glycoprotein.
- The integrated Cottrell equation (Anson plot) can be used to evaluate SARS-CoV-2 spike glycoprotein interaction with the MIP-Ppy-based layer.

- The molecularly imprinted polypyrrole (MIP-Ppy) with MB imprints can be created by choosing the right synthesis conditions.

Contribution of the Author

The author of the dissertation performed the main experiments of electrochemical layer deposition on the electrode. Also, the author performed an electrochemical analysis and carried out an SEM evaluation. The author was responsible for preparing samples for evaluation by AFM or FTIR. In addition, the author conducted the data analysis and the interpretation of the results of experiments, created graphic illustrations, data graphs, and prepared the manuscripts of scientific publications. In addition, the author presented the obtained results at many international conferences (both oral and poster presentations).

LIST OF PUBLICATIONS

The main results of the doctoral thesis were published in 5 scientific publications (P: 1–5) and presented in 16 conference reports (C: 1–16).

P1. **R. Boguzaite,** V. Ratautaite, L. Mikoliunaite, V. Pudzaitis, A. Ramanaviciene, and A. Ramanavicius. Towards analytical application of electrochromic polypyrrole layers modified by phenothiazine derivatives. *Journal of Electroanalytical Chemistry*, 2021, 886, 115132.
https://doi.org/10.1016/j.jelechem.2021.115132

P2. V. Ratautaite, **R. Boguzaite**, M.B. Mickeviciute, L. Mikoliunaite, U. Samukaite-Bubniene, A. Ramanavicius, A. Ramanaviciene. Evaluation of electrochromic properties of polypyrrole/poly(methylene blue) layer doped by polysaccharides, *Sensors*, 2022, 22(1), 232;
https://doi.org/10.3390/s22010232

P3. V. Ratautaite, **R. Boguzaite**, E. Brazys, A. Ramanaviciene, E. Ciplys, M. Juozapaitis, R. Slibinskas, M. Bechelany, A. Ramanavicius. Molecularly imprinted polypyrrole based sensor for the detection of SARS-CoV-2 spike glycoprotein, *Electrochimica Acta*, 2022, 403, 139581;
https://doi.org/10.1016/j.electacta.2021.139581

P4. V. Ratautaite, **R. Boguzaite**, E. Brazys, D. Plausinaitis, S. Ramanavicius, U. Samukaite-Bubniene, M. Bechelany, A. Ramanavicius. Evaluation of the interaction between SARS-CoV-2 spike glycoproteins and the molecularly imprinted polypyrrole, *Talanta*, 2023, 253, 123981.
https://doi.org/10.1016/j.talanta.2022.123981

P5. **R. Boguzaite**, G. Pilvenyte, V. Ratautaite, E. Brazys, A. Ramanaviciene, A. Ramanavicius. Towards Molecularly imprinted polypyrrole-based sensor for the detection of methylene blue, *Chemosensors* 2023, 11, 549.
https://doi.org/10.3390/chemosensors11110549

OTHER PUBLICATIONS

O1. V. Ratautaite; U. Samukaite-Bubniene; D. Plausinaitis; **R. Boguzaite;** D. Balciunas; A. Ramanaviciene; Neunert, G.; Ramanavicius, A. Molecular imprinting technology for determination of uric acid. *International Journal of Molecular Sciences*, 2021, 22, 5032. https://doi.org/10.3390/ijms22095032

O2. V. Liustrovaite, M. Pogorielov, **R. Boguzaite**, V. Ratautaite, A. Ramanaviciene, G. Pilvenyte, V. Holubnycha, V. Korniienko, K. Diedkova, R. Viter, A. Ramanavicius. Towards electrochemical sensor based on molecularly imprinted polypyrrole for the detection of bacteria - *Listeria monocytogenes*, *Polymers*, 2023, 15(7), 1597. https://doi.org/10.3390/polym15071597

O3. G. Pilvenyte, V. Ratautaite, **R. Boguzaite**, A. Ramanavicius, R. Viter, S. Ramanavicius. Molecularly imprinted polymers for the determination of cancer biomarkers, International Journal of Molecular Sciences, 2023, 24(4), 4105. https://doi.org/10.3390/ijms24044105

O4. G. Pilvenyte, V. Ratautaite, **R. Boguzaite**, U. Samukaite-Bubniene, D. Plausinaitis, A. Ramanaviciene, M. Bechelany, A. Ramanavicius, Molecularly imprinted polymers for the recognition of biomarkers of certain neurodegenerative diseases, *Journal of Pharmaceutical and Biomedical Analysis*, 2023, 228, 115343. https://doi.org/10.1016/j.jpba.2023.115343

O5. G. Pilvenyte, V. Ratautaite, **R. Boguzaite**, S. Ramanavicius, C.-F. Chen, R. Viter, A. Ramanavicius. Molecularly imprinted polymer-based electrochemical sensors for the diagnosis of infectious diseases, *Biosensors*, 2023, 13, 620. https://doi.org/10.3390/bios13060620

LIST OF CONFERENCE PRESENTATIONS

C1. **Raimonda Boguzaite**, Vilma Ratautaite, Lina Mikoliunaite Arunas Ramanavicius, *Evaluation of Electrochromic Properties of Polypyrrole Films Modified by Phenothiazine Derivatives*. 6th International Conference on Sensors Engineering and Electronics Instrumentation Advances (**SEIA' 2020**), 23–25 September 2020, Porto, Portugal. Oral presentation. Received 2nd place award for this presentation.

C2. **Raimonda Boguzaite,** Vilma Ratautaite, Karolis Treinys, Ernestas Brazys, Almira Ramanaviciene, Arunas Ramanavicius, *An Application of Polypyrrole for the Design of Electrochromic CO_2 Sensor*. 22nd International Conference – School **"Advanced Materials and Technologies 2020"**, 24–28 August 2020 Palanga, Lithuania. Poster presentation.

C3. **Raimonda Boguzaite**, Vilma Ratautaite, Lina Mikoliunaite, Arunas Ramanavicius, *Electrochemical Deposition of Polypyrrole Films Modified with Phenothiazine Derivatives*. 14th International Scientific Conference **"The Vital Nature Sign"**, 15–16 May 2020 Kaunas, Lithuania. Oral presentation.

C4. **Raimonda Boguzaite**, Vilma Ratautaite, Lina Mikoliunaite, Ernestas Brazys, Arunas Ramanavicius, *Electrochemical Deposition and Modifications of Polypyrrole*. 22–23 October 2020, 10th Conference for PhD Students and Young Scientists of the Center for Physical Sciences and Technology (FTMC) – **"FizTech2020"**, Vilnius, Lithuania. Oral presentation.

C5. **Raimonda Boguzaite**, Vilma Ratautaite, Ernestas Brazys, Arunas Ramanavicius, *The Ppy Layer Thickness Control for The Development of The Sensor*. 64th International Scientific Conference for Students of Physics and Natural Sciences – **"Open Readings 2021"**, 16–19 March 2021, Vilnius, Lithuania. Oral presentation.

C6. **Raimonda Boguzaite,** Vilma Ratautaite, Lina Mikoliunaite, Almira Ramanaviciene, Arunas Ramanavicius, *Electrochemical Deposition of Polypyrrole Layers Modified by Phenothiazine Derivatives*. 23rd International Conference-School **"Advanced Materials and Technologies"** (AMT 2021), 23–27 August 2021 Palanga, Lithuania. Poster presentation.

C7. **Raimonda Boguzaite,** Vilma Ratautaite, Urte Samukaite-Bubniene, Deivis Plausinaitis, Ernestas Brazys, Arunas Ramanavicius,

Application of Molecularly Imprinted Polypyrrole for Electrochemical Sensor Design. 11th Conference for PhD Students and Young Scientists of the Center for Physical Sciences and Technology (FTMC) – **"FizTech2021",** 20–21 October Vilnius, Lithuania. Oral presentation. Award for the best oral presentation.

C8. **Raimonda Boguzaite,** Vilma Ratautaite, Ernestas Brazys, Almira Ramanaviciene, Arunas Ramanavicius, *Towards Electrochemical Polymerization of Polypyrrole/Poly(Methylene Blue) Layer Doped by Polysaccharides*. 65th International Conference for Students of Physics and Natural Sciences – **"Open Readings 2022"**, 15–18 March 2022, Vilnius, Lithuania. Poster presentation.

C9. **Raimonda Boguzaite**, Vilma Ratautaite, Ernestas Brazys, Almira Ramanaviciene, Arunas Ramanavicius, *Molecularly Imprinted Polypyrrole Application for The Detection of SARS-CoV-2 Spike Glycoprotein*. 7th **International Conference on Bio-Sensing Technology**, 22–25 May 2022, Sitges, Spain. A poster presentation was presented. Received the certificate for the most popular poster presentation.

C10. **Raimonda Boguzaite,** Vilma Ratautaite, Ernestas Brazys, Greta Pilvenyte, Almira Ramanaviciene, Arunas Ramanavicius *Molecularly Imprinted Polypyrrole Application for Electrochemical Sensor Design*. International conference **"Chemistry and Chemical Technology 2022"**, 14 October 2022, Kaunas, Lithuania. Oral presentation.

C11. **Raimonda Boguzaite,** Vilma Ratautaite, Migle Beatrice Mickeviciute, Arunas Ramanavicius, *Electrochemical Deposition and Modifications of Polypyrrole with Methylene Blue*. 12th Conference for PhD Students and Young Scientists of the Center for Physical Sciences and Technology (FTMC) – **"FizTech2022"**,19–20 October 2022, Vilnius, Lithuania. Oral presentation. Award for the best oral presentation.

C12. **Raimonda Boguzaite**, Vilma Ratautaite, Greta Pilvenyte, Ernestas Brazys, Arunas Ramanavicius, *Polypyrrole Modifications with Methylene Blue*. International conference **"Chemistry and Chemical Technology 2023"**, 10 March 2023, Vilnius, Lithuania. Poster presentation.

C13. **Raimonda Boguzaite**, Vilma Ratautaite, Greta Pilvenyte, Arunas Ramanavicius, *Determination of Ppy Layer Stability for the Development of the Sensor.* 66th International Scientific Conference

for Students of Physics and Natural Sciences – **"Open Readings 2023"**, 18–21 April 2023, Vilnius, Lithuania. Poster presentation.

C14. **<u>Raimonda Boguzaite,</u>** Vilma Ratautaite, Arunas Ramanavicius *Modification and Application of Polypyrrole for the Development of an Electrochemical Sensor*. Lithuanian Academy of Sciences, 11th conference of young scientists **"Interdisciplinary Research in Physical and Technological Sciences"**, 23 March 2023, Vilnius, Lithuania. Oral presentation. Award for the best oral presentation.

C15. **<u>Raimonda Boguzaite</u>**, Vilma Ratautaite, Ernestas Brazys, Greta Pilvenyte, Arunas Ramanavicius, *Application of Molecularly Imprinted Polypyrrole for Electrochemical Sensor*. 12th **International Colloids Conference**, 11–14 June 2023, Palma de Mallorca, Spain. Poster presentation.

C16. **<u>Raimonda Boguzaite</u>**, Vilma Ratautaite, Greta Pilvenyte, Arunas Ramanavicius, *Determination of Ppy Layer Stability for the Development of the Sensor.* International Summer School **"e-SPARK"**, 19–24 June 2023, Warsaw, Poland. Poster presentation.

OTHER CONFERENCE PRESENTATIONS

OC1. Ernestas Brazys, Vilma Ratautaite, **<u>Raimonda Boguzaite</u>**, Arunas Ramanavicius, *Molecularly Imprinted Polypyrrole Based Sensor for The Detection of SARS-CoV-2 Spike Glycoprotein*. 65th International Conference for Students of Physics and Natural Sciences – **"Open Readings 2022"**, 15–18 March 2022, Vilnius, Lithuania. Poster presentation.

OC2. Ernestas Brazys, Vilma Ratautaite, **<u>Raimonda Boguzaite</u>**, Arunas Ramanavicius, *Evaluation of the Interaction Between SARS-CoV-2 Spike Glycoproteins and the Molecularly Imprinted Polypyrrole.* **"Chemistry and Chemical Technology 2023"**, 10 March 2023, Vilnius, Lithuania. Poster presentation.

OC3. Ernestas Brazys, Vilma Ratautaite, **<u>Raimonda Boguzaite</u>**, Arunas Ramanavicius, *Evaluation of the Interaction Between SARS-CoV-2 Spike Glycoproteins and the Molecularly Imprinted Polypyrrole*. 66th International Scientific Conference for Students of Physics and Natural Sciences – "**Open Readings 2023**", 18–21 April 2023, Vilnius, Lithuania. Poster presentation.

OC4. Ernestas Brazys, Vilma Ratautaite, **<u>Raimonda Boguzaite</u>**, Arunas Ramanavicius, *Molecularly Imprinted Polypyrrole-Based Sensor for the Detection of the SARS-CoV-2 Spike Glycoprotein*. 25th

International Conference-School "**Advanced Materials and Technologies 2023**", 21–25 August 2023, Palanga, Lithuania. Poster presentation

OC4. Greta Pilvenyte, **Raimonda Boguzaite**, Vilma Ratautaite, Ausra Baradoke, Arunas Ramanavicius, *Conducting Polymers in The Design of Biosensors*. 65th International Conference for Students of Physics and Natural Sciences – **"Open Readings 2022"**, 15–18 March 2022, Vilnius, Lithuania. Poster presentation.

OC5. Greta Pilvenyte, **Raimonda Boguzaite**, Vilma Ratautaite, Arunas Ramanavicius, *Molecularly Imprinted Polymer-Based Biosensors for Cancer Biomarkers Detection*. 12th Conference for PhD Students and Young Scientists of the Center for Physical Sciences and Technology (FTMC) – **"FizTech2022"**, 19–20 October 2022, Vilnius, Lithuania. Poster presentation.

OC6. Greta Pilvenyte, **Raimonda Boguzaite**, Vilma Ratautaite, Arunas Ramanavicius, *Molecularly Imprinted Polymer-Based Biosensors for the Detection of Alzheimer's Disease Biomarkers.* 66th International Scientific Conference for Students of Physics and Natural Sciences – **"Open Readings 2023"**, 18–21 April 2023, Vilnius, Lithuania. Poster presentation.

OC7. Greta Pilvenyte, **Raimonda Boguzaite,** Vilma Ratautaite, Arunas Ramanavicius, *Impact of Layer Thickness on Stability of Molecularly Imprinted Polypyrrole on the Indium Tin Oxide Modified Electrode.* 11th International Workshop on Surface Modification for Chemical and Biochemical Sensing (**SMCBS**), 3–7 November 2023, Lochow, Poland. Poster presentation.

OC8. Greta Pilvenyte, **Raimonda Boguzaite**, Vilma Ratautaite, Arunas Ramanavicius, *Formation of MIP based on electrically conductive polymer*. 13th Conference for PhD Students and Young Scientists of the Center for Physical Sciences and Technology (FTMC) – **"FizTech2023"**, 18-19 October 2023, Vilnius, Lithuania. Oral presentation.

Summer School **"Commercialising Biosensors"**, 26 July 2021. During the one-day summer school, the following general topics were covered: How should your technology be protected? Deciding whether to license technology or launch a business? Which inventions are leading the biosensors industry?

International Summer School **"e-SPARK"**, 19–24 June 2023, Warsaw, Poland. It was a five-day training program with laboratory classes covering a wide range of fundamental electrochemical laboratory practices.

1. LITERATURE REVIEW

1.1. Polypyrrole

Ppy is one of conducting polymers which has been widely used for sensor applications [2,3]. It has been used in a wide range of fields, including electronics, energy storage, and biomedical applications [4–7].

Pyrrole is a 5-membered aromatic nitrogen heterocycle that is found in a wide variety of molecules denoted by biological and material relevance [8]. It is a colorless volatile liquid that darkens readily upon exposure to air. The cyclic pattern is frequently the pharmacophore of bioactive pharmaceutical drugs and natural materials [9].

Since the 20th century, it has been known that electrochemically polymerizing Ppy provides a thick, long-lasting layer with improved conductivity and superior electrode properties [10].

The electropolymerization of Ppy generally is achieved by the potentiostatic (constant potential) or galvanostatic (constant current) methods [11]. Ppy is synthesized by electrochemical [12,13], chemical [14,15], chemical vapour deposition [16], enzymatic [17], and/or microorganism-assisted methods [18–20].

Ppy can be produced and placed on a variety of substrates, including electrodes, such as ITO glass [21,22], screen-printed carbon [23–25], platinum [26,27], and transducers [3,28]. The polymerization of Ppy on the ITO electrode has been shown in the previous studies to depend on the electrode surface modification, but it begins above 0.5 V [22,29]. The integration of Ppy into a variety of sensor designs and formats, including microelectrode arrays [30–32], flexible sensors [33,34], and even 3D-printed structures [35–37], is made possible by the adaptability of fabrication techniques.

The presence of the different compounds in the polymerization mixture may be used for tuning the final properties of the polymer. A Ppy layer's electrochemical activity is alternated by Ppy doping or dedoping with certain ions and/or molecules. Ppy can be altered by adding different functional groups or chemical species while it is being synthesized. By adjusting the surface characteristics of the polymer, these alterations enable the selective detection of particular analytes. The Ppy sensor's selectivity and sensitivity can be increased by adding certain functional groups which can interact specifically with the target analyte.

Ppy electrochemical polymerization is illustrated in Figure 1. It consists of oxidation and dimerization of pyrrole followed by aromatization and

oxidation of the dimer. Higher molecular weight oligomers and aromatic dimers are known to oxidize more readily than monomers.
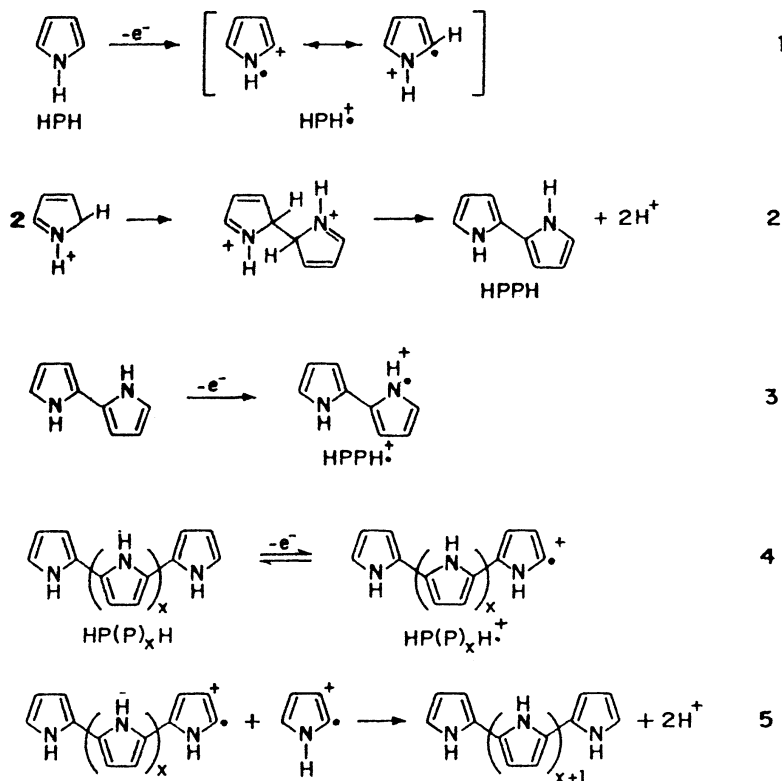

Figure 1. Mechanism for the electrochemical polymerization of Ppy [38]

1.2. Electrochromism

The term *electrochromism* describes the reversible color change that some materials display in response to an external electrical input. To identify and quantify analytes in a solution, electrochromic sensors make use of this characteristic. Electrochromism occurs when a material undergoes persistent, yet reversible color shifts due to an electrochemical reaction [38,39]. Usually, there is a color shift between two colored states or between a transparent (or 'bleached') state and a colored state [40].

Some semiconducting layers based on metal oxides and some organic materials, such as polymers, have electrochromic characteristics as a distinguishing property [39]. Since polymers are characterized by their simplicity, ease of synthesis, stability, biocompatibility, high optical contrasts, quick response, ability to produce thin coatings and form multicolored

electrochromes, they have electrochromic qualities and are thus relatively popular [41–43].

Due to changes in the polymer's π-π conjugated electronic system and their ability to participate in electrochemical oxidation and reduction, conjugated polymers exhibit electrochromism [38,44–46].

Numerous systems, including rechargeable batteries, photovoltaic cells, polymeric light emitting diodes, transistors, smart windows for automobiles, buildings, and greenhouses, electrochromic display devices, and smart sunglasses, have benefited from the use of conjugated polymers [17,40,47–50].

Different variations of the polymer have been applied in the development of electrochromic sensors. For example, polyaniline and *o*-phenylenediamine-based copolymers were formed electrochemically by potential cycling. Copolymer layers were electrochemically deposited on transparent conducting ITO-coated glass electrodes by potential cycling from polymerization solution containing different concentration ratios of monomers and applied for electrochromic sensor design [51].

Some pure PANI films, Ppy, and PEDOT:PSS films enhanced with electrochromic dyes have all shown sufficient sensing parameters, highlighting the significance of composite materials for exceptional electrochromic sensor parameters [40].

It has been presented that gold nanostructures (AuNS) placed on an ITO electrode improve the electrochromic characteristics of the PANI-PEDOT layer [41]. Such a simple and inexpensive substrate pre-modification technique can be applied to further enhance different conducting polymer-based electrochromic devices.

1.2.1. Phenothiazine derivatives

The beginning of the chemistry of phenothiazines is considered to be the end of the 19th century, when the parent compound, 10H-dibenzo-1,4-thiazine, was obtained by Bernthsen in 1883. Since then, several thousand derivatives have been developed [52].

This class of organic molecules became extremely significant due to the wide range of relevant biological and chemical features [53].

Phenothiazine derivatives are biologically active compounds [54] due to their reversible potentials near that of biological compounds such as NADH, redox dyes have been investigated as mediators for the electron transfer between enzymes or microbes and an electrode [55].

The principal application of phenothiazines in medicine is psychopharmacology. These substances can successfully inhibit dopamine, histamine, serotonin, acetylcholine, and adrenergic receptors. Phenothiazines also have a strong antibacterial action in addition to their antipsychotic properties [56].

Phenothiazines belong to the oldest, synthetic antipsychotic drugs. More than 50 years ago, phenothiazines, which have a tricyclic scaffold and a side chain extending from the central ring moiety, were utilized to treat psychoses [57]. Also, phenothiazines show antibacterial and antifungal activities [53].

There are a number of well-known phenothiazines: methylene blue (MB), chlorpromazine, levomepromazine, promethazine, thioridazine, trifluoperazine, thionine (TH), and azure A (AA) (Fig. 2).
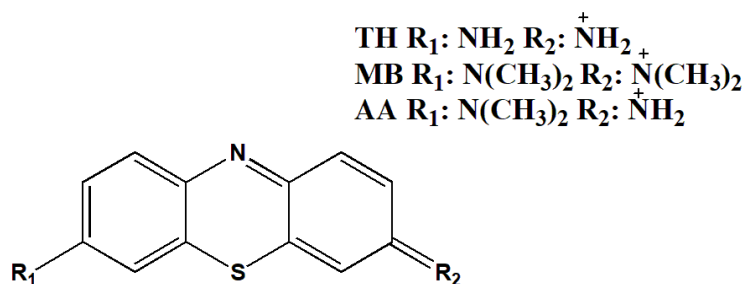
TH R_1: NH_2 R_2: $\overset{+}{N}H_2$
MB R_1: $N(CH_3)_2$ R_2: $\overset{+}{N}(CH_3)_2$
AA R_1: $N(CH_3)_2$ R_2: $\overset{+}{N}H_2$

Figure 2. Structure of phenothiazine derivatives (thionine, methylene blue, azure A)

Chlorpromazine and promethazine derivatives have altered the fields of psychiatry and allergy treatment, respectively [58]. MB was one of the first antimalarial drugs [59]. Also, it is one of the earliest organic dyes still in use today. It has a similar redox potential value to several biomolecules [60,61]. Since MB is a cationic dye, it is used in the textile industry. This leads to certain environmental issues. Despite some downsides and growing concerns about the environment, the usage of dyes is still increasing in many countries through the textile industry and other coloring processes. Among the pollutants, dyes are particularly noted for their harmful effects on the environment and human health [62–64].

Additionally, MB works well as a mediator of electron redox [65]. The sensitizer of choice is typically TH. Concerning redox-active low molecular weight molecules, polythionine (PTH) and monomer TH both have electrocatalytic activity [66].

Phenothiazine derivatives often exhibit a low oxidation potential and a strong propensity to form stable radical cations. Electropolymerization is one of the most common and useful techniques used to obtain oligomer or polymer dye thin films [67]. There are different possible products generated during the electropolymerization of MB. Three linkage schemes, 'nitrogen-to-ring' ('N-to-ring'), 'ring-to-ring', and 'nitrogen-to-nitrogen' ('N-to-N') have been proposed [68]. It is believed that demethylation followed by 'N-to-ring' coupling is the dominant reaction during the electrochemical polymerization of MB. It was observed that the rate of the polymerization increased with an increasing pH, thereby indicating that basic solutions are the optimal media for the polymerization of MB pH 6.8 solution containing 3 mM of MB [68].

Electropolymerization of MB could be performed by using potentiodynamic (cyclic voltammetry) or potentiostatic (constant potential) techniques in a three-electrode cell [67]. The same study also showed that a cathodic peak was observed at –0.235 V, an oxidative peak at –0.22 V, overoxidation of PMB starts after the preparation potential of 1 V and unreacted monomer species in the solution are easily adsorbed to the rough surface of the PMB film [67]. The shift of peaks depends on the type of the electrode and other polymerization conditions, such as the composition of the solution, pH, etc. Another study described the electrochemical polymerization of MB on the platinum foil in the aqueous solutions, which was carried out by using potential cycling; at the region of –0.40 V and 1.10 V, the cathodic peak of MB was at 0.22 V [69]. Polymerization of MB at the carbon fiber electrode surface was performed by the cyclic voltammetry (CV) technique in the range between –1.0 V to +1.5 V during 30 continuous cycles at a scan rate of 50 mV/s. In another case, MB was combined with a conductive polymer and was polymerized on stainless steel by first applying a layer of polymer to inhibit the passivation or corrosion of the metal and to increase the active surface area. PMB was deposited by repeated potential sweeps between +1.05 V and –0.5 V at 100 mV/s [55].

Electrochemical polymerization of other phenothiazine derivatives was also described. The electrochemical polymerization of azure A has been carried out by using repeated potential cycling. The scan potential is set between –0.2 V and +1.3 V (vs. Ag/AgCl). The polymerization rate of azure A and the electrochemical properties of poly(azure A) are affected by the temperature and the pH value of the electrolytic solution [70]. Electropolymerization of TH was performed to create a stable film on the surface of the carbon nanotube paste electrode, at the potential range of −0.5 V to +1.2 V and a scan rate of 40 mV/s [71]. The aforementioned studies

demonstrate that the successful polymerization of phenothiazine derivatives requires a potential value above 1 V.

Table 1 summarizes the applications of phenothiazine derivative MB in the electrochemical sensor design. Table 1 demonstrates that the main purpose of MB application in the electrochemical sensor design is related to its redox properties. MB was applied to detect proteins, enzymes, bacteria, etc.

Meanwhile, the objective of Table 2 is to summarize the electrochemical and microgravimetric methods for sensing MB as the target analyte.

Table 1. Summary of phenothiazine derivative MB applications in electrochemical sensor design

Purpose of MB application	Electrode	MB form in the analytical system	Analytical method	Goal of detection	Ref.
Mediator	GCE	(MB-MWNTs)/GCE	Flow injection analysis with amperometric detection	Detecting haemoglobin (Hb) and myoglobin (Mb) with LOD of 1.5 nM for Hb and 20 nM for Mb	[72]
Redox marker electrochemical indicator	AuE	MB/AuE	DPV, EIS	DNA detection with LOD of 20 fM	[73]
Redox tag redox label	AuE	(MB-based SAM with PEG)/AuE	SWV	Protease activity trypsin with LOD of 250 pM	[74]
Signal tags	AuE	MB@MOF-Apt/MCH/cDNA/AuNPs/CS-ZnO NFs/AuE	EIS and DPV	Detecting patulin (PAT) with LOD of 1.46×10^{-8} µg/mL	[75]
Redox probe	G-GCE	-	CV	*Escherichia coli*	[76]
Redox species	GCE	GS-MB-CS nanocomposite	CV, EIS	Detecting prostate-specific antigen (PSA) with LOD of 13 pg/mL	[77]
Electron transfer mediator	GCE	MB, MOFs, and rGO nanocomposite	CV, DPV	Detecting rutin in tablets and urine samples with LOD of 20 nM	[78]
Electrochemical indicator	AuE	MB/aptamerAuE	DPV	Detecting adenosine with LOD of 1×10^{-8} M.	[79]
Redox tag	AuE	MB/aptamer/AuE	SWV	Detecting aflatoxin B1 (AFB1) with LOD of 6 pM	[80]

Purpose of MB application	Electrode	MB form in the analytical system	Analytical method	Goal of detection	Ref.
Redox mediator	GCE	Nanocomposite of PMB, DES, and AuNP on GCE	CV, EIS	Detecting ascorbic acid with LOD of 0.40 µmol/L and 5-aminosalicylic acid (5-ASA) with LOD of 0.064 µmol/L	[81]
Electrochemical signal indicator	ITO	MOF/MB composite	DPV	Detecting paraoxon (pesticide) with LOD of 1.7 ng/mL	[82]
Dual-signal source	ITO	MB-encapsulated MOF	FL, DPV	Detecting adenosine triphosphate with LOD of 0.38 nM by FL and 0.027 nM for DPV	[83]
	PE	rGO/PMB/AgNPs/PE	CV	Detecting NADH with LOD of 0.072 µM	[84]
Electrochemical reporter	GCE	PMB/GCE	CV, DPV	Detecting acrylamide with LOD of 0.13 nM	[85]

AuE – gold electrode; AuNP –gold nanoparticles; CS – chitosan; DES – deep eutectic solvent; FL – fluorescence; GCE – glassy carbon electrode; G – GCE-graphene electrode; GCE-graphene ink–modified glassy carbon electrode; GS – graphene sheets; ITO – Indium tin oxide; MOF – metal-organic framework; PE – paper electrode; PEG – polyethylene-glycol; rGO – reduced graphene oxide; SAM – self-assembled monolayer; SWV – square wave voltammetry.

Table 2. Sensing platforms dedicated to the detection of MB

Sample	Sensing platform	Polymer modification	Method of analysis	LOD	Ref.
River water	gum Arabic–AgNPs/ GCE		SWV	64 µg/L **MB monomer oxidation** 440 µg/L **PMB oxidation**	[86]
-	MPTMS/CPE	-	CV	400 nM	[87]
-	ibu-AuNps/GCE	-	DPV, CV, SWV	3.9 nM	[88]
-	Co-bhb/CPE	-	CV	0.1 ppm	[89]
-	NH₂-fMWCNTs/GCE	-	SWV	0.21 nM	[90]
Ground, river, and sea water	Ppy/Fe₃O₄NPs/ QCM sensor	MIP	QCM-D	1.4 µg/L	[91]
	PMAA/CPE	MIP	DPV		[92]

CPE – carbon paste electrode; PMAA – poly(methacrylic acid); QCM-D – quartz crystal microbalance with dissipation; QCM – quartz crystal microbalances; NH₂-fMWCNTs – amino-group-functionalized, multi-walled carbon nanotubes; Co-bhb – cobalt-beta hydroxyl benzoate; ibu-AuNPs – ibuprofen benzoate; ibu-AuNPs – ibuprofen coated gold nanoparticles; MPTMS – 3-mercaptopropyltrimethoxysilane; SWV – square wave voltammetry; GCE – glassy carbon electrode.

1.2.2. Application of Ppy in the design of the electrochromic sensor

Electrochromic sensors are one area where Ppy, a conducting polymer, has drawn a lot of interest. High electrical conductivity, environmental stability, and the simplicity of synthesis are only a few of the beneficial characteristics that Ppy offers for the construction of electrochromic sensors.

The Ppy film can serve as a sensing layer for electrochromic detection once it has been deposited. The presence of analytes in the surrounding media has an impact on the redox state of the polymer, which, in turn, affects the color shift of the Ppy film. A reversible color change is caused by the analyte's interaction with the Ppy film, which causes a change in the film's oxidation/reduction state.

Several optical techniques, such as absorbance spectroscopy or colorimetry, can be used to identify the color shift of the Ppy film. The target analyte's presence or concentration can be determined by the color of the film. The electrochromic sensor can give qualitative or quantitative information about the analyte by keeping track of the color change.

1.3. Molecularly Imprinted Polymers

Molecularly imprinted polymers (MIPs) are specialized polymers that can selectively recognize and bind to specific target molecules with high affinity and specificity. Polymers with molecular imprints function as artificial receptors for specific molecules [93,94].

The MIP technique is important today when we are looking for better and more useful sensors and sensing systems for improved diagnosis, treatments, and assays [95,96].

In previous studies, it has been reported that various types of small molecules can be imprinted within polymers [14,97–99]. High molecular mass biomolecules can be also molecularly imprinted within polymers [100–105]. Conducting polymers have undergone molecular imprinting with different proteins [106–109], DNA [30,110,111], and bacteria [23,112,113].

Therefore, MIPs can specifically bind the analytes of interest that serve as templates for their development [114,115]. Furthermore, MIP is a potential technique for a variety of analytical uses, such as food safety, environmental monitoring, and biological diagnostics [96,116,117]. MIPs are exploited in many different fields: chemical sensing [118–121], drug delivery [122–124], sample preparation [125,126], and chromatographic separation [127–129].

In addition to being available for a broad range of targets and having recognition qualities that are similar to those of natural receptors, it may imitate biological receptors-ligand and antibody-antigen-based systems

[96,130,131]. MIPs are appealing, they have better chemical and physical stability compared to biological receptors; it is also claimed that MIPs are characterized by simple and inexpensive preparation, reusability, and potential use for large-scale manufacturing [124,127,132].

Using modified electrodes made with the molecularly imprinted technology (MIT) has shown to be one of the most effective methods in recent years, and it has the potential to create sensor recognition elements [133]. However, the perfect sensor should also be affordable, portable, accurate, responsive to the target analyte instantly in any chosen media, and able to produce a detectable signal within the necessary concentration range [132].

Commercialization of MIPs has been growing (> 1000 patents on *SciFinder* prior to 2020) [93,119]. The global biosensors market size was estimated at US$ 28.44 billion in 2023, and it is expected to grow further [1].

Sensor devices for the detection of a nearly infinite number of analytes of interest can be created by combining MIPs with a wide range of label-free readout techniques [119]. High commercial potential MIP sensors have been developed for use in water monitoring [134–136], food safety [137], soil pollution screening [138], and cancer diagnostics [139].

To combine MIP techniques with the latest smart technology and provide economically viable ways, successful MIP integration will depend on academic stakeholders and commercial partners [140].

The molecular imprinting approach typically consists of multiple phases: 1) the self-assembled pre-polymerization complex is formed by combining functional monomer(s) with a target molecule, known as a template; 2) the mixture is then polymerized; and 3) the template is extracted from the freshly synthesized polymer [96,141].

A schematic diagram of MIP formation and a visual representation of the formation steps are demonstrated in Figure 3.
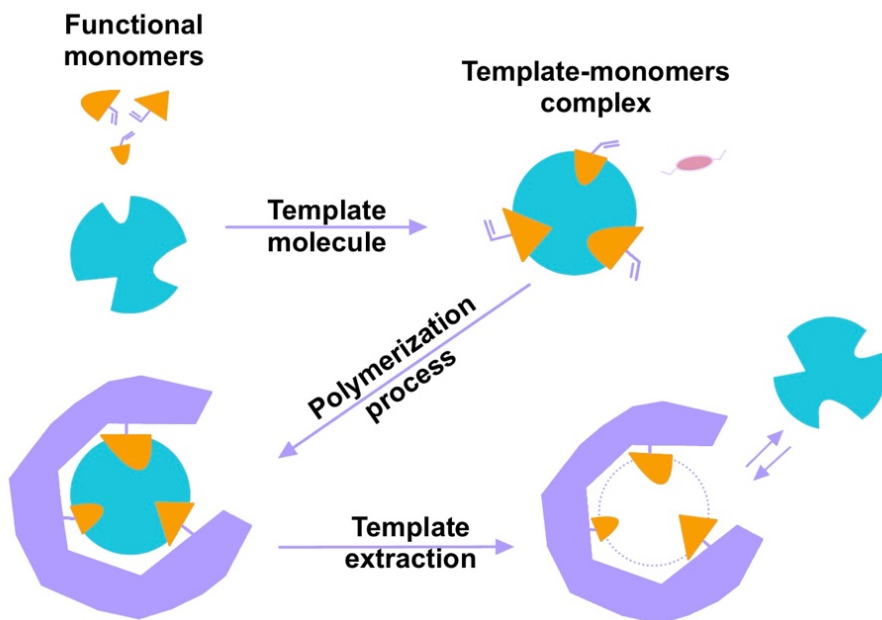
Figure 3. Schematic diagram of MIP formation

The template interacts with monomers to form a cavity around the template molecule, and the template is subsequently removed, leaving behind the empty molecularly imprinted cavity that matches the shape, size, and chemical functionality of the target molecule for rebinding the target molecule [93,132].

The research conducted by Wulff and Sarhan [142] more than 50 years ago laid the groundwork for the modern molecular imprinting technology (MIT) [143]. Other scientists, for instance, K. Mosbach and B. Sellergren, continued working on this topic and published papers that specifically reported an 'imprinted polymer' in the 1980's [144]. These early researchers developed different aspects of science [93].

The common production technique is bulk polymerization [93]. However, such polymerization causes some difficulties, it is longer and more expensive. One of the alternatives is electrochemical polymerization, which is quick, simple, and can be performed in an aqueous medium, without using organic solvents, thus responding to the theme of sustainability. Our scientific team of the FTMC, Department of Nanotechnology usually uses this method for polymerization and MIP formation. During several years of experiments, promising results have been obtained, demonstrating the real possibilities of applying MIP in the development of sensors [116,143,145].

Our scientific team created MIPs on various surface-working electrodes, for example, ITO, Pt, and carbon-printed ones. Furthermore, polymers on the

transduction platform surface can also be electropolymerized [96]. To characterize MIP, the following factors like size and size distribution, the number of binding sites, the imprinting factor, the surface morphology, the crystalline form, the thermal stability, the surface area, the pore parameters (size, specific volume), and the degree of swelling can be evaluated [124].

However, there still are some challenges and limitations [119,146–148]. Kan et al. [149] identified three limitations that are the most critical during protein imprinting. Specifically, after polymerization, it is challenging to extract the template protein from the bulk polymer matrix. Additionally, organic solvents are frequently utilized in the creation of MIPs; however, because of the poor solubility of the protein molecule in these solvents and the potential for denaturation of proteins in organic solvents, they are not appropriate for the synthesis of MIPs imprinted with proteins. Finally, a more significant non-specific binding is caused by the protein's size and structural complexity.

1.3.1. Application of Ppy in the design of the MIP sensor

Among the various types of MIP, a promising polymer pyrrole has emerged for the development of highly sensitive and specific sensors. Pyrrole could be polymerized on different surfaces, by numerous techniques, and in various mediums. It is possible to polymerize pyrrole even in a water solution. Previous experiments have shown that the best polymerization and, later on, effectiveness was seen in an acidic medium. Pyrrole-based MIPs possess unique properties such as high thermal and chemical stability, and tunable molecular recognition properties, making them suitable for a wide range of applications in fields such as biotechnology, environmental monitoring, and pharmaceuticals. Previous studies on Ppy have defined molecular imprints with virus glycoproteins [145,150], bovine serum albumin [151,152], cardiac troponin-I [153], prostate-specific antigen [100], and cardiac troponin T [154]. If electrochemical polymerization is considered, the surface could be chosen from various electrodes: ITO, carbon, carbon-printed, and platinum electrodes. The Ppy-based MIP platform on an ITO-coated glass electrode was created for *K. pneumonia* electrochemical detection and level monitoring [155]. Within the linear detection range of 1 to 10^5 CFU per millilitre, the proposed sensor has a low LOD of 1.352 CFU/ml and good sensitivity (3 µA ml CFU/cm^2).

In the study of Gupta et al. [133], the glassy carbon electrode (GCE) based on molecularly imprinted polypyrrole was fabricated for the determination of tobramycin in milk and eggs. It presented an excellent identification capability

for the template molecule. The current response and tobramycin concentration were shown to have a linear relationship of 5.0×10^{-10}–1.0×10^{-8} M, with a detection limit of 1.4×10^{-10} M. Another study [156] detailed the creation of an electrochemical sensor for the sensitive and precise measurement of 4-ethylphenol in wine, based on a molecularly imprinted polymer (MIP). The working electrode was either a GCE or a MIP-modified GCE (MIP/GCE). For the study of 4-ethylphenol, the sensor demonstrated strong selectivity and sensitivity, a broad linear range (from 0.2 to 34.8 μM), good precision (3.0%), and detection capability (0.2 μM).

High sensitivity and specificity glyphosate (Gly) detection has been achieved by the development of an electrochemical sensor based on molecularly imprinted polypyrrole nanotubes (MIPNs) by applying a thin layer of MIPNs to an electrode that was screen-printed (SPE) [157]. The outcomes show the limit of detection (LOD) of 1.94 ng/mL along with a broad detection range of 2.5–350 ng/mL. One more group of scientists analyzed the detection of glyphosate [158] and used a three-electrode configuration: a gold electrode, a saturated calomel electrode (SCE), and a platinum wire as the working, the reference, and the auxiliary electrodes, respectively. To detect glyphosate specifically, complementary surface acoustic wave (SAW) and electrochemical sensors were functionalized with a Ppy-imprinted polymer. Their respective limits of detection (LOD) were approximately 10^{-12} M. The electrochemical and gravimetric sensors have sensitivity values of approximately (75 ± 41) μA/nM and $(6.9 \pm 2.9) \times 10^{-20}$/nM, respectively, based on their designed sensors.

Other scientists [159] described the development of a simple and cost-effective electrochemical sensor for sulfadimethoxine based on molecularly imprinted overoxidized Ppy on a gold electrode. The role of the cationic electrolyte has been proven to significantly influence the MIP morphology. Ramanaviciene et al. [145], reported the preparation and characterization of a Ppy-based sensor on a modified platinum electrode for direct pulsed amperometric detection of Bovine leukaemia virus proteins glycoprotein gp51. Another research [23] was aimed to create an electrochemical sensor for the detection of *Listeria monocytogenes* by using platinum and screen-printed carbon (SPCE) electrodes modified with a molecularly imprinted polymer (MIP). Based on the research findings, it was hypothesized that the most efficient MIP-Ppy/SPCE sensor might be created by eliminating bacteria using the proteolytic enzyme trypsin. The MIP-Ppy/SPCE has a linear range of 300 to 6700 CFU/mL, with a LOD and LOQ of 70 and 210 CFU/mL, respectively.

These are just a few examples demonstrating the wide application of the pyrrole monomer in the field of the molecular polymer imprinting technology, when different conditions, surfaces, and analytes are chosen.

In conclusion, Ppy is a commonly cited polymer that has been applied to the development of a variety of molecularly imprinted sensors. Ppy usually is chosen among the large variety of conducting polymers for several reasons: its stability in a wide range of pH, the stability over time of the synthesized films, and the ease of electropolymerization on various substrates.

2. MATERIALS AND METHODS

2.1. Materials and Chemicals

Pyrrole was distilled before its utilization. All other chemicals were of analytical grade, and were used as received without further purification unless otherwise stated. The main chemicals which were used in this research are listed below.

Reagent	Source
Acetic acid CAS 64-19-7	*Roth* (Karlsruhe, Germany)
Acetone CAS: 67-64-1	Alfa Aesar (Kandel, Germany)
Ammonium hydroxide (30%) (CAS: 1336-21-6)	*Carl Roth GmbH* (Karlsruhe, Germany)
Azure A CAS: 531-53-3	*Alfa Aesar* (Kandel, Germany)
Boric acid CAS 10043-35-3	*Scharlau* (Barcelona, Spain)
Caffeine (CAS 58-08-2)	*Sigma Aldrich* (Taufkirchen, Germany)
Heparin (Hep) 80020	*Rotexmedica* (Trittau, Germany)
Hydrogen peroxide 35% CAS: 7722-84-1	*Alfa Aesar* (Kandel, Germany)
Lactose (Lac) (CAS 10039-26-6)	*Carl Roth* (Karlsruhe, Germany)
Methylene blue (MB) CAS: 122965-43-9	*Alfa Aesar* (Kandel, Germany)
Phosphoric acid CAS 7664-38-2	*Alfa Aesar* (Kandel, Germany)
Phosphate-buffered saline (PBS) tablets P441750TAB	*Sigma Aldrich* (Steinheim, Germany)
Potassium hexacyanoferrate (II) $K_4[Fe(CN)_6]$	*Reachim* (Donetsk, Ukraine)
Potassium chloride CAS 7447-40-7	*Carl Roth* (Karlsruhe, Germany)
Potassium hexacyanoferrate (III) $K_3[Fe(CN)_6]$ CAS: 13746-66-2	*Carl Roth* (Karlsruhe, Germany)
Pyrrole CAS: 109-97-7	*Alfa Aesar* (Kandel, Germany)
Sodium hydroxide CAS 1310-73-2	*Alfa Aesar* (Kandel, Germany)
Sucrose (Suc) (CAS 57-50-1)	*Sigma Aldrich* (Taufkirchen, Germany)
Theobromine (CAS 83-67-0)	*Alfa Aesar* (Kandel, Germany)
Theophylline (CAS 58-55-9)	*Sigma Aldrich* (Taufkirchen, Germany)
Thionine acetate CAS: 78338-22-4	*Alfa Aesar* (Kandel, Germany)

The Britton–Robinson buffer (BR buffer) consisted of 0.01 M boric acid, 0.01 M acetic acid, and 0.01 M phosphoric acid. The pH value of the BR buffer was adjusted with NaOH.

2.2. Instrumentation

2.2.1. Experiments on ITO electrode

The experiment was carried out in a three-electrode system where the working electrode (WE) was an indium tin oxide (ITO)-coated glass, which was purchased from *Sigma Aldrich* (Steinheim, Germany). The surface resistivity stated by the manufacturer of the glass/ITO electrode was 15–25 Ω/cm^2. The geometric area of the working electrode that was coated with the layer of polypyrrole and the phenothiazine derivative was 2 cm^2. Two reference electrodes (RE) were used to perform the experiments of this study:

a)   Ag/AgCl wire was used as the RE during the electrochemical deposition of the layers because it is less sensitive to contamination with electrochemical polymerization products;

b)   Ag/AgCl$_{(3M\ KCl)}$ (from *CH Instruments* (USA)) was used during the electrochemical evaluation of the obtained polymeric layers by cyclic voltammetry (CV) and chronoamperometry (CA).

A platinum wire (from *CH Instruments* (USA) and (*Alfa Aesar*, Kandel, Germany) was used as the counter electrode (CE). All the experiments were performed at room temperature (approximately 20 °C).

Electrochemical polymerization was performed by using computer-controlled galvanostat-potentiostat *Metrohm DropSens* equipped with the *DropView* software. A glass cuvette (high × depth × width = 32 mm × 18 mm × 30 mm) was used as an electrochemical cell for synthesis.

Electrochemical polymerization was performed by using a computer-controlled potentiostat *PGSTAT 128N* using the *NOVA 1.10* software purchased from *EcoChemie* (The Netherlands). The spectrometer *USB4000-FL* equipped with the *SpectraSuite* software, which was purchased from *Ocean Optics* (USA), was used for the optical measurements.

A spectrometer *USB4000-FL* equipped with the *SpectraSuite* software was purchased from *Ocean Optics* (Largo, FL, USA) and was used for optical measurements.

The changes in pH were followed with a pH-meter *ProLine Plus* (*Q-i-s*, Oosterhout, The Netherlands) or a pH-meter *Seven Compact Mettler-Toledo GmbH* (Greifensee, Switzerland)

2.2.2. Experiments on Pt electrode

The analysis was performed by using a potentiostat/galvanostat *Metrohm-Autolab*, model µAutolabIII/FRA2 µ3AUT71079 controlled by the *NOVA 2.1.3* software (*EcoChemie*, The Netherlands). All measurements were done

in a homemade cell. The total volume of the cell was 250 μL. The three-electrode system consisted of a WE–Pt disk of 1 mm diameter sealed in glass, RE – Ag/AgCl, and a CE – Pt disk of 2 mm diameter.

2.3. Pre-Treatment of Working Electrodes

2.3.1. Pre-treatment of the ITO working electrode

Before the electrochemical deposition of the polymer layer, the glass/ITO was washed for 3 min in the solution consisting of 27% NH_4OH and 30% H_2O_2 mixed at a ratio of 3:1 and preheated up to 50 °C. Later, the electrode was washed at room temperature and subsequently in water, acetone, and water for 15 min in each liquid in an ultrasonic bath.

2.3.2. Pre-treatment of the Pt working electrode

The Pt working electrode was pre-treated before every electrochemical deposition of Ppy following the procedure described in previous studies [145,160] All solutions were thoroughly degassed just before use with a stream of nitrogen (N_2). The Pt electrode was rinsed with concentrated HNO_3 solution in an ultrasonic bath for 10 min, then rinsed with water and polished with alumina paste. Later, it was rinsed with water again, and then with 10 M solution of NaOH, thereafter, with 5 M solution of H_2SO_4 in an ultrasonic bath for 5 min. Electrochemical cleaning of the electrode was carried out in 0.5 M H_2SO_4 by cycling the potential 20 times in the range between −0.1 V and +1.2 V vs. Ag/AgCl at a sweep rate of 100 mV/s. The identification of the bare electrode surface was made possible by a stable indication of the cyclic voltammogram. To improve the adhesion of the Ppy layer to the electrode surface, a layer of 'platinum black' was deposited over the working electrode [160]. The deposition of Pt clusters was performed in a 5 mM solution of H_2PtCl_6 containing 0.1 M of KCl by 10 potential cycles in the range between + 0.5 V and −0.4 V vs Ag/AgCl at a sweep rate of 10 mV/s.

2.4. The Electrochemical Deposition Conditions of Polymer on the Working Electrodes

2.4.1. The electrochemical deposition of Ppy layers on ITO

Depending on the requirements of the experiment, polymer layers on ITO were deposited by potential cycling according to the following conditions:

a)   A potential range was from −0.2 V to +1 V vs Ag/AgCl, at a potential sweep rate of 50 mV/s, by 25 cycles with a step lift of 2.44 mV. A

polymerization solution was prepared in water with 10 mM of the corresponding phenothiazine derivative (methylene blue, azure A, or thionine acetate) and 50 mM of pyrrole. The obtained polymer layers are indicated as Ppy-PMB, Ppy-PAA, and Ppy-PTH, respectively.

b)   A potential range was from −0.5 V to +1.2 V vs. Ag/AgCl, at the sweep rate of 50 mV/s and a step potential of 2.44 mV, by 25 cycles. The electrochemical deposition was carried out from a solution containing 50 mM of pyrrole, 10 mM of MB, and one of the doping materials: 0.1 M lactose (Lac), 0.1 M sucrose (Suc), or 0.01 g/L heparin (Hep). The obtained polymer layers are indicated as (Ppy-PMB)$_{Lac}$, (Ppy-PMB)$_{Suc}$, and (Ppy-PMB)$_{Hep}$, respectively.

The polymerization of all polymer layers was performed at room temperature.

2.4.2. Electrochemical deposition of MIP and NIP layers on Pt electrode

The polymerization solution, which contained 0.5 M of pyrrole in PBS with 0.1 M of KCl and had a pH of 7.4, was electrochemically used to deposit non-imprinted polypyrrole (NIP-Ppy). The polymerization solution, which contained 0.5 M of pyrrole and 50 µg/mL of SARS-CoV-2-S glycoprotein in the same PBS with 0.1 M of KCl, pH 7.4, was used to create molecularly imprinted polypyrrole (MIP-Ppy). The polymeric layers were formed by a sequence of 20 potential pulses of +0.95 V vs. Ag/AgCl for 1 s; between these pulses, 0 V vs. Ag/AgCl potential for 10 s was applied. Further, MIP-Ppy or NIP-Ppy modified electrodes were immersed in 0.05 M H$_2$SO$_4$ solution for 10 min to extract the template molecules and obtain the final structure of the extracted MIP-Ppy.

2.4.3. Electrochemical deposition of MIP and NIP layers on ITO electrode

Polymer layers were electrochemically deposited by potential cycling in a potential range from −0.4 V to +1 V vs Ag/AgCl, at a potential sweep rate of 50 mV/s, by 25, 20, 15, 10, 7, 5 and 3 cycles with a step lift of 2.44 mV. A polymerization solution in the water contained 10 mM MB (in the case of MIP), 50 mM pyrrole, and 5 µg/mL heparin. Hereafter, to form MIP, MB was removed from the created layer. For this, sulfuric acid of 0.1 M concentration was used, in which the washing lasted for 5 min. The NIP was also washed to create the same experimental conditions. In the following part of the research,

the formed MIP and NIP layers were evaluated by observing the change in absorption.

2.5. Evaluation of Ppy Layers

2.5.1. Evaluation of Ppy layers for electrochromic application

a) Chronoamperometry and CV techniques were used to examine the generated Ppy-PMB, Ppy-PAA, and Ppy-PTH layers. Electrochemical measurements were followed simultaneously at several wavelengths by optical absorbance.
    The dependence of the absorbance on the pH value of Ppy-PMB, Ppy-PAA and Ppy-PTH layers was analyzed in the Britton–Robinson buffer (BR-buffer).
    The absorbance changes of Ppy-PMB and Ppy-PTH layers at several different pH values were followed during potential cycling from −0.8 V to +0.8 V vs Ag/AgCl$_{(3M\ KCl)}$, at a scan rate of 50 mV/s and a step lift of 2.44 mV, with 5 cycles. The optical absorbance was followed at 668 nm (for Ppy-PMB), 610 nm (for Ppy-PTH), and 750 nm (for Ppy-PMB and Ppy-PTH); these wavelengths were selected regarding the absorbance spectrum of the corresponding phenothiazine.

b) The electrochromic response of Ppy-PMB and Ppy-PTH layers to the different concentrations of ascorbic acid was analyzed at three pH values of BR-buffer: pH 3.0, pH 4.0, and pH 5.0. During this experiment, a sequence of 5 potential pulses of −0.9 V for 10 s and +0.3 V vs Ag/AgCl$_{(3M\ KCl)}$ for 10 s was applied.

c) A potential pulse sequence (PPS) was applied to evaluate the electrochromic properties of the Ppy-PMB layer. The potential pulses were +0.8 V and −0.8 V. The duration of the pulse was 10 s. Each potential was repeated 5 times.

2.5.2. Evaluation of Ppy layers for application as MIP

MIP-Ppy and NIP-Ppy were analyzed by using pulsed amperometric detection by the sequence of 10 potential pulses of + 0.6 V vs. Ag/AgCl lasting for 2 s; between these pulses, 0 V vs. Ag/AgCl was applied for 2 s. Various aspects of charging-discharging of the conducting polymer polypyrrole were extensively discussed by Heinze et al. [161]. Also, it was stated that overoxidation of Ppy occurs at 0.65 V vs. Ag/AgCl$_{(3M\ KCl)}$ [162]. Hence, taking into account these findings, the potential pulse values of 0 V and +0.6 V were selected for the determination of SARS-CoV-2-S glycoproteins.

The stability of the layer was monitored by analyzing the absorbance changes after washing the layer in water; each wash lasted 3 min. The potential pulse chronoamperometry was used and set to a total of 10 pulses: 5 pulses of –0.8 V, and 5 pulses of +0.8 V in shifts; the potential pulse duration was 10 s. Simultaneously, the optical absorbance was monitored at 530 nm, 668 nm, and 750 nm. ΔA was calculated by using Equation (1):

$$\Delta A = A_0 - A \qquad\qquad (1)$$

Cyclic voltammograms were recorded with and without redox mediators $K_3[Fe(CN)_6]/K_4[Fe(CN)_6]$ weekly in the potential range from -0.2 V to $+0.6$ V vs Ag/AgCl$_{(3M\ KCl)}$, at a scan rate of 50 mV/s and a step lift of 2.44 mV; in total, there were 3 potential cycles.

2.6. Surface Morphology Analysis

The surface morphology of the Ppy-PMB, Ppy-PAA and Ppy-PTH layers was evaluated with a scanning electron microscope (SEM) *TM4000Plus* from *Hitachi* (Japan) and an atomic force microscope (AFM) *Bioscope/Catalyst* from *Bruker* (USA). The AFM images were obtained by using the Contact mode with a silicon nitride probe coated with a gold reflective layer (tip radius 20 nm, nominal resonant frequency 56 kHz, spring constant 0.24 N/m).

Reflection absorption infrared spectroscopy (RAIRS) data were recorded by using a *Vertex 80v* (from *Bruker Inc*., (Leipzig, Germany)) spectrometer equipped with a liquid nitrogen-cooled narrow-band MCT detector. The samples were placed onto a horizontal accessory in an evacuated (~2 mbar) spectrometer chamber, and the measurements were conducted at an angle of 80º. The bare ITO substrate was used as the reference. The spectra were taken after incubation of the samples in a vacuum for 300 s. The spectral resolution was set to 4 cm^{-1}, the aperture to 1.5 mm, the scanner velocity to 40 kHz, and the spectra were acquired by averaging 200 scans.

3. RESULTS AND DISCUSSION

3.1. The Modification of Polypyrrole Properties for the Application as an Electrochromic Sensor

Electrochromism in conjugated polymers occurs as a result of the changes in the polymer's π-π conjugated electronic system and because of the capacity to take part in electrochemical oxidation and reduction.

The combination of polymers in dyes, conducting coatings, and electrochromic devices has a tremendous potential. In this part of the study, the aim was to modify the Ppy by using one of three phenothiazine derivatives in the polymerization mixture. The three-electrode system was used to deposit electrochemically the Ppy layer in the presence of MB on ITO (Fig. 4).
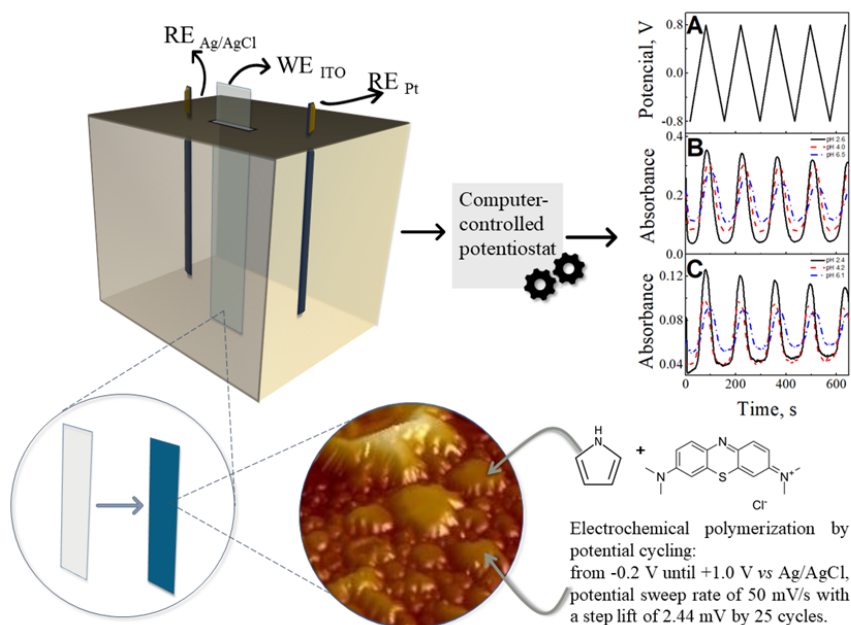
Figure 4. Experimental setup and electrochromic layer. The three-electrode system consisted of the glass/ITO-based electrode (WE), Ag/AgCl$_{(3M\ KCl)}$ (RE), and a platinum wire (CE)

3.1.1. Application of three different phenothiazine derivatives for the modification of the polypyrrole layer properties

Phenothiazine (PT) derivatives are biologically active substances that can also be electrochemically polymerized. Hence, Ppy was modified by three phenothiazine derivatives (MB, AA and TH). These derivatives were chosen for their similar structure, good electrical activity, and due to water solubility.
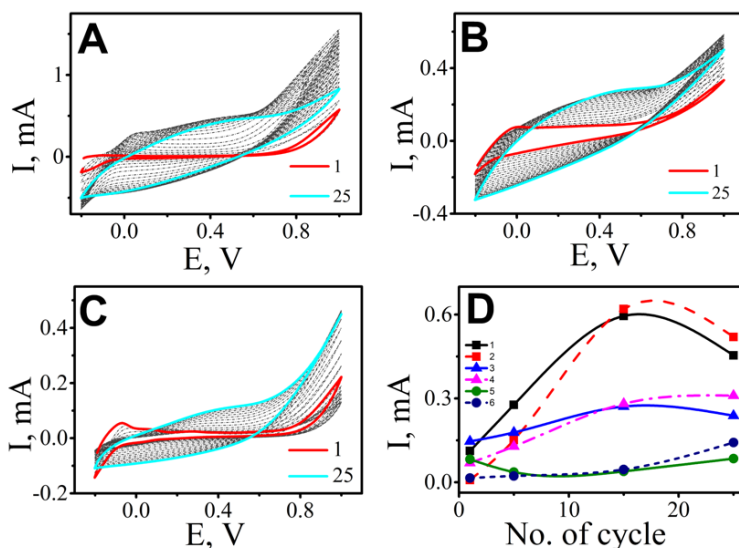
Figure 5. Electrochemical deposition of Ppy-PMB (A), Ppy-PAA (B), Ppy-PTH (C). The width of the cycle loop in mA (ΔI) was measured during potential cycling at potentials of +0.056 V (1) and +0.4 V (2) for Ppy-PMB, −0.007 V (3) and +0.4 V (4) for Ppy-PAA, −0.073 V (5) and +0.4 V (6) for Ppy-PTH, (D). The polymerization solution consisted of 50 mM pyrrole and 10 mM phenothiazine derivative (in water). CV at a scan rate of 50 mV/s, from −0.2 V to +1 V, 25 cycles, step potential 2.44 mV. Electrochemical polymerization was performed in a three-electrode system, where WE – glass/ITO, RE – Ag/AgCl, and CE – platinum wire

Typically, the pyrrole oxidation peak exhibits less expression compared to the oxidation peak of MB. Figure 5 depicts the cyclic voltammograms that were measured when pyrrole and methylene blue were electrochemically polymerizing on ITO-coated glass. Initially, there was a discernible overlap at +0.05 V, the starting point of the oxidation process, when the potential was raised. This shows that nucleation and polymerization occurred on the electrode. The widening of the voltammogram loop indicates the creation of the polymer layer. Up until the 15th cycle of the applied potential, both

cathodic and anodic currents increase, and a subsequent decrease in the voltammogram loop width is seen (Fig. 5D). This decrease in the voltammogram width has been linked to the electrochemical deterioration of the Ppy layer at the applied overpotential in some earlier studies [163,164].

The structure of the layers was characterized by using AFM and scanning electron microscopy (SEM)-based imaging. The Ppy-PAA layer, which was the most unevenly distributed, had the roughest surface with large polymer agglomerations (Fig. 6A). The surface of the Ppy-PMB layer, which forms pleated structures and wrinkles, was relatively smooth (Fig. 6B). The surface of the Ppy-PTH layer is depicted in Figure 6C. This image illustrates that the structure of this layer is fairly evenly distributed, but it consists of larger grains which are formed around shape folds, and, in some places, they are forming larger agglomerations. The observed wrinkles and folds possibly have formed during the drying of the layer.
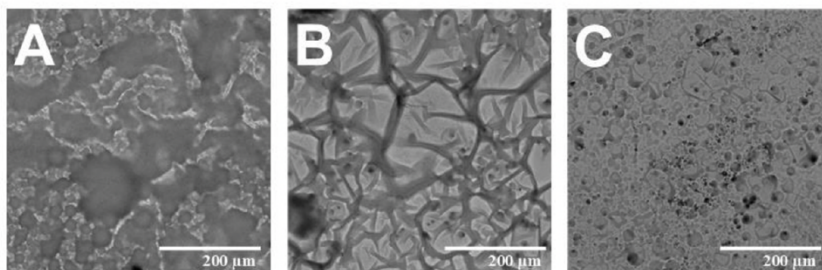
Figure 6. SEM-based evaluation of the Ppy layer surface morphology of all three (A – Ppy-PAA, B – Ppy-PMB, C – Ppy-PTH) electrodes. Magnification for A, B, C was ×500

In the light of this, the SEM results show that the Ppy-PAA layer has the roughest surface, followed by the Ppy-PMB-based layer, which is then smoother, and the Ppy-PTH-based layer, which is finally the smoothest. Visually, the Ppy-PAA layer was the most opaque and non-translucent when compared to the other two samples under identical polymerization conditions, thereby validating our earlier predictions that it is the thickest layer. For these reasons, the sample Ppy-PAA was not further analyzed. The information obtained by AFM also confirmed the SEM results.

Further the optical absorbance spectra of Ppy-PMB, Ppy-PAA, and Ppy-PTH layers at pH values from pH 2.0 to pH 8.0 were measured. When applying 5 potential sweep cycles at the prescribed pH value of the solution, the optical absorbance was measured with potential cycling from −0.8 V to +0.8 V vs. Ag/AgCl$_{(3M\ KCl)}$, at a potential sweep rate of 50 mV/s (Fig. 7).
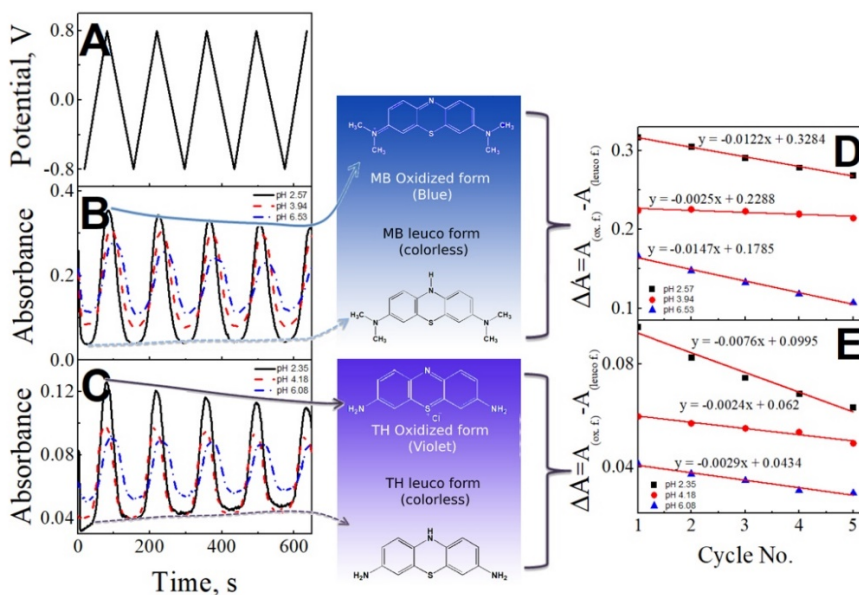
Figure 7. The dependence of optical absorbance on the solution pH value. **A)** potential cycling profile; **B)** Ppy-PMB; **C)** Ppy-PTH. The shift of absorbance (ΔA) of oxidized and leuco forms during potential cycling: **D)** ΔA of Ppy-PMB; **E)** ΔA of Ppy-PTH. The potential during potential cycling was swept from -0.8 V to $+0.8$ V vs. Ag/AgCl$_{(3M\ KCl)}$, the potential sweep rate of 50 mV/s, 5 potential cycles were performed

It was discovered that when a solution becomes more alkaline, the optical absorbance values would decrease, and the electrochromic characteristics of the Ppy-PT-based layer would be well noted up to pH 6.5. The polymeric layer is quickly degraded in a higher pH range. However, that kind of material could be applied as a pH sensor.

The chronoamperometric signals at different pH values and the concentration of ascorbic acid were measured. Three pH ranges were selected for the experiment based on the ascorbic acid $pKa1 = 4.17$. When using a 1 mM increase, the electrochromic response of the Ppy-PMB and Ppy-PTH layers to ascorbic acid was examined at values ranging from 0 mM to 5 mM.

Additionally, it was noted that each potential cycle drops the current of the modified glass/ITO electrode. When Ppy-PMB is formed, it can be seen that the current reduces between the first and the last cycles by 15% (at pH 2.6), 4% (at pH 4.0), and even 35% (at pH 6.5). The current reduction was 33% (at pH 2.4), 18% (at pH 4.2), and 28% (at pH 6.1) during the examination of the Ppy-PTH layer.

The association between the variations in optical absorbance (ΔA) (ΔA = $A_{+0.3V} - A_{-0.9V}$) and ascorbic acid concentrations in the BR-buffer at pH 3.0, pH 4.0, and pH 5.0 is shown in Figure 8B, C, E, and F. The dependence on the concentration at two chosen wavelengths (750 and 610 or 668 nm) is compared. It was shown that ΔA decreases in every instance as the ascorbic acid concentration rises. The electron exchange between phenothiazine and ascorbic acid can account for these alterations. The color of the associated layer changes as a result of this transition.

In the BR-buffer at pH 3.0, pH 4.0, and pH 5.0, Figure 8A and D shows the fluctuation of ΔI vs. the ascorbic acid concentration. A trend that both ΔA and ΔI tend to decrease with the increasing ascorbic acid concentration was identified from the dependence of the current on the ascorbic acid concentration. From the calibration plots produced by these two techniques, it can be inferred that Ppy-PMB and Ppy-PTH have the potential to be employed as electrochromic sensors to measure the ascorbic acid concentration.
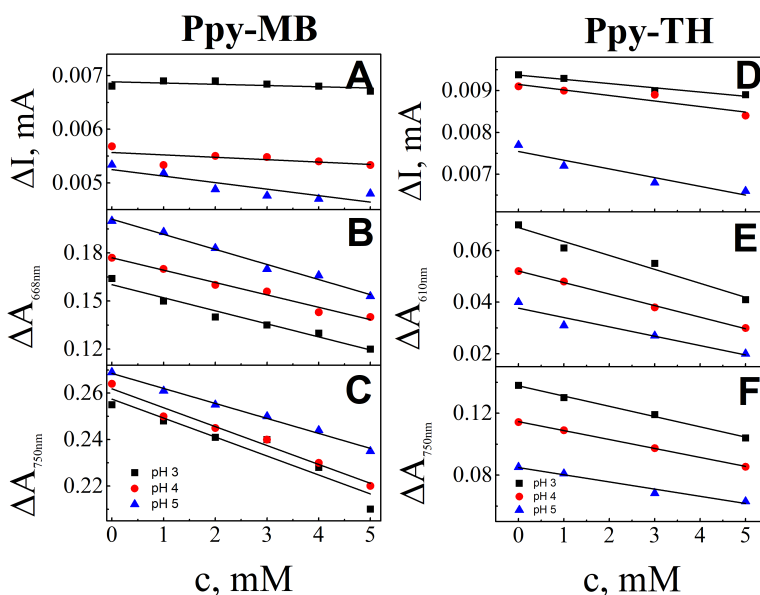
Figure 8. Calibration plots presenting the chronoamperometric signals at the beginning of the pulse (at different pH values: pH 3.0, pH 4.0, and pH 5.0) vs. concentrations of ascorbic acid: A – Ppy-PMB, and D – Ppy-PTH layers. The calibration plots of optical absorbance ($\Delta A = A_{+0.3V} - A_{-0.9V}$) vs. the concentration of ascorbic acid registered by: B – Ppy-PMB layer at a wavelength of 668 nm; C – Ppy-PMB layer at a wavelength of 750 nm; E – Ppy-PTH layer at a wavelength of 610 nm; F – Ppy-PTH layer at a wavelength of 750 nm in the BR-buffer at pH 3.0, pH 4.0, and pH 5.0

3.1.2. Application of three different polysaccharides for the modification of the polypyrrole-methylene blue layer properties

The study was carried out by selecting the layer of Ppy-PMB that was deposited by potential cycling of 25 cycles in the range from −0.5 V to +1.2 V, at a scan rate of 50 mV/s, and a step potential of 2.44 mV.

A thoughtful choice of the dopants can successfully adjust the conductivity of Ppy [165,166]. Small ions of strong acids, such as iodine [167], perchlorate [22], chloride [164], sulphate [168], and others, are exploited as dopants. Small ions of weak acids, like carboxylates, can also be used as dopants [165]. Saccharides are unique chemicals that are included in the list of dopants [169–171]. In order to examine the effects of saccharides, the Ppy-PMB layers were co-deposited on the ITO electrode in the presence of three saccharides (lactose, sucrose, and heparin).

The surface morphology was analyzed by AFM (Fig. 9). As it can be observed, the (Ppy- PMB)$_{Lac}$ (Fig. 9A) layer's surface has the most uniform distribution. On the (Ppy-PMB)$_{Hep}$ layer, the largest surface structures occurred (Fig. 9C). From the length of the cross-section vs. the structure height distribution (Fig. 9D), the height is up to 1.5–2.5 μm for (Ppy-PMB)$_{Lac}$, up to 2 μm for (Ppy-PMB)$_{Suc}$, and up to 3 μm for (Ppy-PMB)$_{Hep}$. The surface height distribution shown in Figure 9E validates that the dominant structural height for all Ppy-PMB layers is around 2.5 μm.
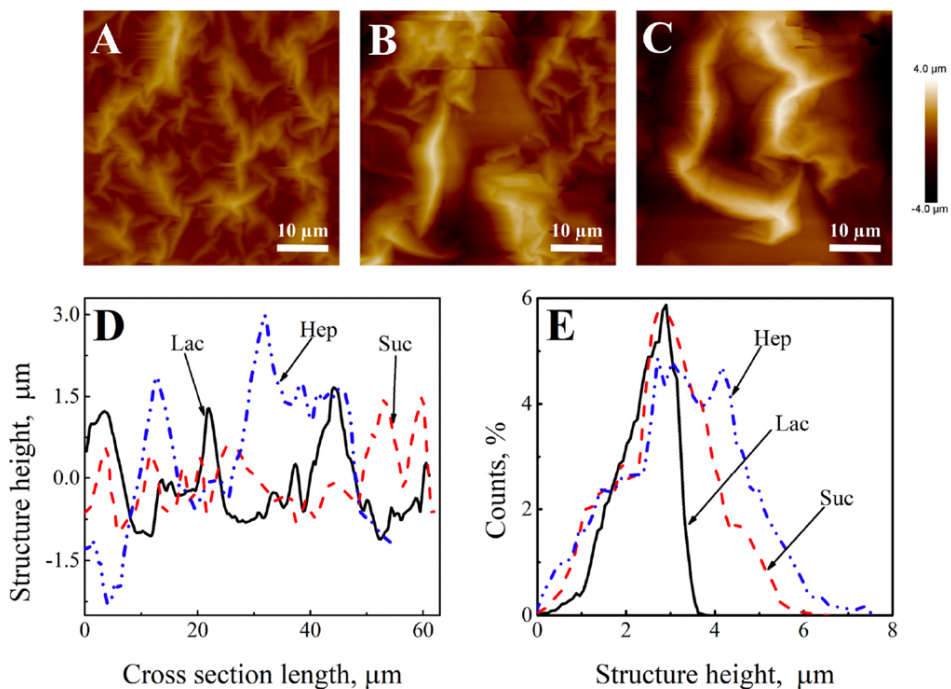
Figure 9. AFM-based evaluation of Ppy-PMB surface morphology of A glass/ITO/(Ppy-PMB)$_{Lac}$, B – glass/ITO/(Ppy-PMB)$_{Suc}$, C – glass/ITO/ (Ppy-PMB)$_{Hep}$. D – a comparison of the cross-sections of the surfaces of the layers, E – height distribution of the formed polymeric structures

The following study's objective was to investigate how lactose, sucrose, and heparin affected the Ppy-PMB layer's electrochromic characteristics. The surface shape is moderately impacted by the saccharides applied. By altering the pH value of the surrounding solution and the potential between +0.8 V and – 0.8 V, the electrochromic characteristics were examined concerning the changes in absorbance of the layer at two wavelengths (668 nm and 750 nm). For the calculation of ΔA, the values of $A_{+0.8V}$ and $A_{-0.8V}$ at the end of the potential pulse were taken. ΔA was calculated by using the following Equation (2):

$$\Delta A = A_{+0.8V} - A_{-0.8V} \qquad (2)$$

The calibration plots of ΔA vs. pH are shown in Figure 10. It was found that ΔA was the highest in the most acidic solutions regardless of the wavelength, and it decreased for all Ppy-PMB layers when the pH of the solution was changed to more alkaline.
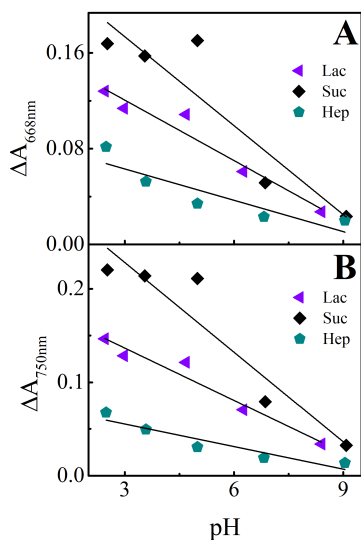
Figure 10. Calibration plot of ΔA (at the wavelengths of **A)** $\lambda = 668$ nm and **B)** $\lambda = 750$ nm) as a function of the pH value of BRB with 0.1 M of KCl solution, when potential pulses were of +0.8 V and –0.8 V with a duration of 10 s. Each potential pulse was repeated 5 times

The dependence of the absorbance changes (at $\lambda = 668$ nm and $\lambda = 750$ nm) on the pH of the BR buffer solution is also shown in Table 3. The electrochromic property of the optical contrast was also analyzed. The response times were very similar in all cases. Changing the pH to the alkaline side showed a visible change – by slowing down the response times in coloration and bleaching. In the case of (Ppy-PMB)$_{Lac}$ layers at 668 nm, a response time of about 8 s for coloration and 2.8 s for bleaching was shown. In the case of (Ppy-PMB)$_{Suc}$, there was a response time of about 5.9 s for coloration and 2.1 s for bleaching. In the case of (Ppy-PMB)$_{Hep}$, the response times were the longest compared to others: about 9.8 s for coloration, and 3.6 s for bleaching.

The Ppy-PMB layers with heparin as a dopant were shown to be more mechanically stable than the layers with lactose and sucrose as the dopants. To create electrochromic sensors for the detection of three xanthine derivatives – caffeine, theobromine, and theophylline – the Ppy-PMB layer doped with heparin was chosen for the subsequent experiment. For all three of the investigated xanthine derivatives, ΔA ($\Delta A = A_{+0.8V} - A_{-0.8V}$) versus concentration was shown to be linear (Fig. 11). Theophylline determination revealed the greatest change in the optical absorption. The slope for the relationship between the concentration of xanthine derivatives (C, µM) and variations in absorbance (at $\lambda = 668$ nm and $\lambda = 750$ nm) was calculated by using the linear regression equation. The slope of the

linear regression for caffeine (at $\lambda = 668$ nm) was –0.001 with an R^2 of 0.978, while it was –0.002 with an R^2 of 0.977 for theophylline, which is two times higher. Theobromine has a slope of linear regression with an R^2 value of 0.939 and a slope of –0.005. Only the first three points are reported since only at low concentrations is there a linear relationship to be seen, followed by a scattering of points (the concentration interval of theobromine was limited by the compound solubility in the BRB solution). The lowest concentration of the analyte that produces an analytical signal greater than the background value plus $3\,\delta$ is referred to as the limit of detection (LOD). The LODs for ΔI vs. the concentrations of caffeine, theophylline, and theobromine were 2.0 µM, 3.9 µM, and 7.48 µM, respectively. Based on registered changes in absorbance at $\lambda = 668$ nm, the LODs for caffeine, theophylline, and theobromine were 3.3 µM, 3.0 µM, and 6.0 µM, respectively; while the changes in absorbance were registered at $\lambda = 750$ nm, the LODs were 3.75 µM, 3.0 µM, and 3.0 µM, respectively. The (Ppy-PMB)$_{Hep}$ layer may be suited for the detection of xanthine derivatives, particularly for theophylline and caffeine, in the light of the results that have been obtained.
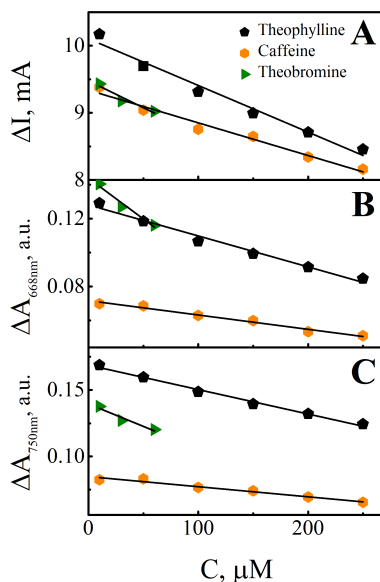

Figure 11. Dependence of absorbance changes (at $\lambda = 668$ nm and $\lambda = 750$ nm) on the concentration of caffeine, theophylline, and theobromine in BRB with 0.1 M of KCl, pH 2.5 solution. **A)** calibration plots of ΔI vs. the concentration of caffeine, theophylline, and theobromine, **B)** calibration plots of ΔA (at 668 nm) vs. the concentration of caffeine, theophylline, and theobromine, **C)** calibration plots of ΔA (at 750 nm) vs. the concentration of caffeine, theophylline, and theobromine

Table 3. Dependence of absorbance changes (at λ = 668 nm and λ = 750 nm) on the pH value of BRB solution. The slope and intercept values of the calibration plots

Wavelength	Layer	Slope	Intercept	R^2
668nm	(Ppy-PMB)$_{Lac}$	−0.017±0.002	0.171±0.001	0.935
	(Ppy-PMB)$_{Suc}$	−0.025±0.006	0.248±0.036	0.790
	(Ppy-PMB)$_{Hep}$	−0.009±0.002	0.089±0.0145	0.742
750nm	(Ppy-PMB)$_{Lac}$	−0.019±0.0023	0.193±0.012	0.944
	(Ppy-PMB)$_{Suc}$	−0.032±0.0064	0.324±0.038	0.857
	(Ppy-PMB)$_{Hep}$	−0.008±0.0017	0.079±0.010	0.851

3.2. The Modification of Polypyrrole Properties for the Application as Molecularly Imprinted Polymer

The severe acute respiratory syndrome coronavirus-2 (SARS-CoV-2) induced COVID-19 pandemic that began in 2019 has caused drastic changes. Countries all over the world were affected by lockdowns, quarantines, economic problems, even people's emotional health has deteriorated. During the pandemic, the understanding and control of the virus was problematic. Although the vaccines became available to society, this viral infection was very active, mutating. Therefore, a much deeper understanding of the virus SARS-CoV-2 was required, and rapid analytical methods that are suitable for the diagnosis of COVID-19 and/or detection of the virus or their parts were demanded.

The focus of this part of the study was later shifted to the development of an MIP-based sensor for the detection of the SARS-CoV-2-S glycoprotein. To do this, Ppy layers were obtained from the polymerization of SARS-CoV-2-S glycoprotein and pyrrole dissolved in phosphate-buffered saline (PBS) solution, pH 7.4, were applied to the working platinum electrode.
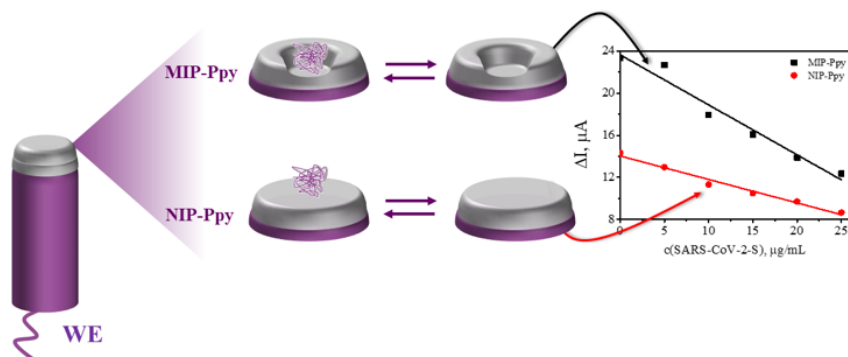

Figure 12. Schematic representation of evaluation by chronoamperometry of Pt electrode modified with non-imprinted polypyrrole (NIP-Ppy) and with molecularly imprinted polypyrrole (MIP-Ppy) with SARS-CoV-2-S glycoprotein imprints. Electrochemical measurements were performed in a phosphate-buffered saline (PBS) solution, pH 7.4

The approach outlined in a preceding chapter (2.4.2. Electrochemical deposition of MIP and NIP layers on Pt electrode) was used to carry out the electrochemical deposition of the polypyrrole layer. The scheme of the investigation and comparison of the performance of the electrode that was

modified with MIP-Ppy and NIP-Ppy (Fig. 12). The performance of the polymer layers was evaluated by pulsed amperometric detection.

3.2.1. Modification of polypyrrole with SARS-CoV-2 spike glycoprotein imprints

The two different types of Ppy layers were electrochemically polymerized by using a series of potential pulses (Fig. 13). The potential pulse sequence profile is depicted in Figure 13A. Figures 13B and C show the current values that were recorded during the electrochemical deposition of the Ppy layer from the polymerization solution containing SARS-CoV-2-S glycoprotein and the Ppy layer from the polymerization solution without SARS-CoV-2-S glycoprotein on the Pt-electrode surface, respectively. The variations in the current at the start I_1 and the end I_2 of pulses with a potential of +0.95 V are shown in Figure 13E. Since the concentrations of the monomer and template molecules near the working electrode are equilibrating during this potential step, the current variations at a potential of 0 V were not the subject of the research. Prior research has shown that the recognition properties of the final polymers are significantly influenced by the self-assembly of monomers and template molecules caused by interactions under thermodynamic control [172]. Ppy polymerizes during the pulses at a voltage of +0.95 V.

Therefore, at a 0 V potential step, the electrode only displayed a minimal Faradaic process. As a result, when the potential was raised to +0.95 V, the current variations during the potential step were examined in greater detail. Two current points at the beginning I_1 and the end I_2 of each potential step was taken into consideration for the visualization of the current changes during the electrochemical deposition of the Ppy layer from polymerization solution containing SARS-CoV-2-S glycoprotein and the Ppy layer from the polymerization solution without SARS-CoV-2-S glycoprotein (Fig. 13D). The current registered during the deposition of the Ppy layer from the polymerization solution without SARS-CoV-2-S glycoprotein is higher than that registered during the deposition of the Ppy layer from the polymerization solution with SARS-CoV-2-S glycoprotein, according to a comparison of the current changes (Fig. 13E).
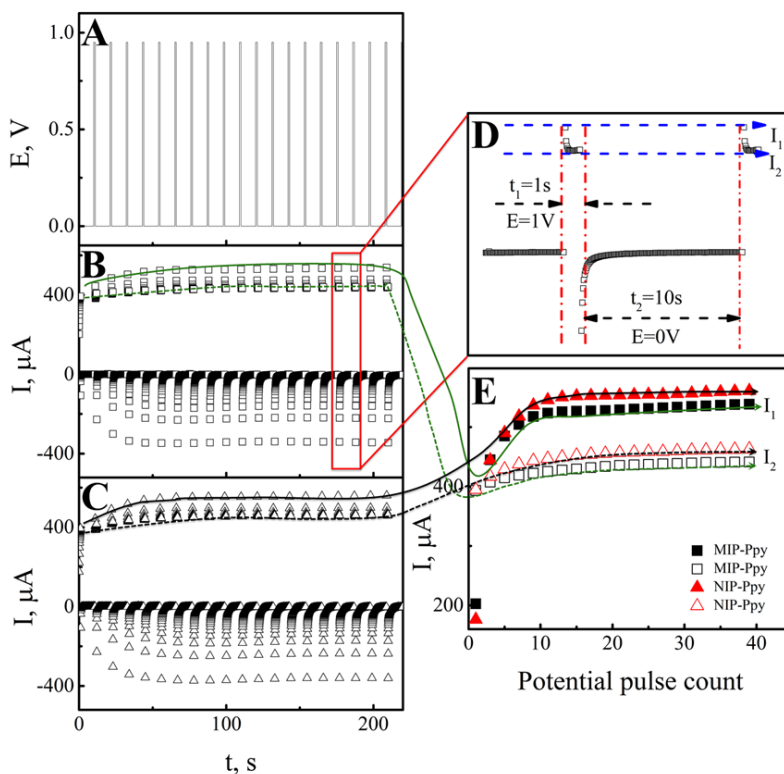
Figure 13. Electrochemical deposition of polypyrrole layers on the Pt electrode: **A)** The profile of the potential applied during the sequence of potential pulses; **B)** The profile of the current registered during the deposition of Ppy layer from polymerization solution containing SARS-CoV-2-S glycoprotein; **C)** The profile of the current registered during the formation of Ppy layer from the polymerization solution without SARS-CoV-2-S glycoproteins; **D)** The profile of the current registered during one potential pulse; **E)** Changes of the current measured instantly after a potential step of +0.95 V

The produced MIP-Ppy and NIP-Ppy layers were evaluated by using pulsed amperometric detection while using a sequence of 10 potential pulses of +0.6 V and 0 V for 2 s each. Heinze et al. [161] provided a thorough discussion of the different features of the charging and discharging of conducting polymer polypyrrole.

The potential pulse sequence was used to evaluate the electrochemical properties of the MIP-Ppy and NIP-Ppy layers (Fig. 14). The SARS-CoV-2-S glycoprotein's concentration ranged from 0 µg/mL to 25 µg/mL. The amperometric response of MIP-Ppy and NIP-Ppy modified Pt electrodes that

were incubated in the SARS-CoV-2-S glycoprotein-containing PBS solution, pH 7.4, is dependent on concentration, as shown in Figures 14A and B. The adsorption of less conductive protein molecules on the MIP-Ppy or NIP-Ppy layer is responsible for the modification in the amperometric response. The registered amperometric response of both MIP-Ppy and NIP-Ppy modified Pt electrodes decreased when the solution's SARS-CoV-2 spike glycoprotein concentration rose. Higher current values were recorded before the electrode's incubation in the SARS-CoV-2-S glycoprotein-containing solution.
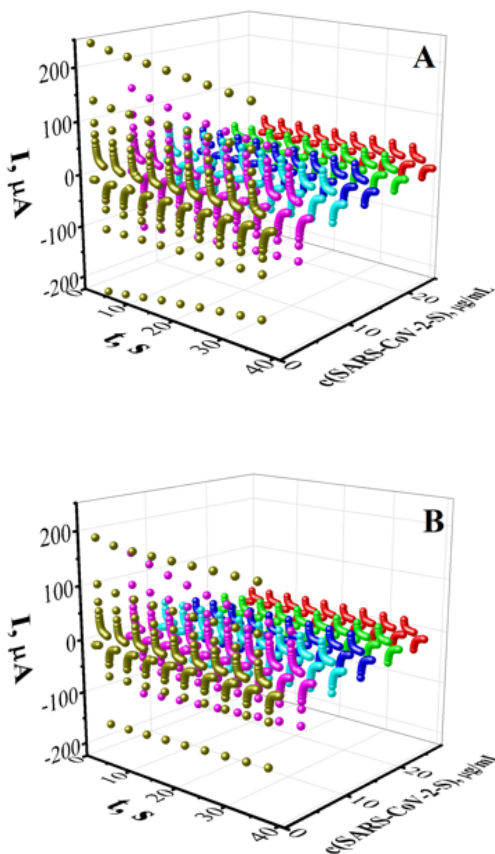
Figure 14. Pulsed amperometry-based evaluation of MIP-Ppy and NIP-Ppy modified electrodes performed by the potential pulse sequence (+0.6 V and 0 V potentials), representing the incubation process of SARS-CoV-2-S glycoprotein. Amperograms were obtained at Pt electrode modified: **A)** with MIP-Ppy modified electrode; and **B)** with NIP-Ppy modified electrode in PBS with 0.1 M of KCl, pH 7.4 in the absence of SARS-CoV-2-S glycoprotein or in the presence of SARS-CoV-2 spike glycoprotein concentrations from 5 µg/mL up to 25 µg/mL

With an increasing SARS-CoV-2-S glycoprotein concentration in the PBS solution, the value of the current differences, which are observed during potential pulses at instants when the potentials were stepped from 0 V up to +0.6 V, and from +0.6 V down to 0 V, decreased (Fig. 15). The current profile that was recorded during potential pulses is shown in Figure 15A, along with a representation of the analytical signals (ΔI) for the calibration plot. According to this calibration plot (Fig. 15B), all the assessed SARS-CoV-2-S glycoprotein concentrations in the range of 0 μg/mL to 25 μg/mL showed the linearity of the analytical signal dependence on the analyte concentration.

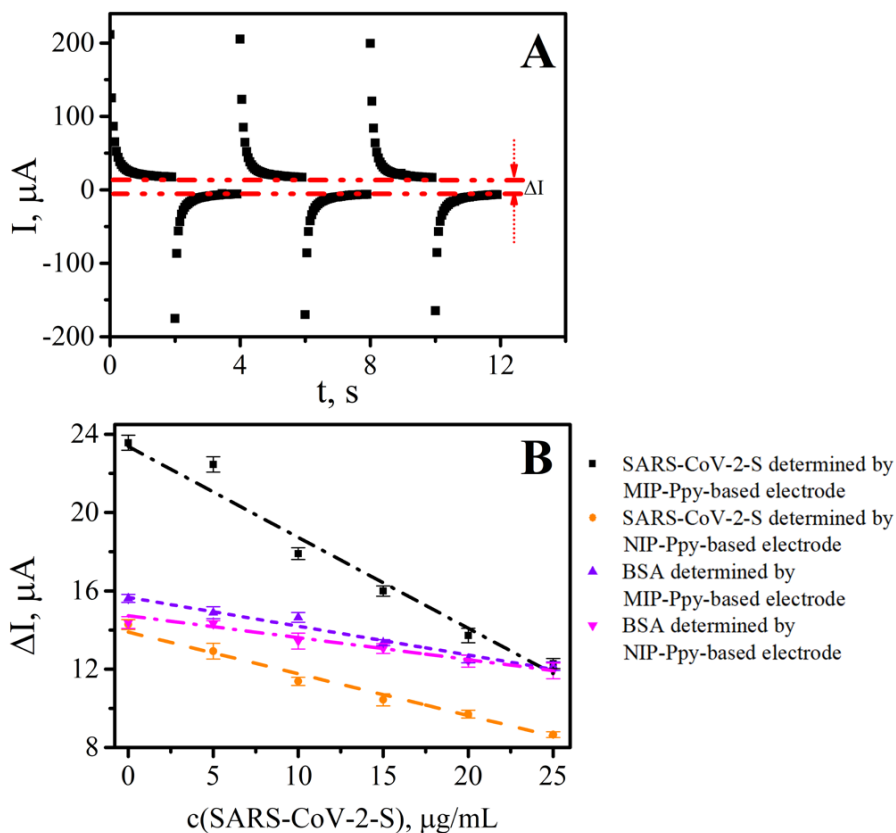**Figure 15.** Calibration plots of ΔI vs. concentration of SARS-CoV-2-S glycoprotein and BSA on MIP-Ppy and NIP-Ppy according to the ΔI calculated in respect to: **A)** the principal of ΔI measuring; **B)** ΔI. RSD% was in the range from 2% to 4.3% of the current values of 5 potential pulses for the listed data points

To assess the selectivity of the MIP-Ppy layer towards various proteins, the same MIP-Ppy and NIP-Ppy modified Pt electrodes were tested for te interaction with BSA (Fig. 15B). Through the use of linear regression, the slope values for these observations were determined (Table 4). The slope value recorded by the MIP-Ppy modified Pt electrodes incubated in a BSA-containing solution was significantly lower (-0.15 µA/(µg/mL)). The results of using MIP-Ppy modified Pt electrodes showed greater fluctuations in the current and can be used for the targeted detection of the imprinted SARS-CoV-2-S glycoprotein. In the light of this, it can be said that the molecular imprinting of the conducting polymer may be used to create an electrochemical sensor for the detection of SARS-CoV-2-S glycoprotein. The novelty of the second part of this research was based on the application of the total charge for the evaluation of the interaction between the electrode and the analyte. The key idea of this work was based on the application of the Anson plots for the elucidation of the interaction between SARS-CoV-2 spike glycoproteins and the molecularly imprinted polypyrrole.

Table 4. Linear regression characteristics of current (ΔI, μA) vs. the concentration of SARS-CoV-2-S glycoprotein (c, μg/mL) on the MIP-Ppy and NIP-Ppy modified Pt electrodes

$y = ax + b$	a	b	R^2
SARS-CoV-2-S glycoprotein determined by MIP-Ppy-based electrode	−0.46 ±0.04	23.4 ±0.7	0.96
SARS-CoV-2-S glycoprotein determined by NIP-Ppy-based electrode	−0.21 ±0.01	13.9 ± 0.3	0.98
BSA determined by MIP-Ppy-based electrode	−0.15 ± 0.01	15.7 ± 0.2	0.97
BSA determined by NIP-Ppy-based electrode	−0.10 ± 0.01	14.7 ± 0.1	0.97

The relation of the cumulative charge passed and time in Ppy-based electrochemical sensors obeys the integrated Cottrell Equation (3) [173,174]:

$$Q = 2nFAC\sqrt{\frac{D}{\pi}}\sqrt{t} + Q_{d.l.} + Q_{ads.} = k\sqrt{t} + Q_{d.l.} + Q_{ads.} \quad (3)$$

where: Q – total charge (C); n – number of electrons; F – Faraday constant (96485 C/mol); A – area of the electrode (cm^2); C – concentration (M); D – diffusion coefficient (cm^2/s); t – time (s); $Q_{d.l.}$ – the charge of the electrical double layer; $Q_{ads.}$ – charge induced by adsorbed ions

The cumulative charge in the Cottrell equation corresponds to the charge passed associated with the redox activity leading to Faradic charges (Q_F), charging, and discharging of the electrode-electrolyte double-layer capacitive charges ($Q_{d.l.}$), and charge changes associated with the adsorbed species ($Q_{ads.}$) [175]. Hence, the plot of Q vs. $t^{1/2}$ has a linear correlation with the slope k and the intercept corresponding to $Q_{ads.} + Q_{d.l.}$.

The simplified reaction of the analyte at the electrode can therefore be described in several steps: the diffusion of the analyte from the solution to the electrode, electrochemical oxidation-reduction reaction, and then the diffusion of the reaction products from the electrode to the solution. Analysis of the slopes and intercepts in the Anson diagram can be used to identify the adsorption of either the analytes or the reaction products at the electrode.

The data from the amperograms are presented in the Anson plots (Fig. 16A, D). The parameters of the related linear equations are presented in Table 5 along with the relationship between Q and $t^{1/2}$ that was fitted by linear regression. The plot of Q vs. $t^{1/2}$ shows a linear association, according to the computed R^2 values (Table 5). It was not anticipated that the oxidation of the SARS-CoV-2-S glycoprotein would take place at a voltage of +0.6 V based on the experimental settings. However, similarly to how it was described for small molecular weight molecules [176,177], the interaction of SARS-CoV-2-S glycoprotein with complementary carboxyl, carbonyl, and hydroxyl groups arranged in imprinted cavities played a significant role in the recognition of SARS-CoV-2-S glycoprotein and the formation of the Ppy/SARS-CoV-2-S glycoprotein complex. After incubating the MIP-Ppy modified electrode, changes in the registered current are detected as a result of the SARS-CoV-2-S glycoprotein replacing the water molecules.
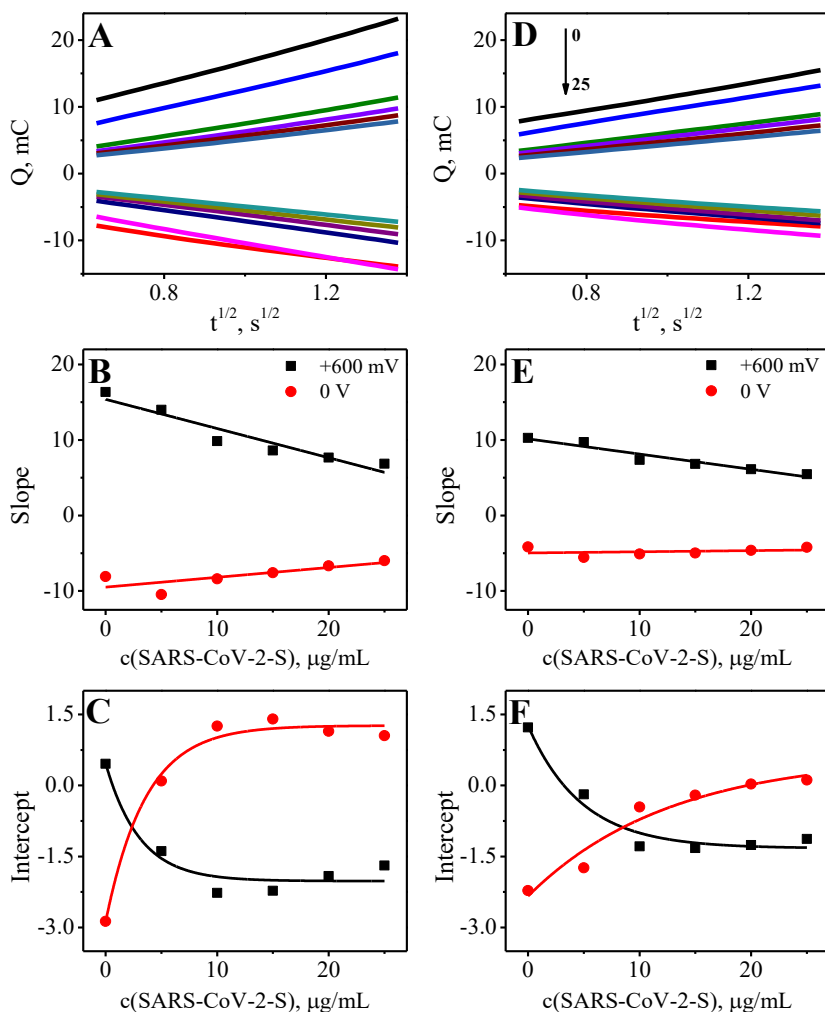
Figure 16. A and D represent the Anson plots (Q, mC vs. $t^{1/2}$, $s^{1/2}$) derived from the amperometric response presented in Figure 14 for: **A)** MIP-Ppy modified electrode; and **D)** NIP-Ppy modified electrode. **B)** and **E)** represent the slope values vs. the concentration of SARS-CoV-2-S glycoprotein (concentration, μg/mL). **C)** and **F)** represent the intercept values vs. the concentration of SARS-CoV-2-S glycoprotein (μg/mL)

The MIP-Ppy modified electrode has a stronger linear dependence of the slope value on the analyte concentration (– 0.387 for +0.6 V pulse and 0.1303 for 0 V pulse; Fig. 16B) than the NIP-Ppy modified electrode (–0.2015 for +0.6 V pulse and 0.0156 for 0 V pulse; Fig. 16E). This demonstrates that the analyte interacts with NIP-Ppy less favorably than MIP-Ppy. In the absence of the SARS-CoV-2-

S glycoprotein, there is one point that deviates from the general trend (Fig. 16B, E).

Only when MIP-Ppy and NIP-Ppy modified Pt electrodes were incubated in SARS-CoV-2-S glycoprotein-free PBS solution was the intercept determined to have a positive value. It was thought that the pyrrole oxidation process operates under the tenets of heterogeneous kinetics. The working principles of the MIP are the foundation of the investigation as detailed above. This refers to the complementary cavities that emerge in the polymer during the polymerization stage and their presence in a particular analyte interaction during the assessment stage. The heterogeneous kinetics of the pyrrole oxidation and reduction reaction are thus hampered by molecules adsorbed on the Ppy surface.

The information in Figure 16B, E shows that as the concentration of SARS-CoV-2-S glycoprotein rises, the slope 'k' of the Anson equation, which was computed by using Equation (3), decreases. This impact is far more noticeable at an electrode potential of +0.6 V than it is at a potential of 0 V. The slope 'k', denoted by Equation (3), depends on the concentration of the material 'C', the diffusion coefficient 'D', the equivalent number of electrons 'n' transported during the electrochemical reaction, the electrochemically active area 'A', and the slope 'k'. The diminution in the electrochemically active area (A) is connected to the opposite dependency of slope k on glycoprotein concentration C. This conclusion is based on the assumption that the values of the n and D parameters are constant at all of the SARS-CoV-2-S glycoprotein concentrations evaluated here because the concentration of all other solution constituents and, consequently, physicochemical properties (such as density and viscosity), are the same. It should be observed that the reliance of 'k' on the concentration of SARS-CoV-2-S glycoprotein is more strongly expressed in the case of the MIP-Ppy-modified electrode than it is in the case of the NIP-Ppy-modified electrode. The dependence of the 'k' value on C is 1.9 times more expressed in the case of the MIP-Ppy modified electrode in comparison to the value of the NIP-Ppy modified electrode at +0.6 V, even though the dependence of 'k' on the concentration of SARS-CoV-2-S glycoprotein 'C' is linear. The active area of MIP-Ppy (AMIP-Ppy) is 1.9 times larger than that of NIP-Ppy (ANIP-Ppy), according to the slope.

As it was already mentioned, the blockage of the MIP-Ppy surface by a non-conducting material – SARS-CoV-2-S glycoprotein – is what causes the drop in the surface charge at greater concentrations of SARS-CoV-2-S glycoprotein. In this chronoamperometric experiment, all electrical charge passage is governed by the adsorption and desorption of ions on the MIP-Ppy or NIP-Ppy layers as well as the doping and dedoping of Ppy-based layers with anions such as PO_4^{3-}, HPO_4^{2-}, $H_2PO_4^-$, and Cl^-. Figure 16B and D presents how Ppy-based layers interact with SARS-CoV-2-S glycoprotein and, respectively, how the Ppy surface is partially blocked.

The Anson plot-based evaluation indicates that a SARS-CoV-2-S glycoprotein molecule is an analyte in this situation which interacts with MIP-Ppy and non-specifically adsorbs on NIP-Ppy layers.

Table 5. Linear regression parameters of the Anson plot (Q, mC vs. $t^{1/2}$, $s^{1/2}$) (derived from Fig. 14) on the MIP-Ppy and NIP-Ppy modified Pt electrodes for the last (10th) pulse of the potential pulse sequence.

C, μg/mL	y = ax + b	MIP-Ppy modified electrode			NIP-Ppy modified electrode		
		a	b	R^2	a	b	R^2
0	+0.6 V	16.35	0.46	0.99	10.26	1.22	0.99
	0 V	-8.09	-2.87	0.99	-4.17	-2.22	0.99
5	+0.6 V	13.99	-1.39	0.99	9.70	-0.19	0.99
	0 V	-10.48	0.095	0.99	-5.56	-1.74	0.99
10	+0.6 V	9.84	-2.27	0.99	7.37	-1.29	0.99
	0 V	-8.39	1.25	0.99	-5.10	-0.46	0.99
15	+0.6 V	8.61	-2.22	0.99	6.83	-1.32	0.99
	0 V	-7.57	1.40	0.99	-4.97	-0.20	0.99
20	+0.6 V	7.65	-1.91	0.99	6.12	-1.26	0.99
	0 V	-6.68	1.14	0.99	-4.61	0.03	0.99
25	+0.6 V	6.85	-1.69	0.99	5.47	-1.13	0.99
	0 V	-5.98	1.05	0.99	-4.22	0.12	0.99

3.2.2. Modification of polypyrrole with methylene blue as the imprint template

This section of the study was focused on combining the MIP technology and applying it to the determination of MB on an ITO electrode.

Figure 17A displays a schematic representation of the investigation. With MB serving as a template molecule, the goal of this study was to produce a molecularly imprinted Ppy. A glass/ITO electrode with an imprinted Ppy layer is shown in Figure 17B. The impact of the surface polymer's variable thickness on the strength and effectiveness of the MIP characteristics was also examined.

A

B
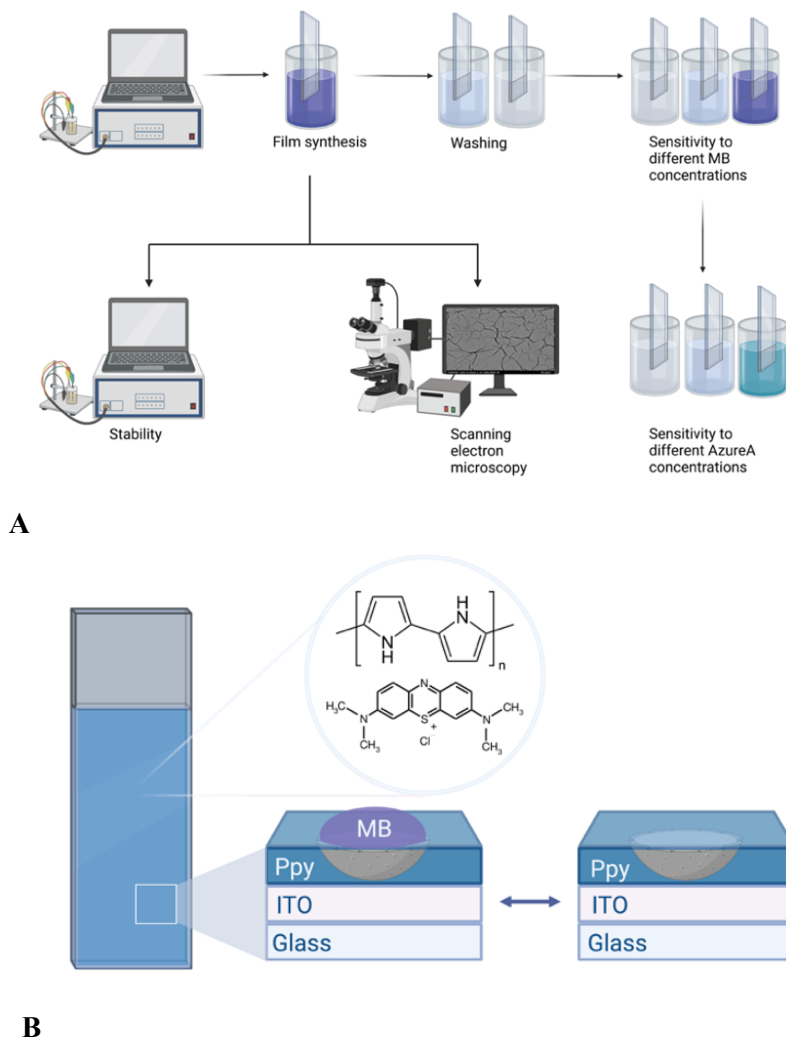
Figure 17. Schematic representation of the study. **A)** Scheme of MB-based sensor evaluation steps; **B)** Visualization of an imprinted Ppy layer on an ITO electrode

According to the aforementioned conditions and by using 3, 5, 7, 10, 15, 20, or 25 potential cycles, polymer layers containing entrapped MB as a template were electrochemically deposited. Several potential ranges were tested, including – 0.4 V to +1 V (1), –0.5 V to +1.2 V (2), –0.4 V to +0.8 V (3), and –0.4 V to +0.6 V (4), to determine the best synthesis conditions to imprint MB onto the Ppy layer (Ppy-MB). Cyclic voltammograms from the electrochemical polymerization of the polymer layers with imprinted MB are compared (Fig. 18). In the ranges from −0.4 V to +0.6 V and from −0.4 V to +0.8 V, the voltammograms lack sufficient anodic peaks to investigate the pyrrole polymerization. For further studies, a smaller potential window (– 0.4 V to +1 V) was chosen.
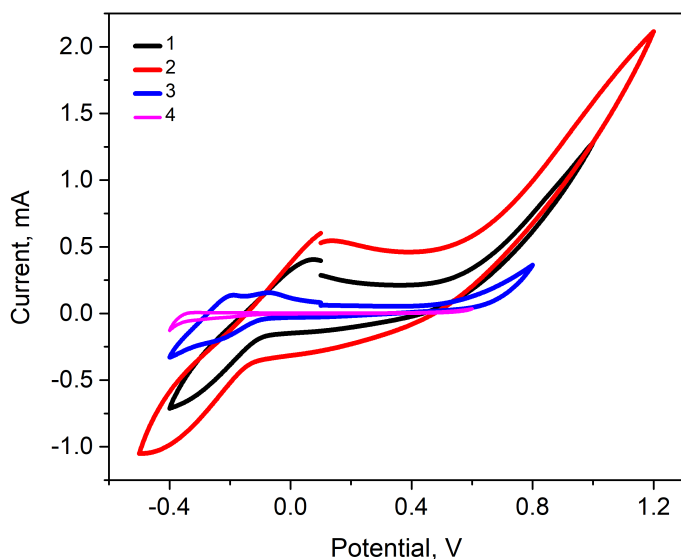
Figure 18. Electrochemical deposition of Ppy-MB during potential cycling at different conditions: 1) from –0.4 V to +1 V; 2) from –0.5 V to +1.2 V; 3) from –0.4 V to +0.8 V; 4) from –0.4 V to +0.6 V. CV at a scan rate of 50 mV/s, and a step potential of 2.44 mV. Electrochemical polymerization was performed in a three-electrode system, in which glass/ITO was used as WE, Ag/AgCl as RE, and platinum wire as CE

Changes in optical absorbance (A) in the BR-buffer solution, wherein the pH value was equal to 3, was determined right after deposition (Fig. 19). The pulse chronoamperometry was used and set to a total of 10 pulses: 5 pulses of –0.8 V, and 5 pulses of +0.8 V in shifts, with each pulse being set for 10 s. At

wavelengths of 530 nm, 668 nm, and 750 nm, optical absorbance was monitored. The trends indicate that the change in absorption rises with the layer thickness are discernible.
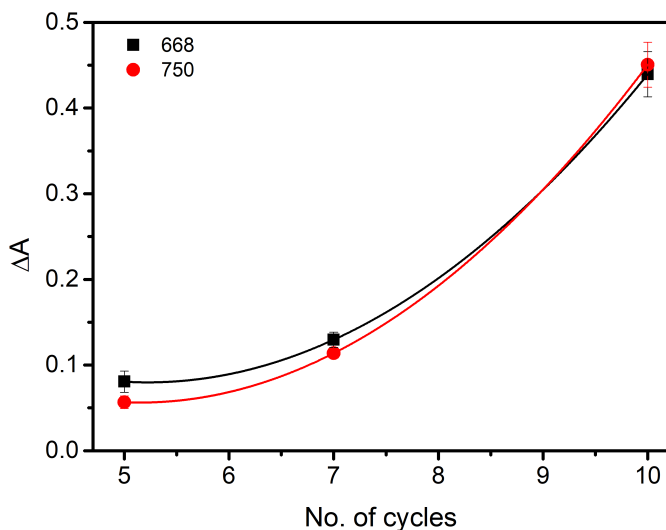

Figure 19. Impact of the number of Ppy-MB polymerization cycles on the absorbance: Ppy-MB-5, Ppy-MB-7, Ppy-MB-10. The absorbance was measured at $\lambda = 668$ nm and $\lambda = 750$ nm

The electrode modified by the deposited MIP-Ppy layer imprinted with MB was examined for its performance and stability (i.e., its ability to remain mechanically on the electrode surface and the reproducibility of experiments employing the same layer). The storage circumstances listed below were examined: BR-buffer in air, water, and an acidic medium. The obtained results of this and previous studies proved that storage of the polypyrrole in the air is more convenient.

An analysis of the layer's performance and the impact of the washing and determination processes on the polymer layer's properties was the goal of the additional part of this investigation. The Ppy-MB-5, Ppy-MB-7, and Ppy-MB-10 layers were washed in water to verify their stability. The shift in optical absorbance (ΔA) was noted following each wash, which lasted for three minutes. Five pulses were chronoamperometrically measured by using the potential pulse method. Five pulses, each with a voltage between –0.8 V and +0.8 V and a time setting of 10s, were employed in the pulse chronoamperometry. The absorbance was tracked concurrently. The optical

absorbance was observed simultaneously. Figure 20 depicts a pattern that has been steadily declining. It was noted that, during the third wash (or a comparable number of washes), the Ppy-MB-5 layer on the electrode lost mechanical stability, and absorption was not detectable.
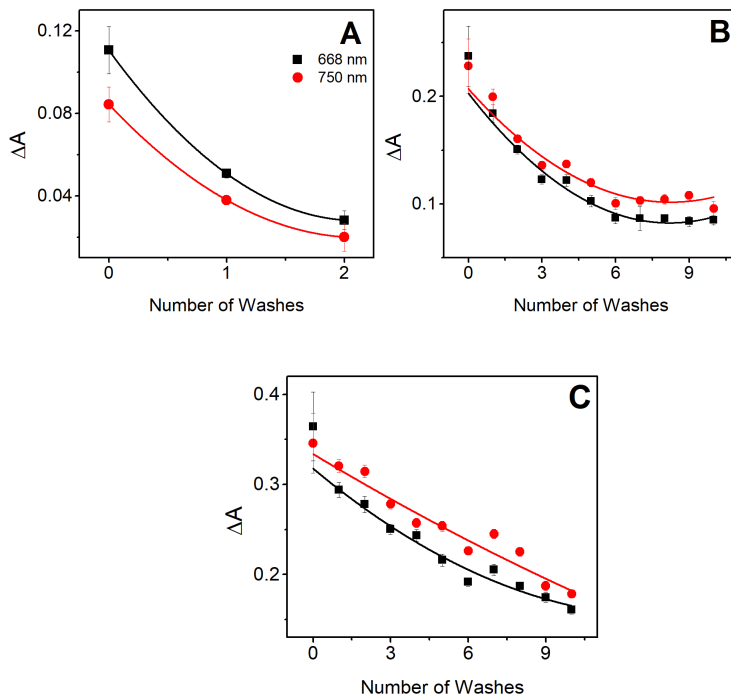

Figure 20. Dependence of the change in absorption on the number of times the layer was washed in water. **A)** Ppy-MB-5, **B)** Ppy-MB-7, **C)** Ppy-MB-10. Absorbance was measured at $\lambda = 668$ nm and $\lambda = 750$ nm. Error bars represent the standard deviation of ΔA from N=3

According to an analysis of the earlier phases of this research, the layer that was deposited by using 7 potential cycles is probably the most trustworthy and efficient. Since it is not very thick, it adheres to the electrode's surface for a longer period. It is also clear, yet it does not wash off even after numerous washings. This layer was carefully used to conduct additional research and verify the sensor's status as an imprinted Ppy-MB. The imprinted MB from the newly generated layer has to be removed first. Sulfuric acid of a concentration of 0.1 M was employed for this, and the washing process took 5 minutes.

To create identical experimental settings, NIP-Ppy was likewise washed. The produced MIP-Ppy and NIP-Ppy layers were assessed in the subsequent section of the research by tracking changes in absorption. The range of MB concentrations was from 0.1 μM to 10 mM. The outcomes are displayed in Figure 21.
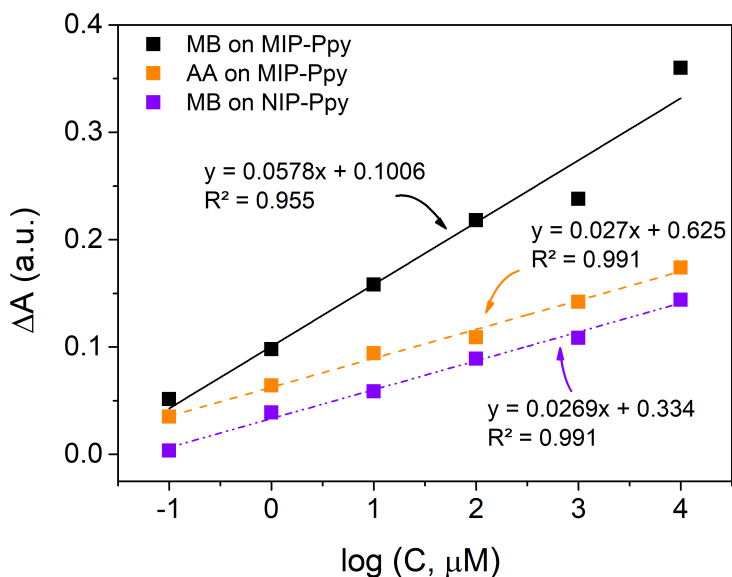

Figure 21. Calibration plots (ΔA vs log [C, μM]) present the change in absorption on Ppy-MB-7 layers as MIP-Ppy or NIP-Ppy, in the presence of adsorption of MB and azure A

Figure 21 presents the calibration plots that show how the presence of MB or azure A alters the absorption (A) on the MIP-Ppy and NIP-Ppy layers. All of the tested calibration graphs in the concentration range of 0.1 μM to 10 mM showed linearity. R^2 is higher than 0.9 because MB on MIP-Ppy is 0.955, AA on MIP-Ppy is 0.976, and MB on NIP-Ppy is 0.991. When MB interaction is contrasted with MIP-Ppy or NIP-Ppy, the apparent imprinting factor is approximately 2.15. This represents that, compared to the rival molecule azure A, the target MB molecules are more complimentary to the imprinted holes of the layer. While the slope for the calibration plot of MB on MIP-Ppy is noticeably steeper, the slope values for the calibration plots of AA on MIP-Ppy and MB on NIP-Ppy are approximately the same. The strength of the target molecule interactions with the polymer layers can be used to determine the magnitude of the slope values for the calibration plots. Since there was no

imprinting procedure during the sensor's fabrication, the slope for MB on MIP-Ppy was expected to be greater than that of MB on NIP-Ppy. Complementary holes and imprints allowed MB to interact with MIP-Ppy in both specific and non-specific ways. Conversely, MB only had a non-specific interaction with NIP-Ppy, which led to reduced slope values. Moreover, there is a similar difference in the slope values for MB and AA on MIP-Ppy, suggesting that MIP-Ppy is selective for MB molecules. Considering the aforementioned observations, it is possible to conclude that the methods outlined above can be used to create imprinted Ppy-based sensors that are capable of MB detection.

CONCLUSIONS

Polypyrrole layers were successfully modified with phenothiazine derivatives or molecular imprints.

The investigation has revealed that, among the three phenothiazine derivatives – methylene blue, azure A, and thionine – methylene blue emerged as the most promising candidate for designing an effective electrochromic sensor.

The study has also demonstrated the positive impact of polysaccharides, particularly heparin, in the polymerization mixture, contributing to an improved layer adhesion.

Furthermore, the research has emphasized the significance of the polymerized layer's thickness, highlighting its direct correlation with an enhanced adhesion and the overall durability.

The developed MIP-Ppy-based layer exhibited potential as a sensor for the determination of the SARS-CoV-2-S glycoprotein, showcasing its versatility in practical applications.

The integrated Cottrell equation (the Anson plot) has emerged as a valuable tool for calculating the amount of charge passed through both the MIP-Ppy and NIP-Ppy layers.

Additionally, the study has highlighted the possibility of creating the MIP-Ppy with methylene blue as a template, where methylene blue does not fully polymerize and is effectively imprinted, thereby presenting an innovative approach to the sensor design.

SANTRAUKA LIETUVIŲ KALBA

ĮVADAS

Elektrocheminiai jutikliai atlieka svarbų vaidmenį įvairiose pramonės šakose ir pritaikyme skirtingose srityse, nes gali aptikti ir kiekybiškai įvertinti konkrečius cheminius junginius ar elementus. Jie naudojami aplinkos stebėjimui, sveikatos priežiūros ir medicinos reikmėms, pramoniniams procesams, saugai bei kitiems tikslams.

Elektrocheminių jutiklių rinka sparčiai plečiasi dėl technologijų pažangos, sustiprėjusių aplinkosaugos taisyklių ir augančių sveikatos priežiūros poreikių. Apskaičiuota, kad 2023 m. pasaulinės biojutiklių rinkos dydis siekė 28.44 mlrd. JAV dolerių, o iki 2033 m. manoma, kad ji pasieks 58.44 mlrd. [1]

Literatūroje aprašoma daug įvairių elektrocheminių jutiklių konstrukcijų skirtingoms medžiagoms aptikti. Žinoma, mokslininkai susiduria su sunkumais, lėtinančiais jutiklių realizavimą rinkoje: pakartojamumo ir jutiklių stabilumo problemomis, nepakankamai žemomis aptikimo ribomis, ieškoma tvaresnių sprendimų ir jutiklių integravimo į praktiškus, patogius įrenginius, teisiniu reglamentavimu.

Dėl morfologinių ir fizikinių laidžių polimerų savybių jie gali būti pritaikomi įvairiose pramonės srityse, taip pat ir kuriant jutiklių konstrukcijas. Polipirolas (Ppy) yra laidus polimeras, vienas iš dažniausiai naudojamų elektrocheminiams jutikliams gaminti, nes jame dera elektrinis laidumas, elektrocheminis aktyvumas, stabilumas ir pritaikomumas. Ppy pasižymi ypatingomis savybėmis, tad jo pagrindu buvo sukurti jutikliai, taikomi aptinkant įvairias analites, tokias kaip dujos, jonai, biomolekulės ir aplinkos teršalai.

Tyrimo tikslas:

Įvertinti Ppy savybių modifikavimo galimybes kuriant elektrocheminį jutiklį. Šiuo tikslu Ppy sluoksnis buvo modifikuotas fenotiazino dariniais arba molekuliniais įspaudais.

Tyrimo uždaviniai:

1. Polimerizuoti pirolo sluoksnį, modifikuotą fenotiazino dariniais ir kitais priedais, ant stiklo padengto plonu indžio alavo oksido (ITO) sluoksniu.

2. Kuriant jutiklio konstrukciją, nustatyti tinkamiausias sąlygas stabilesnio polipirolo sluoksnio nusodinimui ant ITO.
3. Pirolo sluoksnį polimerizuoti ant platinos elektrodo ir pritaikyti jutiklio, grįsto molekulių įspaudais modifikuotu polimeru, kūrimui.
4. Įvertinti gautas struktūras ir jų panaudojimą.
5. Pritaikyti integruotą Cottrell lygtį siekiant įvertinti molekulių įspaudais modifikuotą polipirolą (MIP-Ppy) ir molekulių įspaudais nemodifikuotą polipirolą (NIP-Ppy).

Naujumas:

• Trys fenotiazino dariniai (metileno mėlynasis (MB), azūras A (AA) ir tioninas (TH)) buvo naudojami elektrochrominio jutiklio konstrukcijai sukurti. Tyrimu buvo siekiama parodyti, kad polisacharidai gali būti naudojami sluoksnio modifikavimui, siekiant pagerinti polimero sluoksnio savybes. Tuo metu literatūroje šios modifikacijos buvo randamos retai.

• 2019 m. pabaigoje Kinijoje kilusios COVID-19 pandemijos pradžioje buvo svarbu atlikti aktualius tyrimus. Siekiant kuo greičiau suvaldyti pandemiją bei reaguojant į vyriausybės politiką, buvo atlikti eksperimentai. Fizinių ir technologijos mokslų centro (FTMC) Nanotechnologijų skyriaus mokslinė komanda buvo viena pirmųjų, kuri paskelbė, kaip panaudoti molekulių įspaudais modifikuoto polimero (MIP) technologiją, kuriant elektrocheminį jutiklį SARS-CoV-2 spyglio (SARS-CoV-2-S) baltymui aptikti.

• Jutiklio konstrukcija, skirta MB atpažinimui, paremta molekulių įspaudais modifikuotu polipirolu, buvo sukurta siekiant užpildyti metileno mėlynojo aptikimo metodų spragą.

Ginamieji teiginiai:

1. Elektrochrominio jutiklio konstrukcijai gaminti gali būti naudojami trys fenotiazino dariniai: metileno mėlynasis, azūras A ir tioninas, kurie gali pagerinti jutiklio savybes.
2. Polimerizacijos mišinyje panaudojami polisacharidai prisideda prie sluoksnio, kuris pritaikomas jutiklio kūrime, teigiamo savybių pokyčio – heparinas yra tinkama medžiaga sluoksnio sukibimui pagerinti.
3. Molekulių įspaudais modifikuoto polipirolo (MIP-Ppy) pagrindu sukurtas sluoksnis gali būti pritaikomas kaip jutiklis, skirtas SARS-CoV-2 spyglio baltymui nustatyti.

4. Integruota Cottrell (Anson tiesė) lygtis gali būti naudojama SARS-CoV-2 spyglio baltymo sąveikai su MIP-Ppy įvertinti.

5. Molekulių įspaudais modifikuotas polipirolas (MIP-Ppy) su metileno mėlynojo įspaudais gali būti sukurtas pasirinkus tinkamas sintezės sąlygas.

LITERATŪROS APŽVALGA

Polipirolas. Polipirolas (Ppy) yra vienas iš laidžių polimerų, plačiai naudojamas jutikliams gaminti [2,3]. Jis taip pat pritaikomas įvairiose srityse: elektronikoje, energijos kaupime ir biomedicinoje [4–7].

Nuo praėjusio amžiaus buvo žinoma, kad elektrochemiškai polimerizuojant pirolą gaunamas ilgai išliekantis sluoksnis, pasižymintis geru laidumu [10]. Ppy elektropolimerizacija paprastai atliekama potenciostatiniais (pastovus potencialas) arba galvanostatiniais (pastovios srovės) metodais [11]. Ppy gali būti sintetinamas elektrocheminiais metodais [12,13], cheminiu [14,15], cheminiu garų nusodinimu [16], fermentiniu [17] ir (arba) mikroorganizmų pagalba [18–20]. Įvairių junginių buvimas polimerizacijos mišinyje gali būti naudojamas polimero sluoksnio savybėms pagerinti.

Elektrochromizmas. Terminas „elektrochromizmas" apibūdina grįžtamąjį spalvos pokytį, kurį kai kurios medžiagos demonstruoja reaguodamos į elektrinio potencialo pokytį. Elektrochromizmas atsiranda tada, kai medžiagoje, dėl elektrocheminės reakcijos, vyksta nuolatiniai, tačiau grįžtami spalvos pokyčiai [38,39]. Paprastai spalvų poslinkis atsiranda tarp dviejų spalvotų būsenų arba tarp skaidrios (arba „balintos") ir spalvotos būsenos [40]. Kai kurie puslaidininkiniai sluoksniai, kurių pagrindą sudaro metalų oksidai ir kai kurios organinės medžiagos, pavyzdžiui, polimerai, pasižymi elektrochrominėmis savybėmis [39]. Daugeliui sistemų, įskaitant įkraunamas baterijas, fotovoltinius elementus, polimerinius šviesos diodus, tranzistorius, išmaniuosius automobilių, pastatų ir šiltnamių langus, elektrochrominius ekranus ir išmaniuosius akinius nuo saulės, yra naudinga naudoti konjuguotus polimerus [17,40,47–50].

Fenotiazino dariniai. Fenotiazinai priklauso seniausiems sintetiniams antipsichoziniams vaistams. Dėl plataus šios klasės organinių molekulių biologinių ir cheminių savybių spektro, jos tapo itin reikšmingos [53]. Fenotiazino dariniai yra biologiškai aktyvūs junginiai [54]. Dėl jų grįžtamojo potencialo jie buvo naudojami kaip elektronų perdavimo tarpininkai tarp fermentų ar mikrobų ir elektrodo [55,65]. Politioninas (PTH) ir monomeras

tioninas pasižymi elektrokataliziniu aktyvumu [66]. Metileno mėlynasis (MB), chlorpromazinas, levomepromazinas, prometazinas, tioridazinas, trifluoperazinas, tioninas ir azūras A yra plačiausiai žinomi fenotiazino dariniai. MB buvo vienas pirmųjų vaistų nuo maliarijos [59]. Tai yra vienas iš pirmųjų organinių dažiklių, vis dar naudojamų ir šiandien, be to – jo potencialas panašus į kelių biomolekulių redokso potencialą [60,61]. Kadangi MB yra katijoninis dažiklis bei naudojamas ir tekstilės pramonėje, tai sukelia tam tikrų aplinkosaugos problemų – dažikliai ypač išskiriami dėl žalingo poveikio aplinkai ir žmonių sveikatai [62–64].

Fenotiazino dariniai dažnai pasižymi žemu oksidacijos potencialu ir stipriu polinkiu formuoti stabilius radikalų katijonus. Elektropolimerizacija yra vienas iš labiausiai paplitusių ir naudingiausių metodų, naudojamų plonoms oligomerų arba polimerinių dažų plėvelėms gauti [66]. Fenotiazino dariniai gali būti naudojami elektrocheminių jutiklių modeliavimui.

Molekulių įspaudais modifikuoti polimerai (MIP). MIP yra polimerai, naudojami selektyviai atpažinti ir prisijungti prie konkrečių tikslinių molekulių, turinčių didelį giminingumą ir specifiškumą. Polimeriniai sluoksniai su molekulių įspaudais veikia kaip dirbtiniai specifinių molekulių receptoriai [93,94].

Ankstesniuose tyrimuose buvo pranešta, kad polimeruose gali būti įspaustos įvairių tipų molekulės – tiek mažos molekulės [14,97–99], tiek didelės molekulinės masės molekulės [100–105].

MIP yra patrauklūs, nes turi geresnį cheminį ir fizinį stabilumą, lyginant su biologiniais receptoriais. Taip pat MIP pasižymi paprastu ir nebrangiu paruošimu, pakartotiniu panaudojimu bei galimybėmis gaminti didelius kiekius [124,127,132].

MIP paruošimas paprastai susideda iš kelių fazių: 1) monomero (-ų) ir tikslinės molekulės, žinomos kaip šablonas, komplekso susidarymas polimerizacijos mišinyje; 2) po to monomerai polimerizuojami; ir 3) šablonas išplaunamas iš šviežiai susintetinto polimero [96,141].

Pirolo pagrindu pagaminti MIP pasižymi savybėmis, tokiomis kaip didelis terminis ir cheminis stabilumas bei molekulinės atpažinimo savybės, tad jie tinkami pritaikyti įvairiose srityse, tokiose kaip biotechnologijos, aplinkos stebėjimas ir farmacija. Ppy literatūroje dažnai minimas polimeras, kuris buvo panaudotas kuriant įvairius jutiklius su MIP, pvz.: galvijų serumo albuminą [151,152], širdies troponiną-I [153], prostatos specifinį antigeną [100] ir širdies troponiną T [154]. Pirolas gali būti polimerizuojamas ant skirtingų elektrodų paviršių ir iš skirtingų terpių.

METODIKA

ITO darbinio elektrodo išankstinis apdorojimas. Prieš elektrocheminį polimero sluoksnio nusodinimą, ITO buvo 3 minutes plaunamas tirpale, sudarytame iš 27% NH_4OH ir 30% H_2O_2, sumaišyto santykiu 3:1, ir pakaitintame iki 50 °C. Vėliau elektrodas buvo plaunamas kambario temperatūros vandenyje, acetone ir vėl vandenyje, po 15 minučių kiekviename tirpale, ultragarso vonelėje.

Pradinis Pt darbinio elektrodo paruošimas. Prieš elektrocheminį Ppy nusodinimą, Pt darbinis elektrodas buvo paruoštas pagal ankstesniuose tyrimuose aprašytą procedūrą [145,160]. Prieš naudojimą visi tirpalai buvo degazuojami azoto (N_2) dujomis. Pt elektrodas buvo 10 minučių plaunamas koncentruotu HNO_3 tirpalu ultragarso vonioje, po to nuplaunamas vandeniu, o tada poliruojamas aliuminio oksido pasta. Vėliau dar kartą skalaujamas vandeniu ir 10 M NaOH tirpalu, o tuomet – 5 M H_2SO_4 tirpalu ultragarso vonioje 5 minutes. Elektrocheminis elektrodo valymas buvo atliekamas 0,5 M H_2SO_4, 20 kartų skleidžiant intervale nuo –0,1 V iki +1,2 V Ag/AgCl elektrodo atžvilgiu, esant 100 mV/s potencialo skleidimo greičiui. Siekiant pagerinti Ppy sluoksnio sukibimą su elektrodo paviršiumi, ant darbinio elektrodo buvo nusodinamas platinos juodžių sluoksnis [160]. Pt juodžių nusodinimas buvo atliktas 5 mM H_2PtCl_6 su 0,1 M KCl tirpale, 10 potencialų ciklų intervale nuo +0,5 V iki –0,4 V Ag/AgCl elektrodo atžvilgiu, esant 10 mV/s potencialo skleidimo greičiui.

Elektrocheminis Ppy sluoksnių nusodinimas ant ITO. Priklausomai nuo eksperimento reikalavimų, polimero sluoksniai ant ITO buvo nusodinami ciklinės voltamperometrijos metodu tokiomis sąlygomis:
a) Potencialų diapazonas buvo nuo –0,2 V iki +1 V Ag/AgCl elektrodo atžvilgiu, esant 50 mV/s potencialo skleidimo greičiui, 25 ciklai su 2,44 mV žingsniu. Polimerizacijos tirpalas buvo paruoštas vandenyje su 10 mM atitinkamo fenotiazino darinio (metileno mėlynojo, azūro A arba tionino acetato) ir 50 mM pirolo. Gauti polimero sluoksniai žymimi atitinkamai Ppy-PMB, Ppy-PAA ir Ppy-PTH.
b) Potencialų diapazonas buvo nuo –0,5 V iki +1,2 V Ag/AgCl elektrodo atžvilgiu, esant 50 mV/s potencialo skleidimo greičiui, 25 ciklai su 2,44 mV žingsniu. Elektrocheminis nusodinimas buvo atliktas iš tirpalo, kuriame yra 50 mM pirolo, 10 mM MB ir vienos iš priedo medžiagų: 0,1 M laktozės (Lac), 0,1 M sacharozės (Suc) arba 0,01 g/l heparino (Hep).

Gauti polimero sluoksniai žymimi atitinkamai (Ppy-PMB)$_{Lac}$, (Ppy-PMB)$_{Suc}$ ir (Ppy-PMB)$_{Hep}$.

MIP ir NIP sluoksnių elektrocheminis nusodinimas ant Pt elektrodo.
Polimerizacijos tirpalas, kuriame buvo 0,5 M pirolo (PBS buferyje) su 0,1 M KCl ir pH 7,4, buvo elektrochemiškai naudojamas neįspaustam Ppy (NIP-Ppy) sluoksniui nusodinti. Polimerizacijos tirpalas, kuriame buvo 0,5 M pirolo ir 50 µg/ml SARS-CoV-2-S glikoproteino tame pačiame PBS su 0,1 M KCl, pH 7,4, buvo naudojamas molekulių įspaudais modifikuoto Ppy (MIP-Ppy) sluoksniui nusodinti. Polimeriniai sluoksniai buvo nusodinami naudojant 20 potencialo impulsų +0,95 V Ag/AgCl palyginamojo elektrodo atžvilgiu, 1 s su 0 V Ag/AgCl palyginamojo elektrodo atžvilgiu, 10 s tarp impulsų. Po to MIP-Ppy arba NIP-Ppy modifikuoti elektrodai buvo panardinti į 0,05 M H$_2$SO$_4$ tirpalą 10 minučių, siekiant išplauti šablono molekules.

MIP ir NIP sluoksnių elektrocheminis nusodinimas ant ITO elektrodo.
Polimerų sluoksniai buvo nusodinami skleidžiant potencialą nuo –0,4 V iki +1 V Ag/AgCl palyginamojo elektrodo atžvilgiu, esant 50 mV/s potencialo skleidimo greičiui, su 2,44 mV žingsniu. Polimerų sluoksnių nusodinimui buvo keičiamas potencialo skleidimo ciklų skaičius: 25, 20, 15, 10, 7, 5 ir 3. MIP atveju polimerizacijos tirpale buvo 10 mM MB, 50 mM pirolo ir 5 µg/mL heparino. NIP atveju: 50 mM pirolo ir 5 µg/mL heparino. MB buvo išplaunamas 0,1 M H$_2$SO$_4$ tirpalu, 5 minutes.

REZULTATŲ APTARIMAS

Trijų skirtingų fenotiazino darinių taikymas modifikuojant Ppy sluoksnio savybes. Pirmajame straipsnyje buvo analizuotas Ppy sluoksnio savybių modifikavimas, atliktas su trimis fenotiazino dariniais: metileno mėlynuoju, azūru A ir tioninu. Šie dariniai pasirinkti todėl, nes yra panašios struktūros, pasižymi geru elektriniu aktyvumu ir yra tirpūs vandenyje. 5 paveiksle parodytos ciklinės voltamperogramos, kurios gautos, kai Ppy ir fenotiazino darinys elektrochemiškai polimerizuojamas ant ITO. Iki 15-ojo potencialo ciklo didėja ir katodinė, ir anodinė srovė, o vėliau buvo pastebėtas voltamperogramos kilpos pločio sumažėjimas. Kai kuriuose ankstesniuose tyrimuose šis voltamperogramos pločio sumažėjimas susiejamas su Ppy sluoksnio elektrocheminiu irimu [163, 164].

Sluoksnių morfologija analizuota atominės jėgos mikroskopijos (AFM) ir skenuojančios elektroninės mikroskopijos (SEM) metodais. Vertinant SEM analizę (6 pav.), Ppy-PAA sluoksnis, kuris buvo pasiskirstęs netolygiausiai,

pasižymėjo paviršiumi su didelėmis polimerų aglomeracijomis. Ppy-PMB sluoksnio paviršius, kuriame matomos klostuotos struktūros ir raukšlės, buvo gana lygus (6B pav.). Ppy-PTH sluoksnio paviršius parodytas 6C paveiksle. Šiame sluoksnyje matomos struktūros buvo gana tolygiai pasiskirsčiusios, bet įžvelgiami grūdeliai, apvalios formos raukšlės ir vietomis besiformuojančios didesnės sankaupos. Klostuotos struktūros ir raukšlės galėjo susiformuoti polimerinio sluoksnio džiūvimo metu. AFM gauta informacija taip pat patvirtino SEM rezultatus.

Kitame tyrimų etape buvo išmatuota optinės absorbcijos priklausomybė nuo tirpalo pH vertės. Nustatyta, kad tirpalui tampant baziškesniu, optinė absorbcija mažėja ir palaipsniui blogėja. Ppy-PT pagrindu pagaminto sluoksnio elektrochrominės charakteristikos buvo fiksuojamos iki pH 6,5.

Toliau išmatuoti chronoamperometriniai signalai esant skirtingoms pH vertėms ir askorbo rūgšties koncentracijai (kas 1 mM padidėjimas, nuo 0 mM iki 5 mM). Ryšys tarp optinės absorbcijos (ΔA) ($\Delta A = A_{+0,3V} - A_{-0,9V}$) ir askorbo rūgšties koncentracijos BR buferyje, kai pH 3,0, pH 4,0 ir pH 5,0, svyravimų parodytas 8 paveiksle. Remiantis kalibravimo kreivėmis daroma išvada, kad Ppy-PMB ir Ppy-PTH gali būti naudojami kaip elektrochrominiai jutikliai askorbo rūgšties (vitamino C) koncentracijai matuoti.

Trijų skirtingų polisacharidų taikymas polipirolo-metileno mėlynojo sluoksnio savybėms modifikuoti. Apgalvotas legiruojančių priedų pasirinkimas gali pagerinti Ppy laidumą [165,166]. Antrame straipsnyje buvo siekiama Ppy-PMB sluoksnį legiruoti trimis sacharidais (laktoze, sacharoze ir heparinu) bei palyginti jų poveikį elektrochrominėms savybėms. Vertinant AFM duomenis buvo matoma, jog visų sluoksnių paviršiuje raukšlių ir klosčių yra nuo mažesnių ((Ppy-PMB)$_{Lac}$) iki didesnių ((Ppy-PMB)$_{Hep}$). 9E paveiksle parodytas paviršiaus aukščio pasiskirstymas patvirtina, kad visų Ppy-PMB sluoksnių dominuojantis konstrukcijų aukštis yra apie 2,5 μm. Sluoksnio savybės buvo analizuojamos atsižvelgiant į absorbcijos pokyčius, keičiant tirpalo pH (10 pav.). Pastebėta, jog Ppy-PMB sluoksniai su heparinu kaip priedu yra mechaniškai stabilesni nei sluoksniai, kurių priedai yra laktozė ir sacharozė.

Norint sukurti elektrochrominius jutiklius trijų ksantino darinių – kofeino, teobromino ir teofilino – aptikimui, tolesniam eksperimentui buvo pasirinktas heparinu legiruotas Ppy-PMB sluoksnis. Įrodyta, kad visų trijų tirtų ksantino darinių ΔA ($\Delta A = A_{+0.8V} - A_{-0.8V}$) priklausomybė nuo koncentracijos yra tiesinė (11 pav.). Teofilino nustatymas atskleidė didžiausią optinės sugerties pokytį. Teofilino tiesinės regresijos nuolydis (esant $\lambda = 668$ nm) buvo –0,002,

o R^2 – 0,977, o tai yra du kartus didesnis nei kofeino atveju. Šis tyrimas rodė, kad Ppy-PMB gali būti naudojamas kuriant elektrochrominius jutiklius.

Polipirolo savybių modifikavimas, siekiant jį panaudoti kaip MIP. Trečiasis ir ketvirtasis straipsniai buvo skirti sukurti MIP pagrįstą jutiklį SARS-CoV-2-S glikoproteinui nustatyti. Sunkaus ūminio kvėpavimo sindromo koronaviruso-2 (SARS-CoV-2) sukelta COVID-19 pandemija, prasidėjusi 2019 m., sukėlė drastiškus pokyčius. Viso pasaulio šalys buvo paveiktos karantino, ekonominių problemų, pablogėjo žmonių emocinė sveikata. Nors vakcinos tapo prieinamos visuomenei, ši virusinė infekcija išliko itin aktyvi, mutavo, todėl vis dar yra reikalingas gilesnis SARS-CoV-2 viruso supratimas ir greitesni analizės metodai, tinkami COVID-19 diagnostikai ir (arba) viruso bei jo dalių aptikimui.

Šiuo tikslu ant darbinio platinos elektrodo buvo nusodinti Ppy sluoksniai iš polimerizacijos mišinio, kuriame buvo SARS-CoV-2-S glikoproteino ir pirolo, ištirpinto fosfatiniame buferiniame tirpale (PBS), kai pH 7,4. Ištirtas elektrodo su MIP-Ppy sluoksniu (įspaustas SARS-CoV-2-S glikoproteinu) veikimas ir palygintas su neįspaustu elektrodu (12 pav.). Polimerų sluoksnių nusodinimas atliktas pulsinės amperometrijos metodu. Pagaminti MIP-Ppy ir NIP-Ppy sluoksniai taip pat buvo įvertinti naudojant pulsinės amperometrijos metodą, naudojant 10 potencialių impulsų: +0,6 V ir 0 V po 2 s. SARS-CoV-2-S glikoproteino koncentracija buvo nuo 0 µg/mL iki 25 µg/mL (14, 15 pav.). Taikant tiesinės regresijos lygtį, buvo nustatytos tiesinės regresijos lygties nuolydžio vertės. MIP-Ppy modifikuotų Pt elektrodų, inkubuotų BSA turinčiame tirpale, nuolydžio vertė buvo žymiai mažesnė (–0,15 µA/(µg/mL)).

Ketvirtojo straipsnio naujovė buvo pagrįsta elektros krūvio Q kitimo kreivių taikymu elektrodo ir analitės sąveikai įvertinti. Pagrindinė šio darbo idėja buvo pagrįsta integruotos Cottrell (Anson tiesės) lygties taikymu, siekiant pateikti įžvalgų apie SARS-CoV-2 glikoproteinų ir molekuliniu būdu įspausto Ppy sąveiką.

Krūvio Q ir laiko santykis Ppy pagrindu veikiančiuose elektrocheminiuose jutikliuose paklūsta integruotai Cottrell lygčiai (3) [173,174]:

$$Q = 2nFAC\sqrt{\frac{D}{\pi}}\sqrt{t} + Q_{d.l.} + Q_{ads.} = k\sqrt{t} + Q_{d.l.} + Q_{ads.} \quad (3)$$

Supaprastintą analitės reakciją prie elektrodo galima apibūdinti keliais etapais: analitės difuzija iš tirpalo į elektrodą, elektrocheminė oksidacijos-redukcijos reakcija ir tada reakcijos produktų difuzija iš elektrodo į tirpalą.

Anson tiesės lygties koeficientų analizė gali būti naudojama analičių arba reakcijos produktų adsorbcijai elektrode nustatyti.

Chronoamperogramų duomenys rodomi Anson tiesei (16A, D pav.). Susijusių tiesės lygčių koeficientai pateikti 5-oje lentelėje. MIP-Ppy modifikuotas elektrodas turi stipresnę tiesės lygties nuolydžio vertės priklausomybę nuo analitės koncentracijos (16B pav.) nei NIP-Ppy modifikuotas elektrodas (16E pav.). Tai rodo, kad analitė sąveikauja su NIP-Ppy mažiau palankiai nei MIP-Ppy.

Polipirolo modifikacija naudojant metileno mėlynąjį kaip įspaudo šabloną. Penktuoju straipsniu buvo siekiama pritaikyti molekulinių polimerinių įspaudų technologiją metileno mėlynojo nustatymui. 17A paveiksle parodyta tyrimo sekos schema. Pirolas, kartu su metileno mėlynuoju, buvo nusodinamas ant ITO elektrodo. Polimerizacijos metu taikyti 3, 5, 7, 10, 15, 20 arba 25 potencialų ciklai elektrocheminiam nusodinimui. Buvo išbandyti keli potencialų diapazonai, įskaitant nuo –0,4 V iki +1 V (1), –0,5 V iki +1,2 V (2), –0,4 V iki +0,8 V (3) ir –0,4 V iki +0,6 V (4), siekiant, kad būtų nustatomos geriausios sintezės sąlygos MB įspaudimui ant Ppy sluoksnio (Ppy-MB). Tolimesniems tyrimams pasirinktas diapazonas nuo –0,4 V iki +1 V.

Optinė absorbcija (A) BR buferiniame tirpale (pH 3) buvo nustatyta iškart po nusodinimo. Elektrodas, modifikuotas MIP-Ppy sluoksniu su MB įspaudais, buvo tiriamas dėl jo veikimo ir stabilumo (t.y. jo gebėjimo mechaniškai likti ant elektrodo paviršiaus ir eksperimentų, kuriuose naudojamas tas pats sluoksnis, atkuriamumą). Eksperimento metu buvo vertinamos toliau išvardytos laikymo aplinkybės: BR buferyje, ore, vandenyje ir rūgštinėje terpėje. Gauti šio ir ankstesnių tyrimų rezultatai įrodė, kad Ppy laikyti ore yra tinkamiau. Kitos šio tyrimo dalies tikslas buvo sluoksnio eksploatacinių savybių ir plovimo bei nustatymo procesų įtakos polimero sluoksnio savybėms analizė. Ppy-MB-5, Ppy-MB-7 ir Ppy-MB-10 sluoksniai buvo plaunami vandenyje. Remiantis ankstesnių šio tyrimo etapų analize, sluoksnis, kuris buvo nusodintas naudojant 7 ciklus, yra bene patikimiausias ir efektyviausias.

Pagaminti MIP-Ppy ir NIP-Ppy sluoksniai buvo įvertinti tolesniame tyrime, stebint optinės absorbcijos pokyčius. MB koncentracijų diapazonas buvo nuo 0,1 µM iki 10 mM (21 pav.). Paveiksle demonstruojamos kalibracinės kreivės, rodančios kaip MB arba azūro A buvimas pakeičia absorbciją (A) MIP-Ppy ir NIP-Ppy sluoksniuose. Paveiksle matoma, kad koncentracijos diapazone nuo 0,1 µM iki 10 mM matomas tiesiškumas. Kai MB sąveika lyginama su MIP-Ppy arba NIP-Ppy, tariamas įspaudimo

koeficientas yra maždaug 2,15. Atsižvelgiant į pirmiau minėtus pastebėjimus, daroma išvada, kad aukščiau aprašyti metodai gali būti naudojami kuriant įspaustus Ppy jutiklius, gebančius aptikti MB.

IŠVADOS

Polipirolo sluoksniai buvo modifikuoti fenotiazino dariniais arba molekuliniais įspaudais. Gauti rezultatai rodo, kad iš trijų fenotiazino darinių – metileno mėlynojo, azūro A ir tionino – metileno mėlynasis yra perspektyviausias siekiant sukurti efektyvų elektrochrominį jutiklį.

Gauti tyrimo rezultatai taip pat parodė teigiamą polisacharidų, ypač heparino, poveikį polimerizacijos mišinyje, prisidedantį prie geresnio sluoksnio sukibimo.

Be to, tyrimo rezultatai parodė polimerizuoto sluoksnio storio svarbą bei tiesioginę koreliaciją su padidintu sukibimu ir bendru patvarumu.

Sukurtas MIP-Ppy sluoksnis turėjo potencialą kaip jutiklis, nustatant SARS-CoV-2-S glikoproteiną, parodydamas savo universalumą praktikoje.

Integruotos Cottrell (Anson tiesė) lygties koeficientų analizė pasirodė kaip vertingas įrankis įvertinti analičių arba reakcijos produktų adsorbcijai elektrode.

Tyrime taip pat pademonstruota galimybė sukurti MIP-Ppy, naudojant metileno mėlynąjį kaip šabloną, kur metileno mėlynasis ne visiškai polimerizuojasi ir yra efektyviai įspaustas. Tai rodo naujovišką požiūrį į jutiklių dizainą.

ACKNOWLEDGMENTS

I would like to express my gratitude to everyone who contributed to the development of the dissertation, as well as to anyone whoever provided support and motivation to me. Please accept my most sincere *Thank you* everyone who has collaborated on the scientific experiments and research. My sincere appreciation goes out to my adviser, Dr. Vilma Ratautaitė, for her wise counsel, support, and patience during the process. I am also grateful to my family and friends, who have been a source of encouragement and inspiration.

CURRICULUM VITAE

PERSONAL INFORMATION

Name, Surname	Raimonda Bogužaitė
E-mail	raimonda.boguzaite@ftmc.lt

ACADEMIC EDUCATION

2013–2017	Vilnius University, Chemistry BSc Bachelor's Degree in Specialist Teacher Training, qualification of Teacher.
2017–2019	Vilnius University, Physical Sciences MSc

PROFESSIONAL EXPERIENCE

2016	Trainee, University of Iceland, Department of Chemistry
2019–2021	Engineer, Center for Physical Sciences and Technology, Department of Functional Materials and Electronics, Laboratory of Nanotechnology, Vilnius, Lithuania
2021–present	Junior Researcher, Center for Physical Sciences and Technology, Department of Nanotechnology, Laboratory of Bioanalysis, Vilnius, Lithuania

REFERENCES

1. Ltd., P.R.P. Biosensors Market Available online: https://www.precedenceresearch.com/biosensors-market.

2. Ramanavičius, A.; Ramanavičiene, A.; Malinauskas, A. Electrochemical Sensors Based on Conducting Polymer-Polypyrrole. *Electrochim. Acta* **2006**, *51*, 6025–6037, doi:10.1016/j.electacta.2005.11.052.

3. Dzulkurnain, N.A.; Mokhtar, M.; Rashid, J.I.A.; Knight, V.F.; Wan Yunus, W.M.Z.; Ong, K.K.; Mohd Kasim, N.A.; Mohd Noor, S.A. A Review on Impedimetric and Voltammetric Analysis Based on Polypyrrole Conducting Polymers for Electrochemical Sensing Applications. *Polymers (Basel).* **2021**, *13*, 2728, doi:10.3390/polym13162728.

4. Cui, S.; Mao, J.; Rouabhia, M.; Elkoun, S.; Zhang, Z. A Biocompatible Polypyrrole Membrane for Biomedical Applications. *RSC Adv.* **2021**, *11*, 16996–17006, doi:10.1039/d1ra01338f.

5. Ezika, A.C.; Sadiku, E.R.; Ray, S.S.; Hamam, Y.; Folorunso, O.; Adekoya, G.J. Emerging Advancements in Polypyrrole MXene Hybrid Nanoarchitectonics for Capacitive Energy Storage Applications. *J. Inorg. Organomet. Polym. Mater.* **2022**, *32*, 1521–1540, doi:10.1007/s10904-022-02280-6.

6. Ansar, M.T.; Ali, A.; Mustafa, G.M.; Afzal, F.; Ishaq, S.; Kanwal, F.; Naseem, S.; Atiq, S. Polypyrrole-Based Nanocomposites Architecture as Multifunctional Material for Futuristic Energy Storage Applications. *J. Alloys Compd.* **2021**, *855*, 157341, doi:10.1016/j.jallcom.2020.157341.

7. Yoon, H.; Jang, J. Conducting-Polymer Nanomaterials for High-Performance Sensor Applications: Issues and Challenges. *Adv. Funct. Mater.* **2009**, *19*, 1567–1576, doi:10.1002/adfm.200801141.

8. Philkhana, S.C.; Badmus, F.O.; Dos Reis, I.C.; Kartika, R. Recent Advancements in Pyrrole Synthesis. *Synth.* **2021**, *53*, 1531–1555, doi:10.1055/s-0040-1706713.

9. Gholap, S.S. Pyrrole: An Emerging Scaffold for Construction of Valuable Therapeutic Agents. *Eur. J. Med. Chem.* **2016**, *110*, 13–31, doi:10.1016/j.ejmech.2015.12.017.

10. Diaz, A.F.; Kanazawa, K.K.; Gardini, G.P. Electrochemical Polymerization of Pyrrole. *J. Chem. Soc. Chem. Commun.* **1979**, 635–636, doi:10.1039/C39790000635.

11. Sabouraud, G.; Sadki, S.; Brodie, N. The Mechanisms of Pyrrole Electropolymerization. *Chem. Soc. Rev.* **2000**, *29*, 283–293, doi:10.1039/a807124a.

12. Plausinaitis, D.; Ratautaite, V.; Mikoliunaite, L.; Sinkevicius, L.; Ramanaviciene, A.; Ramanavicius, A. Quartz Crystal Microbalance-Based Evaluation of the Electrochemical Formation of an Aggregated

Polypyrrole Particle-Based Layer. *Langmuir* **2015**, *31*, 3186–3193, doi:10.1021/la504340u.

13. Plausinaitis, D.; Sinkevicius, L.; Samukaite-bubniene, U.; Ratautaite, V. Evaluation of Electrochemical Quartz Crystal Microbalance Based Sensor Modified by Uric Acid-Imprinted Polypyrrole. *Talanta* **2020**, *220*, 121414, doi:10.1016/j.talanta.2020.121414.

14. Ratautaite, V.; Nesladek, M.; Ramanaviciene, A.; Baleviciute, I.; Ramanavicius, A. Evaluation of Histamine Imprinted Polypyrrole Deposited on Boron Doped Nanocrystalline Diamond. *Electroanalysis* **2014**, *26*, 2458–2464, doi:https://doi.org/10.1002/elan.201400294.

15. Leonavicius, K.; Ramanaviciene, A.; Ramanavicius, A. Polymerization Model for Hydrogen Peroxide Initiated Synthesis of Polypyrrole Nanoparticles. *Langmuir* **2011**, *27*, 10970–10976, doi:10.1021/la201962a.

16. Kim, Y.K.; Shin, K.Y. Dopamine-Assisted Chemical Vapour Deposition of Polypyrrole on Graphene for Flexible Supercapacitor. *Appl. Surf. Sci.* **2021**, *547*, 149141, doi:10.1016/j.apsusc.2021.149141.

17. German, N.; Ramanaviciene, A.; Ramanavicius, A. Formation of Polyaniline and Polypyrrole Nanocomposites with Embedded Glucose Oxidase and Gold Nanoparticles. *Polymers (Basel).* **2019**, *11*, 19–24, doi:10.3390/POLYM11020377.

18. Apetrei, R.M.; Carac, G.; Ramanaviciene, A.; Bahrim, G.; Tanase, C.; Ramanavicius, A. Cell-Assisted Synthesis of Conducting Polymer – Polypyrrole – for the Improvement of Electric Charge Transfer through Fungal Cell Wall. *Colloids Surfaces B Biointerfaces* **2019**, *175*, 671–679, doi:10.1016/j.colsurfb.2018.12.024.

19. Ramanavicius, A.; Andriukonis, E.; Stirke, A.; Mikoliunaite, L.; Balevicius, Z.; Ramanaviciene, A. Synthesis of Polypyrrole within the Cell Wall of Yeast by Redox-Cycling of [Fe(CN)6]3-/[Fe(CN)6]4-. *Enzyme Microb. Technol.* **2016**, *83*, 40–47, doi:10.1016/j.enzmictec.2015.11.009.

20. Andriukonis, E.; Reinikovaite, V.; Ramanavicius, A. Comparative Study of Polydopamine and Polypyrrole Modified Yeast Cells Applied in Biofuel Cell Design. *Sustain. Energy Fuels* **2022**, *6*, 4209–4217, doi:10.1039/d2se00634k.

21. Arjomandi, J.; Raoufi, D.; Ghamari, F. Surface Characterization and Morphology of Conducting Polypyrrole Thin Films during Polymer Growth on ITO Glass Electrode. *J. Phys. Chem. C* **2016**, *120*, 18055–18065, doi:10.1021/acs.jpcc.6b04913.

22. Ratautaite, V.; Bagdziunas, G.; Ramanavicius, A.; Ramanaviciene, A. An Application of Conducting Polymer Polypyrrole for the Design of Electrochromic PH and CO 2 Sensors . *J. Electrochem. Soc.* **2019**, *166*, B297–B303, doi:10.1149/2.1221904jes.

23. Liustrovaite, V.; Pogorielov, M.; Boguzaite, R.; Ratautaite, V.; Ramanaviciene, A.; Pilvenyte, G.; Holubnycha, V.; Korniienko, V.;

Diedkova, K.; Viter, R.; et al. Towards Electrochemical Sensor Based on Molecularly Imprinted Polypyrrole for the Detection of Bacteria—Listeria Monocytogenes. *Polymers (Basel).* **2023**, *15*, doi:10.3390/polym15071597.

24. Gonçalves, M. de L.; Truta, L.A.N.; Sales, M.G.F.; Moreira, F.T.C. Electrochemical Point-of Care (PoC) Determination of Interleukin-6 (IL-6) Using a Pyrrole (Py) Molecularly Imprinted Polymer (MIP) on a Carbon-Screen Printed Electrode (C-SPE). *Anal. Lett.* **2021**, *54*, 2611–2623, doi:10.1080/00032719.2021.1879108.

25. Geană, E.I.; Artem, V.; Apetrei, C. Discrimination and Classification of Wines Based on Polypyrrole Modified Screen-Printed Carbon Electrodes Coupled with Multivariate Data Analysis. *J. Food Compos. Anal.* **2021**, *96*, 103704, doi:10.1016/j.jfca.2020.103704.

26. Lu, J.J.; Ma, J.Q.; Yi, J.M.; Shen, Z.L.; Zhong, Y.J.; Ma, C.A.; Li, M.C. Electrochemical Polymerization of Pyrrole Containing TEMPO Side Chain on Pt Electrode and Its Electrochemical Activity. *Electrochim. Acta* **2014**, *130*, 412–417, doi:10.1016/j.electacta.2014.03.028.

27. Yalçinkaya, S.; Demetgül, C.; Timur, M.; Çolak, N. Electrochemical Synthesis and Characterization of Polypyrrole/Chitosan Composite on Platinum Electrode: Its Electrochemical and Thermal Behaviors. *Carbohydr. Polym.* **2010**, *79*, 908–913, doi:10.1016/j.carbpol.2009.10.022.

28. Hamami, M.; Bouaziz, M.; Raouafi, N.; Bendounan, A.; Korri-Youssoufi, H. Mos2/Ppy Nanocomposite as a Transducer for Electrochemical Aptasensor of Ampicillin in River Water. *Biosensors* **2021**, *11*, doi:10.3390/bios11090311.

29. Kim, S.; Jang, L.K.; Park, H.S.; Lee, J.Y. Electrochemical Deposition of Conductive and Adhesive Polypyrrole-Dopamine Films. *Sci. Rep.* **2016**, *6*, 1–8, doi:10.1038/srep30475.

30. Ratautaite, V.; Topkaya, S.N.; Mikoliunaite, L.; Ozsoz, M.; Oztekin, Y.; Ramanaviciene, A.; Ramanavicius, A. Molecularly Imprinted Polypyrrole for DNA Determination. *Electroanalysis* **2013**, *25*, 1169–1177, doi:10.1002/elan.201300063.

31. Yang, Y.; Deng, Y.; Xu, S.; Liu, Y.; Liang, W.; Zhang, K.; Lv, S.; Sha, L.; Yin, H.; Wu, Y.; et al. PPy/SWCNTs-Modified Microelectrode Array for Learning and Memory Model Construction through Electrical Stimulation and Detection of In Vitro Hippocampal Neuronal Network. *ACS Appl. Bio Mater.* **2023**, *6*, 3414–3422, doi:10.1021/acsabm.3c00105.

32. Aqrawe, Z.; Montgomery, J.; Travas-Sejdic, J.; Svirskis, D. Conducting Polymers for Neuronal Microelectrode Array Recording and Stimulation. *Sensors Actuators, B Chem.* **2018**, *257*, 753–765, doi:10.1016/j.snb.2017.11.023.

33. Han, Y.; Sun, L.; Wen, C.; Wang, Z.; Dai, J.; Shi, L. Flexible

Conductive Silk-PPy Hydrogel toward Wearable Electronic Strain Sensors. *Biomed. Mater.* **2022**, *17*, 24107, doi:10.1088/1748-605X/ac5416.

34. Chen, J.; Liu, J.; Thundat, T.; Zeng, H. Polypyrrole-Doped Conductive Supramolecular Elastomer with Stretchability, Rapid Self-Healing, and Adhesive Property for Flexible Electronic Sensors. *ACS Appl. Mater. Interfaces* **2019**, *11*, 18720–18729, doi:10.1021/acsami.9b03346.

35. Qi, Z.; Ye, J.; Chen, W.; Biener, J.; Duoss, E.B.; Spadaccini, C.M.; Worsley, M.A.; Zhu, C. 3D-Printed, Superelastic Polypyrrole–Graphene Electrodes with Ultrahigh Areal Capacitance for Electrochemical Energy Storage. *Adv. Mater. Technol.* **2018**, *3*, 1–8, doi:10.1002/admt.201800053.

36. Vijayavenkataraman, S.; Kannan, S.; Cao, T.; Fuh, J.Y.H.; Sriram, G.; Lu, W.F. 3D-Printed PCL/PPy Conductive Scaffolds as Three-Dimensional Porous Nerve Guide Conduits (NGCs) for Peripheral Nerve Injury Repair. *Front. Bioeng. Biotechnol.* **2019**, *7*, 1–14, doi:10.3389/fbioe.2019.00266.

37. Ajdary, R.; Ezazi, N.Z.; Correia, A.; Kemell, M.; Huan, S.; Ruskoaho, H.J.; Hirvonen, J.; Santos, H.A.; Rojas, O.J. Multifunctional 3D-Printed Patches for Long-Term Drug Release Therapies after Myocardial Infarction. *Adv. Funct. Mater.* **2020**, *30*, 1–10, doi:10.1002/adfm.202003440.

38. Prakash R. Somani, S.R. Electrochromic Materials and Devices: Present and Future. *Mater. Chem. Phys.* **2002**, *77*, 117–133, doi:10.1002/9783527679850.

39. Argun, A.A.; Aubert, P.H.; Thompson, B.C.; Schwendeman, I.; Gaupp, C.L.; Hwang, J.; Pinto, N.J.; Tanner, D.B.; MacDiarmid, A.G.; Reynolds, J.R. Multicolored Electrochromism in Polymers: Structures and Devices. *Chem. Mater.* **2004**, *16*, 4401–4412, doi:10.1021/cm049669l.

40. Celiesiute, R.; Ramanaviciene, A.; Gicevicius, M.; Ramanavicius, A. Electrochromic Sensors Based on Conducting Polymers, Metal Oxides, and Coordination Complexes. *Crit. Rev. Anal. Chem.* **2019**, *49*, 195–208, doi:10.1080/10408347.2018.1499009.

41. Popov, A.; Brasiunas, B.; Damaskaite, A.; Plikusiene, I.; Ramanavicius, A.; Ramanaviciene, A. Electrodeposited Gold Nanostructures for the Enhancement of Electrochromic Properties of Pani–Pedot Film Deposited on Transparent Electrode. *Polymers (Basel).* **2020**, *12*, 1–14, doi:10.3390/polym12122778.

42. Deshmukh, M.A.; Gicevicius, M.; Ramanaviciene, A.; Shirsat, M.D.; Viter, R.; Ramanavicius, A. Hybrid Electrochemical/Electrochromic Cu(II) Ion Sensor Prototype Based on PANI/ITO-Electrode. *Sensors Actuators, B Chem.* **2017**, *248*, 527–535, doi:10.1016/j.snb.2017.03.167.

43. Hyodo, K. Electrochromism of Conducting Polymers. *Electrochim. Acta* **1994**, *39*, 265–272, doi:10.1016/0013-4686(94)80062-6.

44. Chu, T.; Ju, X.; Han, X.; Du, H.; Zhang, Y.; Zhao, J.; Zhang, J. Synthesis and Electrochromic Properties of Cross-Linked and Soluble Conjugated Polymers Based on 5, 8, 14, 17-Tetrabromoquinoxaline[2′, 3':9,10]Phenanthro[4,5-Abc]Phenazine as the Multifunctionalized Acceptor Unit. *Org. Electron.* **2019**, *73*, 43–54, doi:10.1016/j.orgel.2019.06.004.

45. In, Y.R.; Han, J.M.; Kwon, J.E.; Kim, B.G.; Moon, H.C. Rational Molecular Design of Electrochromic Conjugated Polymers: Toward High-Performance Systems with Ultrahigh Coloration Efficiency. *Chem. Eng. J.* **2022**, *433*, 133808, doi:10.1016/j.cej.2021.133808.

46. Yue, H.; Kong, L.; Wang, B.; Yuan, Q.; Zhang, Y.; Du, H.; Dong, Y.; Zhao, J. Synthesis and Characterization of Novel D-A Type Neutral Blue Electrochromic Polymers Containing. *Polymers (Basel).* **2019**, *11*, doi:10.3390/polym11122023.

47. Ramanavicius, S.; Jagminas, A.; Ramanavicius, A. Advances in Molecularly Imprinted Polymers Based Affinity Sensors (Review). *Polymers (Basel).* **2021**, *13*, doi:10.3390/polym13060974.

48. Sadasivuni, K.K.; Hegazy, S.M.; Abdullah Aly, Aa.A.M.; Waseem, S.; Karthik, K. *Polymers in Electronics*; INC, 2020; ISBN 9780128168080.

49. Jinno, H.; Yokota, T.; Koizumi, M.; Yukita, W.; Saito, M.; Osaka, I.; Fukuda, K.; Someya, T. Self-Powered Ultraflexible Photonic Skin for Continuous Bio-Signal Detection via Air-Operation-Stable Polymer Light-Emitting Diodes. *Nat. Commun.* **2021**, *12*, 4–12, doi:10.1038/s41467-021-22558-6.

50. Bagdžiūnas, G.; Palinauskas, D.; Ramanavičius, A. Towards Colourless-to-green Electrochromic Smart Glass Based on a Redox Active Polymeric Semiconductor Containing Carbazole Moiety. *Dye. Pigment.* **2020**, *177*, doi:10.1016/j.dyepig.2020.108328.

51. Gicevicius, M.; Kucinski, J.; Ramanaviciene, A.; Ramanavicius, A. Tuning the Optical PH Sensing Properties of Polyaniline-Based Layer by Electrochemical Copolymerization of Aniline with o-Phenylenediamine. *Dye. Pigment.* **2019**, *170*, 107457, doi:10.1016/j.dyepig.2019.04.002.

52. Okafor, C. 0. The Chemistry and Applications of Angular Phenothiazine Derivatives. *Dye. Pigment.* **1986**, *7*, 249–287.

53. Pluta, K.; Morak-Młodawska, B.; Jeleń, M. Recent Progress in Biological Activities of Synthesized Phenothiazines. *Eur. J. Med. Chem.* **2011**, *46*, 3179–3189, doi:10.1016/j.ejmech.2011.05.013.

54. Froimowitz, M.; Cody, V. Biologically Active Conformers of Phenothiazines and Thioxanthenes. Further Evidence for a Ligand Model of Dopamine D2 Receptor Antagonists. *J. Med. Chem.* **1993**, *36*, 2219–2227, doi:10.1021/jm00067a019.

55. J. M. Godwin, R.W.E.; Department Polypyrrole/Poly(Methylene Blue) Composite Electrode Films on Stainless Steel. *Angew. Chemie Int. Ed. 6(11), 951–952.* **2011**, *33*, 181–188, doi:10.1149/1.3565513.

56. Varga, B.; Csonka, Á.; Csonka, A.; Molnár, J.; Amaral, L.; Spengler, G. Possible Biological and Clinical Applications of Phenothiazines. *Anticancer Res.* **2017**, *37*, 5983–5993, doi:10.21873/anticanres.12045.

57. Korth, C.; May, B.C.H.; Cohen, F.E.; Prusiner, S.B.; Korth, C.; Mayt, B.C.H.; Cohen, F.E.; Prusiner, B. Acridine and Phenothiazine Derivatives as Pharmacotherapeutics for Pri on Disease. *Proc. Natl. Acad. Sci. U. S. A.* **2001**, *98*, 9836–9841, doi:10.1073/161274798.

58. Boyd-Kimball, D.; Gonczy, K.; Lewis, B.; Mason, T.; Siliko, N.; Wolfe, J. Classics in Chemical Neuroscience: Chlorpromazine. *ACS Chem. Neurosci.* **2019**, *10*, 79–88, doi:10.1021/acschemneuro.8b00258.

59. Schirmer, R.H.; Coulibaly, B.; Stich, A.; Scheiwein, M.; Merkle, H.; Eubel, J.; Becker, K.; Becher, H.; Müller, O.; Zich, T.; et al. Methylene Blue as an Antimalarial Agent. *Redox Rep.* **2003**, *8*, 272–275, doi:10.1179/135100003225002899.

60. Lin, X.H.; Wu, P.; Chen, W.; Zhang, Y.F.; Xia, X.H. Electrochemical DNA Biosensor for the Detection of Short DNA Species of Chronic Myelogenous Leukemia by Using Methylene Blue. *Talanta* **2007**, *72*, 468–471, doi:10.1016/j.talanta.2006.11.015.

61. Erdem, A.; Kerman, K.; Meric, B.; Akarca, U.S.; Ozsoz, M. Novel Hybridization Indicator Methylene Blue for the Electrochemical Detection of Short DNA Sequences Related to the Hepatitis B Virus. *Anal. Chim. Acta* **2000**, *422*, 139–149, doi:10.1016/S0003-2670(00)01058-8.

62. Samyn, L.M.; Suresh Babu, R.; Devendiran, M.; de Barros, A.L.F. One-Step Electropolymerization of Methylene Blue Films on Highly Flexible Carbon Fiber Electrode as Supercapacitors. *Micro Nano Syst. Lett.* **2021**, *9*, 0–9, doi:10.1186/s40486-021-00130-7.

63. Zulfikar, M.A.; Mustapa; Amran, M.B.; Alni, A.; Wahyuningrum, D. Adsorption of Cationic Dye from Aqueous Solution Using Molecularly Imprinted Polymers (MIPs). *Desalin. Water Treat.* **2018**, *103*, 102–112, doi:10.5004/dwt.2018.21936.

64. Houas, A.; Lachheb, H.; Ksibi, M.; Elaloui, E.; Guillard, C.; Herrmann, J.M. Photocatalytic Degradation Pathway of Methylene Blue in Water. *Appl. Catal. B Environ.* **2001**, *31*, 145–157, doi:10.1016/S0926-3373(00)00276-9.

65. Pfaffen, V.; Ortiz, P.I.; Córdoba de Torresi, S.I.; Torresi, R.M. On the PH Dependence of Electroactivity of Poly(Methylene Blue) Films. *Electrochim. Acta* **2010**, *55*, 1766–1771, doi:10.1016/j.electacta.2009.10.062.

66. Li, F.; Guo, Y.; Sun, X.; Wang, X. Aptasensor Based on Thionine, Graphene-Polyaniline Composite Film, and Gold Nanoparticles for

Kanamycin Detection. *Eur. Food Res. Technol.* **2014**, *239*, 227–236, doi:10.1007/s00217-014-2211-2.

67. Kaplan, I.H.; Dağci, K.; Alanyalioğlu, M. Nucleation and Growth Mechanism of Electropolymerization of Methylene Blue: The Effect of Preparation Potential on Poly(Methylene Blue) Structure. *Electroanalysis* **2010**, *22*, 2694–2701, doi:10.1002/elan.201000304.

68. Kertesz, V.; Van Berkel, G.J. Electropolymerization of Methylene Blue Investigated Using On-Line Electrochemistry/Electrospray Mass Spectrometry. *Electroanalysis* **2001**, *13*, 1425–1430, doi:10.1002/1521-4109(200111)13:17<1425::AID-ELAN1425>3.0.CO;2-R.

69. Liu, J.; Mu, S. Electrochemical Polymerization of Methylene Blue and Properties of Polymethylene Blue. *Synth. Met.* **1999**, *107*, 159–165, doi:10.1016/S0379-6779(99)00146-0.

70. Chen, C.; Mu, S. Electrochemical Polymerization of Azure A and Properties of Poly(Azure A). *J. Appl. Polym. Sci.* **2003**, *88*, 1218–1224, doi:10.1002/app.11780.

71. Jahromi, Z.; Afzali, M.; Mostafavi, A.; Nekooie, R.; Mohamadi, M. Electropolymerization of Thionine as a Stable Film along with Carbon Nanotube for Sensitive Detection of Tetracycline Antibiotic Drug. *Iran. Polym. J. (English Ed.* **2020**, *29*, 241–251, doi:10.1007/s13726-020-00788-7.

72. Pakapongpan, S.; Palangsuntikul, R.; Surareungchai, W. Electrochemical Sensors for Hemoglobin and Myoglobin Detection Based on Methylene Blue-Multiwalled Carbon Nanotubes Nanohybrid-Modified Glassy Carbon Electrode. *Electrochim. Acta* **2011**, *56*, 6831–6836, doi:10.1016/j.electacta.2011.05.089.

73. Lin, C.; Wu, Y.; Luo, F.; Chen, D.; Chen, X. A Label-Free Electrochemical DNA Sensor Using Methylene Blue as Redox Indicator Based on an Exonuclease III-Aided Target Recycling Strategy. *Biosens. Bioelectron.* **2014**, *59*, 365–369, doi:10.1016/j.bios.2014.03.053.

74. González-Fernández, E.; Avlonitis, N.; Murray, A.F.; Mount, A.R.; Bradley, M. Methylene Blue Not Ferrocene: Optimal Reporters for Electrochemical Detection of Protease Activity. *Biosens. Bioelectron.* **2016**, *84*, 82–88, doi:10.1016/j.bios.2015.11.088.

75. He, B.; Dong, X. Hierarchically Porous Zr-MOFs Labelled Methylene Blue as Signal Tags for Electrochemical Patulin Aptasensor Based on ZnO Nano Flower. *Sensors Actuators, B Chem.* **2019**, *294*, 192–198, doi:10.1016/j.snb.2019.05.045.

76. Duan, R.; Fang, X.; Wang, D. A Methylene Blue Assisted Electrochemical Sensor for Determination of Drug Resistance of Escherichia Coli. *Front. Chem.* **2021**, *9*, 1–7, doi:10.3389/fchem.2021.689735.

77. Mao, K.; Wu, D.; Li, Y.; Ma, H.; Ni, Z.; Yu, H.; Luo, C.; Wei, Q.; Du,

B. Label-Free Electrochemical Immunosensor Based on Graphene/Methylene Blue Nanocomposite. *Anal. Biochem.* **2012**, *422*, 22–27, doi:10.1016/j.ab.2011.12.047.

78. Wang, Z.; Yu, G.; Xia, J.; Zhang, F.; Liu, Q. One-Step Synthesis of a Methylene Blue@ZIF-8-Reduced Graphene Oxide Nanocomposite and Its Application to Electrochemical Sensing of Rutin. *Microchim. Acta* **2018**, *185*, doi:10.1007/s00604-018-2796-4.

79. Wang, J.; Wang, F.; Dong, S. Methylene Blue as an Indicator for Sensitive Electrochemical Detection of Adenosine Based on Aptamer Switch. *J. Electroanal. Chem.* **2009**, *626*, 1–5, doi:10.1016/j.jelechem.2008.08.008.

80. Wang, C.; Zhao, Q. A Reagentless Electrochemical Sensor for Aflatoxin B1 with Sensitive Signal-on Responses Using Aptamer with Methylene Blue Label at Specific Internal Thymine. *Biosens. Bioelectron.* **2020**, *167*, 112478, doi:10.1016/j.bios.2020.112478.

81. Abad-Gil, L.; Brett, C.M.A. Poly(Methylene Blue)-Ternary Deep Eutectic Solvent/Au Nanoparticle Modified Electrodes as Novel Electrochemical Sensors: Optimization, Characterization and Application. *Electrochim. Acta* **2022**, *434*, 141295, doi:10.1016/j.electacta.2022.141295.

82. Li, X.; Gao, X.; Gai, P.; Liu, X.; Li, F. Degradable Metal-Organic Framework/Methylene Blue Composites-Based Homogeneous Electrochemical Strategy for Pesticide Assay. *Sensors Actuators, B Chem.* **2020**, *323*, 128701, doi:10.1016/j.snb.2020.128701.

83. Chang, J.; Lv, W.; Li, Q.; Li, H.; Li, F. One-Step Synthesis of Methylene Blue-Encapsulated Zeolitic Imidazolate Framework for Dual-Signal Fluorescent and Homogeneous Electrochemical Biosensing. *Anal. Chem.* **2020**, *92*, 8959–8964, doi:10.1021/acs.analchem.0c00952.

84. Topçu, E.; Dağcı, K.; Alanyalıoğlu, M. Free-Standing Graphene/Poly(Methylene Blue)/AgNPs Composite Paper for Electrochemical Sensing of NADH. *Electroanalysis* **2016**, *28*, 2058–2069, doi:10.1002/elan.201600108.

85. Esokkiya, A.; Sudalaimani, S.; Sanjeev Kumar, K.; Sampathkumar, P.; Suresh, C.; Giribabu, K. Poly(Methylene Blue)-Based Electrochemical Platform for Label-Free Sensing of Acrylamide. *ACS Omega* **2021**, *6*, 9528–9536, doi:10.1021/acsomega.0c06315.

86. Zahran, M.; Khalifa, Z.; Zahran, M.A.H.; Azzem, M.A. Gum Arabic-Capped Silver Nanoparticles for Electrochemical Amplification Sensing of Methylene Blue in River Water. *Electrochim. Acta* **2021**, *394*, 139152, doi:10.1016/j.electacta.2021.139152.

87. Tonlé, I.K.; Ngameni, E.; Tcheumi, H.L.; Tchiéda, V.; Carteret, C.; Walcarius, A. Sorption of Methylene Blue on an Organoclay Bearing Thiol Groups and Application to Electrochemical Sensing of the Dye. *Talanta* **2008**, *74*, 489–497, doi:10.1016/j.talanta.2007.06.006.

88.	Hassan, S.S.; Nafady, A.; Sirajuddin; Solangi, A.R.; Kalhoro, M.S.; Abro, M.I.; Sherazi, S.T.H. Ultra-Trace Level Electrochemical Sensor for Methylene Blue Dye Based on Nafion Stabilized Ibuprofen Derived Gold Nanoparticles. *Sensors Actuators, B Chem.* **2015**, *208*, 320–326, doi:10.1016/j.snb.2014.11.021.

89.	Sangeetha, S.; Krishnamurthy, G.; Raghavan, M.S. Electrochemical Sensing and Photocatalytic Degradation of Methylene Blue (MB) Dye by Cobalt-Beta Hydroxy Benzoate Complex. *Mater. Sci. Semicond. Process.* **2019**, *101*, 164–173, doi:10.1016/j.mssp.2019.05.016.

90.	Hayat, M.; Shah, A.; Nisar, J.; Shah, I.; Haleem, A.; Ashiq, M.N. A Novel Electrochemical Sensing Platform for the Sensitive Detection and Degradation Monitoring of Methylene Blue. *Catalysts* **2022**, *12*, doi:10.3390/catal12030306.

91.	Hu, Y.; Xing, H.; Li, G.; Wu, M. Magnetic Imprinted Polymer-Based Quartz Crystal Microbalance Sensor for Sensitive Label-Free Detection of Methylene Blue in Groundwater. *Sensors (Switzerland)* **2020**, *20*, 1–13, doi:10.3390/s20195506.

92.	Soysal, M.; Muti, M.; Esen, C.; Gençdağ, K.; Aslan, A.; Erdem, A.; Karagözler, A.E. A Novel and Selective Methylene Blue Imprinted Polymer Modified Carbon Paste Electrode. *Electroanalysis* **2013**, *25*, 1278–1285, doi:10.1002/elan.201200569.

93.	Belbruno, J.J. Molecularly Imprinted Polymers. *Chem. Rev.* **2019**, *119*, 94–119, doi:10.1021/acs.chemrev.8b00171.

94.	Dong, C.; Shi, H.; Han, Y.; Yang, Y.; Wang, R.; Men, J. Molecularly Imprinted Polymers by the Surface Imprinting Technique. *Eur. Polym. J.* **2021**, *145*, 110231, doi:10.1016/j.eurpolymj.2020.110231.

95.	Piletsky, S.A.; Alcock, S.; Turner, A.P.F. Molecular Imprinting: At the Edge of the Third Millennium. *Trends Biotechnol.* **2001**, *19*, 9–12, doi:10.1016/S0167-7799(00)01523-7.

96.	Vasapollo, G.; Sole, R. Del; Mergola, L.; Lazzoi, M.R.; Scardino, A.; Scorrano, S.; Mele, G. Molecularly Imprinted Polymers: Present and Future Prospective. *Int. J. Mol. Sci.* **2011**, *12*, 5908–5945, doi:10.3390/ijms12095908.

97.	Ratautaite, V.; Plausinaitis, D.; Baleviciute, I.; Mikoliunaite, L.; Ramanaviciene, A.; Ramanavicius, A. Characterization of Caffeine-Imprinted Polypyrrole by a Quartz Crystal Microbalance and Electrochemical Impedance Spectroscopy. *Sensors Actuators, B Chem.* **2015**, *212*, 63–71, doi:10.1016/j.snb.2015.01.109.

98.	Ávila, M.; Zougagh, M.; Ríos, Á.; Escarpa, A. Molecularly Imprinted Polymers for Selective Piezoelectric Sensing of Small Molecules. *TrAC - Trends Anal. Chem.* **2008**, *27*, 54–65, doi:10.1016/j.trac.2007.10.009.

99.	Cowen, T.; Cheffena, M. Template Imprinting Versus Porogen Imprinting of Small Molecules: A Review of Molecularly Imprinted Polymers in Gas Sensing. *Int. J. Mol. Sci.* **2022**, *23*,

doi:10.3390/ijms23179642.

100. Mazouz, Z.; Mokni, M.; Fourati, N.; Zerrouki, C.; Barbault, F.; Seydou, M.; Kalfat, R.; Yaakoubi, N.; Omezzine, A.; Bouslema, A.; et al. Biosensors and Bioelectronics Computational Approach and Electrochemical Measurements for Protein Detection with MIP-Based Sensor. *Biosens. Bioelectron.* **2020**, *151*, 111978, doi:10.1016/j.bios.2019.111978.

101. Tlili, A.; Attia, G.; Khaoulani, S.; Mazouz, Z.; Zerrouki, C.; Yaakoubi, N.; Othmane, A.; Fourati, N. Contribution to the Understanding of the Interaction between a Polydopamine Molecular Imprint and a Protein Model: Ionic Strength and PH Effect Investigation. *Sensors (Switzerland)* **2021**, *21*, 1–13, doi:10.3390/s21020619.

102. Ansari, S.; Masoum, S. Molecularly Imprinted Polymers for Capturing and Sensing Proteins: Current Progress and Future Implications. *TrAC - Trends Anal. Chem.* **2019**, *114*, 29–47, doi:10.1016/j.trac.2019.02.008.

103. Stojanovic, Z.; Erdőssy, J.; Keltai, K.; Scheller, F.W.; Gyurcsányi, R.E. Electrosynthesized Molecularly Imprinted Polyscopoletin Nanofilms for Human Serum Albumin Detection. *Anal. Chim. Acta* **2017**, *977*, 1–9, doi:10.1016/j.aca.2017.04.043.

104. Tamboli, V.K.; Bhalla, N.; Jolly, P.; Bowen, C.R.; Taylor, J.T.; Bowen, J.L.; Allender, C.J.; Estrela, P. Hybrid Synthetic Receptors on MOSFET Devices for Detection of Prostate Specific Antigen in Human Plasma. *Anal. Chem.* **2016**, *88*, 11486–11490, doi:10.1021/acs.analchem.6b02619.

105. Zeng, Q.; Huang, X.; Ma, M. A Molecularly Imprinted Electrochemical Sensor Based on Polypyrrole/Carbon Nanotubes Composite for the Detection of S-Ovalbumin in Egg White. *Int. J. Electrochem. Sci.* **2017**, *12*, 3965–3981, doi:10.20964/2017.05.61.

106. Moreira, F.T.C.; Dutra, R.A.F.; Noronha, J.P.C.; Sales, M.G.F. Electrochemical Biosensor Based on Biomimetic Material for Myoglobin Detection. *Electrochim. Acta* **2013**, *107*, 481–487, doi:10.1016/j.electacta.2013.06.061.

107. Lai, Y.; Zhang, C.; Deng, Y.; Yang, G.; Li, S.; Tang, C.; He, N. A Novel α-Fetoprotein-MIP Immunosensor Based on AuNPs/PTh Modified Glass Carbon Electrode. *Chinese Chem. Lett.* **2019**, *30*, 160–162, doi:10.1016/j.cclet.2018.07.011.

108. Karami, P.; Bagheri, H.; Johari-Ahar, M.; Khoshsafar, H.; Arduini, F.; Afkhami, A. Dual-Modality Impedimetric Immunosensor for Early Detection of Prostate-Specific Antigen and Myoglobin Markers Based on Antibody-Molecularly Imprinted Polymer. *Talanta* **2019**, *202*, 111–122, doi:10.1016/j.talanta.2019.04.061.

109. Yarman, A.; Dechtrirat, D.; Bosserdt, M.; Jetzschmann, K.J.; Gajovic-Eichelmann, N.; Scheller, F.W. Cytochrome C-Derived Hybrid Systems Based on Molecular Imprinted Polymers. *Electroanalysis*

2015, *27*, 573–586, doi:10.1002/elan.201400592.

110. Nawaz, N.; Abu Bakar, N.K.; Muhammad Ekramul Mahmud, H.N.; Jamaludin, N.S. Molecularly Imprinted Polymers-Based DNA Biosensors. *Anal. Biochem.* **2021**, *630*, 114328, doi:10.1016/j.ab.2021.114328.

111. Ramanavičius, S.; Morkvėnaitė-Vilkončienė, I.; Samukaitė-Bubnienė, U.; Ratautaitė, V.; Plikusienė, I.; Viter, R.; Ramanavičius, A. Electrochemically Deposited Molecularly Imprinted Polymer-Based Sensors. *Sensors* **2022**, *22*, doi:10.3390/s22031282.

112. Chen, S.; Chen, X.; Zhang, L.; Gao, J.; Ma, Q. Electrochemiluminescence Detection of Escherichia Coli O157:H7 Based on a Novel Polydopamine Surface Imprinted Polymer Biosensor. *ACS Appl. Mater. Interfaces* **2017**, *9*, 5430–5436, doi:10.1021/acsami.6b12455.

113. Ait Lahcen, A.; Arduini, F.; Lista, F.; Amine, A. Label-Free Electrochemical Sensor Based on Spore-Imprinted Polymer for Bacillus Cereus Spore Detection. *Sensors Actuators, B Chem.* **2018**, *276*, 114–120, doi:10.1016/j.snb.2018.08.031.

114. Nguy, T.P.; Van Phi, T.; Tram, D.T.N.; Eersels, K.; Wagner, P.; Lien, T.T.N. Development of an Impedimetric Sensor for the Label-Free Detection of the Amino Acid Sarcosine with Molecularly Imprinted Polymer Receptors. *Sensors Actuators, B Chem.* **2017**, *246*, 461–470, doi:10.1016/j.snb.2017.02.101.

115. Teng, Y.; Liu, F.; Kan, X. Voltammetric Dopamine Sensor Based on Three-Dimensional Electrosynthesized Molecularly Imprinted Polymers and Polypyrrole Nanowires. *Microchim. Acta* **2017**, *184*, 2515–2522, doi:10.1007/s00604-017-2243-y.

116. Uzun, L.; Turner, A.P.F. Molecularly-Imprinted Polymer Sensors: Realising Their Potential. *Biosens. Bioelectron.* **2016**, *76*, 131–144, doi:10.1016/j.bios.2015.07.013.

117. Xing, X.; Liu, S.; Yu, J.; Lian, W.; Huang, J. Electrochemical Sensor Based on Molecularly Imprinted Film at Polypyrrole-Sulfonated Graphene/Hyaluronic Acid-Multiwalled Carbon Nanotubes Modified Electrode for Determination of Tryptamine. *Biosens. Bioelectron.* **2012**, *31*, 277–283, doi:10.1016/j.bios.2011.10.032.

118. Sharma, P.S.; Pietrzyk-Le, A.; D'Souza, F.; Kutner, W. Electrochemically Synthesized Polymers in Molecular Imprinting for Chemical Sensing. *Anal. Bioanal. Chem.* **2012**, *402*, 3177–3204, doi:10.1007/s00216-011-5696-6.

119. Lowdon, J.W.; Diliën, H.; Singla, P.; Peeters, M.; Cleij, T.J.; van Grinsven, B.; Eersels, K.; Lowdon, J.W.; Dili, H.; Grinsven, B. Van; et al. MIPs for Commercial Application in Low-Cost Sensors and Assays – An Overview of the Current Status Quo. *Sensors Actuators B Chem.* **2020**, *325*, 128973, doi:10.1016/j.snb.2020.128973.

120. Huynh, T.P.; Kutner, W. Molecularly Imprinted Polymers as

Recognition Materials for Electronic Tongues. *Biosens. Bioelectron.* **2015**, *74*, 856–864, doi:10.1016/j.bios.2015.07.054.

121. Ma, J.; Yan, M.; Feng, G.; Ying, Y.; Chen, G.; Shao, Y.; She, Y.; Wang, M.; Sun, J.; Zheng, L.; et al. An Overview on Molecular Imprinted Polymers Combined with Surface-Enhanced Raman Spectroscopy Chemical Sensors toward Analytical Applications. *Talanta* **2021**, *225*, 122031, doi:10.1016/j.talanta.2020.122031.

122. Zaidi, S.A. Molecular Imprinting: A Useful Approach for Drug Delivery. *Mater. Sci. Energy Technol.* **2020**, *3*, 72–77, doi:10.1016/j.mset.2019.10.012.

123. Liu, R.; Poma, A. Advances in Molecularly Imprinted Polymers as Drug Delivery Systems. *Molecules* **2021**, *26*, doi:10.3390/molecules26123589.

124. He, S.; Zhang, L.; Bai, S.; Yang, H.; Cui, Z.; Zhang, X.; Li, Y. Advances of Molecularly Imprinted Polymers (MIP) and the Application in Drug Delivery. *Eur. Polym. J.* **2021**, *143*, 110179, doi:10.1016/j.eurpolymj.2020.110179.

125. Mpupa, A.; Selahle, S.K.; Mizaikoff, B.; Nomngongo, P.N. Recent Advances in Solid-Phase Extraction (Spe) Based on Molecularly Imprinted Polymers (Mips) for Analysis of Hormones. *Chemosensors* **2021**, *9*, doi:10.3390/chemosensors9070151.

126. Kaya, S.I.; Cetinkaya, A.; Ozkan, S.A. Molecularly Imprinted Polymers as Highly Selective Sorbents in Sample Preparation Techniques and Their Applications in Environmental Water Analysis. *Trends Environ. Anal. Chem.* **2023**, *37*, e00193, doi:10.1016/j.teac.2022.e00193.

127. Rebelo, P.; Costa-Rama, E.; Seguro, I.; Pacheco, J.G.; Nouws, H.P.A.; Cordeiro, M.N.D.S.; Delerue-Matos, C. Molecularly Imprinted Polymer-Based Electrochemical Sensors for Environmental Analysis. *Biosens. Bioelectron.* **2021**, *172*, 112719, doi:10.1016/j.bios.2020.112719.

128. Arabi, M.; Ostovan, A.; Bagheri, A.R.; Guo, X.; Wang, L.; Li, J.; Wang, X.; Li, B.; Chen, L. Strategies of Molecular Imprinting-Based Solid-Phase Extraction Prior to Chromatographic Analysis. *TrAC - Trends Anal. Chem.* **2020**, *128*, 115923, doi:10.1016/j.trac.2020.115923.

129. Song, Z.; Li, J.; Lu, W.; Li, B.; Yang, G.; Bi, Y.; Arabi, M.; Wang, X.; Ma, J.; Chen, L. Molecularly Imprinted Polymers Based Materials and Their Applications in Chromatographic and Electrophoretic Separations. *TrAC - Trends Anal. Chem.* **2022**, *146*, doi:10.1016/j.trac.2021.116504.

130. Karasu, T.; Özgür, E.; Uzun, L. MIP-on-a-Chip: Artificial Receptors on Microfluidic Platforms for Biomedical Applications. *J. Pharm. Biomed. Anal.* **2023**, *226*, doi:10.1016/j.jpba.2023.115257.

131. Haupt, K.; Medina Rangel, P.X.; Bui, B.T.S. Molecularly Imprinted

Polymers: Antibody Mimics for Bioimaging and Therapy. *Chem. Rev.* **2020**, *120*, 9554–9582, doi:10.1021/acs.chemrev.0c00428.

132. Leibl, N.; Haupt, K.; Gonzato, C.; Duma, L. Molecularly Imprinted Polymers for Chemical Sensing: A Tutorial Review. *Chemosensors* **2021**, *9*, 1–19, doi:10.3390/chemosensors9060123.

133. Gupta, V.K.; Yola, M.L.; Özaltin, N.; Atar, N.; Üstündağ, Z.; Uzun, L. Molecular Imprinted Polypyrrole Modified Glassy Carbon Electrode for the Determination of Tobramycin. *Electrochim. Acta* **2013**, *112*, 37–43, doi:10.1016/j.electacta.2013.08.132.

134. Yaroshenko, I.; Kirsanov, D.; Marjanovic, M.; Lieberzeit, P.A.; Korostynska, O.; Mason, A.; Frau, I.; Legin, A. Real-Time Water Quality Monitoring with Chemical Sensors. *Sensors* 2020, *20*.

135. Uka, B.; Kieninger, J.; Urban, G.A.; Weltin, A. Electrochemical Microsensor for Microfluidic Glyphosate Monitoring in Water Using MIP-Based Concentrators. *ACS Sensors* **2021**, *6*, 2738–2746, doi:10.1021/acssensors.1c00884.

136. Karimian, N.; Stortini, A.M.; Moretto, L.M.; Costantino, C.; Bogialli, S.; Ugo, P. Electrochemosensor for Trace Analysis of Perfluorooctanesulfonate in Water Based on a Molecularly Imprinted Poly(o-Phenylenediamine) Polymer. *ACS Sensors* **2018**, *3*, 1291–1298, doi:10.1021/acssensors.8b00154.

137. Khadem, M.; Faridbod, F.; Norouzi, P.; Rahimi Foroushani, A.; Ganjali, M.R.; Shahtaheri, S.J.; Yarahmadi, R. Modification of Carbon Paste Electrode Based on Molecularly Imprinted Polymer for Electrochemical Determination of Diazinon in Biological and Environmental Samples. *Electroanalysis* **2017**, *29*, 708–715, doi:10.1002/elan.201600293.

138. Aylaz, G.; Kuhn, J.; Lau, E.C.H.T.; Yeung, C.C.; Roy, V.A.L.; Duman, M.; Yiu, H.H.P. Recent Developments on Magnetic Molecular Imprinted Polymers (MMIPs) for Sensing, Capturing, and Monitoring Pharmaceutical and Agricultural Pollutants. *J. Chem. Technol. Biotechnol.* **2021**, *96*, 1151–1160, doi:10.1002/jctb.6681.

139. Pacheco, J.G.; Silva, M.S.V.; Freitas, M.; Nouws, H.P.A.; Delerue-Matos, C. Molecularly Imprinted Electrochemical Sensor for the Point-of-Care Detection of a Breast Cancer Biomarker (CA 15-3). *Sensors Actuators, B Chem.* **2018**, *256*, 905–912, doi:10.1016/j.snb.2017.10.027.

140. Dixit, C.K.; Bhakta, S.; Reza, K.K.; Kaushik, A. Exploring Molecularly Imprinted Polymers as Artificial Antibodies for Efficient Diagnostics and Commercialization: A Critical Overview. *Hybrid Adv.* **2022**, *1*, 100001, doi:10.1016/j.hybadv.2022.100001.

141. Mohsenzadeh, E.; Ratautaite, V.; Brazys, E.; Ramanavicius, S.; Zukauskas, S.; Plausinaitis, D.; Ramanavicius, A. Application of Computational Methods in the Design of Molecularly Imprinted Polymers (Review). *TrAC - Trends Anal. Chem.* **2024**, *171*, 117480,

doi:10.1016/j.trac.2023.117480.

142. Wulff, G.; Sarhan, A. Use of Polymers with Enzyme-Analogous Structures for the Resolution of Racemates. *Angew. Chemie Int. Ed.* **1972**, *11*, 341–344.

143. El-Schich, Z.; Zhang, Y.; Feith, M.; Beyer, S.; Sternbæk, L.; Ohlsson, L.; Stollenwerk, M.; Wingren, A.G. Molecularly Imprinted Polymers in Biological Applications. *Biotechniques* **2020**, *69*, 407–420, doi:10.2144/btn-2020-0091.

144. Sarpong, K.A.; Xu, W.; Huang, W.; Yang, W. The Development of Molecularly Imprinted Polymers in the Clean-Up of Water Pollutants: A Review. *Am. J. Anal. Chem.* **2019**, *10*, 202–226, doi:10.4236/ajac.2019.105017.

145. Ramanaviciene, A.; Ramanavicius, A. Molecularly Imprinted Polypyrrole-Based Synthetic Receptor for Direct Detection of Bovine Leukemia Virus Glycoproteins. *Biosens. Bioelectron.* **2004**, *20*, 1076–1082, doi:10.1016/j.bios.2004.05.014.

146. Crapnell, R.D.; Dempsey-Hibbert, N.C.; Peeters, M.; Tridente, A.; Banks, C.E. Molecularly Imprinted Polymer Based Electrochemical Biosensors: Overcoming the Challenges of Detecting Vital Biomarkers and Speeding up Diagnosis. *Talanta Open* **2020**, *2*, 100018, doi:10.1016/j.talo.2020.100018.

147. Yarman, A.; Scheller, F.W. How Reliable Is the Electrochemical Readout of MIP Sensors? *Sensors (Switzerland)* **2020**, *20*, doi:10.3390/s20092677.

148. Ndunda, E.N. Molecularly Imprinted Polymers — A Closer Look at the Control Polymer Used in Determining the Imprinting Effect : A Mini Review. *J. Mol. Recognit.* **2020**, 1–11, doi:10.1002/jmr.2855.

149. Kan, X.; Xing, Z.; Zhu, A.; Zhao, Z.; Xu, G.; Li, C.; Zhou, H. Molecularly Imprinted Polymers Based Electrochemical Sensor for Bovine Hemoglobin Recognition. *Sensors Actuators, B Chem.* **2012**, *168*, 395–401, doi:10.1016/j.snb.2012.04.043.

150. Yadav, A.K.; Verma, D.; Dalal, N.; Kumar, A.; Solanki, P.R. Molecularly Imprinted Polymer-Based Nanodiagnostics for Clinically Pertinent Bacteria and Virus Detection for Future Pandemics. *Biosens. Bioelectron. X* **2022**, *12*, 100257, doi:10.1016/j.biosx.2022.100257.

151. Gandarilla, A.M.D.; Matos, R.S.; Barcelay, Y.R.; da Fonseca Filho, H.D.; Brito, W.R. Molecularly Imprinted Polymer on Indium Tin Oxide Substrate for Bovine Serum Albumin Determination. *J. Polym. Res.* **2022**, *29*, 1–11, doi:10.1007/s10965-022-03022-5.

152. Chen, H.J.; Zhang, Z.H.; Luo, L.J.; Yao, S.Z. Surface-Imprinted Chitosan-Coated Magnetic Nanoparticles Modified Multi-Walled Carbon Nanotubes Biosensor for Detection of Bovine Serum Albumin. *Sensors Actuators, B Chem.* **2012**, *163*, 76–83, doi:10.1016/j.snb.2012.01.010.

153. Yola, M.L.; Atar, N. Development of Cardiac Troponin-I Biosensor

Based on Boron Nitride Quantum Dots Including Molecularly Imprinted Polymer. *Biosens. Bioelectron.* **2019**, *126*, 418–424, doi:10.1016/j.bios.2018.11.016.

154. Silva, B.V.M.; Rodríguez, B.A.G.; Sales, G.F.; Sotomayor, M.D.P.T.; Dutra, R.F. An Ultrasensitive Human Cardiac Troponin T Graphene Screen-Printed Electrode Based on Electropolymerized-Molecularly Imprinted Conducting Polymer. *Biosens. Bioelectron.* **2016**, *77*, 978–985, doi:10.1016/j.bios.2015.10.068.

155. Sharma, R.; Lakshmi, G.B.V.S.; Kumar, A.; Solanki, P. Polypyrrole Based Molecularly Imprinted Polymer Platform for Klebsiella Pneumonia Detection. *ECS Sensors Plus* **2022**, *1*, 010603, doi:10.1149/2754-2726/ac612c.

156. Domínguez-Renedo, O.; Navarro-Cuñado, A.M.; Arnáiz-Lozano, V.; Alonso-Lomillo, M.A. Molecularly Imprinted Polypyrrole Based Electrochemical Sensor for Selective Determination of 4-Ethylphenol. *Talanta* **2020**, *207*, 120351, doi:10.1016/j.talanta.2019.120351.

157. Ding, S.; Lyu, Z.; Li, S.; Ruan, X.; Fei, M.; Zhou, Y.; Niu, X.; Zhu, W.; Du, D.; Lin, Y. Molecularly Imprinted Polypyrrole Nanotubes Based Electrochemical Sensor for Glyphosate Detection. *Biosens. Bioelectron.* **2021**, *191*, 113434, doi:10.1016/j.bios.2021.113434.

158. Mazouz, Z.; Rahali, S.; Fourati, N.; Zerrouki, C.; Aloui, N.; Seydou, M.; Yaakoubi, N.; Chehimi, M.M.; Othmane, A.; Kalfat, R. Highly Selective Polypyrrole MIP-Based Gravimetric and Electrochemical Sensors for Picomolar Detection of Glyphosate. *Sensors (Switzerland)* **2017**, *17*, 1–15, doi:10.3390/s17112586.

159. Turco, A.; Corvaglia, S.; Mazzotta, E. Electrochemical Sensor for Sulfadimethoxine Based on Molecularly Imprinted Polypyrrole: Study of Imprinting Parameters. *Biosens. Bioelectron.* **2015**, *63*, 240–247, doi:10.1016/j.bios.2014.07.045.

160. Ramanavicius, A.; Oztekin, Y.; Ramanaviciene, A. Electrochemical Formation of Polypyrrole-Based Layer for Immunosensor Design. *Sensors Actuators, B Chem.* **2014**, *197*, 237–243, doi:10.1016/j.snb.2014.02.072.

161. Heinze, J.; Frontana-Uribe, B.A.; Ludwigs, S. Electrochemistry of Conducting Polymers-Persistent Models and New Concepts. *Chem. Rev.* **2010**, *110*, 4724–4771, doi:10.1021/cr900226k.

162. Lewis, T.W.; Wallace, G.G.; Kim, C.Y.; Kim, D.Y. Studies of the Overoxidation of Polypyrrole. *Synth. Met.* **1997**, *84*, 403–404, doi:10.1016/s0379-6779(97)80803-x.

163. Li, C.M.; Sun, C.Q.; Chen, W.; Pan, L. Electrochemical Thin Film Deposition of Polypyrrole on Different Substrates. *Surf. Coatings Technol.* **2005**, *198*, 474–477, doi:10.1016/j.surfcoat.2004.10.065.

164. Ratautaite, V.; Ramanaviciene, A.; Oztekin, Y.; Voronovic, J.; Balevicius, Z.; Mikoliunaite, L.; Ramanavicius, A. Electrochemical Stability and Repulsion of Polypyrrole Film. *Colloids Surfaces A*

Physicochem. Eng. Asp. **2013**, *418*, 16–21, doi:10.1016/j.colsurfa.2012.10.052.

165. Kuwabata, S.; Nakamura, J.; Yoneyama, H. The Effect of Basicity of Dopant Anions on the Conductivity of Polypyrrole Films. *J. Chem. Soc. Chem. Commun.* **1988**, 779–780, doi:10.1039/C39880000779.

166. Fonner, J.M.; Schmidt, C.E.; Ren, P. A Combined Molecular Dynamics and Experimental Study of Doped Polypyrrole. *Polymer (Guildf).* **2010**, *51*, 4985–4993, doi:10.1016/j.polymer.2010.08.024.

167. John, J.; Sivaraman, S.; Jayalekshmy, S.; Anantharaman, M.R. Investigations on the Mechanism of Carrier Transport in Plasma Polymerized Pyrrole Thin Films. *J. Phys. Chem. Solids* **2010**, *71*, 935–939, doi:10.1016/j.jpcs.2010.03.047.

168. Aboutorab, S.; Izadan, H.; Tavanai, H.; Nezhad, A.Z.; Bayat, M. An Investigation on the Effect of Acid Dyes as Dopants on the Electrical Conductivity and Heat Generation of Polypyrrole Coated Polyester Fabric. *Prog. Org. Coatings* **2023**, *185*, 107917, doi:10.1016/j.porgcoat.2023.107917.

169. Serra Moreno, J.; Panero, S.; Materazzi, S.; Martinelli, A.; Sabbieti, M.G.; Agas, D.; Materazzi, G. Polypyrrole-Polysaccharide Thin Films Characteristics: Electrosynthesis and Biological Properties. *J. Biomed. Mater. Res. - Part A* **2009**, *88*, 832–840, doi:10.1002/jbm.a.32230.

170. Alizadeh, N.; Tavoli, F. Enhancing Electrochromic Contrast and Redox Stability of Nanostructure Polypyrrole Film Doped by Heparin as Polyanion in Different Solvents. *J. Polym. Sci. Part A Polym. Chem.* **2014**, *52*, 3365–3371, doi:10.1002/pola.27398.

171. Nirmala Devi, G.; Chitra, S.; Selvasekarapandian, S.; Premalatha, M.; Monisha, S.; Saranya, J. Synthesis and Characterization of Dextrin-Based Polymer Electrolytes for Potential Applications in Energy Storage Devices. *Ionics (Kiel).* **2017**, *23*, 3377–3388, doi:10.1007/s11581-017-2135-5.

172. Svenson, J.; Andersson, H.S.; Piletsky, S.A.; Nicholls, I.A. Spectroscopic Studies of the Molecular Imprinting Self-Assembly Process. *J. Mol. Recognit.* **1998**, *11*, 83–86, doi:https://doi.org/10.1002/(SICI)1099-1352(199812)11:1/6<83::AID-JMR395>3.0.CO;2-P.

173. Anson, F.C. Innovations in the Study of Adsorbed Reactants by Chronocoulometry. *Anal. Chem.* **1966**, *38*, 54–57, doi:10.1021/ac60233a014.

174. Anson, F.C.; Christie, J.H.; Osteryoung, R.A. A Study of the Adsorption of Cadmium(II) on Mercury from Thiocyanate Solutions by Double Potential-Step Chronocoulometry. *J. Electroanal. Chem.* **1967**, *13*, 343–353, doi:10.1016/0022-0728(67)80037-8.

175. Zhou, K.; Wang, H.; Zhang, Y.; Liu, J.; Yan, H. An Advanced Technique to Evaluate the Electrochromic Performances of NiO Films by Multi-Cycle Double-Step Potential Chronocoulometry. *J.*

Electrochem. Soc. **2016**, *163*, H1033–H1040, doi:10.1149/2.1011610jes.

176. Tsai, T.C.; Han, H.Z.; Cheng, C.C.; Chen, L.C.; Chang, H.C.; Chen, J.J.J. Modification of Platinum Microelectrode with Molecularly Imprinted Over-Oxidized Polypyrrole for Dopamine Measurement in Rat Striatum. *Sensors Actuators, B Chem.* **2012**, *171–172*, 93–101, doi:10.1016/j.snb.2011.07.052.

177. Syritski, V.; Reut, J.; Menaker, A.; Gyurcsányi, R.E.; Öpik, A. Electrosynthesized Molecularly Imprinted Polypyrrole Films for Enantioselective Recognition of L-Aspartic Acid. *Electrochim. Acta* **2008**, *53*, 2729–2736, doi:10.1016/j.electacta.2007.10.032.

COPIES OF PUBLICATIONS

1st publication / 1 publikacija
R. Boguzaite, V. Ratautaite, L. Mikoliunaite, V. Pudzaitis, A. Ramanaviciene, A. Ramanavicius,
Towards analytical application of electrochromic polypyrrole layers modified by phenothiazine derivatives,
Journal of Electroanalytical Chemistry, 886 (2021) 115132.
https://doi.org/10.1016/j.jelechem.2021.115132

Towards analytical application of electrochromic polypyrrole layers modified by phenothiazine derivatives

Raimonda Boguzaite [a,b], Vilma Ratautaite [a,b], Lina Mikoliunaite [b,c], Vaidas Pudzaitis [c], Almira Ramanaviciene [d], Arunas Ramanavicius [a,b,d,*]

[a] Laboratory of Nanotechnology, Department of Functional Materials and Electronics, Center for Physical Sciences and Technology, Sauletekio av. 3, Vilnius LT-10257, Lithuania
[b] Department of Physical Chemistry, Institute of Chemistry, Faculty of Chemistry and Geosciences, Vilnius University, Naugarduko str. 24, Vilnius LT-03225, Lithuania
[c] Laboratory of Spectroelectrochemistry, Department of Organic Chemistry, Center for Physical Sciences and Technology, Sauletekio av. 3, Vilnius LT-10257, Lithuania
[d] NanoTechnas – Center of Nanotechnology and Materials Science at Vilnius University, Faculty of Chemistry and Geosciences, Naugarduko 24, LT-03225 Vilnius, Lithuania

ARTICLE INFO

ABSTRACT

Electrochromism is the phenomenon, which is based on the change of material color when particular voltage is applied to electrochemical system. This feature is of high importance for a wide range of actuating devices such as smart windows, screens, thermal modulators and various sensors. During this research we have formed and investigated polypyrrole (Ppy) based layers, which were electrochemically deposited on the indium tin oxide coated glass in the presence of three phenothiazine (PT) derivatives - methylene blue (MB), azure A (AA), and thionine (TH). The surface morphology of the coatings was determined by atomic force microscopy (AFM) and scanning electron microscopy (SEM). It was found that the thickness of the surface irregularities ranged from 1 to 3 μm. The reflection absorption infrared spectroscopy (RAIRS) was chosen for the evaluation of the layer due to the possibility to measure reflection spectra of thin layers avoiding influence of the glass substrate present under the ITO layer. Polypyrrole and poly(Azure A) (Ppy-PAA) layer was the thickest one and non-translucent, therefore, it was not suitable for optical evaluation. The polypyrrole and poly(methylene blue) (Ppy-PMB) and polypyrrole and polythionine (Ppy-PTH) layers also were analyzed by cyclic voltammetry and chronoamperometry methods. The applicability of Ppy-PMB, Ppy-PAA, and Ppy-PTH in chemical sensing was evaluated. The investigated polymeric coatings exhibited electrochromic properties (color change at different potential), reacted to pH changes and to ascorbic acid concentration.

1. Introduction

Electrochromism is a phenomenon in which the color of a material changes depending on the values of electrical potential applied to the system [1]. This feature is very important for a wide range of applications such as smart windows, screens, thermal modulators, sensors, electrochromic supercapacitors, and versatile functional electrochromic displays [2–8]. Electrochromic properties are characteristic feature for some semiconducting layers based on metal oxides and some organic materials such as polymers [2]. Polymers can also have electrochromic properties and are rather popular due to their simplicity, ability to form thin coatings, easy synthesis, stability, high optical contrasts, fast response, ability to form multicolored electrochromes [9,10]. In conjugated polymers, electrochromism occurs due to changes in the π-π conjugated electronic system of the polymer and ability to participate in electrochemical oxidation and reduction. Among many conducting polymers, polyaniline (PANI) [2] and polypyrrole (Ppy) [11] has received considerable attention. In the middle of 19th century, Henry Letheby, a British chemical analyst during the study of polyaniline (PANI), observed that the reduced PANI layer was colorless but after oxidation it become dark blue [12]. In 1979 Diaz published the first article on the electrochemical synthesis of polypyrrole (Ppy) and the preparation of a conjugated electrochromic polymer based coating [13].

Phenothiazine (PT) derivatives (Fig. 1A) are biologically active compounds and also can be electrochemically polymerized. Chlorpromazine and promethazine derivatives have altered the fields of psychiatry and allergy treatment, respectively. Methylene blue (MB) was one of the first antimalarial drugs, and other PT derivatives are being studied as possible anti-infection drugs. These derivatives were

chosen for their similar structure, good electrical activity, and due to water solubility. MB is one of the oldest organic dyes used in chemistry, having a potential close to the redox potentials of many biomolecules [14]. Also, it is an effective electron redox mediator [15]. Thionine (TH) is usually selected as the sensitizer. Both thionine monomer and the polythionine (PTH) have excellent electrocatalytic activity towards redox-active low molecular weight compounds [16]. Combined polymers have significant potential when they are used for the application in dyes, conducting coatings and electrochromic devices [9].

Combining polymers such as Ppy with phenothiazine derivatives can be the key to create electrochromic coatings with advanced properties, faster response, and responsive towards environmental changes [17,18]. Phenothiazine derivatives can be applied in the manufacture of electrochemical devices, sensors, imaging [2,14,19,20].

Polypyrrole can be obtained by chemical polymerization, chemical vapor deposition (CVD), electrochemical polymerization [21,22]. Electrochemical polymerization is also a convenient method to form layers using the phenothiazine derivatives discussed in the study [23,24]. The conjugated polymers can be synthesized by chemical and electrochemical polymerization methods in a variety of organic solvents and aqueous media. Physical properties of chemically synthesized conductive polymers, such as particle size and morphology, can be controlled by optimizing the synthesis conditions [11,25].

The advantage of electrochemical polymerization is a possibility to cover electrodes by layers made of conductive polymers and/or their composites with high conductivity. Moreover, the electrochemical polymerization method meets the requirements of the green chemistry and, therefore, it is preferable for practical applications [26]. Methylene blue, thionine, azure A can be electrochemically polymerized in aqueous solution to produce new polymers with unique functions and electrochemical properties [17,23,27,28]. The study analyzing the ultrathin layers of poly(methylene blue) (PMB) and their properties by electrochemical surface plasmon resonance (SPR) demonstrated that the effects of the adsorption and desorption processes are important only for thick layers, but for thinner layers only redox activity of PMB was affecting SPR signal [29].

A plausible polymer of MB structure determined by DFT calculations [30,31] and possible mechanism of azine polymerization and formed tetramer structure of polyphenazine was predicted [32].

The layer of polypyrrole and phenothiazine derivatives were electrochemically deposited by potential cycling, while conditions for here applied electrochemical polymerization were chosen according to that reported in other researches [17,23,33–35]. Ascorbic acid is an important analyte, because it is redox-active compound and has a significant role as an antioxidant in the living cells, therefore, it is used as an additive for the improvement of food and beverages [36–39].

The aim of this work was to investigate the synthesis of Ppy, which was modified by three phenothiazine derivatives (methylene blue, azure A and thionine) and to study electrochromic properties of the formed layers. The applicability of Ppy layers modified with phenothiazine derivatives in the design of ascorbic acid (vitamin C) sensor has been investigated, assuming that due to the structure of the compounds, electron transfer from ascorbic acid should occur while forming a charge transfer complex.

2. Materials and methods

2.1. Chemicals and instrumentation

Azure A (AA), methylene blue (MB), thionine (TH) acetate were purchased from *Alfa Aesar* (Germany) and used as received. Other chemicals were purchased as follows: ascorbic acid –from *Aldrich* (Germany), NaOH –from *Merck* (Germany), H_3BO_3 – from *Scharlau* (Spain),

H_3PO_4 – from *Fluka* (Germany) and CH_3COOH – from *Carl Roth* (Germany), $LiClO_4$ – from *Alfa Aesar* (Germany), 27% NH_4OH – from *Carl Roth* (Germany) and 30% H_2O_2 – from *Chempur* (Poland).

Electrochemical polymerization was performed using computer controlled potentiostat PGSTAT 128N using NOVA 1.10 software purchased from *EcoChemie* (The Netherlands). A glass cuvette (high × depth × width = 32 mm × 18 mm × 30 mm) was used as an electrochemical cell for synthesis. Another glass cuvette (32 mm × 18 mm × 50 mm) was used for analytical purposes. The experiment was carried out in a three-electrode system where the working electrode was an indium tin oxide (ITO) coated glass, which was purchased from *Sigma-Aldrich* (Germany). The surface resistivity stated by manufacturer of glass/ITO electrode was of 15–25 Ω/cm^2. The geometric area of the working electrode that was coated with the layer of polypyrrole and the phenothiazine derivative was 2 cm^2. Two reference electrodes were used to perform the experiments of this study: (i) Ag/AgCl wire was used as the reference electrode during the electrochemical deposition of the layers, because it is less sensitive to contamination with electrochemical polymerization products; (ii) Ag/AgCl$_{(3M\ KCl)}$ (from *CH Instruments* (USA)) was used during electrochemical evaluation of the obtained polymeric layers by cyclic voltammetry (CV) and chronoamperometry (CA). A platinum wire (from *CH Instruments* (USA)) was used as the counter electrode. All the experiments were performed at room temperature (approx. 20 °C). The spectrometer USB4000-FL equipped with "SpectraSuite" software, which was purchased from *Ocean Optics* (USA), was used for the optical measurements.

2.2. Electrochemical deposition of polypyrrole/phenothiazine derivative layer on ITO

Before electrochemical deposition of the Ppy layer modified with phenothiazine derivatives, the glass/ITO was washed in the solution consisting of 27% NH_4OH and 30% H_2O_2 mixed at ratio 3:1 preheated up to 50 °C for 3 min. Later the electrode was cleaned at room temperature in ultrasonic bath subsequently in water, acetone, and water for 15 min in each liquid.

Electrochromic layers were electrochemically deposited by potential cycling in a potential range from −0.2 V until +1.0 V vs Ag/AgCl, at potential sweep rate of 50 mV/s, by 25 cycles with a step lift of 2.44 mV. A polymerization solution was prepared in water with 10 mM of corresponding phenothiazine derivative (methylene blue, azure A or thionine acetate) and 50 mM of pyrrole formed layers are indicated as Ppy-PMB, Ppy-PAA and Ppy-PTH, respectively.

2.3. The evaluation of electrochemical and electrochromic properties of Ppy-PMB, Ppy-PAA and Ppy-PTH layers

The formed Ppy-PMB, Ppy-PAA and Ppy-PTH layers were analyzed by chronoamperometry and CV methods. Optical absorbance was followed at several wavelengths simultaneously to electrochemical measurements.

The dependence of absorbance on the pH value of Ppy-PMB, Ppy-PAA and Ppy-PTH layers was analyzed in Britton–Robinson buffer (BR-buffer). BR-buffer consisted of 0.040 M H_3BO_3, 0.040 M H_3PO_4, and 0.040 M CH_3COOH. 0.10 M $LiClO_4$, which was used to support the ionic strength of BR-buffer. The required pH of BR-buffer was regulated with 0.10 M of NaOH solution.

The color changes of Ppy-PMB and Ppy-PTH layers at several different pH values were followed during potential cycling from −0.8 V to +0.8 V vs Ag/AgCl$_{(3M\ KCl)}$, at the scan rate of 50 mV/s and step lift of 2.44 mV, 5 cycles. Optical absorbance was followed at 668 nm (for Ppy-PMB), 610 nm (for Ppy-PTH), and 750 nm (for Ppy-PMB and Ppy-PTH), these wavelengths were selected with regard on the absorbance spectrum of corresponding phenothiazine. The wavelength of

2

750 nm was chosen taking into account optical absorbance spectra of polypyrrole layer and the results of previous our studies [40].

The electrochromic response of Ppy-PMB and Ppy-PTH layers to the different concentrations of ascorbic acid was analyzed at three pH values of BR-buffer: pH 3.0, pH 4.0, and pH 5.0. Such pH values were selected regarding the ascorbic acid pK_a values, which are $pK_{a1} = 4.17$; $pK_{a2} = 11.57$. pH values close to pH 11.57 were not included to the study taking into account properties of Ppy [40]. During this experiment sequence of 5 potential pulses of -0.9 V for 10 s and $+0.3$ V vs Ag/AgCl$_{(3M\ KCl)}$ for 10 s was applied.

The surface morphology of the Ppy-PMB, Ppy-PAA and Ppy-PTH layers was evaluated by scanning electron microscope (SEM) TM4000Plus from Hitachi (Japan) and atomic force microscope (AFM) 'Bioscope/Catalyst' from *Bruker* (USA). AFM images were obtained using Contact-mode with a silicone nitride probe coated with a gold reflective layer (tip radius 20 nm, nominal resonant frequency 56 kHz, spring constant 0.24 N/m).

Reflection absorption infrared spectroscopy (RAIRS) data were recorded using Vertex 80v (from Bruker Inc., (Leipzig, Germany)) spectrometer equipped with liquid nitrogen cooled narrow-band MCT detector. Samples were placed onto a horizontal accessory in evacuated (~2 mbar) spectrometer chamber, measurements were conducted at 80 deg angle. The bare ITO substrate was used as a reference. The spectra were taken after incubation of the samples in vacuum for 300 s. Spectral resolution was set to 4 cm^{-1}, aperture to 1.5 mm, scanner velocity to 40 kHz and spectra were acquired by averaging 200 scans.

3. Results and discussions

Scheme of the experiment is demonstrated in Fig. 1B. It shows that a three-electrode system was used during electrochemical deposition of polypyrrole layer modified with a PT derivative. Upon polymerization, the Ppy layer is deposited on the glass/ITO electrode (glass/ITO/

TH R$_1$: NH$_2$ R$_2$: $\overset{+}{N}$H$_2$
MB R$_1$: N(CH$_3$)$_2$ R$_2$: $\overset{+}{N}$(CH$_3$)$_2$
AA R$_1$: NH$_2$ R$_2$: $\overset{+}{N}$(CH$_3$)$_2$
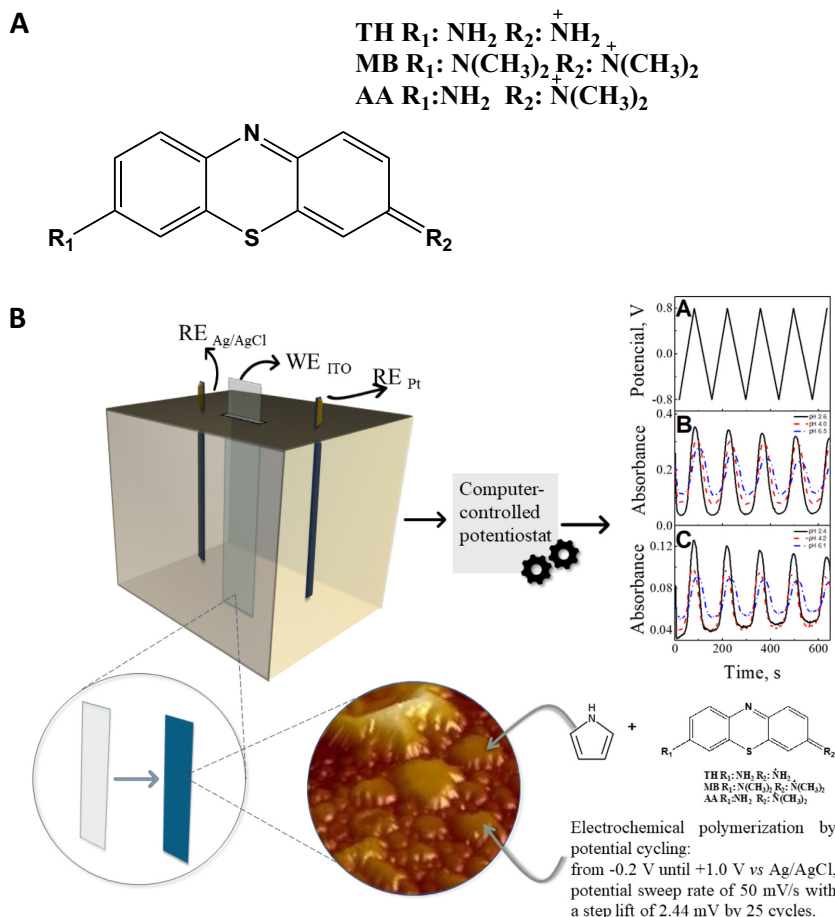
Fig. 1. A. Structures of phenothiazine derivatives (thionine (TH), methylene blue (MB), azure A (AA)). **B.** Experimental setup and electrochromic layer. The three-electrode system consisted of: glass/ITO-based electrode (WE), Ag/AgCl$_{(3M\ KCl)}$ (RE) and platinum wire (CE).

Ppy) and it is clearly visible by naked eye (Fig. 1B) in various shades of dark blue (depending on applied PT derivative). Further, the layers obtained using the three-electrode system were subjected to various voltammetry and chronoamperometry based experiments to elucidate their electrochromic properties with respect to pH changes in the medium. The sensitivity of Ppy-PMB and Ppy-PTH layers towards different concentrations of ascorbic acid was tested.

3.1. Electrochemical deposition of Ppy layers modified by PMB, PAA, PTH on glass/ITO electrode

Cyclic voltammetry is the most widely used technique for acquiring qualitative information about electrochemical reactions. The power of cyclic voltammetry is based on the ability to provide rapidly considerable information on the thermodynamics of redox process, on the kinetics of heterogenous electron-transfer reactions, and on coupled chemical reactions or adsorption processes [41].

Fig. 2A represents CV recorded during electrochemical polymerization of pyrrole and methylene blue on glass/ITO (Ppy-PMB). Initially, when the potential is raised, there was a visible overlap at the beginning of the oxidation process at +0.050 V. This identifies the nucleation and polymer formation on the electrode. The formation of the polymer layer is indicated by the increase of the voltammogram loop width (Fig. 2D, 1 and 2 curves). Both cathodic and anodic currents increase with a number of applied potential cycles until 15th cycle, and later some decrease of the voltammogram loop width has been observed. In some previous researches such reduction of the voltammogram width is associated with some electrochemical degradation of Ppy layer at applied overpotential [42,43]. At the same time the overoxidation of PMB occurs at the potential values higher than 1000 mV [44]. Moreover, in the same study it is claimed that the overoxidized rough surface of PMB layer absorbs remaining unreacted monomer.

Fig. 2B demonstrates CVs recorded by electropolymerization of pyrrole and AA on a glass/ITO electrode. The shape of this CV registered during the polymerization of Ppy-PAA has some similarities to the previously presented CVs registered during the synthesis of Ppy-PMB, with the most pronounced expansion of cyclic voltammogram at +0.55 V vs. Ag/AgCl. Fig. 2C shows cyclic voltammograms recorded by electropolymerization of pyrrole and thionine on a glass/ITO electrode. The overall width of the cyclic voltammogram has increased during polymerization. This reaction shows a strong overlap and a slight increase in the voltammogram width. The oxidation process is identified at −0.07 V and a sharp rise from +0.62 V is observed, which evidences the formation of the polymeric layer.

During the formation of Ppy-PMB layer it can be seen that the beginning of the process is very reminiscent only of the polymerization of pyrrole [40,45] but during the course of polymerization some additional signs of the formation of a polymer coating consisting of both Ppy and PMB becomes visible. At the first polymerization cycle much wider oxidation peak has been observed that indicates the initiation of the oxidation process followed by nucleation. The variation of CV shape, which is observed during the course of polymerization, illustrate that the ongoing formation of polymer layer on the electrode reduces the number of nucleation sites where the polymer can buildup. The width of cyclic voltammogram during the formation of Ppy-PTH ((Fig. 2D 5 and 6 curves) decreased after the first potential cycle, but later it tended continuously to increase until the last potential cycle. The last cyclic voltammograms registered during the formation of Ppy-PMB (Fig. 2D 1 and 2 curves) and Ppy-PAA (Fig. 2D 3 and 4 curves) here presented cases are very widespread, which indicates that the electrochemically active layer becomes rather thick and is failing to discharge and recharge as quickly when the potential of the electrode is changing.

Surface structure and roughness were analysed by AFM. Three different layers (Ppy-PAA (Fig. 3A), Ppy-PTH (Fig. 3B), Ppy-PMB
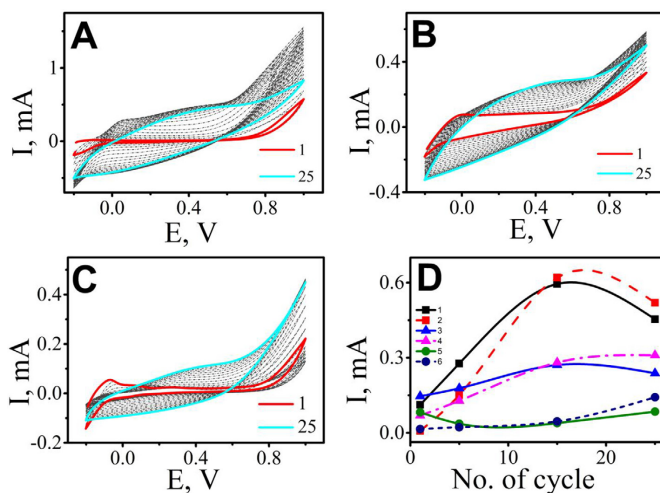

Fig. 2. Electrochemical deposition of Ppy-PMB (**A**), Ppy-PAA (**B**), Ppy-PTH (**C**). The width of the cycle loop in mA (ΔI) was measured during potential cycling at potentials of +0.056 V (1) and +0.40 V (2) for Ppy-PMB, −0.007 V (3) and +0.40 V (4) for Ppy-PAA, −0.073 V (5) and +0.40 V (6) for Ppy-PTH, (**D**). Polymerization solution consisted of 50 mM pyrrole and 10 mM phenothiazine derivative (in water). CV at scan rate of 50 mV/s, from −0.20 V to +1.0 V, 25 cycles, step potential 2.44 mV. Electrochemical polymerization was performed in a three-electrode system, where WE was glass/ITO, RE – Ag/AgCl, and CE – platinum wire.
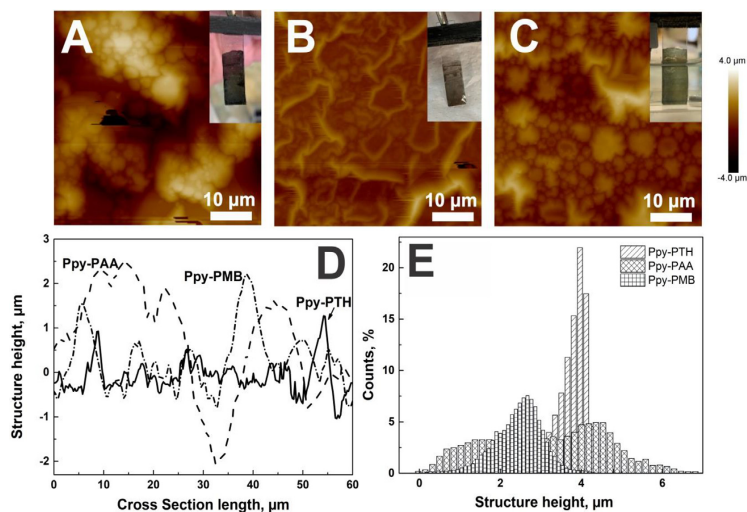
4

Fig. 3. The AFM-based evaluation of Ppy layer surface morphology of all three (**A** – glass/ITO/Ppy-PAA, **B** – glass/ITO/Ppy-PTH, **C** – glass/ITO/Ppy-PMB) electrodes. Imaged area is of 50 μm × 50 μm, the height amplitude for all images was of 8 μm; photographic images of each electrode are presented in corresponding insets. **D** – Comparison of cross sections of all three-electrode surfaces, obtained by AFM measurements. **E** – Height distribution of formed polymeric structures. Other experimental conditions were the same as that reported in Fig. 2.

(Fig. 3C)) were of rather different surface morphology. The roughest surface was observed on Ppy-PAA layer (Fig. 3A), which consisted of large polymerised structures. From the cross section data (Fig. 3 D) it is visible that the width of these structures can reach up to 30 μm and the height of such structures is up to 2–3 μm. In Ppy-PTH layer (Fig. 3B) surface structures were the finest and distributed the most evenly. Formed polymeric layer consisted of small grains and round shape wrinkles. The latter could be formed during layer drying process. Size of the grains do not exceed 1 μm. The surface of Ppy-PMB layer was grained (Fig. 3C), however, the height of the structures distributed from 1 up to 3 μm and the width from 5 to 10 μm. Surface height distribution (Fig. 3E) confirms the former observations drawn from the Figures 3A, 3B and 3C about layers surface roughness. The surface of Ppy-PTH layer is the smoothest and the roughness in this layer is distributed the most evenly, while Ppy-PAA layer is based on the widest structures, and the width of structures that are forming the Ppy-PMB layer is in between of that of Ppy-PTH and Ppy-PAA. Hence, the AFM data illustrate, that the Ppy-PAA layer has the roughest surface, while the Ppy-PMB-based layer is smoother, and the Ppy-PTH-based layer is the smoothest one. Visually Ppy-PAA layer was opaquest and non-translucent at the same polymerization conditions if compared to other two samples, thus confirming our previously presented expectations that this layer is the thickest one.

The structure of the obtained layers was also characterized using scanning electron microscopy (SEM) based imaging. Fig. 4A and 4D represent surface of Ppy-PAA layer, which is the most unevenly distributed, while large polymer agglomerations of different sizes are formed. Fig. 4B and 4E illustrate the surface of Ppy-PMB layer, where fairly smooth but pleated structures are formed. In Fig. 4C and F the surface of Ppy-PTH layer is imaged, this picture illustrates that the structure of this layer consists of larger grains, which are formed round shape folds and in some places they are forming larger agglomerations, while the average particle size is 6 μm. The SEM data confirms the information obtained using the AFM technique. Ppy-PAA layer has

the roughest surface, Ppy-PMB has the smoother one and Ppy-PTH has the smoothest one. Moreover, in SEM and AFM images some wrinkles are observed on the surfaces of Ppy-PTH (Fig. 4F) and Ppy-PMB (Fig. 4E), which possibly have formed during drying of the layer.

The reflection absorption infrared spectroscopy (RAIRS) was chosen due to the possibility to evaluate thin polymer layers and to avoid the influence of glass substrate. For the obtained spectra, the influence of water vapor was removed, baseline correction and min/max normalization were conducted. RAIRS spectra of Ppy-PAA, Ppy-PMB and Ppy-PTH are shown in Fig. 5. The presented spectra were shifted along the y-axis for clarity. At the higher wavenumber region the broad absorption band at 3400 cm^{-1} is associated with N—H bond stretching [46]. 3097 cm^{-1} peak is associated with symmetrical stretching of functional group =C—H of the ring. The peaks 2962 cm^{-1} and 2921 cm^{-1} are antisymmetric stretching of the CH$_3$ and CH$_2$ groups respectively. 2850 cm^{-1} peak is dedicated to CH$_2$ symmetrical stretching with barely noticeable shoulder assigned to symmetric stretching of CH$_3$ group. It could be noted that the biggest difference observed between Ppy-PAA, Ppy-PMB, and Ppy-PTH spectra in higher wavenumber region is related to a conjugated system of aromatic rings', which can be also strongly affected by overoxidation.

In the 'fingerprint' region (Fig. 5B) 1702 cm^{-1} peak corresponds to C=O vibration [47].The presence of this functional group indicates that the polymer chain is overoxidized [46], confirming 3097 cm^{-1} peak variations. The absorption bands in the range from 1560 to 1547 cm^{-1} attributed to pyrrole ring C—C stretching mode [46–49]. The peak at 1480 cm^{-1} can be associated with C—N asymmetric stretching of Py ring [48,49]. 1323 cm^{-1} corresponds to the plane vibration of =C—H [46]. The peak at 1294 cm^{-1} is characteristic band attributed to the N—H in-plane and C—H in-plane vibrations. The peaks in the region of 1200–1170 cm^{-1} are characteristic of pyrrole ring 'breathing-like' vibrations [50]. The peak at 1039 cm^{-1} can be associated with in-plane C—H and N—H stretching vibrations [46–49]. The band corresponding to the C—C out of the plane ring
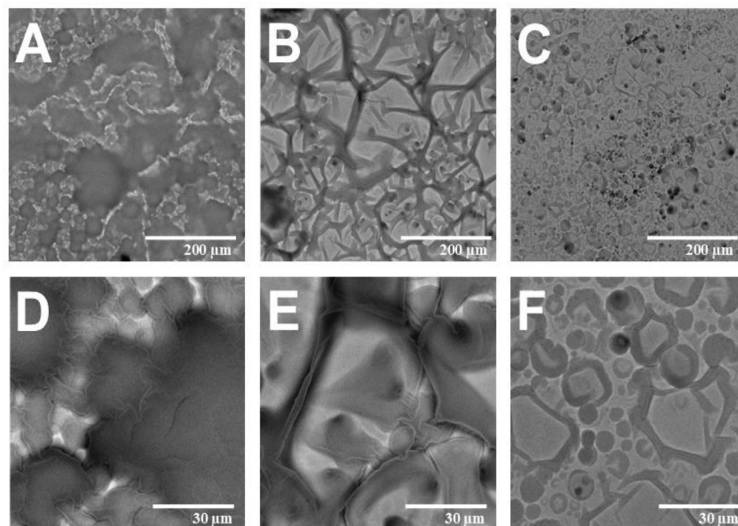
Fig. 4. SEM images of A, D - Ppy-PAA B, E – Ppy-PMB C, F – Ppy-PTH. Magnification for A, B, C was ×500 and for D, E, F was ×3000. Imaged area for A, B, and C is of 87.5 μm × 87.5 μm and for D, E, F is 500 μm × 500 μm.

deformation vibration is situated at 964 cm^{-1} [46] and 923 cm^{-1} [47]. As could be seen from the spectra most of the bands are the same for all of three samples just with some minor differences that the most probably are appearing due to the difference modifiers applied during the formation of these layers.

3.2. The applicability of Ppy-PMB and Ppy-PTH layers in pH and ascorbic acid electrochromic sensors

Research was continued by measuring the optical absorbance spectra of Ppy-PMB, Ppy-PAA and Ppy-PTH layers at pH range from pH 2.0 to pH 8.0. Such pH range was selected because it is the most relevant for the establishment of electrochromic properties of Ppy and taking into account that the conductivity of Ppy in the oxidized form is pH-depended with significant increase of electrical resistance at pH > 12 [40]. The same pH range was also chosen in the work analyzing poly(neutral red) obtained from the phenazine dye neutral red, and poly(methylene green) and poly(methylene blue) (PMB)

[27]. Analysis was carried out in BR-buffer by increasing pH of the medium with NaOH solution (0.10 M). During experiments, higher pH values also were tested, but some shrinking and exfoliation of the polymer layers from the electrode were observed. The most problematic in this respect was Ppy-PAA layer (Fig. 3B) because it was too thick and not translucent, therefore, optical absorbance was not measurable.

Fig. 6 represents optical absorbance of Ppy-PMB (Fig. 6B) and Ppy-PTH (Fig. 6C), which both points the variation of optical absorbance of the phenothiazine-derivative based layers deposited on glass/ITO substrate as a function of the pH of BR-buffer and applied potential value (Fig. 6A). Optical absorbance was measured during potential cycling from −0.8 V to +0.8 V *vs.* Ag/AgCl$_{(3M\ KCl)}$, at potential sweep rate of 50 mV/s applying 5 potential sweep cycles at the specified pH of solution. It was determined that when the medium becomes more alkaline, then optical absorbance decreases, over time it starts to deteriorate. Moreover, it was observed that the registered current of modified glass/ITO electrode also decreased by each potential cycle
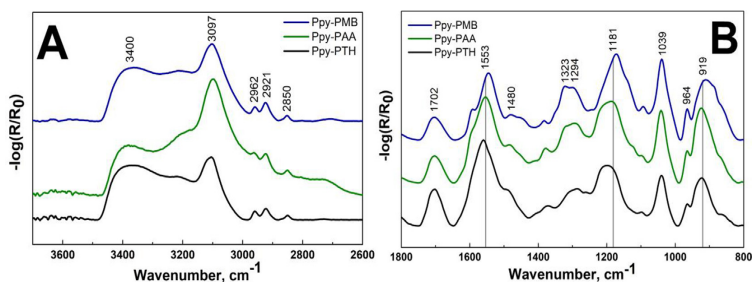
Fig. 5. The RAIRS spectrum at higher wavenumber region (A) and at "fingerprint" region (B) of the Ppy-PT layers (Ppy-PAA, Ppy-PMB, Ppy-PTH). Vertical grey lines in part B are presented for the 'eye-based guidance'.
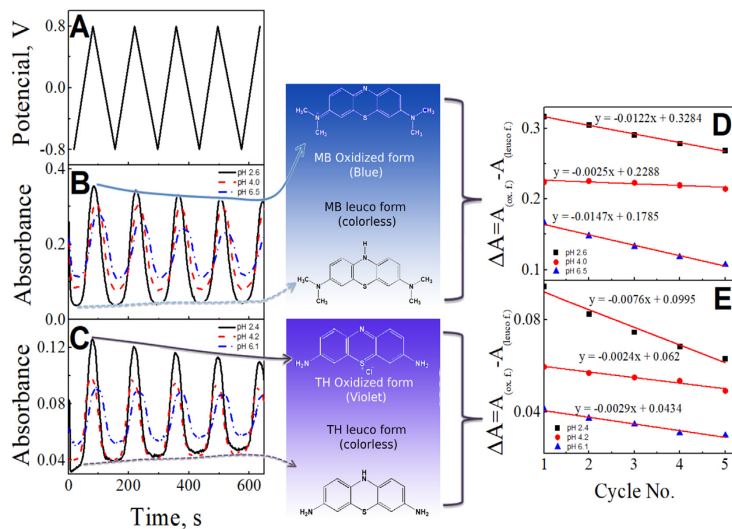
Fig. 6. The dependence of optical absorbance on pH value of the solution. **A**. potential cycling profile. **B** – Ppy-PMB; **C** – Ppy-PTH. BR-buffer with NaOH solution (0.10 M). The shift ΔAbsorbance of oxidized and leuco forms during potential cycling: **D**. ΔAbsorbance of Ppy-PMB; **E**. ΔAbsorbance of Ppy-PTH. Potential cycling conditions: the potential was swept from −0.8 V to +0.8 V *vs* Ag/AgCl$_{(3M\ KCl)}$, potential sweep rate of 50 mV/s, 5 potential cycles were performed.
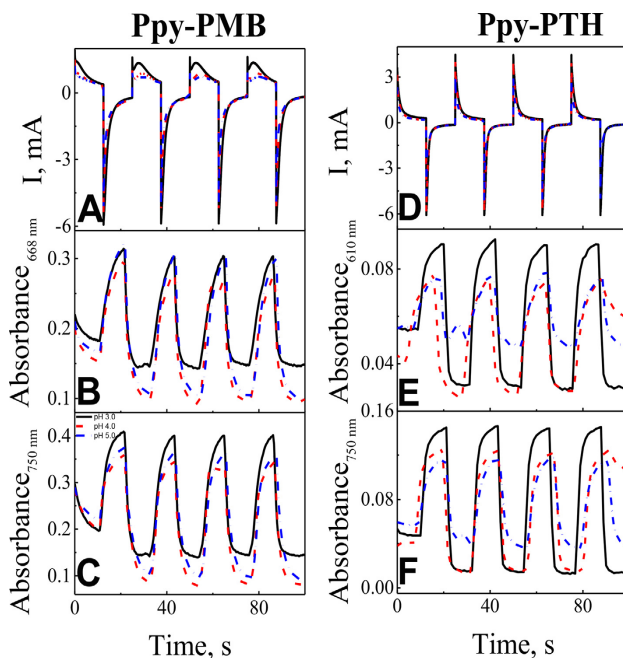
Fig. 7. Chronoamperometric signals at different pHs (at pH 3.0, pH 4.0, and pH 5.0) in the presence of 1 mM of ascorbic acid: **A** – Ppy-PMB layer; **D** – Ppy-PTH layer; and changes of absorbance at three pH values (pH 3.0, pH 4.0 and pH 5.0) of Ppy-PMB at **B** – λ = 668 nm; **C** – λ = 750 nm; and of Ppy-PTH at **E** – λ = 610 nm; **F** – λ = 750 nm. Chronoamperometric signals were registered by applying −0.9 V and +0.3 V *vs.* Ag/AgCl$_{(3M\ KCl)}$ potential pulses. The duration of each potential pulse was 10 s.

7

(Fig. 6D and E). It can be observed that in the case of the formation of Ppy-PMB, the current decreases by 15% (at pH 2.6), 4% (at pH 4.0) and even 35% (at pH 6.5) comparing the first and last cycles. During the investigation of Ppy-PTH layer, the current diminution was 33% (at pH 2.4), 18% (at pH 4.2) and 28% (at pH 6.1). It can be assumed that optical absorbance value decreases with increasing pH value and electrochromic properties of the Ppy-PT-based layer are well observed until pH 6.5. But when pH exceeded value of pH = 6.5, then rapid destruction of the polymeric layer is observed.

Three pH values were selected for the experiment based on the ascorbic acid $pK_{a1} = 4.17$. The electrochromic response of Ppy-PMB and Ppy-PTH layers to the ascorbic acid was analyzed in the concentrations interval from 0 mM until 5 mM, by the increment of 1 mM. In order to provide information well suitable for the evaluation measurement results are presented when the concentration of ascorbic acid was 1 mM (Fig. 7). Chronoamperometric assay was subjected between −0.9 V and + 0.3 V *vs.* Ag/AgCl$_{(3M\ KCl)}$ (the duration of each potential pulse was of 10 s) [40]. Analytical signals were recorded at pH 3.0, pH 4.0, and pH 5.0.

It was determined that the value of optical absorbance for the Ppy-PMB layer is greater than that for the Ppy-PTH layer (Fig. 7) but optical absorbance of both (Ppy-PMB and Ppy-PTH) layers are not significantly changed by the increase of ascorbic acid concentration. The intensity of optical absorbance decreases when the medium becomes more alkaline (Fig. 7).

Fig. 8B, C, E, and F depicts the relationship between the variation of optical absorbance (ΔA) ($\Delta A = A_{0.3\ V} - A_{-0.9\ V}$) on the concentration of ascorbic acid in BR-buffer at pH 3.0, pH 4.0, and pH 5.0. The slope and R^2 values of linear dependence of current or optical absorbance *vs* ascorbic acid concentration of Ppy-PMB, Ppy-PTH layers in BR-buffer at pH 3.0, pH 4.0, and pH 5.0 are represented in Table 1. ΔA dependence on concentration is compared at two selected wavelengths (750 and 610 or 668 nm). It was observed, that when the concentration of ascorbic acid increases, ΔA decreases in all cases. Such changes

can be explained by the electron exchange between phenothiazine and ascorbic acid. This transition results in a change of the color of the corresponding layer. Fig. 8A and D depicts the variation of ΔI *vs* ascorbic acid concentration in BR-buffer at pH 3.0, pH 4.0, and pH 5.0. From the dependence of current on concentration of ascorbic acid it was determined a tendency that with increasing concentration of ascorbic acid both ΔA and ΔI are decreasing. From these calibration curves obtained by these two methods it can be concluded that Ppy-PMB and Ppy-PTH, can be used as the electrochromic sensor suitable for the determination of ascorbic acid concentration.

4. Conclusions

Electrochemical deposition of polypyrrole layer modified with phenothiazine derivatives (methylene blue, azure A and thionine) was performed by cyclic voltammetry with a potential range of −0.2 V to +1.0 V *vs* Ag/AgCl, 50 mV/s, 25 cycles with a step lift of 2.44 mV and in the polymerization mixture containing 10 mM of phenothiazine derivative and 50 mM of pyrrole. The morphology of the layers was analyzed by the AFM method. It was determined that the structure height of Ppy-PAA reached up to 4 μm. This Ppy-PAA layer was the roughest from all three here investigated layers. The Ppy-PTH layer was quite evenly covered on the surface, and this layer was the smoothest one. The SEM data confirmed the information obtained using the AFM technique: the Ppy-PAA layer has the roughest surface, while the Ppy-PMB layer has the smoother one and the Ppy-PTH layer has the smoothest. Also, in SEM images as well as in AFM wrinkles of the layers are observed for Ppy-PTH and Ppy-PMB layers, which the most possibly were formed during the drying of these layers.

The Reflection absorption infrared spectroscopy illustrated that most of the bands were the same for all of the samples just with minor differences the most probably appearing due to different compounds used for polymerization. The electrochromic properties of Ppy-PMB and Ppy-PTH layers were analyzed, however, the Ppy-PAA layer was
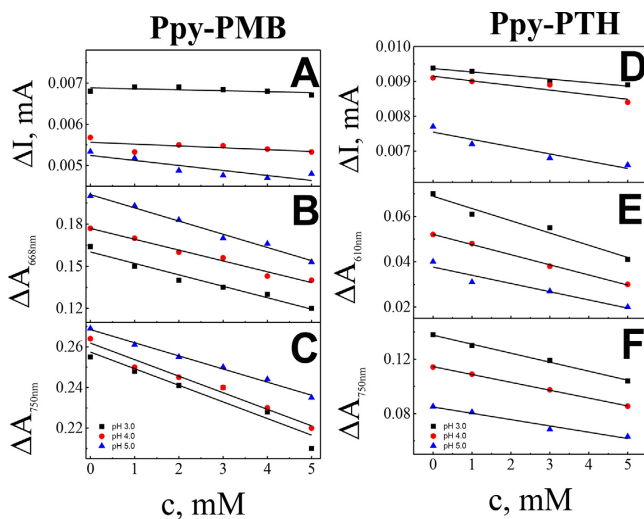

Fig. 8. The calibration curves, which are presenting the chronoamperometric signals at the beginning of the pulse (at different pHs: pH 3.0, pH 4.0, and pH 5.0) *vs.* concentrations of ascorbic acid: **A** – Ppy-PMB and **D** – Ppy-PTH layers. The calibration curves of optical absorbance ($\Delta A = A_{0.3\ V} - A_{-0.9\ V}$) *vs.* concentration of ascorbic acid registered by: **B** – Ppy-PMB layer at wavelength of 668 nm; **C** – Ppy-PMB layer at wavelength of 750 nm; **E** – Ppy-PTH layer at wavelength of 610 nm; **F** – Ppy-PTH layer at wavelength of 750 nm in BR-buffer at pH 3.0, pH 4.0, and pH 5.0 and at the same other conditions as it is described in Fig. 7.

8

Table 1

The slope and R^2 values of linear dependence of current and absorbance of Ppy-PMB, Ppy-PTH layers on the concentration of ascorbic acid in BR-buffer at pH 3.0, pH 4.0, and pH 5.0.

Layer	Name	Description		Slope	R^2
Ppy-PMB	A	ΔI, mA	pH 3.0	−2.314	0.2015
			pH 4.0	−4.457	0.2465
			pH 5.0	−1.213	0.7399
	B	$\Delta Absorbance_{668\ nm}$	pH 3.0	−0.009	0.985
			pH 4.0	−0.007	0.976
			pH 5.0	−0.008	0.958
	C	$\Delta Absorbance_{750\ nm}$	pH 3.0	−0.0064	0.990
			pH 4.0	−0.0081	0.971
			pH 5.0	−0.0081	0.891
Ppy-PTH	D	ΔI, mA	pH 3.0	−1.012	0.940
			pH 4.0	−1.322	0.833
			pH 5.0	−2.085	0.859
	E	$\Delta Absorbance_{610\ nm}$	pH 3.0	−0.005	0.954
			pH 4.0	−0.004	0.997
			pH 5.0	−0.004	0.893
	F	$\Delta Absorbance_{750\ nm}$	pH 3.0	−0.007	0.993
			pH 4.0	−0.006	0.999
			pH 5.0	−0.005	0.957

too thick and non-translucent. Ppy-PMB and Ppy-PTH exhibited electrochromic properties, reacted to pH changes, and ascorbic acid concentration. Color change could be seen in acidic medium and the change of the color was reversible. The obtained color change during potential cycling was the most stable in the BR-buffer at pH 4.0. It can be assumed that electrochromic properties of Ppy-PT-based coatings are well observed up to pH 6.5. The evaluation of absorbance changes in presence of different concentrations of ascorbic acid and by applying potential pulses demonstrated that Ppy-PMB and Ppy-PTH layers can be applied in electrochromic sensors, which can be suitable for the determination of ascorbic acid concentration in aqueous solutions.

CRediT authorship contribution statement

Raimonda Boguzaite: Investigation, Formal analysis, Data curation, Writing - review & editing. **Vilma Ratautaite:** Conceptualization, Methodology, Validation, Visualization, Writing - original draft, Writing - review & editing. **Lina Mikoliunaite:** Investigation, Writing - review & editing. **Vaidas Pudzaitis:** Investigation. **Almira Ramanaviciene:** Conceptualization, Writing - review & editing. **Arunas Ramanavicius:** Supervision, Conceptualization, Writing - review & editing, Funding acquisition.

Declaration of Competing Interest

The authors declare that they have no known competing financial interests or personal relationships that could have appeared to influence the work reported in this paper.

Acknowledgement

Appendix A. Supplementary data

Supplementary data to this article can be found online at https://doi.org/10.1016/j.jelechem.2021.115132.

References

[1] C.G. Granqvist, Oxide electrochromics: an introduction to devices and materials, Sol. Energy Mater. Sol. Cells 99 (2012) 1–13, https://doi.org/10.1016/j.solmat.2011.08.021.

[2] A.A. Argun, P.-H. Aubert, B.C. Thompson, I. Schwendeman, C.L. Gaupp, J. Hwang, N.J. Pinto, D.B. Tanner, A.G. MacDiarmid, J.R. Reynolds, Multicolored electrochromism in polymers: structures and devices, Chem. Mater. 16 (2004) 4401–4412, https://doi.org/10.1021/cm049669l.

[3] Q. Guo, X. Zhao, Z. Li, D. Wang, G. Nie, A novel solid-state electrochromic supercapacitor with high energy storage capacity and cycle stability based on poly (5-formylindole)/WO3 honeycombed porous nanocomposites, Chem. Eng. J. 384 (2020) 123370, https://doi.org/10.1016/j.cej.2019.123370.

[4] Y.R. In, Y.M. Kim, Y. Lee, W.Y. Choi, S.H. Kim, S.W. Lee, H.C. Moon, Ultra-low power electrochromic heat shutters through tailoring diffusion-controlled behaviors, ACS Appl. Mater. Interfaces 12 (2020) 30635–30642, https://doi.org/10.1021/acsami.0c05918.

[5] T.Y. Yun, X. Li, S.H. Kim, H.C. Moon, Dual-function electrochromic supercapacitors displaying real-time capacity in color, ACS Appl. Mater. Interfaces 10 (2018) 43993–43999, https://doi.org/10.1021/acsami.8b15066.

[6] H. Oh, J.K. Lee, Y.M. Kim, T.Y. Yun, U. Jeong, H.C. Moon, User-customized, multicolor, transparent electrochemical displays based on oxidatively tuned electrochromic ion gels, ACS Appl. Mater. Interfaces 11 (2019) 45959–45968, https://doi.org/10.1021/acsami.9b15288.

[7] P. Andersson Ersman, J. Kawahara, M. Berggren, Printed passive matrix addressed electrochromic displays, Org. Electron. 14 (2013) 3371–3378, https://doi.org/10.1016/j.orgel.2013.10.008.

[8] Q. Guo, X. Zhao, Z. Li, B. Wang, D. Wang, G. Nie, High performance multicolor intelligent supercapacitor and its quantitative monitoring of energy storage level by electrochromic parameters, ACS Appl. Energy Mater. 3 (2020) 2727–2736, https://doi.org/10.1021/acsaem.9b02392.

[9] K. Hyodo, Electrochromism of conducting polymers, Electrochim Acta 39 (1994) 265–272, https://doi.org/10.1016/0013-4686(94)80062-6.

[10] M.A. Deshmukh, M. Gicevicius, A. Ramanaviciene, M.D. Shirsat, R. Viter, A. Ramanavicius, Hybrid electrochemical/electrochromic Cu(II) ion sensor prototype based on PANI/ITO-electrode, Sensors Actuators, B Chem. 248 (2017) 527–535, https://doi.org/10.1016/j.snb.2017.03.167.

[11] P. Moarref, M. Pishvaei, A. Soleimani-Gorgani, F. Najafi, Synthesis of polypyrrole/indium tin oxide nanocomposites via miniemulsion polymerization, Des. Monomers Polym. 19 (2016) 138–144, https://doi.org/10.1080/15685551.2015.1124321.

[12] S.S. Shinde, J.A. Kher, A review on polyaniline and its noble metal composites, Int. J. Innov. Res. Sci. Eng. Technol. 03 (2014) 16570–16576, https://doi.org/10.15680/ijirset.2014.0310023.

[13] G. Sabouraud, S. Sadki, N. Brodie, The mechanisms of pyrrole electropolymerization, Chem. Soc. Rev. 29 (2000) 283–293, https://doi.org/10.1039/a807124a.

[14] A. Erdem, K. Kerman, B. Meric, U.S. Akarca, M. Ozsoz, Novel hybridization indicator methylene blue for the electrochemical detection of short DNA sequences related to the hepatitis B virus, Anal. Chim. Acta 422 (2000) 139–149, https://doi.org/10.1016/S0003-2670(00)01058-8.

[15] V. Pfaffen, P.I. Ortiz, S.I. Córdoba de Torresi, R.M. Torresi, On the pH dependence of electroactivity of poly(methylene blue) films, Electrochim. Acta 55 (2010) 1766–1771, https://doi.org/10.1016/j.electacta.2009.10.062.

[16] F. Li, Y. Guo, X. Sun, X. Wang, Aptasensor based on thionine, graphene-polyaniline composite film, and gold nanoparticles for kanamycin detection, Eur. Food Res. Technol. 239 (2014) 227–236, https://doi.org/10.1007/s00217-014-2211-2.

[17] B. Liu, H. Cang, L. Cui, H. Zhang, Electrochemical polymerization of methylene blue on glassy carbon electrode, Int. J. Electrochem. Sci. 12 (2017) 9907–9913, https://doi.org/10.20964/2017.10.49.

[18] R.M. Ion, F. Scarlat, F. Scarlat, V.I.R. Niculescu, Methylene - Blue modified polypyrrole film electrode for optoelectronic applications, J. Optoelectron. Adv. Mater. 5 (2003) 109–115.

[19] S.B. Adeloju, M. Sohail, Azure a mediated polypyrrole-based amperometric nitrate biosensor, Electroanalysis 23 (2011) 987–996, https://doi.org/10.1002/elan.201000386.

[20] Q. Gao, X. Cui, F. Yang, Y. Ma, X. Yang, Preparation of poly(thionine) modified screen-printed carbon electrode and its application to determine NADH in flow injection analysis system, Biosens. Bioelectron. 19 (2003) 277–282, https://doi.org/10.1016/S0956-5663(03)00212-4.

[21] R. Ansari, Polypyrrole conducting electroactive polymers: synthesis and stability studies, E-Journal Chem. 3 (2006) 186–201, https://doi.org/10.1155/2006/860413.

[22] S. Machida, S. Miyata, A. Techagumpuch, Chemical synthesis of highly electrically conductive polypyrrole, Synth. Met. 31 (1989) 311–318, https://doi.org/10.1016/0379-6779(89)90798-4.

[23] C. Chen, S. Mu, Electrochemical polymerization of azure A and properties of poly (azure A), J. Appl. Polym. Sci. 88 (2003) 1218–1224, https://doi.org/10.1002/app.11780.

[24] A.A. Karyakin, A.K. Strakhova, E.E. Karyakina, S.D. Varfolomeyev, A.K. Yatslmirsky, The electrochemical polymerization of Methylene Blue and bioelectrochemical activity of the resulting film, Synth. Met. 60 (1993) 289–292, https://doi.org/10.1016/0379-6779(93)91294-C.

[25] X. Kong, A.P. Kulkarni, S.A. Jenekhe, Phenothiazine-based conjugated polymers: synthesis, electrochemistry, and light-emitting properties, Macromolecules 36 (2003) 8992–8999, https://doi.org/10.1021/ma035087y.

[26] R. Viveiros, S. Rebocho, T. Casimiro, Green strategies for molecularly imprinted polymer development, Polymers (Basel) 10 (2018) 306, https://doi.org/10.3390/polym10030306.

[27] M.M. Barsan, E.M. Pinto, C.M.A. Brett, Electrosynthesis and electrochemical characterisation of phenazine polymers for application in biosensors, Electrochim. Acta 53 (2008) 3973–3982, https://doi.org/10.1016/j.electacta.2007.10.012.

[28] E. Topçu, M. Alanyalıoğlu, Electrochemical formation of poly(thionine) thin films: the effect of amine group on the polymeric film formation of phenothiazine dyes, J. Appl. Polym. Sci. 131 (2014) n/a–n/a, https://doi.org/10.1002/app.39686.

[29] F.S. Damos, R.C.S. Luz, L.T. Kubota, Study of poly(methylene blue) ultrathin films and its properties by electrochemical surface plasmon resonance, J. Electroanal. Chem. 581 (2005) 231–240, https://doi.org/10.1016/j.jelechem.2005.04.021.

[30] N. Ajami, A. Ehsani, F. Babaei, R. Safari, Electrochemical properties, optical modeling and electrocatalytic activity of pulse-electropolymerized ternary nanocomposite of poly (methylene blue) in aqueous solution, J. Mol. Liq. 215 (2016) 24–30, https://doi.org/10.1016/j.molliq.2015.12.023.

[31] A. Ehsani, N. Ajami, F. Babaei, H. Mostaanzadeh, Electrosynthesis and characterization of poly methylene blue and its nanocomposite with ZnO nanoparticles, Synth. Met. 197 (2014) 80–85, https://doi.org/10.1016/j.synthmet.2014.08.017.

[32] R. Pauliukaite, M.E. Ghica, M.M. Barsan, C.M.A. Brett, Phenazines and polyphenazines in electrochemical sensors and biosensors, Anal. Lett. 43 (2010) 1588–1608, https://doi.org/10.1080/00032711003653791.

[33] P. Kara, K. Kerman, D. Ozkan, B. Meric, A. Erdem, Z. Ozkan, M. Ozsoz, Electrochemical genosensor for the detection of interaction between methylene blue and DNA, Electrochem. Commun. 4 (2002) 705–709, https://doi.org/10.1016/S1388-2481(02)00428-9.

[34] P.K. Sharma, G. Gupta, V.V. Singh, B.K. Tripathi, P. Pandey, M. Boopathi, B. Singh, R. Vijayaraghavan, Synthesis and characterization of polypyrrole by cyclic

[35] voltammetry at different scan rate and its use in electrochemical reduction of the simulant of nerve agents, Synth. Met. 160 (2010) 2631–2637, https://doi.org/10.1016/j.synthmet.2010.10.016.

[35] J. Liu, S. Mu, Electrochemical polymerization of methylene blue and properties of polymethylene blue, Synth. Met. 107 (1999) 159–165, https://doi.org/10.1016/S0379-6779(99)00146-0.

[36] C.L. Sun, H.H. Lee, J.M. Yang, C.C. Wu, The simultaneous electrochemical detection of ascorbic acid, dopamine, and uric acid using graphene/size-selected Pt nanocomposites, Biosens. Bioelectron. 26 (2011) 3450–3455, https://doi.org/10.1016/j.bios.2011.01.023.

[37] B. Frei, Ascorbic acid protects lipids in human plasma and low-density lipoprotein against oxidative damage, Am. J. Clin. Nutr. 54 (1991) 1113S–1118S, https://doi.org/10.1093/ajcn/54.6.1113sa.

[38] B. Kaur, T. Pandiyan, B. Satpati, R. Srivastava, Simultaneous and sensitive determination of ascorbic acid, dopamine, uric acid, and tryptophan with silver nanoparticles-decorated reduced graphene oxide modified electrode, Colloids Surfaces B Biointerfaces. 111 (2013) 97–106, https://doi.org/10.1016/j.colsurfb.2013.05.023.

[39] C.G. Fraga, P.A. Motchnik, M.K. Shigenaga, H.J. Helbock, R.A. Jacob, B.N. Ames, Ascorbic acid protects against endogenous oxidative DNA damage in human sperm, Proc. Natl. Acad. Sci. U. S. A. 88 (1991) 11003–11006, https://doi.org/10.1073/pnas.88.24.11003.

[40] V. Ratautaite, G. Bagdziunas, A. Ramanavicius, A. Ramanaviciene, An application of conducting polymer polypyrrole for the design of electrochromic pH and CO 2 sensors, J. Electrochem. Soc. 166 (2019) B297–B303, https://doi.org/10.1149/2.1221904jes.

[41] J. Wang, Analytical electrochemistry, Second ed., New York, 2001.

[42] C.M. Li, C.Q. Sun, W. Chen, L. Pan, Electrochemical thin film deposition of polypyrrole on different substrates, Surf. Coatings Technol. 198 (2005) 474–477, https://doi.org/10.1016/j.surfcoat.2004.10.065.

[43] V. Ratautaite, A. Ramanaviciene, Y. Oztekin, J. Voronovic, Z. Balevicius, L. Mikoliunaite, A. Ramanavicius, Electrochemical stability and repulsion of polypyrrole film, Colloids Surfaces A Physicochem. Eng. Asp. 418 (2013) 16–21, https://doi.org/10.1016/j.colsurfa.2012.10.052.

[44] İ.H. Kaplan, K. Dağcı, M. Alanyalıoğlu, Nucleation and growth mechanism of electropolymerization of methylene blue: the effect of preparation potential on poly(methylene blue) structure, Electroanalysis 22 (2010) 2694–2701, https://doi.org/10.1002/elan.201000304.

[45] B. Schweiger, J. Kim, Y. Kim, M. Ulbricht, Electropolymerized molecularly imprinted polypyrrole film for sensing of clofibric acid, Sensors 15 (2015) 4870–4889, https://doi.org/10.3390/s150304870.

[46] F. López García, G. Canché-Escamilla, A. Ocampo-Flores, P. Roquero, L. Ordonez, Controlled size nano-polypyrrole synthetized in micro- emulsions as Pt support for the ethanol electro-oxidation reaction, Int. J. Electrochem. Sci. 8 (2013) 3794–3813.

[47] A. Nan, I. Craciunescu, R. Turcu, Aspects on Fundaments and Applications of Conducting Polymers, 2012. https://doi.org/10.5772/1106.

[48] N. Su, H.B. Li, S.J. Yuan, S.P. Yi, E.Q. Yin, Synthesis and characterization of polypyrrole doped with anionic spherical polyelectrolyte brushes, Express Polym. Lett. 6 (2012) 697–705, https://doi.org/10.3144/expresspolymlett.2012.75.

[49] T. Wu, H. Chang, Y. Lin, Synthesis and characterization of conductive polypyrrole with improved conductivity and processability, Polym. Int. 58 (2009) 1065–1070, https://doi.org/10.1002/pi.2634.

[50] S. Maruthamuthu, J. Chandrasekaran, D. Manoharan, R. Magesh, Conductivity and dielectric analysis of nanocolloidal polypyrrole particles functionalized with higher weight percentage of poly (styrene sulfonate) using the dispersion polymerization method, J. Polym. Eng. 37 (2016) 481–492, https://doi.org/10.1515/polyeng-2015-0321.

10

2nd publication / 2 publikacija

V. Ratautaite, **R. Boguzaite**, M.B. Mickeviciute, L. Mikoliunaite, U. Samukaite-Bubniene, A. Ramanavicius, A. Ramanaviciene,

Evaluation of Electrochromic Properties of Polypyrrole/Poly(Methylene Blue) Layer Doped by Polysaccharides,

Sensors, 22 (2022) 232.

Article

Evaluation of Electrochromic Properties of Polypyrrole/Poly(Methylene Blue) Layer Doped by Polysaccharides

Vilma Ratautaite [1,2], **Raimonda Boguzaite** [1,2], **Migle Beatrice Mickeviciute** [2], **Lina Mikoliunaite** [2,3], **Urte Samukaite-Bubniene** [1,2], **Arunas Ramanavicius** [1,2,4] and **Almira Ramanaviciene** [4,*]

1. Laboratory of Nanotechnology, Department of Functional Materials and Electronics, Center for Physical Sciences and Technology, Sauletekio Ave. 3, LT-10257 Vilnius, Lithuania; vilma.ratautaite@ftmc.lt (V.R.); raimonda.boguzaite@ftmc.lt (R.B.); urte.samukaite-bubniene@chf.vu.lt (U.S.-B.); arunas.ramanavicius@chf.vu.lt (A.R.)
2. Department of Physical Chemistry, Faculty of Chemistry and Geosciences, Institute of Chemistry, Vilnius University, Naugarduko Str. 24, LT-03225 Vilnius, Lithuania; miglebeatricemick@gmail.com (M.B.M.); lina.mikoliunaite@chf.vu.lt (L.M.)
3. Laboratory of Spectroelectrochemistry, Department of Organic Chemistry, Center for Physical Sciences and Technology, Sauletekio Ave. 3, LT-10257 Vilnius, Lithuania
4. NanoTechnas—Center of Nanotechnology and Materials Science, Faculty of Chemistry and Geosciences, Institute of Chemistry, Vilnius University, Naugarduko Str. 24, LT-03225 Vilnius, Lithuania
* Correspondence: almira.ramanaviciene@chf.vu.lt

Abstract: Polypyrrole (Ppy) and poly(methylene blue) (PMB) heterostructure (Ppy-PMB) was electrochemically formed on the indium tin oxide (ITO) coated glass slides, which served as working electrodes. For electropolymerization, a solution containing pyrrole, methylene blue, and a saccharide (lactose, sucrose, or heparin) that served as dopant was used. The aim of this study was to compare the effect of the saccharides (lactose, sucrose, and heparin) on the electrochromic properties of the Ppy-PMB layer. AFM and SEM have been used for the analysis of the surface dominant features of the Ppy-PMB layers. From these images, it was concluded that the saccharides used in this study have a moderate effect on the surface morphology. Electrochromic properties were analyzed with respect to the changes of absorbance of the layer at two wavelengths (668 nm and 750 nm) by changing the pH of the surrounding solution and the potential between +0.8 V and −0.8 V. It was demonstrated that the highest absorbance changes are characteristic for all layers in the acidic media. Meanwhile, the absorbance changes of the layers were decreased in the more alkaline media. It was determined that the Ppy-PMB layers with heparin as a dopant were more mechanically stable in comparison to the layers doped with lactose and sucrose. Therefore, the Ppy-PMB layer doped with heparin was selected for the further experiment and it was applied in the design of electrochromic sensors for the determination of three xanthine derivatives: caffeine, theobromine, and theophylline. A linear relationship of ΔA ($\Delta A = A_{+0.8V} - A_{-0.8V}$) vs. concentration was determined for all three xanthine derivatives studied. The largest change in optical absorption was observed in the case of theophylline determination.

Keywords: methylene blue; polypyrrole (Ppy); polysaccharides; heparin; electrochromic polymers; caffeine; theophylline; theobromine

1. Introduction

Electrochromic properties are characteristic features not only for non-organic materials but also for some conjugated (conducting) polymers (e.g., polypyrrole (Ppy) and poly(methylene blue) (PMB) possess remarkable electrochromic properties). In conducting polymers, electrochromism occurs due to changes in the π-π conjugated electronic system and the ability to participate in electrochemical oxidation and reduction. Electrochromism

describes the phenomenon in which the color of the material depends on the applied potential. The key parameters of the electrochromism are (i) response time; (ii) optical contrast; (iii) electrochromic efficiency; (iv) durability; and (v) optical memory [1].

Ppy is one of the most analyzed conducting polymers used for the development of various types of sensors. Ppy is easily synthesized by chemical [2–4], enzymatic [5,6], electrochemical [7–9], or other methods. Firstly, it was synthesized electrochemically by A. F. Diaz and K. Keiji Kanazawa. The resulting layer was characterized by appropriate adsorption and high conductivity [10].

Methylene blue (MB) is a phenothiazine (PT) derivative (Figure 1). This is a hetero-cyclic organic compound, which is well known for biomedical applications. In analytical chemistry, it is used as a redox mediator that undergoes color changes from bright blue to colorless when the oxidized form becomes reduced [11]. In previous studies, cyclic voltammetry was the mostly applied method for the electrochemical polymerization of PMB [11–16].
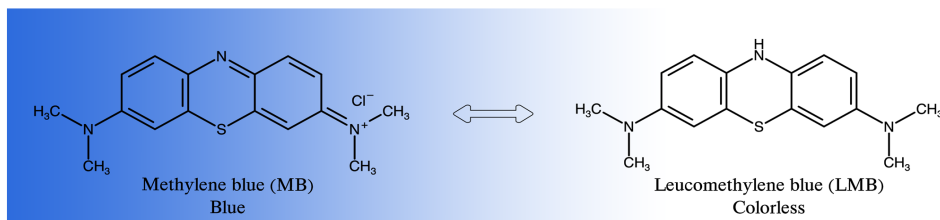
Figure 1. Chemical structures of methylene blue and leucomethylene blue.

Overall, electrochemical polymerization has a remarkable advantage as polymer preparation method due to the ability to form layers with controllable properties on various types and shapes of electrodes. The controllable parameters of the electrochemical poly-merization include the value of potential or current density, time, electrochemical method (cyclic voltammetry (CV), chronoamperometry, etc.).

Moreover, the composition and pH of the polymerization mixture also have a signifi-cant influence on the properties, including electrochromic ones, of the polymer layer [17]. The conductivity of Ppy can be effectively tuned by a careful selection of dopants [18–20]. In most cases, small ions of strong acids are used as dopants, for instance, chloride [21], sulfate [8], perchlorate [22], iodine [23], and others. Small ions of a weak acid can be used as dopants too, for example, carboxylates [18]. Among the various dopants, saccharides are special substances [19,24,25]. The characteristics of polypyrrole-polysaccharide thin layers and the influence of three polysaccharides, namely, heparin, chondroitin-4-sulphate, and hyaluronic acid on the polypyrrole chemical and physicochemical properties were evaluated [19]. The polypyrrole layers in the aforementioned study were deposited on the ITO electrodes. This study found a strong correlation between the sample morphology and the current density during polymerization of Ppy in the presence of polysaccharides: a smooth surface morphology was observed when the current density was in the range of 100–700 $\mu A/cm^2$, whereas high current (synthesis charge > 1.0 mA/cm^2) or longer time (synthesis charge > 100 mC/cm^2) led to form rough surfaces. It is noteworthy that in the above-mentioned study, extremely high concentrations of pyrrole (1 M) and doping anion (heparin, hyaluronic acid, or chondroitin-4-sulphate) (2.0 mg/mL) were used. Water, propylene carbonate, and acetonitrile were used as different solvents for the preparation of polymerization mixtures containing pyrrole and heparin as a polyanion [24]. The Ppy layer was deposited on the fluorine-doped tin oxide (FTO)-coated glass surface. The aforemen-tioned study evaluated the electrochromic contrast and redox stability. Ppy layer doped by heparin was characterized by cyclic voltammetry and by in situ spectroelectrochemistry. It was concluded that the presence of heparin caused a drastic enhancement of electro-optical

stability of Ppy. The evaluation of surface dominant features has demonstrated a Ppy and heparin layer composed of quasi-spherical grains (50–80 nm in dimensions). The layers were grown anodically at constant potential mode at 0.8 V vs. Ag/AgCl and by passing a charge of 100 mC from aqueous solution containing 0.1 M pyrrole and 0.01 mg/mL heparin. The previous works demonstrated the effect of polysaccharides on Ppy properties, but the understanding of the impact on the electric and electrochromic properties of Ppy can still be improved, for instance, stability and response speed.

Several studies describing the combination of Ppy and PMB have been published [26–31]. The results of electrochemical polymerization of pyrrole are better when the polymerization is carried out in an acidic solution, preferably ≤pH 7 [17,32]. The pH of the solution for polymerization of methylene blue is preferably around pH 6.0. An electrochemical activity of PMB after polymerization is well established as good and reversible in the pH region from 2.0 to 8.0 [14]. Usually, salts such as KCl, Na_2SO_4, etc. are added to ensure ionic strength in the polymerization mixture formulation. In the polymerization mixture of pyrrole and methylene blue, no additional salts are required because methylene blue itself acts as a supporting electrolyte [26]. Regarding the optimal pH values for polymerization of pyrrole and methylene blue, the sandwich-type of Ppy-PMB layer was formed. Such sandwich-type of the layer was obtained in two steps of polymerization of Ppy and PMB. In the first polymerization step, Ppy was electro-polymerized on the electrode from solution at low pH and in the second step, PMB was electro-polymerized from solution at high pH [27,28]. Such sandwich-type of Ppy-PMB layer was applied as a mediator in a microbial fuel cell with a Ppy-PMB composite electrode [27], and as an additive that was able to decrease significantly the charge transfer resistance of Ppy [28]. In previous studies, Ppy-PMB layers were also used for optoelectronic applications [26], as a photosensitizer for medical applications in deep tissue treatment [29], or in the solid-state photo-electrochemical cells [30]. Summarizing the aforementioned studies, we can see that although the Ppy and PMB co-deposited layer have been previously studied, the electrochromic properties of such a layer, especially of the Ppy-PMB doped with heparin, have not been studied yet. In addition, the possibility of applying the Ppy-PMB layer as an electrochromic sensor has been very little investigated. The most recent study of application of Ppy-PMB was published by our scientific group [31].

Therefore, the aim of this study was to co-deposit the Ppy-PMB layer on the ITO electrode in the presence of three saccharides (lactose, sucrose, and heparin) during a single-step procedure and compare the effect of different saccharides on the electrochromic properties. The properties of the layer were analyzed with respect to the changes of absorbance by changing the pH of the surrounding solution. The most mechanically stable layer was tested as an electrochromic sensor for xanthine derivatives. This study demonstrates that Ppy-PMB can be used in the design of electrochromic sensors.

2. Materials and Methods

2.1. Chemicals and Materials

Ultra-pure H_2O was obtained by Crystal 7 water purification system received from Adrona (Riga, Latvia). The conductivity of purified water was 0.055 μS/cm. The pyrrole was purchased from Sigma-Aldrich (Darmstadt, Germany) and was distilled before use. Methylene blue from Alfa Aesar (Karlsruhe, Germany), lactose (Lac) from Carl Roth (Karlsruhe, Germany), sucrose (Suc) from Fluka (Darmstadt, Germany), heparin (Hep) from Rotexmedica (Trittau, Germany), and acetone from Reachem (Petržalka, Slovakia) were of analytical grade and were used as obtained. Ammonium hydroxide (27%) and hydrogen peroxide (30%) were from Chempur (Piekary Śląskie, Poland). Xanthine derivatives used in this study were theophylline, caffeine from Sigma Aldrich (Germany), and theobromine from Alfa Aesar (Germany).

Britton–Robinson buffer (BRB) solution [33] was made of 0.01 M boric acid from Scharlau (Barcelona, Spain), 0.01 M acetic acid from Carl Roth (Germany), and 0.01 M phosphoric acid from Fluka (Germany). The ionic strength of BRB was supported with

0.1 M potassium chloride from Scharlau (Spain). The pH of solutions to the required value was adjusted with 1 M sodium hydroxide from Merck (Darmstadt, Germany).

2.2. Pretreatment of ITO-Coated Glass Slide

Pretreatment of ITO-coated glass slide was carried out as it was described in a previous study [22]. ITO-coated glass slide (glass/ITO) with surface resistivity of 15–25 Ω/cm^2 was purchased from Sigma-Aldrich (Steinheim, Germany). Glass/ITO surface was washed in a solution consisting of 27% NH_4OH and 30% H_2O_2 mixed at ratio 3:1 and preheated up to 50 °C degrees for 4 min. Later on, glass/ITO was treated by ultrasound subsequently in water, acetone, and water for 15 min in each liquid. After the pretreatment procedure, the glass/ITO was dried out with argon stream and stored in dry conditions.

2.3. Co-Deposition of Ppy-PMB Layer on ITO Glass Electrode

A computer-controlled potentiostat/galvanostat PGSTAT 128N equipped with Nova 1.10 software from Eco-Chemie (Utrecht, The Netherlands) was used for electrochemical polymerization of conducting polymer and electrochemical measurements. A three-electrode system was applied for all electrochemical depositions. Ag/AgCl wire was used as a reference electrode and platinum wire as a counter electrode (CH Instruments, Austin, TX, USA). ITO electrode was used as a working electrode. The electrochemical deposition was carried out from a solution containing of 50 mM of pyrrole, 10 mM of methylene blue, and one of the doping materials: 0.1 M Lac, 0.1 M Suc, or 0.01 g/L Hep. The formed Ppy and PMB layers doped with saccharides were indicated as (Ppy-PMB)$_{Lac}$, (Ppy-PMB)$_{Suc}$, and (Ppy-PMB)$_{Hep}$. The parameters of electrochemical polymerization were selected according to our previous research [31]. Polymerization was performed at a room temperature during 25 potential cycles in the range from −0.5 V to +1.2 V vs. Ag/AgCl, at the sweep rate of 50 mV/s and step potential of 2.44 mV.

2.4. Evaluation of Dominant Features by Atomic Force Microscopy and Scanning Electron Microscopy

Visualization and evaluation of surface dominant features were performed by atomic force microscope (AFM) 'Bioscope/Catalyst' from Bruker (Santa Barbara, CA, USA). AFM images were obtained with a silicon nitride probe coated with a gold reflective layer (tip radius 20 nm, nominal resonant frequency 56 kHz, spring constant 0.24 N/m). Additionally, layers were evaluated using scanning electron microscope (SEM) TM4000-Plus from Hitachi (Hitachinaka, Japan).

2.5. Evaluation of Electrochromic Properties of Ppy-PMB Layer at Different PH of the Solution

A spectrometer USB4000-FL equipped with SpectraSuite software was purchased from Ocean Optics (Largo, FL, USA) and was used for optical measurements.

The changes of pH were followed with pH-meter ProLine Plus (Q-i-s, Oosterhout, The Netherlands) in BRB with 0.1 M KCl solution by increasing the pH with 1 M NaOH. Continuous measurements of the UV absorbance at particular wavelengths (668 nm and 750 nm) vs. time were performed at each pH value of BRB solution. Appropriate wavelengths were selected taking into account the absorbance spectra of methylene blue with the maximum at 668 nm [34] and of Ppy with the maximum at 750 nm [22].

Different reference electrodes were used during co-deposition of Ppy-PMB and evaluation of electrochromic response. Ag/AgCl$_{(3M\ KCl)}$ (CH Instruments, Austin, TX, USA) was used as a reference electrode and platinum wire as a counter electrode. ITO electrode modified with Ppy-PMB layer was used as a working electrode.

A potential pulse sequence (PPS) was applied to evaluate the electrochromic properties of Ppy-PMB layer. Potential pulses were +0.8 V and −0.8 V. Duration of the pulse was 10 s. Each potential was repeated 5 times.

2.6. Application of (Ppy-PMB)$_{Hep}$ Layer for Sensing Xanthine Derivatives

The ITO electrode coated with (Ppy-PMB)$_{Hep}$ layer was used for sensing of xanthine derivatives. The changes of absorbance at different theophylline, theobromine, and caffeine concentrations and potential values were evaluated. The potential was alternated in BRB with 0.1 M KCl, pH 2.5 according to the following procedure: +0.8 V for 10 s, then −0.8 V for 10 s. Each potential was replicated 5 times. The changes of absorbance were registered at 668 nm and 750 nm wavelengths.

3. Results

In the previous study, it was mentioned that some destruction of Ppy-Phenothiazine (Ppy-PT) layer on ITO electrode was observed at a certain pH value [31]. To overcome such limitation, some measures can be applied: (1) modification of the ITO electrode surface with silanes without specific functional groups in order to form the silane-based self-assembled monolayers (SAM) and so to improve the non-covalent interaction of the polymer layer with electrode surface [22] or with silane-based SAM with pyrrolyl end-groups, e.g., 11-(1H-Pyrrol-1-yl)undecane-1-thiol; (2) doping with some polysaccharides, for example, heparin, which can be electrochemically incorporated into Ppy to enhance adhesion [19,24].

Electrochemical polymerization of Ppy-PMB layers doped with lactose (Lac), sucrose (Suc), and heparin (Hep) was carried out by conditions described in Section 2.3. In total, 25 potential cycles were applied to obtain the layers. The voltammograms obtained during electropolymerization by potential cycling are represented in Figure 2A–C. Comparison of the current changes obtained during the first cycle demonstrates the visible cathodic peak of current at the beginning of the oxidation process at −0.20 V for the (Ppy-PMB)$_{Lac}$, −0.28 V for the (Ppy-PMB)$_{Suc}$, and −0.277 V for the (Ppy-PMB)$_{Hep}$ layers. This increment of current could identify the beginning of polymer formation on the ITO electrode. During the next potential cycles, it was observed that the cathodic peak was moved to the higher potential values.

The comparison of the current changes obtained during electropolymerization of Ppy-PMB described in this and other studies demonstrate that the shift of cathodic peak depends on the type of electrode and other polymerization conditions, such as composition of the solution, pH, etc. The cathodic peak of methylene blue on platinum foil was at −0.22 V and it is attributed to the oxidation of methylene blue [14]. The oxidation peak of methylene blue during electropolymerization on the gold electrode moved to more negative potential values ($\approx$−0.4 V) [15], whereas the oxidation peak ($\approx$−0.255 V) of methylene blue during electro-polymerization on glassy carbon electrode was very similar as it was obtained in this study on ITO electrode. Thus, this confirms that the cathodic peak at the $\approx$−0.2 V (Figure 2A–C) is attributed to the oxidation of methylene blue.

The oxidation peak of pyrrole usually is less expressed than the oxidation peak of methylene blue. In the previous study, it was demonstrated that polymerization of pyrrole on ITO electrode depending on the modification of electrode surface started at +0.53 and +0.70 V vs. Ag/AgCl$_{(3M\ KCl)}$ [22]. It is notable that the oxidation potentials get lower with increasing chain length [35]. In this study, the nucleation of pyrrole during electro-polymerization of Ppy-PMB (Figure 2A–C) is not clearly expressed and cannot be clearly distinguished from non-Faradaic processes.

Evaluation of the width of the cycle loop ΔI (Figure 2D) gives a deeper insight into electrical conductivity changes of the Ppy-PMB layer during the electropolymerization process. The width of the cycle loop was compared at two potential values: +0.08 V and +0.7 V. An increase in loop width identifies the growth of the polymer layer. However, approximately from the 10th cycle, a decrease in the loop width can be attributed to some overoxidation of the Ppy layer as it was demonstrated in the previous study [21]. Moreover, it was stated that cause of the induced overoxidation process could be nucleophilic solvents, for instance, water [35].
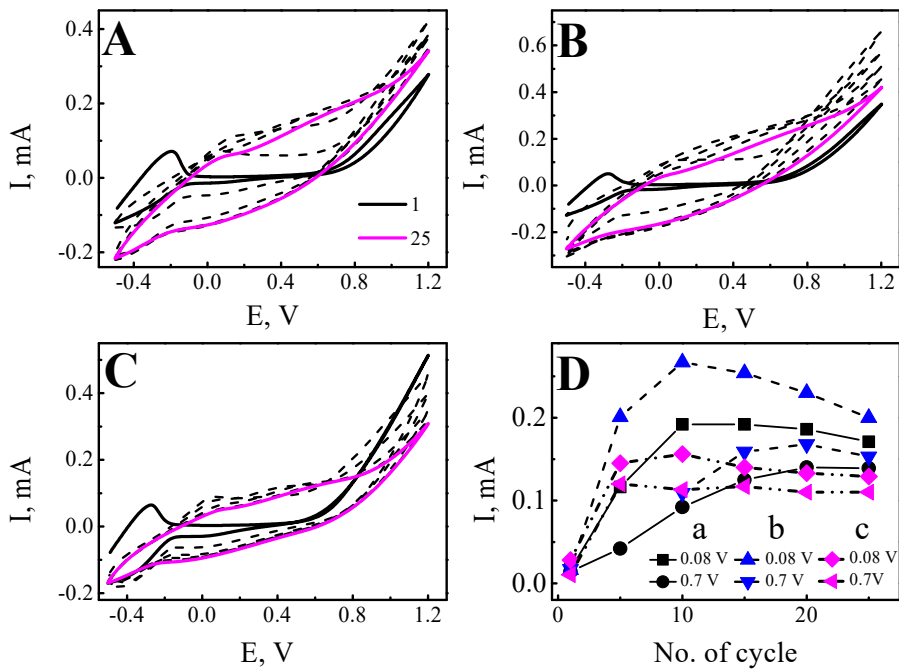
Figure 2. Electropolymerization of Ppy-PMB layers by potential cycling. Voltammograms at different cycles (1, 5, 10, 15, 20, 25): (**A**)—(Ppy-PMB)$_{Lac}$, (**B**)—(Ppy-PMB)$_{Suc}$, (**C**)—(Ppy-PMB)$_{Hep}$, (**D**)—the width of the cycle loop in mA (ΔI) was compared at potentials +0.08 V and +0.7 V. a—(Ppy-PMB)$_{Lac}$, b—(Ppy-PMB)$_{Suc}$, c—(Ppy-PMB)$_{Hep}$. Polymerization solution consisted of 50 mM pyrrole, 10 mM methylene blue, and 0.1 M lactose, 0.1 M sucrose, or 0.01 g/L heparin. Ppy-PMB layers were obtained by potential cycling 25 cycles, from −0.5 V to +1.2 V, at scan rate of 50 mV/s, and step potential of 2.44 mV. WE—glass/ITO, RE—Ag/AgCl wire, CE—platinum wire.

Surface morphology and roughness were analyzed by AFM (Figure 3). The dominant features of all three electrodes surfaces were fairly different. Figure 2B,C and Figure 3A demonstrate the appearance of the layers. It can be seen that the surface of the (Ppy-PMB)$_{Lac}$ (Figure 3A) layer is most evenly distributed. The most massive surface structures were formed on the (Ppy-PMB)$_{Hep}$ layer (Figure 3C). From the length of cross-section vs. structure height distribution (Figure 3D), it is obvious that the height is up to 1.5–2.5 μm for (Ppy-PMB)$_{Lac}$, up to 2 μm for (Ppy-PMB)$_{Suc}$, and up to 3 μm for (Ppy-PMB)$_{Hep}$. Figure 3E depicts surface height distribution and confirms that dominant height is around 2.5 μm for all Ppy-PMB layers. It confirms the previous observations about layers' surface roughness. From the AFM images, it could be seen that all layers have wrinkles on the surface from smaller ((Ppy-PMB)$_{Lac}$) to larger ((Ppy-PMB)$_{Hep}$). These wrinkles could be formed during the drying process of the layer after synthesis procedure. Possibly, in a solution, the synthesized layer is filled up with water molecules that evaporate during drying procedure. Different wrinkle size could be due to a different Ppy-PMB layer thickness or the strength and compactness of the structure itself. Therefore, from the analysis by AFM it can be concluded that the saccharides used in this study have a moderate effect on the surface morphology and roughness of Ppy-PMB layers.
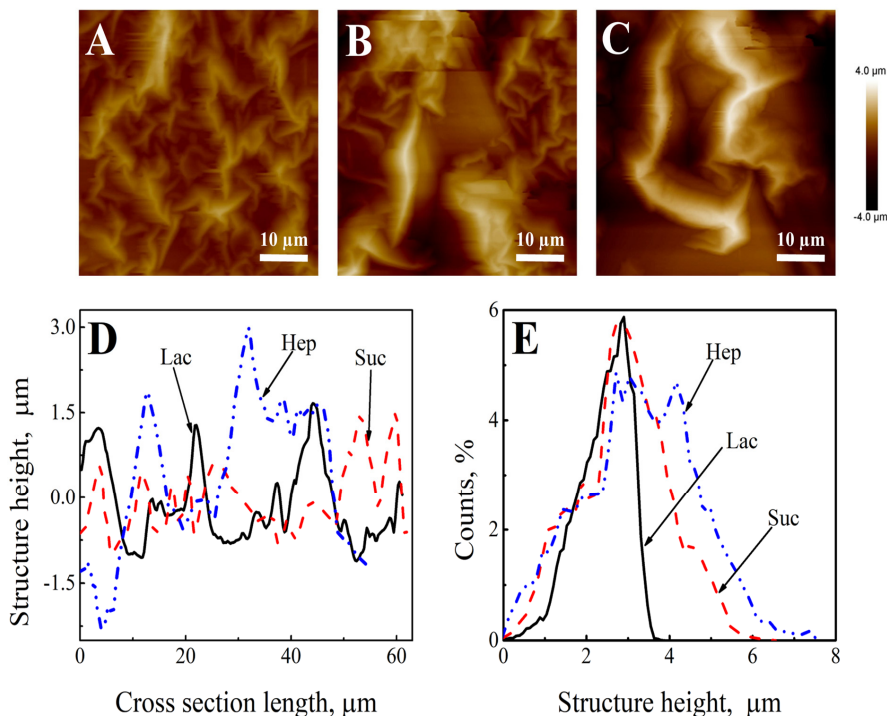
Figure 3. The AFM-based evaluation of surface morphology dominant features of (**A**)—(Ppy-PMB)$_{Lac}$; (**B**)—(Ppy-PMB)$_{Suc}$; (**C**)—(Ppy-PMB)$_{Hep}$. (**D**)—The comparison of the cross-sections of surfaces of the layers. (**E**)—Height distribution. Electrochemical deposition conditions are indicated in Figure 1.

The structure of the obtained layers was characterized using SEM-based imaging. These images also confirmed the AFM analysis. The surface of (Ppy-PMB)$_{Lac}$ is represented in Figure 4A,D and is evenly distributed, some polymer agglomerations are formed. Figure 4B,E represent surface images of (Ppy-PMB)$_{Suc}$ layer, which is also fairly evenly distributed, the structures are minor, but the folds are more expressive than in the previous layer. In Figure 4C,F, the surface of (Ppy-PMB)$_{Hep}$ layer is illustrated. The surface structure of this layer is the most massive and wrinkles are the largest. Thus, SEM results verify AFM images and conclusions, that the largest wrinkles are formed using heparin and the smallest in the sample with lactose.

In the further part of the study, the layers were examined by varying the pH of the BRB solution and the potential. The pH of the BRB solution was increased using 1 M NaOH from pH 2.5 up to pH 9. The sequence of potential pulses was applied to evaluate the absorbance changes with respect to the changing potential of Ppy-PMB layers at each pH value. Potential pulses were +0.8 V and −0.8 V. Duration of the pulse was 10 s. Each potential pulse was repeated 5 times. The pH value of BRB solutions was stepwise increased from acidic to basic and the absorbance at the wavelengths 668 nm and 750 nm was followed (Figure 5). The tendency to increase the absorption at the positive potentials and to decrease at the negative potentials was observed.
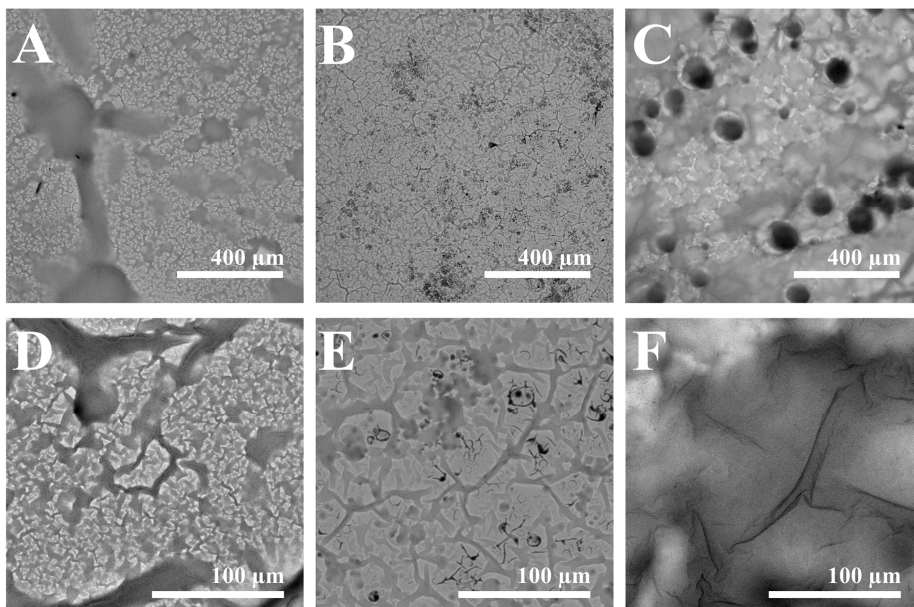
Figure 4. SEM images of (**A,D**)—(Ppy-PMB)$_{Lac}$, (**B,E**)—(Ppy-PMB)$_{Suc}$, (**C,F**)—(Ppy-PMB)$_{Hep}$. Magnification for (**A–C**) was × 200 and for (**D–F**) was × 1000. Imaged area for (**A–C**) is of 1125 μm × 1125 μm and for (**D–F**) is 225 μm × 225 μm.

In previous studies, the evaluation of absorbance spectra of PMB when potential was changed from −0.3 V to +0.5 V by an increment of potential by 0.1 V demonstrated that the position of absorbance peaks at 613 nm and 654 nm do not change with the potential values [14]. The main significant changes occur in the ratio of absorbance at these two wavelengths and which are assigned to the absorption bands of the monomeric and dimeric forms of methylene blue [26]. Another study reported that Ppy doped with Hep is an effective strategy to enhance the electrochromic lifetime of polymer films [24]. The investigated layer was characterized by long-term electro-optical stability: the optical contrast changed from 48% to 42% after 100 steps. In the case of our study, the resulting (Ppy-PMB)$_{Hep}$ layer was incomparably more mechanically stable on the electrode than (Ppy-PMB)$_{Lac}$ and (Ppy-PMB)$_{Suc}$ layers. However, response times were more than two times longer than they were in the recent study and the absorption curves are not as orderly as the other two layers studied. It can be assumed that the same electro-optical stability cannot be seen due to the incorporation of methylene blue.

During the comparison of absorbance at the wavelength 668 nm (Figure 5B,E,H) and 750 nm (Figure 5C,F,I), it was observed that the value of optical absorbance for the (Ppy-PMB)$_{Suc}$ layer is greater than that for the (Ppy-PMB)$_{Lac}$ and (Ppy-PMB)$_{Hep}$. The intensity of optical absorbance decreases when the medium becomes more alkaline (Figure 5).

Analysis of the (Ppy-PMB)$_{Lac}$ layer showed that in all cases, the absorption maximum decreases with the increasing number of pulses, for example, in an acidic medium the absorption ranges from 0.30 to 0.280 at 668 nm and from 0.264 to 0.242 at 750 nm. At neutral and basic pH values, the layer becomes less stable to potential change, resulting in a reduction in the difference between the absorption maxima. As the medium becomes more basic, a drop in values is seen, but it is not as abrupt as when observing other layers. In the case of the (Ppy-PMB)$_{Suc}$ layer, the absorption values at 668 nm wavelengths range from

0.494 to 0.478 and at 750 nm wavelengths from 0.462 to 0.450. At a more alkaline pH, it can be seen that (Ppy-PMB)$_{Suc}$ at both wavelengths reaches the highest absorption maximum during the first potential pulse and decreases markedly during the second pulse. From the second pulse, the absorption narrows slightly at these two pH values. The electrochromic properties of the (Ppy-PMB)$_{Suc}$ layer are best expressed in acidic pH. The (Ppy-PMB)$_{Hep}$ layer exhibits rather similar properties and tendencies in an acidic medium as the other two, but in the presence of neutral and acidic media, a slight increase in the absorption maximum is seen.

ΔA was calculated by using the following Equation (1):

$$\Delta A = A_{+0.8V} - A_{-0.8V} \tag{1}$$

For the calculation of ΔA, the values of $A_{+0.8V}$ and $A_{-0.8V}$ at the end of the potential pulse were taken. It was found that ΔA was the highest in the most acidic solutions regardless of the wavelength and it decreased for all Ppy-PMB layers when the pH of the solution was changed to more alkaline (Figure 6 and Table 1).
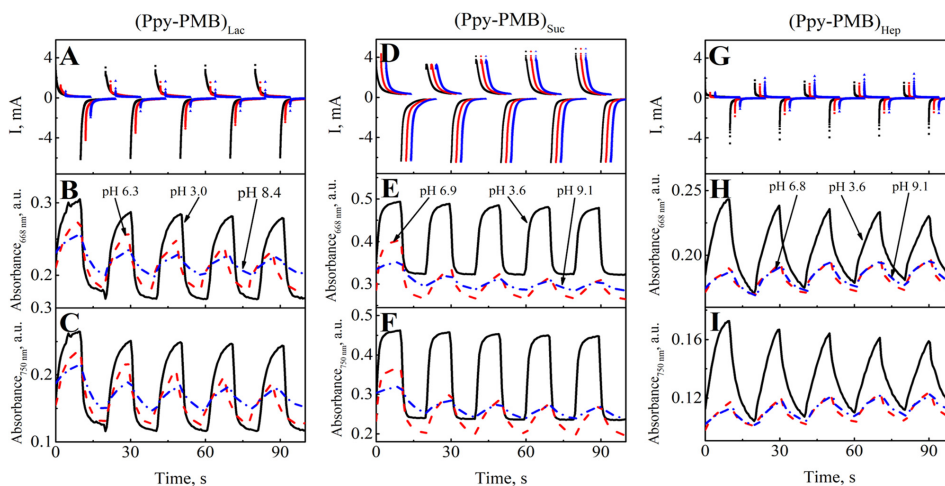
Figure 5. Evaluation of Ppy-PMB layers during potential pulsation. (**A**)—potential pulse sequence of (Ppy-PMB)$_{Lac}$, (**D**)—(Ppy-PMB)$_{Suc}$, (**G**)—(Ppy-PMB)$_{Hep}$ (pH 6 offset 2, pH 9 offset 4). Changes of absorbance at different pH values (at pH 3.0–4.0, pH 6.0–7.0, and pH 8.0–9.0): for (Ppy-PMB)$_{Lac}$ at (**B**)—λ = 668 nm, and (**C**)—λ = 750 nm; for (Ppy-PMB)$_{Suc}$ at (**E**)—λ = 668 nm, and (**F**)—λ = 750 nm; and for (Ppy-PMB)$_{Hep}$ at (**H**)—λ = 668 nm and (**I**)—λ = 750 nm. Potential pulses were +0.8 V and −0.8 V. Duration of the pulse was 10 s. Each potential was repeated 5 times. The dependence of optical absorbance was measured in BRB with 0.1 M of KCl solution. WE—glass/ITO electrode with Ppy-PMB layer, CE—platinum wire, RE—Ag/AgCl$_{(3M\ KCl)}$.

Thus, we can conclude that by changing the pH of the solution and potential value from +0.8 V to −0.8 V, the decrease of the change of absorbance can be observed. Therefore, the highest absorbance changes are observed in the acidic pH of the solution for all Ppy-PMB layers. A similar conclusion was drawn and for the Ppy layers but without PMB [22].

Studies have shown that combining conductive polymers with tunable coloration can lead to smarter electrochromic devices [1]. Electrochromism can be characterized by optical contrast, which is the transmittance difference between the bleached and colored states.
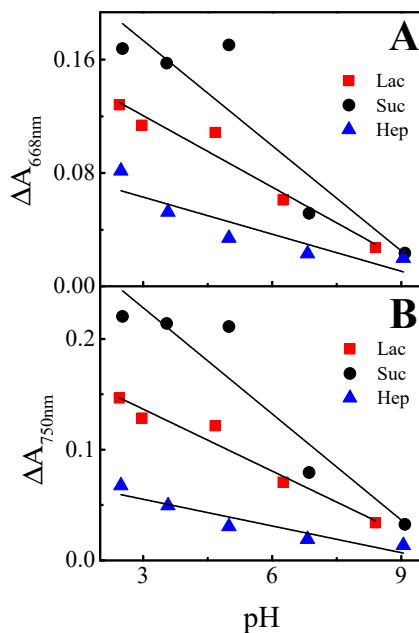
Figure 6. Calibration curve of ΔA (at the wavelengths of: (**A**)—λ = 668 nm and (**B**)—λ = 750 nm) as function of the pH value of BRB with 0.1 M of KCl solution, when potential pulses were of +0.8 V and –0.8 V with duration of 10 s. Each potential pulse was repeated for 5 times.

Table 1. Dependence of absorbance changes (at λ = 668 nm and λ = 750 nm) on the pH of BRB solution. The slope and intercept values of the calibration curves.

Wavelength	Layer	Slope	Intercept	R^2
668 nm	$(Ppy\text{-}PMB)_{Lac}$	-0.017 ± 0.002	0.171 ± 0.001	0.935
	$(Ppy\text{-}PMB)_{Suc}$	-0.025 ± 0.006	0.248 ± 0.036	0.790
	$(Ppy\text{-}PMB)_{Hep}$	-0.009 ± 0.002	0.089 ± 0.0145	0.742
750 nm	$(Ppy\text{-}PMB)_{Lac}$	-0.019 ± 0.002	0.193 ± 0.012	0.944
	$(Ppy\text{-}PMB)_{Suc}$	-0.032 ± 0.006	0.324 ± 0.038	0.857
	$(Ppy\text{-}PMB)_{Hep}$	-0.008 ± 0.002	0.079 ± 0.010	0.851

It was observed that the ΔA value of the $(Ppy\text{-}PMB)_{Suc}$ layer dropped by 86% at 750 nm and 668 nm wavelengths. The ΔA value of $(Ppy\text{-}PMB)_{Lac}$ and $(Ppy\text{-}PMB)_{Hep}$ layers changed in a descending direction, too. The ΔA value of the $(Ppy\text{-}PMB)_{Lac}$ layer dropped by 80% at 750 nm and 78% at 668 nm. In the case of the $(Ppy\text{-}PMB)_{Hep}$ layer, the ΔA value dropped by 78% at 750 nm and 81% at 668 nm.

The electrochromic property of optical contrast was also analyzed. Response times were very similar in all cases. Changing the pH to the alkaline side showed visible change—slowing down response times in coloration and bleaching. In the case of $(Ppy\text{-}PMB)_{Lac}$ layers at 668 nm, a response time of about 8 s for coloration and 2.8 s for bleaching was shown. In the case of $(Ppy\text{-}PMB)_{Suc}$, there was a response time of about 5.9 s for coloration and 2.1 s for bleaching. In the case of $(Ppy\text{-}PMB)_{Hep}$, response times were the longest compared to others: about 9.8 s for coloration and 3.6 s for bleaching. Very similar results were obtained at 750 nm.

The last part of the study was attributed to the application of the formed Ppy-PMB layer for sensing three xanthine derivatives: theophylline, caffeine, and theobromine. Such xanthine derivatives were selected taking into account that these compounds: (1) are soluble

in water-based solutions (solubility in water are 0.330 g/L of theobromine, 7.360 g/L of theophylline, and 21.6 g/L caffeine of at 25 °C); (2) xanthine derivatives differ from each other only by a methylene group, therefore they are convenient for model systems. Xanthine derivatives are found in the biological fluids of humans and some other species and are receiving a lot of interest because of their bio-activity. They are used as pharmaceutics because they have such bio-activities: antimicrobial, antiasthmatic, CNS stimulating, anti-inflammatory, and antagonism to adenosine receptor [8,36,37]. Methylxanthine homologues include such compounds such as caffeine, theophylline, and theobromine. Methylxanthines have some typical parameters suitable for analytical applications.

In previous studies, some applications of polyphenazines for the determination of xanthine derivatives were described [11,38,39]. The study by Bukkitgar and Shetti [39] described the electrochemical behavior of theophylline at the methylene blue dye modified carbon paste. The main analytical methods used for the determination of theophylline were cyclic voltammetry and differential pulse voltammetry (DPV). The obtained results demonstrated that modification of carbon paste electrode with methylene blue during analysis by cyclic voltammetry CV leads to the peak current of theophylline sharpening and increased current values about 2–3 folds in comparison to the peak current obtained on the bare carbon paste electrode. Ppy was also used for the determination of theophylline [4,40–42]. The mentioned studies applied molecular imprinting technology for improved sensitivity/selectivity of theophylline on Ppy by electrochemical analysis (cyclic voltammetry, electrochemical impedance spectroscopy (EIS)) or microgravimetric (quartz crystal microbalances (QCM)) methods.

In comparison to the previously published studies, the experiment described in this article is unique. First of all, this time the combination of polypyrrole and methylene blue was applied as a sensor of xanthine derivatives. In contrast to the previously published study where carbon paste electrode modified with PMB was used as a working electrode [39], in this study, ITO modified with (Ppy-PMB)$_{Hep}$ was used as a working electrode. Secondly, in this study, the (Ppy-PMB)$_{Hep}$ layer was applied as a possible electrochromic surface for the xanthine derivatives detection.

The heparin-doped (Ppy-PMB)$_{Hep}$ layer was chosen to sense xanthine derivatives as the most mechanically stable layer. Evaluation of absorbance dependence (at λ = 668 nm (Figure 7B) and λ = 750 nm (Figure 7C)) on the concentration of caffeine, theophylline, and theobromine was performed in BRB solution with 0.1 M of KCl, pH 2.5. The concentration interval of the theobromine was limited by the compound solubility in the BRB solution. The pH value of BRB solution was selected based on results in the prior section where it was demonstrated that the absorbance changes in the most acidic BRB solution was highest. The potential pulses profile was used unchanged: +0.8 V and −0.8 V with a duration of 10 s.

It was obtained that absorbance dependence (at λ = 668 nm and λ = 750 nm) on the concentration of caffeine, theophylline, and theobromine was linear and the correlation coefficient R^2 for the ΔA at wavelength 668 nm and 750 nm was even higher than for the ΔI (Figure 7A).

Linearity was observed at all evaluated calibration curves of xanthine derivatives. The slope was derived using the linear regression equation for the changes of absorbance changes (at λ = 668 nm and λ = 750 nm) vs. the concentration of xanthine derivatives (c, μM). In the case of caffeine (at λ = 668 nm) slope of linear regression was −0.001 with R^2 = 0.978 (Table 2), while in the case of theophylline slope was −0.002 with R^2 = 0.977 (Table 2), which is 2 times higher. In the case of theobromine, the slope of linear regression was −0.005 with R^2 = 0.939. A linear relationship is observed only in low concentrations, followed by scattering of points, so only the first three points are reported. The limit of detection (LOD) as the lowest concentration of analyte, which gives an analytical signal greater than the background value plus 3 δ, was estimated. The LODs for ΔI vs. concentration of caffeine, theophylline, and theobromine were 2.0 μM, 3.9 μM, and 7.48 μM, respectively. The LODs for caffeine, theophylline, and theobromine based on registered changes of absorbance at

λ = 668 nm were 3.3 μM, 3.0 μM, and 6.0 μM, respectively; while changes of absorbance registered at λ = 750 nm LODs were 3.75 μM, 3.0 μM, and 3.0 μM, respectively. Accordingly to the given results, it is presupposed that the (Ppy-PMB)$_{Hep}$ layer might be used for the detection of xanthine derivatives, especially for theophylline and caffeine.
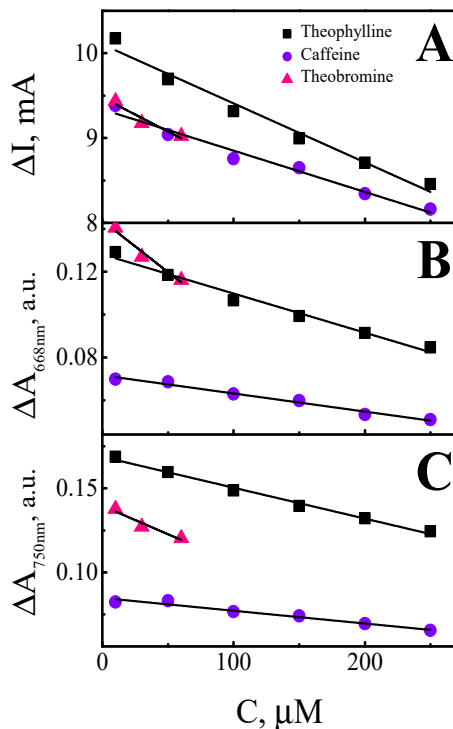

Figure 7. Dependence of absorbance changes (at λ = 668 nm and λ = 750 nm) on the concentration of caffeine, theophylline, and theobromine in BRB with 0.1 M of KCl, pH 2.5 solution. (**A**)—calibration curves of Δ*I* vs. concentration of caffeine, theophylline, and theobromine, (**B**)—calibration curves of Δ*A* (at 668 nm) vs. concentration of caffeine, theophylline, and theobromine, (**C**)—calibration curves of Δ*A* (at 750 nm) vs. concentration of caffeine, theophylline, and theobromine.

Table 2. Dependence of absorbance changes (at λ = 668 nm and λ = 750 nm) on the concentration of caffeine, theophylline, and theobromine. The slope and intercept values of the calibration curves.

		Slope	**Intercept**	**R^2**
	Theophylline	−0.007 ± 0.0005	10.1 ± 0.079	0.973
Δ*I*	Caffeine	−0.005 ± 0.0004	9.35 ± 0.059	0.969
	Theobromine	−0.008 ± 0.0021	9.48 ± 0.082	0.872
	Theophylline	−0.0002 ± 0.00001	0.13 ± 0.002	0.977
668 nm	Caffeine	−0.0001 ± 0.00001	0.07 ± 0.001	0.978
	Theobromine	−0.0005 ± 0.00009	0.14 ± 0.003	0.939
	Theophylline	−0.0002 ± 0.00001	0.17 ± 0.001	0.990
750 nm	Caffeine	−0.0001 ± 0.00001	0.08 ± 0.001	0.958
	Theobromine	−0.0003 ± 0.00008	0.14 ± 0.003	0.884

4. Conclusions

The electrochemical deposition of the polypyrrole layer was carried out by cyclic voltammetry from a solution containing of 50 mM of pyrrole, 10 mM of methylene blue, and one of the doping materials: 0.1 M Lac, 0.1 M Suc, 0.01 g/L Hep. Surface morphology was analyzed by AFM and SEM methods. From the AFM analysis, these layers were compared with each other. It can be concluded that the saccharides used in this study have a moderate effect on the surface morphology and roughness of Ppy-PMB layers. From the length of cross-section vs. structure height distribution, it is obvious that the height is up to 1.5–2.5 μm for (Ppy-PMB)$_{Lac}$, up to 2 μm for (Ppy-PMB)$_{Suc}$, and up to 3 μm for (Ppy-PMB)$_{Hep}$.

The Ppy-PMB layers were examined by varying the pH of the BRB solution and the potential. The tendency to increase the absorption at the positive potentials and to decrease at the negative potentials was observed at each pH value. It was observed that the value of optical absorbance for the (Ppy-PMB)$_{Suc}$ layer is greater than that for the (Ppy-PMB)$_{Lac}$ and (Ppy-PMB)$_{Hep}$. Moreover, it was found that the intensity of optical absorbance itself and the change of absorbance was the highest in the most acidic solutions regardless of the wavelength and it decreased for all Ppy-PMB layers when the pH of the solution was changed to more alkaline. The (Ppy-PMB)$_{Suc}$ layer had the best conductivity properties, and the fastest bleaching and coloration times. The suitability of the Ppy-PMB layer for use as an electrochromic sensor of xanthine derivatives—caffeine, theophylline, and theobromine—was investigated using the (Ppy-PMB)$_{Hep}$ layer. Linearity was observed at evaluated calibration curves (concentration vs. the change of absorbance) of all xanthine derivatives. According to the given results, it is presupposed that the (Ppy-PMB)$_{Hep}$ layer might be used for the detection of xanthine derivatives, especially for theophylline and caffeine.

Author Contributions: Conceptualization, V.R. and A.R. (Arunas Ramanavicius); methodology, V.R.; formal analysis, V.R. and R.B.; investigation, M.B.M., R.B. and L.M.; resources, V.R. and A.R. (Arunas Ramanavicius); data curation, V.R. and A.R. (Almira Ramanaviciene); writing—original draft preparation, V.R. and R.B.; writing—review and editing, V.R., U.S.-B., A.R. (Arunas Ramanavicius), and A.R. (Almira Ramanaviciene); visualization, V.R. and R.B.; supervision, A.R. (Almira Ramanaviciene); project administration, U.S.-B.; funding acquisition, A.R. (Arunas Ramanavicius). All authors have read and agreed to the published version of the manuscript.

Institutional Review Board Statement: Not applicable.

Informed Consent Statement: Not applicable.

Data Availability Statement: The data presented in this study are available on request from the first author.

Conflicts of Interest: The authors declare that they have no known competing financial interests or personal relationships that could have appeared to influence the work reported in this paper.

References

1. Wolfart, F.; Hryniewicz, B.M.; Góes, M.S.; Corrêa, C.M.; Torresi, R.; Minadeo, M.A.; de Torresi, S.I.C.; Oliveira, R.D.; Marchesi, L.F.; Vidotti, M. Conducting polymers revisited: Applications in energy, electrochromism and molecular recognition. *J. Solid State Electrochem.* **2017**, *21*, 2489–2515. [CrossRef]
2. Leonavicius, K.; Ramanaviciene, A.; Ramanavicius, A. Polymerization Model for Hydrogen Peroxide Initiated Synthesis of Polypyrrole Nanoparticles. *Langmuir* **2011**, *27*, 10970–10976. [CrossRef] [PubMed]
3. Ratautaite, V.; Nesladek, M.; Ramanaviciene, A.; Baleviciute, I.; Ramanavicius, A. Evaluation of Histamine Imprinted Polypyrrole Deposited on Boron Doped Nanocrystalline Diamond. *Electroanalysis* **2014**, *26*, 2458–2464. [CrossRef]
4. Ratautaite, V.; Janssens, S.D.; Haenen, K.; Nesládek, M.; Ramanaviciene, A.; Baleviciute, I.; Ramanavicius, A. Molecularly Imprinted Polypyrrole Based Impedimentric Sensor for Theophylline Determination. *Electrochim. Acta* **2014**, *130*, 361–367. [CrossRef]

5. German, N.; Ramanaviciene, A.; Ramanavicius, A. Formation of polyaniline and polypyrrole nanocomposites with embedded glucose oxidase and gold nanoparticles. *Polymers* **2019**, *11*, 377. [CrossRef] [PubMed]

6. Ramanaviciene, A.; Kausaite-Minkstimiene, A.; Oztekin, Y.; Carac, G.; Voronovic, J.; German, N.; Ramanavicius, A. Visualization of red-ox proteins on the gold surface using enzymatic polypyrrole formation. *Microchim. Acta* **2011**, *175*, 79–86. [CrossRef]

7. Plausinaitis, D.; Sinkevicius, L.; Samukaite-Bubniene, U.; Ratautaite, V.; Ramanavicius, A. Evaluation of Electrochemical Quartz Crystal Microbalance Based Sensor Modified by Uric Acid-imprinted Polypyrrole. *Talanta* **2020**, *220*, 121414. [CrossRef]

8. Ratautaite, V.; Plausinaitis, D.; Baleviciute, I.; Mikoliunaite, L.; Ramanaviciene, A.; Ramanavicius, A. Characterization of Caffeine-Imprinted Polypyrrole by a Quartz Crystal Microbalance and Electrochemical Impedance Spectroscopy. *Sens. Actuators B* **2015**, *212*, 63–71. [CrossRef]

9. Plausinaitis, D.; Ratautaite, V.; Mikoliunaite, L.; Sinkevicius, L.; Ramanaviciene, A.; Ramanavicius, A. Quartz Crystal Microbalance-Based Evaluation of the Electrochemical Formation of an Aggregated Polypyrrole Particle-Based Layer. *Langmuir* **2015**, *31*, 3186–3193. [CrossRef]

10. Diaz, A.F.; Kanazawa, K.K.; Gardini, G.P. Electrochemical polymerization of pyrrole. *J. Chem. Soc. Chem. Commun.* **1979**, *14*, 635–636. [CrossRef]

11. Pauliukaite, R.; Ghica, M.E.; Barsan, M.M.; Brett, C.M.A. Phenazines and Polyphenazines in Electrochemical Sensors and Biosensors. *Anal. Lett.* **2010**, *43*, 1588–1608. [CrossRef]

12. Manasa, G.; Mascarenhas, R.J.; Satpati, A.K.; D'Souza, O.J.; Dhason, A. Facile preparation of poly(methylene blue) modified carbon paste electrode for the detection and quantification of catechin. *Mater. Sci. Eng. C* **2017**, *73*, 552–561. [CrossRef]

13. Liu, B.; Cang, H.; Cui, L.; Zhang, H. Electrochemical polymerization of methylene blue on glassy carbon electrode. *Int. J. Electrochem. Sci.* **2017**, *12*, 9907–9913. [CrossRef]

14. Liu, J.; Mu, S. The electrochemical polymerization of methylene blue and properties of polymethylene blue. *Synth. Met.* **1999**, *107*, 159–165. [CrossRef]

15. Damos, F.S.; Luz, R.C.S.; Kubota, L.T. Study of poly(methylene blue) ultrathin films and its properties by electrochemical surface plasmon resonance. *J. Electroanal. Chem.* **2005**, *581*, 231–240. [CrossRef]

16. Brett, C.M.A.; Inzelt, G.; Kertesz, V. Poly(methylene blue) modified electrode sensor for haemoglobin. *Anal. Chim. Acta* **1999**, *385*, 119–123. [CrossRef]

17. Samukaite-Bubniene, U.; Valiūnienė, A.; Bucinskas, V.; Genys, P.; Ratautaite, V.; Ramanaviciene, A.; Aksun, E.; Tereshchenko, A.; Zeybek, B.; Ramanavicius, A. Towards supercapacitors: Cyclic voltammetry and fast Fourier transform electrochemical impedance spectroscopy based evaluation of polypyrrole electrochemically deposited on the pencil graphite electrode. *Colloids Surf. A Physicochem. Eng. Asp.* **2020**, *610*, 125750. [CrossRef]

18. Kuwabata, S.; Nakamura, J.; Yoneyama, H. The effect of basicity of dopant anions on the conductivity of polypyrrole films. *J. Chem. Soc. Chem. Commun.* **1988**, *12*, 779–780. [CrossRef]

19. Serra Moreno, J.; Panero, S.; Materazzi, S.; Martinelli, A.; Sabbieti, M.G.; Agas, D.; Materazzi, G. Polypyrrole-polysaccharide thin films characteristics: Electrosynthesis and biological properties. *J. Biomed. Mater. Res. A* **2009**, *88A*, 832–840. [CrossRef]

20. Fonner, J.M.; Schmidt, C.E.; Ren, P. A combined molecular dynamics and experimental study of doped polypyrrole. *Polymer* **2010**, *51*, 4985–4993. [CrossRef]

21. Ratautaite, V.; Ramanaviciene, A.; Oztekin, Y.; Voronovic, J.; Balevicius, Z.; Mikoliunaite, L.; Ramanavicius, A. Electrochemical stability and repulsion of polypyrrole film. *Colloids Surf. A Physicochem. Eng. Asp.* **2013**, *418*, 16–21. [CrossRef]

22. Ratautaite, V.; Bagdziunas, G.; Ramanavicius, A.; Ramanaviciene, A. An Application of Conducting Polymer Polypyrrole for the Design of Electrochromic pH and CO_2 Sensors. *J. Electrochem. Soc.* **2019**, *166*, B297–B303. [CrossRef]

23. John, J.; Sivaraman, S.; Jayalekshmy, S.; Anantharaman, M.R. Investigations on the mechanism of carrier transport in plasma polymerized pyrrole thin films. *J. Phys. Chem. Solids* **2010**, *71*, 935–939. [CrossRef]

24. Alizadeh, N.; Tavoli, F. Enhancing electrochromic contrast and redox stability of nanostructure polypyrrole film doped by heparin as polyanion in different solvents. *J. Polym. Sci. A Polym. Chem.* **2014**, *52*, 3365–3371. [CrossRef]

25. Horikawa, M.; Fujiki, T.; Shirosaki, T.; Ryu, N.; Sakurai, H.; Nagaoka, S.; Ihara, H. The development of a highly conductive PEDOT system by doping with partially crystalline sulfated cellulose and its electric conductivity. *J. Mater. Chem. C* **2015**, *3*, 8881–8887. [CrossRef]

26. Ion, R.M.; Scarlat, F.; Scarlat, F.; Niculescu, V.I.R. Methylene—Blue modified polypyrrole film electrode for optoelectronic applications. *J. Optoelectron. Adv. Mater.* **2003**, *5*, 109–115.

27. Godwin, J.M.; Evitts, R.W.; Kennell, G.F. Microbial fuel cell with a polypyrrole/poly(methylene blue) composite electrode. *Rep. Electrochem.* **2012**, *2*, 3–11.

28. Godwin, J.M.; Evitts, R. Polypyrrole/Poly(Methylene Blue) Composite Electrode Films on Stainless Steel. *ECS Trans.* **2019**, *33*, 181–188. [CrossRef]

29. Vy Phan, T.T.; Bharathiraja, S.; Nguyen, V.T.; Moorthy, M.S.; Manivasagan, P.; Lee, K.D.; Oh, J. Polypyrrole–methylene blue nanoparticles as a single multifunctional nanoplatform for near-infrared photo-induced therapy and photoacoustic imaging. *RSC Adv.* **2017**, *7*, 35027–35037. [CrossRef]

30. Somani, P.R.; Radhakrishnan, S. Sensitization effect in doped and undoped state of polypyrrole by methylene blue in solid state electrochemical cells. *Chem. Phys. Lett.* **2003**, *379*, 401–405. [CrossRef]

31. Boguzaite, R.; Ratautaite, V.; Mikoliunaite, L.; Pudzaitis, V.; Ramanaviciene, A.; Ramanavicius, A. Towards analytical application of electrochromic polypyrrole layers modified by phenothiazine derivatives. *J. Electroanal. Chem.* **2021**, *886*, 115132. [CrossRef]

32. Sadki, S.; Schottland, P.; Brodie, N.; Sabouraud, G. The mechanisms of pyrrole electropolymerization. *Chem. Soc. Rev.* **2000**, *29*, 283–293.

33. Britton, H.T.S.; Robinson, R.A. CXCVIII.—Universal buffer solutions and the dissociation constant of veronal. *J. Chem. Soc.* **1931**, 1456–1462. [CrossRef]

34. Ion, R.M.; Blair, D.F.; Radovici, O. Spectral properties of methylene blue modified polypyrrole film. *J. Serb. Chem. Soc.* **1997**, *62*, 1063–1068.

35. Heinze, J.; Frontana-Uribe, B.A.; Ludwigs, S. Electrochemistry of Conducting Polymers—Persistent Models and New Concepts. *Chem. Rev.* **2010**, *110*, 4724–4771. [CrossRef] [PubMed]

36. Spătaru, N.; Sarada, B.V.; Tryk, D.A.; Fujishima, A. Anodic Voltammetry of Xanthine, Theophylline, Theobromine and Caffeine at Conductive Diamond Electrodes and Its Analytical Application. *Electroanalysis* **2002**, *14*, 721–728. [CrossRef]

37. Matissek, R. Evaluation of xanthine derivatives in chocolate—Nutritional and chemical aspects. *Z. Lebensm Unters Forsch. A* **1997**, *205*, 175–184. [CrossRef]

38. Ulyanova, Y.V.; Blackwell, A.E.; Minteer, S.D. Poly(methylene green) employed as molecularly imprinted polymer matrix for electrochemical sensing. *Analyst* **2006**, *131*, 257–261. [CrossRef]

39. Bukkitgar, S.D.; Shetti, N.P. Electrochemical behavior of theophylline at methylene blue dye modified electrode and its analytical application. *Mater. Today Proc.* **2018**, *5*, 21474–21481. [CrossRef]

40. Baleviciute, I.; Ratautaite, V.; Ramanaviciene, A.; Balevicius, Z.; Broeders, J.; Croux, D.; McDonald, M.; Vahidpour, F.; Thoelen, R.; Ceuninck, W.D.; et al. Evaluation of theophylline imprinted polypyrrole film. *Synth. Met.* **2015**, *209*, 206–211. [CrossRef]

41. Kim, J.M.; Yang, J.C.; Park, J.Y. Quartz crystal microbalance (QCM) gravimetric sensing of theophylline via molecularly imprinted microporous polypyrrole copolymers. *Sens. Actuators B* **2015**, *206*, 50–55. [CrossRef]

42. Kim, J.-M.; Lee, U.-H.; Chang, S.-M.; Park, J.Y. Gravimetric detection of theophylline on pore-structured molecularly imprinted conducting polymer. *Sens. Actuators B* **2014**, *200*, 25–30. [CrossRef]

Molecularly imprinted polypyrrole based sensor for the detection of SARS-CoV-2 spike glycoprotein

Vilma Ratautaite [a,c], Raimonda Boguzaite [a,c], Ernestas Brazys [c], Almira Ramanaviciene [c], Evaldas Ciplys [c,d], Mindaugas Juozapaitis [c,d], Rimantas Slibinskas [c,d], Mikhael Bechelany [e], Arunas Ramanavicius [b,c,*]

[a] Laboratory of Nanotechnology, Department of Functional Materials and Electronics, Center for Physical Sciences and Technology, Sauletekio av. 3, Vilnius LT-10257, Lithuania
[b] Department of Physical Chemistry, Institute of Chemistry, Faculty of Chemistry and Geosciences, Vilnius University, Naugarduko str. 24, Vilnius LT-03225 Lithuania
[c] NanoTechnas – Center of Nanotechnology and Materials Science at Faculty of Chemistry and Geosciences, Vilnius University, Naugarduko str. 24, LT-03225, Vilnius, Lithuania
[d] Institute of Biotechnology, Life Sciences Center, Vilnius University, Sauletekio av. 7, LT-10257 Vilnius, Lithuania
[e] Institut Européen des Membranes, IEM, UMR 5635, University of Montpellier, CNRS, ENSCM, 34090 Montpellier, France

ARTICLE INFO

ABSTRACT

This study describes the application of a polypyrrole-based sensor for the determination of SARS-CoV-2-S spike glycoprotein. The SARS-CoV-2-S spike glycoprotein is a spike protein of the coronavirus SARS-CoV-2 that recently caused the worldwide spread of COVID-19 disease. This study is dedicated to the development of an electrochemical determination method based on the application of molecularly imprinted polymer technology. The electrochemical sensor was designed by molecular imprinting of polypyrrole (Ppy) with SARS-CoV-2-S spike glycoprotein (MIP-Ppy). The electrochemical sensors with MIP-Ppy and with polypyrrole without imprints (NIP-Ppy) layers were electrochemically deposited on a platinum electrode surface by a sequence of potential pulses. The performance of polymer layers was evaluated by pulsed amperometric detection. According to the obtained results, a sensor based on MIP-Ppy is more sensitive to the SARS-CoV-2-S spike glycoprotein than a sensor based on NIP-Ppy. Also, the results demonstrate that the MIP-Ppy layer is more selectively interacting with SARS-CoV-2-S glycoprotein than with bovine serum albumin. This proves that molecularly imprinted MIP-Ppy-based sensors can be applied for the detection of SARS-CoV-2 virus proteins.

© 2021 Elsevier Ltd. All rights reserved.

1. Introduction

The severe acute respiratory syndrome coronavirus-2 (SARS-CoV-2) induced COVID-19 pandemic that began in 2019 has caused drastic changes in the world. 197 countries were affected [1]: lockdowns [2], quarantine, economic problems hit the most significant part of the world, people's emotional health has deteriorated. Even at the beginning of the 2021, this pandemic is still not adequately controlled. Although the vaccines became available to society, this viral infection is still very active and the virus is rather rapidly mutating and appears in new even more infectious forms. Therefore, a much deeper understanding of the virus SARS-CoV-2 is required and rapid analytical methods that are suitable for the diagnosis of COVID-19 and/or detection of virus or their parts are demanded

to overcome and defeat this infection. Thus, various aspects of the virus itself [3], genome [4–7], research of the structure, function of proteins, and nucleocapsid, envelope, spike, and membrane protein interactions with drugs [8–11], and some other aspects [12, 13] were investigated. Better and easier detection methods could improve the diagnosis of viral infection and enable more efficient ways of defeating the COVID-19 pandemic. Recently, label-free protein detection has become relevant in research and clinical practice [14, 15]. The discovery and detection of biomarkers during the diagnosis of human diseases is required for biomedical purposes [15, 16].

In biosensors, the analyte recognition elements are typically based on bio-macromolecules such as enzymes, antibodies, DNA, aptamers, etc. However, such bioanalytical systems have some limitations due to operating conditions and expensive production. Therefore, the development of artificial biorecognition-systems based on synthetic receptors and molecularly imprinted polymers

* Corresponding author.
E-mail address: arunas.ramanavicius@chf.vu.lt (A. Ramanavicius).

(MIPs) has attracted a great interest as a potential alternative [14, 17-19]. Researchers have been focused on the development of a system that replicates the natural recognition process. Therefore, the interest in the development of MIPs has grown during recent years [15, 16, 20-27]. The technique of molecular imprinting allows the formation of specific molecular recognition sites that operate on the principle of complementarity between the imprinted sites and the analyte. Therefore, MIPs can selectively bind the analytes of interest, which were used as templates during formation of these MIPs [14, 16, 28-30]. MIPs also have some benefits including low-cost, easy way of preparation, advanced storage stability, and rather good specificity [14, 31]. In previous studies, it was reported that various types of small molecules can be imprinted within polymers [24, 29, 32, 33]. In some researches, it was demonstrated that high molecular mass biomolecules including proteins [15, 22, 23, 34-43] can be also molecularly imprinted within polymers. Polypyrrole (Ppy) is among several other polymers that can be very efficiently applied for the design of MIP-based sensors [24, 29, 32, 33, 44-47]. Ppy is a conducting polymer, which can be easily electropolymerized and used as a polymeric matrix of MIPs for the detection of low and high molecular weight analytes [15, 44]. Electrochemical methods like cyclic voltammetry, differential pulse voltammetry, and electrochemical impedance spectroscopy were used for the detection of the proteins both on the polypyrrole modified with molecular imprints and on the unmodified in previous studies [15, 48-54]. Meanwhile, there is only few reports on the application of chronoamperometry for determination of virus-proteins [44]. In chronoamperometry the changes in the current appear in response to increase or decrease of the diffuse layer thickness at the surface of the working electrode [55]. Therefore, the application of chronoamperometry (in pulsed amperometric mode) and the analysis of data gathered by this method using Cottrell or Anson plots are providing interesting and useful insights into the evaluation of interaction between analytes and the electrode [56].

At the moment, there are some explorations reported that are already applying MIP technology for SARS-CoV-2 [57, 58]. The development of so called 'monoclonal-type plastic antibodies' based on MIPs was described [57]. Such 'antibodies' were able to selectively bind a spike protein of the novel coronavirus SARS-CoV-2 to block its function. The obtained nanoparticles were analyzed by SDS-PAGE electrophoresis. The results of the electrophoretic analysis demonstrated promising results in the formulation of 'free-drug therapeutics' due to their ability to bind the virus spike glycoprotein and, thus, to block the infection process. According to reported results it was concluded that the 'monoclonal-type plastic antibodies' could be potentially used as free-drug therapeutics in the treatment of infection by novel coronavirus (2019-nCoV). In another research, SARS-CoV-2 nucleoprotein (ncovNP) was qualitatively and quantitatively determined by MIP-based layer on poly-m-phenylenediamine (PmPD), which was deposited on the Au-TFE electrode [58]. Cyclic voltammetry (CV) was applied for the characterization of the preparation steps of the sensor. Meanwhile, the rebinding of SARS-CoV-2 nucleoprotein on the sensors was studied by differential pulse voltammetry (DPV) in the solution of 1 M KCl containing a redox probe $K_3[Fe(CN)_6]/K_4[Fe(CN)_6]$. The obtained results demonstrated the linear increase of the sensor response with increasing ncovNP concentration. The feasibility of sensor performance in clinical samples was tested. For this purpose, they analyzed the samples prepared from nasopharyngeal swab specimens. Genetically engineered receptor-binding domain of SARS-CoV-2-RBD protein was imprinted in ortho-phenylenediamine and deposited on a macroporous gold screen-printed electrode [59].

The aim of our recent research was to design the MIP-based sensor for the determination of SARS-CoV-2-S glycoprotein. For this purpose, Ppy layers were deposited on the working platinum elec-

trode from the polymerization mixture containing SARS-CoV-2-S glycoprotein and pyrrole dissolved in phosphate buffered saline (PBS) solution, pH 7.4. The performance of the electrode modified by the deposited MIP-Ppy layer imprinted with SARS-CoV-2-S glycoprotein was investigated and compared with that of non-imprinted (NIP-Ppy) layer.

2. Materials and methods

2.1. Chemicals and instrumentation

Pyrrole 98% (*Alfa Aeser*, Germany), H_2SO_4 (96%) (*Lachner*, Czech Republic), HNO_3, NaOH (*Merck*, Germany), H_2PtCl_6 (*Merck*, Germany), and bovine serum albumin (BSA) (*Carl Roth*, Germany) were used as received. KH_2PO_4 (*Honeywell Riedel-de Haen*, Germany), NaCl, KCl, and Na_2HPO_4 (*Roth*, Germany) salts were used for the preparation of buffer. The detailed description of expression and purification of SARS-CoV-2-S spike glycoprotein is presented in supporting material.

Experiment was performed using potentiostat/galvanostat Metrohm AutoLAB model μAutolabIII/FRA2 μ3AUT71079 controlled by NOVA 2.1.3 software (*EcoChemie*, The Netherlands). All measurements were done in a homemade cell. The total volume of the cell was 250 μL. Three-electrode system consisted of Pt disk with 1 mm diameter sealed in glass as the working electrode, Ag/AgCl in 3 M KCl solution electrode as a reference electrode (Ag/AgCl), and Pt disk of 2 mm diameter as a counter electrode.

2.2. Pretreatment of working electrode

The working electrode was pretreated before electrochemical deposition of Ppy following the procedure described in previous studies [44, 60]. All solutions were thoroughly degassed just before use with a stream of nitrogen (N_2). According to this procedure, the Pt electrode was rinsed with concentrated HNO_3 solution in an ultrasonic bath for 10 min, then rinsed with water and polished with alumina paste. Later, it was rinsed with water again and then with 10 M solution of NaOH, thereafter – with 5 M solution of H_2SO_4 in an ultrasonic bath for 5 min. Electrochemical cleaning of the electrode was carried out in 0.5 M H_2SO_4 by cycling the potential for 20 times in the range between -100 mV and $+1200$ mV *vs* Ag/AgCl at a sweep rate of 100 mV s^{-1}. The identification of the bare electrode surface was made possible by a stable indication of the cyclic voltammogram. To improve the adhesion of the Ppy layer to the electrode surface, a layer of 'platinum black' was deposited over the working electrode [60]. Deposition of Pt clusters was performed in 5 mM solution of H_2PtCl_6 containing 0.1 M of KCl by 10 potential cycles in the range between $+500$ mV and -400 mV *vs* Ag/AgCl at a sweep rate of 10 mV s^{-1}.

2.3. The electrochemical deposition of MIP and NIP and evaluation of sensor signal

The electrochemical deposition of the polypyrrole layer was performed in the same electrochemical cell. NIP-Ppy was electrochemically deposited from the polymerization solution containing 0.5 M solution of pyrrole in PBS. The preparation of MIP-Ppy was carried out in two steps. Step I: deposition of polymeric layer was carried out from the polymerization solution containing 0.5 M solution of pyrrole and 50 μg/mL of SARS-CoV-2-S glycoprotein all dissolved in PBS solution. The polymeric layers were formed by a sequence of 20 potential pulses of $+950$ mV for 1 s, between these pulses 0 V potential for 10 s was applied [44, 60]. Step II: the MIP-Ppy was formed when the imprinted protein molecules were extracted by incubation in 0.05 M H_2SO_4 for 10 min. In the
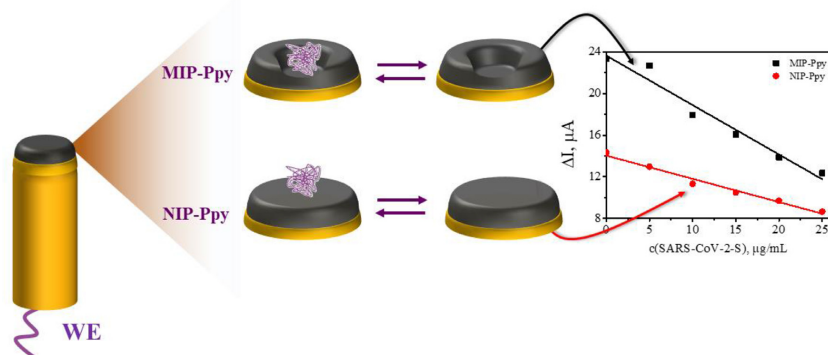
Fig. 1. Schematic representation of evaluation by chronoamperometry of Pt electrode modified with non-imprinted polypyrrole (NIP-Ppy) and with molecularly imprinted polypyrrole (MIP-Ppy) with SARS-CoV-2-S glycoprotein imprints. Electrochemical measurements were performed in phosphate-buffered saline (PBS) solution, pH 7.4.
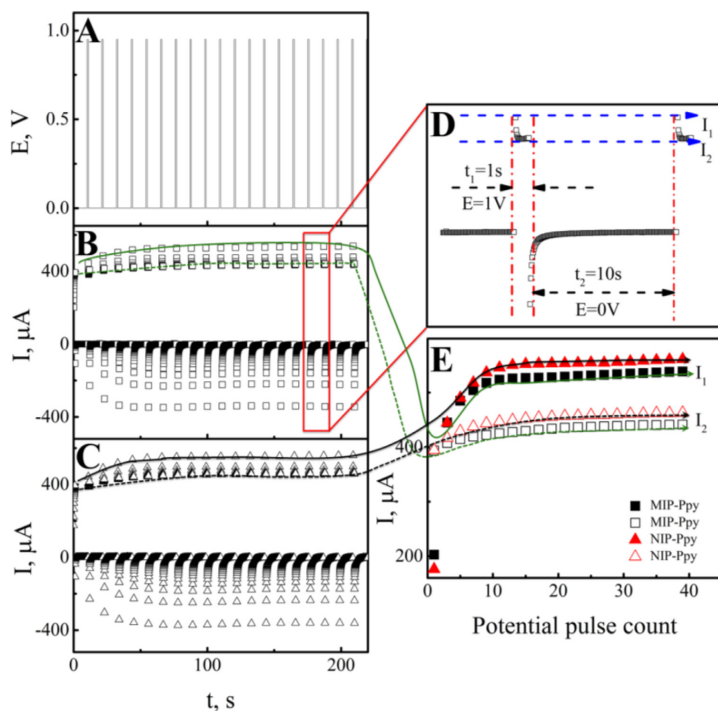

Fig. 2. Electrochemical deposition of the polypyrrole layers on the Pt electrode: **A** – The profile of potential applied during the sequence of potential pulses; **B** – The profile of current registered during the deposition of Ppy layer from polymerization solution containing SARS-CoV-2-S glycoprotein; **C** – The profile of current registered during the formation of Ppy layer from polymerization solution without SARS-CoV-2-S glycoprotein. **D** – The profile of current registered during one potential pulse. **E** – Changes of current measured instantly after a potential step of +950 mV.

same way as MIP-Ppy, NIP-Ppy was also exposed to 0.05 M solution of H_2SO_4. MIP-Ppy and NIP-Ppy were analyzed using pulsed amperometric detection by the sequence of 10 potential pulses of +600 mV *vs* Ag/AgCl lasting for 2 s, between these pulses 0 V *vs* Ag/AgCl was applied for 2 s (Fig. 1).

3. Results and discussions

Electrochemical polymerization of the two types of Ppy layers was performed by a sequence of potential pulses (Fig. 2). The profile of potential pulses sequence is represented in Fig. 2A. Figs. 2B
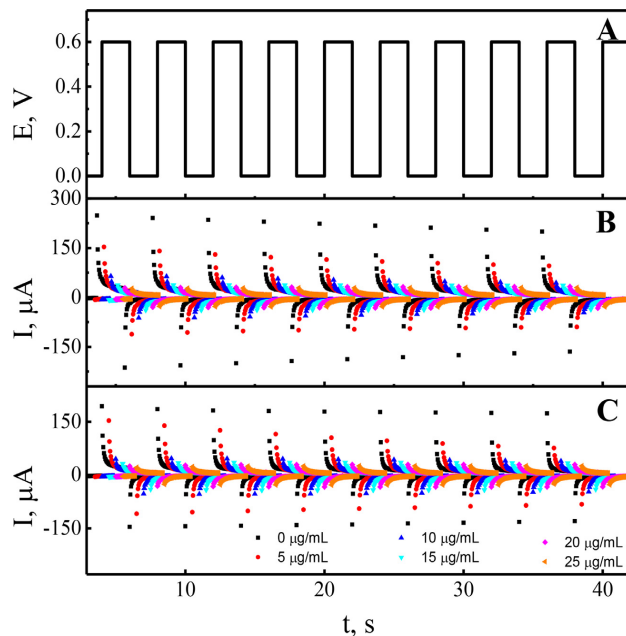
Fig. 3. Electrochemical evaluation of MIP-Ppy and NIP-Ppy layers was performed by the potential pulse sequence. **A** – potential pulse profile. Typical chronoamperograms (during pulsed amperometric detection) were obtained at: **B** – MIP-Ppy and **C** – NIP-Ppy modified Pt electrodes in the absence of SARS-CoV-2-S glycoprotein (•) and in the presence of SARS-CoV-2-S glycoprotein from 5 μg/mL up to 25 μg/mL in PBS solution, pH 7.4 (offset 0.5).

and 2C demonstrate the currents registered during the electrochemical deposition of Ppy layer from polymerization solution containing SARS-CoV-2-S glycoprotein and Ppy layer from polymerization solution without SARS-CoV-2-S glycoprotein on Pt-electrode surface.

The changes of current at the beginning I_1 and at the end I_2 of pulses of the potential at +950 mV are presented in Fig. 2E. The current changes at the potential of 0 V were not the object of analysis, because during this potential step the equilibration of monomer and template molecule concentrations in the neighborhood of the working electrode is happening. Previous studies demonstrated that the self-assembly of monomers and template molecules due to the interactions under thermodynamic control prior to polymerization, is significant for the recognition characteristics of the final polymers [61]. Polymerization of Ppy occurs during the pulses at a potential value of +950 mV. Therefore, only an insignificant Faradaic process was observed on the electrode at the 0 V potential step. Thus, the current changes during the potential step when the potential was elevated up to +950 mV were analyzed in more detail. For the visualization of the current changes during the electrochemical deposition of Ppy layer from polymerization solution containing SARS-CoV-2-S glycoprotein and Ppy layer from polymerization solution without SARS-CoV-2-S glycoprotein, two current points at the beginning I_1 and end I_2 of each potential step were taken into account (Fig. 2D). The comparison of the current changes demonstrated that the current registered during deposition of Ppy layer from polymerization solution without SARS-CoV-2-S glycoprotein is higher than that registered during deposition of Ppy layer from polymerization solution containing SARS-CoV-2-S glycoprotein (Fig. 2E). However, the observed difference of current changes is not very significant in com-

parison with that registered in our previous researches [29] and in other researches [29, 62]. The collation of current changes on Pt electrode during the electrochemical deposition of Ppy/SARS-CoV-2-S and NIP-Ppy layers have illustrated that current during the deposition of NIP-Ppy increased just by 1.05 times in comparison to that registered during the deposition of Ppy/SARS-CoV-2-S. From the current changes observed during the polymerization, it can be presumed that the entrapped protein molecules just insignificantly affect the conductivity of the formed layers. During the next MIP-Ppy preparation step, the entrapped SARS-CoV-2-S glycoproteins were removed from the formed Ppy/SARS-CoV-2-S layer and MIP-Ppy was formed. In the same way, as MIP-Ppy, NIP-Ppy was also exposed to 0.05 M H$_2$SO$_4$ to eliminate any differences caused by the extraction procedure on the formed MIP-Ppy, NIP-Ppy layer properties.

In the following part of the research, the formed MIP-Ppy and NIP-Ppy layers were evaluated using pulsed amperometric detection by a sequence of 10 potential pulses of +600 mV and 0 V for 2 s each as it was suggested in our previous research [44]. Various aspects of charging-discharging of conducting polymer polypyrrole were well discussed by Heinze et al. [63]. Also, there was stated that overoxidation of the un-substituted Ppy already occurs at 0.65 V vs Ag/AgCl(3 M $_{KCl}$) [64]. Hence, taking into account these findings potential pulse values of 0 V and +600 mV were selected for the determination of SARS-CoV-2-S glycoproteins.

The profile of the potential pulse sequence is presented in Fig. 3A.

The concentration of SARS-CoV-2-S glycoprotein was varying in the range from 0 μg/mL to 25 μg/mL. Some other reports described instability of the proteins in presence of salts [65, 66], but during the preparation of required concentrations no signs

4

Table 1
Linear regression characteristics of current (ΔI, μA) vs concentration of SARS-CoV-2-S glycoprotein (c, μg/mL) on the MIP-Ppy and NIP-Ppy modified Pt electrodes.

$y = axe+b$	a	b	R^2
SARS-CoV-2-S determined by MIP-Ppy-based electrode	−0.46±0.04	23.4 ± 0.7	0.96
SARS-CoV-2-S determined by NIP-Ppy-based electrode	−0.21±0.01	13.9 ± 0.3	0.98
BSA determined by MIP-Ppy-based electrode	−0.15±0.01	15.7 ± 0.2	0.97
BSA determined by NIP-Ppy-based electrode	−0.10±0.01	14.7 ± 0.1	0.97

of instability of the SARS-CoV-2-S glycoprotein solubilized in PBS were observed. Figs. 3B and C demonstrate the dependence of the chronoamperometric response (during pulsed amperometric detection) of MIP-Ppy and NIP-Ppy modified electrodes to SARS-CoV-2-S glycoprotein. The change in the chronoamperometric response is related to the adsorption of less conductive protein molecules on the MIP-Ppy and NIP-Ppy layers. When SARS-CoV-2-S glycoprotein concentration in solution was increased, the registered chronoamperometric response of both MIP-Ppy and NIP-Ppy-modified Pt electrodes decreased. Higher currents were registered before the incubation of electrode in SARS-CoV-2-S glycoprotein containing solution. This effect is determined by the presence of water molecules and electrolyte ions in the places where molecular imprints were formed. After the incubation in SARS-CoV-2-S glycoprotein containing solution, the ions of solvent and the electrolyte were replaced by the molecules of SARS-CoV-2-S glycoprotein and thus the registered current at the potential of +600 mV decreased.

The magnitude of current differences, which are registered during potential pulses at instants when potentials were stepped from 0 mV up to +600 mV and +600 mV down to 0 mV, has decreased with increasing SARS-CoV-2-S glycoprotein concentration in PBS solution (Fig. 4). Fig. 4A represents the current profile, which was registered during potential pulses, and the way in which the analytical signals (ΔI) for the calibration curve was depicted. According to this calibration curve, linearity of analytical signal dependence on analyte concentration was observed at all evaluated SARS-CoV-2-S glycoprotein concentrations in the range from 0 μg/mL to 25 μg/mL.

The slope derived using the linear regression equation for the changes of current (ΔI, μA) vs concentration of SARS-CoV-2-S glycoprotein (concentration expressed in μg/mL) registered by NIP-Ppy-modified Pt electrode was of −0.22 μA/(μg/mL) with $R^2 = 0.98$ (Table 1). While the slope of linear regression for the Pt electrode modified with SARS-CoV-2-S glycoprotein imprinted MIP-Ppy was −0.47 μA/(μg/mL) with $R^2 = 0.96$ (Table 1). The sensitivity calculated from the calibration curves of the MIP-Ppy modified Pt electrode towards SARS-CoV-2-S glycoprotein in the linear dependence interval according to the ΔI measurements was approximately 2.1 times higher than that of NIP-Ppy modified Pt electrode. This difference is significant and therefore can be applied in the design of sensors based on MIP-Ppy modified Pt electrodes.

The same MIP-Ppy and NIP-Ppy modified Pt electrodes were evaluated for the interaction with BSA (Fig. 4B) to evaluate the selectivity of MIP-Ppy layer towards different proteins. The slope values for these measurements were derived using linear regression and they are represented in Table 1. The slope value (−0.15 μA/(μg/mL)) registered by the MIP-Ppy modified Pt electrodes incubated in BSA containing solution was significantly lower.

The comparison of the sensitivity/selectivity results among studies, which are reporting MIPs sensors based on the different polymers is rather complicated, because several factors are playing an important role on the final result: (i) the design of the electrochemical cell, (ii) the electrochemical method used for evaluation of the sensor, (iii) nature of the polymer, etc.
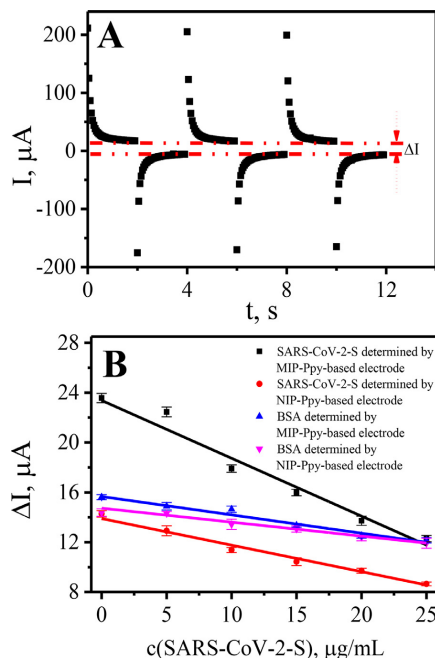

Fig. 4. Calibration curves of ΔI vs concentration of SARS-CoV-2-S glycoprotein and BSA on MIP-Ppy and NIP-Ppy according to the ΔI calculated in respect to: **A** – the principal of ΔI measuring; **B** – ΔI. RSD% was in range from 2 to 4.3% of current values of 5 potential pulses for the listed data points.

Only very few studies are published concerning the application of molecular imprinting technology for the analysis of SARS-CoV-2 proteins. There was a study describing the application of o-phenylenediamine o-phenylenediamine deposited on the macroporous gold screen-printed electrode with the receptor-binding domain of SARS-CoV-2-RBD for impedimetric measurements [59]. The described sensor was sensitive to the concentrations of SARS-CoV-2-RBD molecules in the range of pg/mL. In another study m-phenylenediamine (mPD) was imprinted with SARS-CoV-2 nucleoprotein (ncovNP). The sensitivity of the sensor according to the DPV signal was in the range of fM [58]. In order to demonstrate the selectivity of the sensor, BSA among others were used in the study. The Ppy was imprinted with gp51 and was applied in the design of electrochemical sensor [44]. The sensitivity of the sensor according to the results of simplified pulsed amperometric detection was in the range of μg/mL. The electrochemical sensors based on Ppy with imprints of prostate-specific antigen (PSA) was reported in 2020 [15]. The square wave voltammetry technique was used to determinate PSA concentration. The described sensor was sensi-

tive to the concentrations of PSA molecules in the range of pg/mL. The electrochemical MIP sensor based on Ppy and aminophenylboronic acid (p-APBA) bilayer was imprinted with lysozyme [48]. The sensitivity of the sensor according to the CV signal was in the range of ppm. Hence, several factors govern the sensitivity of the MIP sensors. The electrochemical method of chronoamperometry (pulsed amperometric detection) by the sequence of potential pulses was only occasionally used in previous studies. In this study, we demonstrated that the obtained MIP-Ppy modified Pt electrodes can be applied for the determination of imprinted SARS-CoV-2-S glycoproteins.

Conclusions

Pt electrode was modified by two types of Ppy layers: (i) MIP-Ppy layer, which was modified by imprints of SARS-CoV-2-S glycoprotein and (ii) NIP-Ppy, which was formed without the imprint of any proteins. The comparison of the current changes on Pt electrode during the electrochemical deposition of MIP-Ppy and NIP-Ppy has demonstrated that the current for NIP-Ppy increased approximately by only 1.05 times more than that registered during the deposition of MIP-Ppy layer. This means that the SARS-CoV-2-S glycoprotein, which serves as the template molecule for MIP-Ppy layer, does not have a crucial effect on the thickness of the deposited polymer layer and the initial characteristics of the formed MIP-Ppy and NIP-Ppy layers are comparable. The comparison of calibration curves registered after the incubation of MIP-Ppy and NIP-Ppy modified Pt electrodes revealed that the interaction of SARS-CoV-2-S glycoprotein with MIP-Ppy generates 2.1 times higher change of current for MIP-Ppy modified electrode, in comparison with that registered for NIP-Ppy modified Pt electrode. The selectivity of SARS-CoV-2-S imprinted MIP-Ppy modified Pt electrode was tested in comparison to BSA solution. The obtained slope values during the evaluation of MIP-Ppy modified Pt electrode sensitivity towards BSA were significantly lower when compared with that towards SARS-CoV-2-S glycoprotein. The results of application of MIP-Ppy modified Pt electrodes demonstrated higher current changes and can be applied for selective determination of the imprinted SARS-CoV-2-S glycoprotein. Therefore, it can be concluded that the molecular imprinting of the conducting polymer might be applied for the development of the electrochemical sensor for the detection of SARS-CoV-2-S glycoprotein.

Supporting Material

Supporting material_AR.docx

Declaration of Competing Interest

The authors declare that they have no known competing financial interests or personal relationships that could have appeared to influence the work reported in this paper.

Credit authorship contribution statement

Vilma Ratautaite: Methodology, Investigation, Writing – original draft. **Raimonda Boguzaite:** Methodology, Investigation, Writing – original draft. **Ernestas Brazys:** Methodology, Investigation, Writing – original draft.   **Arunas Ramanavicius:** Supervision, Conceptualization, Writing – review & editing, Funding acquisition.

Acknowledgement

Supplementary materials

Supplementary material associated with this article can be found, in the online version, at doi:10.1016/j.electacta.2021.139581.

References

[1] B. Shan, Y.Y. Broza, W. Li, Y. Wang, S. Wu, Z. Liu, J. Wang, S. Gui, L. Wang, Z. Zhang, W. Liu, S. Zhou, W. Jin, Q. Zhang, D. Hu, L. Lin, Q. Zhang, W. Li, J. Wang, H. Liu, Y. Pan, H. Haick, Multiplexed nanomaterial-based sensor array for detection of COVID-19 in exhaled breath, ACS Nano. 14 (2020) 12125–12132.

[2] R.D. Lamboll, C.D. Jones, R.B. Skeie, S. Fiedler, B.H. Samset, N.P. Gillett, J. Rogelj, P.M. Forster, Modifying emission scenario projections to account for the effects of COVID-19: protocol for COVID-MIP, Geoscientific model development discussions (2020) 1–20 (2020).

[3] D. Wu, T. Wu, Q. Liu, Z. Yang, The SARS-CoV-2 outbreak: what we know, Int. J. Infect. Dis. 94 (2020) 44–48.

[4] T. Koyama, D. Platt, L. Parida, Variant analysis of SARS-CoV-2 genomes, Bull. World Health Organ. 98 (2020) 495–504.

[5] Y.-Z. Zhang, E.C. Holmes, A genomic perspective on the origin and emergence of SARS-CoV-2, Cell 181 (2020) 223–227.

[6] R.L. Tillett, J.R. Sevinsky, P.D. Hartley, H. Kerwin, N. Crawford, A. Gorzalski, C. Laverdure, S.C. Verma, C.C. Rossetto, D. Jackson, M.J. Farrell, S. Van Hooser, M. Pandori, Genomic evidence for reinfection with SARS-CoV-2: a case study, Lancet Infect. Dis. 21 (2021) 52–58.

[7] R.J. Rockett, A. Arnott, C. Lam, R. Sadsad, V. Timms, K.-A. Gray, J.-S. Eden, S. Chang, M. Gall, J. Draper, E.M. Sim, N.L. Bachmann, I. Carter, K. Basile, R. Byun, M.V. O'Sullivan, S.C.A. Chen, S. Maddocks, T.C. Sorrell, D.E. Dwyer, E.C. Holmes, J. Kok, M. Prokopenko, V. Sintchenko, Revealing COVID-19 transmission in Australia by SARS-CoV-2 genome sequencing and agent-based modeling, Nat. Med. 26 (2020) 1398–1404.

[8] L. Yurkovetskiy, X. Wang, K.E. Pascal, C. Tomkins-Tinch, T.P. Nyalile, Y. Wang, A. Baum, W.E. Diehl, A. Dauphin, C. Carbone, K. Veinotte, S.B. Egri, S.F. Schaffner, J.E. Lemieux, J.B. Munro, A. Rafique, A. Barve, P.C. Sabeti, C.A. Kyratsous, N.V. Dudkina, K. Shen, J. Luban, Structural and functional analysis of the D614G SARS-CoV-2 Spike Protein Variant, Cell 183 (2020) 739–751.e738.

[9] A.C. Walls, Y.-J. Park, M.A. Tortorici, A. Wall, A.T. McGuire, D. Veesler, Structure, function, and antigenicity of the SARS-CoV-2 spike glycoprotein, Cell 181 (2020) 281–292.e286.

[10] P. Calligari, S. Bobone, G. Ricci, A. Bocedi, Molecular investigation of SARS—CoV-2 proteins and their interactions with antiviral drugs, Viruses 12 (2020) 445.

[11] Y. Huang, C. Yang, X.-f. Xu, W. Xu, S.-w. Liu, Structural and functional properties of SARS-CoV-2 spike protein: potential antivirus drug development for COVID-19, Acta Pharmacol. Sin. 41 (2020) 1141–1149.

[12] F. Amanat, F. Krammer, SARS-CoV-2 Vaccines: status Report, Immunity 52 (2020) 583–589.

[13] B. Hu, H. Guo, P. Zhou, Z.-L. Shi, Characteristics of SARS-CoV-2 and COVID-19, Nat. Rev. Microbiol. (2020).

[14] A. Tretjakov, V. Syritski, J. Reut, R. Boroznjak, A. Öpik, Molecularly imprinted polymer film interfaced with Surface Acoustic Wave technology as a sensing platform for label-free protein detection, Anal. Chim. Acta 902 (2016) 182–188.

[15] Z. Mazouz, M. Mokni, N. Fourati, C. Zerrouki, F. Barbault, M. Seydou, R. Kalfat, N. Yaakoubi, A. Omezzine, A. Bouslema, A. Othmane, Computational approach and electrochemical measurements for protein detection with MIP-based sensor, Biosens. Bioelectron. 151 (2020) 111978.

[16] A. Kidakova, R. Boroznjak, J. Reut, A. Öpik, M. Saarma, V. Syritski, Molecularly imprinted polymer-based SAW sensor for label-free detection of cerebral dopamine neurotrophic factor protein, Sens. Actuators B 308 (2020) 127708.

[17] R. Thoelen, R. Vansweevelt, J. Duchateau, F. Horemans, J. D'Haen, L. Lutsen, D. Vanderzande, M. Ameloot, M. VandeVen, T.J. Cleij, P. Wagner, A MIP-based impedimetric sensor for the detection of low-MW molecules, Biosens. Bioelectron. 23 (2008) 913–918.

[18] S. Ramanavicius, A. Ramanavicius, Conducting Polymers in the Design of Biosensors and Biofuel Cells, Polymers (Basel) 13 (2021) 49.

[19] S. Ramanavicius, A. Jagminas, A. Ramanavicius, Advances in molecularly imprinted polymers based affinity sensors (Review), Polymers (Basel) 13 (2021) 974.

[20] C. Malitesta, E. Mazzotta, R.A. Picca, A. Poma, I. Chianella, S.A. Piletsky, MIP sensors - the electrochemical approach, Anal. Bioanal. Chem. 402 (2012) 1827–1846.

[21] A.G. Ayankojo, J. Reut, V. Ciocan, A. Öpik, V. Syritski, Molecularly imprinted polymer-based sensor for electrochemical detection of erythromycin, Talanta 209 (2020) 120502.

[22] S. Ansari, S. Masoum, Molecularly imprinted polymers for capturing and sensing proteins: current progress and future implications, TrAC Trends Anal. Chem. 114 (2019) 29–47.

[23] H.F. El-Sharif, D. Stevenson, S.M. Reddy, MIP-based protein profiling: a method for interspecies discrimination, Sens. Actuators B 241 (2017) 33–39.

[24] V. Ratautaite, S.D. Janssens, K. Haenen, M. Nesládek, A. Ramanaviciene, I. Baleviciute, A. Ramanavicius, Molecularly imprinted polypyrrole based impedimentric sensor for theophylline determination, Electrochim. Acta 130 (2014) 361–367.

[25] E.N. Ndunda, Molecularly imprinted polymers—A closer look at the control polymer used in determining the imprinting effect: a mini review, J. Mol. Recognit. 33 (2020) e2855.

[26] O.S. Ahmad, T.S. Bedwell, C. Esen, A. Garcia-Cruz, S.A. Piletsky, Molecularly imprinted polymers in electrochemical and optical sensors, Trends Biotechnol. 37 (2019) 294–309.

[27] B. Yang, C. Fu, J. Li, G. Xu, Frontiers in highly sensitive molecularly imprinted electrochemical sensors: challenges and strategies, TrAC Trends Anal. Chem. 105 (2018) 52–67.

[28] T. Alizadeh, M.R. Ganjali, M. Zare, P. Norouzi, Development of a voltammetric sensor based on a molecularly imprinted polymer (MIP) for caffeine measurement, Electrochim. Acta 55 (2010) 1568–1574.

[29] D. Plausinaitis, L. Sinkevicius, U. Samukaite-Bubniene, V. Ratautaite, A. Ramanavicius, Evaluation of electrochemical quartz crystal microbalance based sensor modified by uric acid-imprinted polypyrrole, Talanta 220 (2020) 121414.

[30] J.W. Lowdon, H. Diliën, P. Singla, M. Peeters, T.J. Cleij, B. van Grinsven, K. Eersels, MIPs for commercial application in low-cost sensors and assays – An overview of the current status quo, Sens. Actuators B 325 (2020) 128973.

[31] G. Selvolini, G. Marrazza, MIP-based sensors: promising new tools for cancer biomarker determination, Sensors 17 (2017) 718.

[32] V. Ratautaite, D. Plausinaitis, I. Baleviciute, L. Mikoliunaite, A. Ramanaviciene, A. Ramanavicius, Characterization of caffeine-imprinted polypyrrole by a quartz crystal microbalance and electrochemical impedance spectroscopy, Sens. Actuators B 212 (2015) 63–71.

[33] V. Ratautaite, M. Nesladek, A. Ramanaviciene, I. Baleviciute, A. Ramanavicius, Evaluation of histamine imprinted polypyrrole deposited on boron doped nanocrystalline diamond, Electroanalysis 26 (2014) 2458–2464.

[34] M. Dabrowski, P. Lach, M. Cieplak, W. Kutner, Nanostructured molecularly imprinted polymers for protein chemosensing, Biosens. Bioelectron. 102 (2018) 17–26.

[35] V.K. Tamboli, N. Bhalla, P. Jolly, C.R. Bowen, J.T. Taylor, J.L. Bowen, C.J. Allender, P. Estrela, Hybrid synthetic receptors on MOSFET devices for detection of prostate specific antigen in human plasma, Anal. Chem. 88 (2016) 11486–11490.

[36] Q. Zeng, X. Huang, M. Ma, A molecularly imprinted electrochemical sensor based on polypyrrole/carbon nanotubes composite for the detection of S-ovalbumin in egg white, Int. J. Electrochem. Sci. 12 (2017) 3965–3981.

[37] V.V. Shumyantseva, T.V. Bulko, L.V. Sigolaeva, A.V. Kuzikov, A.I. Archakov, Electrosynthesis and binding properties of molecularly imprinted poly-o-phenylenediamine for selective recognition and direct electrochemical detection of myoglobin, Biosens. Bioelectron. 86 (2016) 330–336.

[38] Z. Stojanovic, J. Erdőssy, K. Keltai, F.W. Scheller, R.E. Gyurcsányi, Electrosynthesized molecularly imprinted polyscopoletin nanofilms for human serum albumin detection, Anal. Chim. Acta 977 (2017) 1–9.

[39] J. Erdőssy, V. Horváth, A. Yarman, F.W. Scheller, R.E. Gyurcsányi, Electrosynthesized molecularly imprinted polymers for protein recognition, TrAC Trends Anal. Chem. 79 (2016) 179–190.

[40] A. Yarman, D. Dechtrirat, M. Bosserdt, K.J. Jetzschmann, N. Gajovic-Eichelmann, F.W. Scheller, Cytochrome c-derived hybrid systems based on molecular imprinted polymers, Electroanalysis 27 (2015) 573–586.

[41] L.-W. Qian, X.-L. Hu, P. Guan, B. Gao, D. Wang, C.-L. Wang, J. Li, C.-B. Du, W.-Q. Song, Thermal preparation of lysozyme-imprinted microspheres by using ionic liquid as a stabilizer, Anal. Bioanal. Chem. 406 (2014) 7221–7231.

[42] S. Wu, W. Tan, H. Xu, Protein molecularly imprinted polyacrylamide membrane: for hemoglobin sensing, Analyst 135 (2010) 2523–2527.

[43] A. Tlili, G. Attia, S. Khaoulani, Z. Mazouz, C. Zerrouki, N. Yaakoubi, A. Othmane, N. Fourati, Contribution to the understanding of the interaction between a polydopamine molecular imprint and a protein model: ionic strength and ph effect investigation, Sensors 21 (2021) 619.

[44] A. Ramanaviciene, A. Ramanavicius, Molecularly imprinted polypyrrole-based synthetic receptor for direct detection of bovine leukemia virus glycoproteins, Biosens. Bioelectron. 20 (2004) 1076–1082.

[45] I. Baleviciute, V. Ratautaite, A. Ramanaviciene, Z. Balevicius, J. Broeders, D. Croux, M. McDonald, F. Vahidpour, R. Thoelen, W.D. Ceuninck, K. Haenen, M. Nesladek, A. Reza, A. Ramanavicius, Evaluation of theophylline imprinted polypyrrole film, Synth. Met. 209 (2015) 206–211.

[46] V. Ratautaite, S.N. Topkaya, L. Mikoliunaite, M. Ozsoz, Y. Oztekin, A. Ramanaviciene, A. Ramanavicius, Molecularly Imprinted Polypyrrole for DNA Determination, Electroanalysis 25 (2013) 1169–1177.

[47] R. Viter, K. Kunene, P. Genys, D. Jevdokimovs, D. Erts, A. Sutka, K. Bisetty, A. Viksna, A. Ramanaviciene, A. Ramanavicius, Photoelectrochemical bisphenol S sensor based on ZnO-nanoroads modified by molecularly imprinted polypyrrole, Macromol. Chem. Phys., 221 (2020) 1900232.

[48] J. Rick, T.-C. Chou, Amperometric protein sensor – fabricated as a polypyrrole, poly-aminophenylboronic acid bilayer, Biosens. Bioelectron. 22 (2006) 329–335.

[49] X. Kan, Z. Xing, A. Zhu, Z. Zhao, G. Xu, C. Li, H. Zhou, Molecularly imprinted polymers based electrochemical sensor for bovine hemoglobin recognition, Sens. Actuators B 168 (2012) 395–401.

[50] H.-J. Chen, Z.-H. Zhang, L.-J. Luo, S.-Z. Yao, Surface-imprinted chitosan-coated magnetic nanoparticles modified multi-walled carbon nanotubes biosensor for detection of bovine serum albumin, Sens. Actuators B 163 (2012) 76–83.

[51] M.L. Yola, N. Atar, Development of cardiac troponin-I biosensor based on boron nitride quantum dots including molecularly imprinted polymer, Biosens. Bioelectron. 126 (2019) 418–424.

[52] B.V.M. Silva, B.A.G. Rodríguez, G.F. Sales, M.D.P.T. Sotomayor, R.F. Dutra, An ultrasensitive human cardiac troponin T graphene screen-printed electrode based on electropolymerized-molecularly imprinted conducting polymer, Biosens. Bioelectron. 77 (2016) 978–985.

[53] Z. Wang, F. Li, J. Xia, L. Xia, F. Zhang, S. Bi, G. Shi, Y. Xia, J. Liu, Y. Li, L. Xia, An ionic liquid-modified graphene based molecular imprinting electrochemical sensor for sensitive detection of bovine hemoglobin, Biosens. Bioelectron. 61 (2014) 391–396.

[54] L. Li, L. Yang, Z. Xing, X. Lu, X. Kan, Surface molecularly imprinted polymers-based electrochemical sensor for bovine hemoglobin recognition, Analyst 138 (2013) 6962–6968.

[55] S. Ramanavicius, A. Ramanavicius, Charge transfer and biocompatibility aspects in conducting polymer-based enzymatic biosensors and biofuel cells, Nanomaterials 11 (2021) 371.

[56] D. Plausinaitis, V. Ratautaite, L. Mikoliunaite, L. Sinkevicius, A. Ramanaviciene, A. Ramanavicius, Quartz crystal microbalance-based evaluation of the electrochemical formation of an aggregated polypyrrole particle-based layer, Langmuir 31 (2015) 3186–3193.

[57] O.I. Parisi, M. Dattilo, F. Patitucci, R. Malivindi, V. Pezzi, I. Perrotta, M. Ruffo, F. Amone, F. Puoci, Monoclonal-type" plastic antibodies for SARS-CoV-2 based on molecularly imprinted polymers, bioRxiv (2020) 2020.2005.2028.120709.

[58] A. Raziq, A. Kidakova, R. Boroznjak, J. Reut, A. Öpik, V. Syritski, Development of a portable MIP-based electrochemical sensor for detection of SARS-CoV-2 antigen, Biosens. Bioelectron. 178 (2021) 113029.

[59] M.A. Tabrizi, J.P. Fernández-Blázquez, D.M. Medina, P. Acedo, An ultrasensitive molecularly imprinted polymer-based electrochemical sensor for the determination of SARS-CoV-2-RBD by using macroporous gold screen-printed electrode, Biosens. Bioelectron. (2021) 113279.

[60] A. Ramanavicius, Y. Oztekin, A. Ramanaviciene, Electrochemical formation of polypyrrole-based layer for immunosensor design, Sens. Actuators B 197 (2014) 237–243.

[61] J. Svenson, H.S. Andersson, S.A. Piletsky, I.A. Nicholls, Spectroscopic studies of the molecular imprinting self-assembly process, J. Mol. Recognit. 11 (1998) 83–86.

[62] N. Ermis, N. Tınkılıc, Preparation of molecularly imprinted polypyrrole modified gold electrode for determination of tyrosine in biological samples, Int. J. Electrochem. Sci. 13 (2018) 2286–2298.

[63] J. Heinze, B.A. Frontana-Uribe, S. Ludwigs, Electrochemistry of conducting polymers—persistent models and new concepts, Chem. Rev. 110 (2010) 4724–4771.

[64] T.W. Lewis, G.G. Wallace, C.Y. Kim, D.Y. Kim, Studies of the overoxidation of polypyrrole, Synth. Met. 84 (1997) 403–404.

[65] J.N. de Wit, T.v. Kessel, Effects of ionic strength on the solubility of whey protein products. A colloid chemical approach, Food Hydrocoll. 10 (1996) 143–149.

[66] D.L. Beauchamp, M. Khajehpour, Studying salt effects on protein stability using ribonuclease t1 as a model system, Biophys. Chem. 161 (2012) 29–38.

7

129

Evaluation of the interaction between SARS-CoV-2 spike glycoproteins and the molecularly imprinted polypyrrole

Vilma Ratautaite [a,c], Raimonda Boguzaite [a], Ernestas Brazys [b], Deivis Plausinaitis [b], Simonas Ramanavicius [b,c], Urte Samukaite-Bubniene [a,b], Mikhael Bechelany [d], Arunas Ramanavicius [a,b,*]

[a] *Department of Nanotechnology, Center for Physical Sciences and Technology, Sauletekio av. 3, Vilnius, LT-10257, Lithuania*
[b] *Department of Physical Chemistry, Institute of Chemistry, Faculty of Chemistry and Geosciences, Vilnius University, Naugarduko str. 24, Vilnius, LT-03225, Lithuania*
[c] *Department of Electrochemical Material Science, Center for Physical Sciences and Technology, Sauletekio av. 3, Vilnius, LT-10257, Lithuania*
[d] *Institut Européen des Membranes, IEM, UMR 5635, University of Montpellier, CNRS, ENSCM, 34090, Montpellier, France*

ARTICLE INFO

ABSTRACT

The SARS-CoV-2 spike glycoprotein (SARS-CoV-2-S) was used as a template molecule and polypyrrole (Ppy) was applied as an electro-generated conducting polymer, which was acting as a matrix for the formation of molecular imprints. Two types of Ppy-layers: molecularly imprinted polypyrrole (MIP-Ppy) and non-imprinted polypyrrole (NIP-Ppy) were electrochemically deposited on the working platinum electrode. The performance of electrodes modified by MIP-Ppy and NIP-Ppy layers was evaluated by pulsed amperometric detection (PAD). During the assessment of measurement results registered by PAD, the integrated Cottrell equation (Anson plot) was used to calculate the amount of charge passed through the MIP-Ppy and NIP-Ppy layers. The interaction between SARS-CoV-2 spike glycoproteins and molecularly imprinted polypyrrole (MIP-Ppy) was assessed by the Anson plot based calculations. This assessment reveals that SARS-CoV-2-S glycoproteins are interacting with MIP-Ppy more strongly than with NIP-Ppy.

1. Introduction

Molecularly imprinted polymers (MIPs) are artificially formed polymer structures suitable for the design of highly specific, selective, and sensitive analytical systems. Conducting polymers are frequently used for the development of MIPs and can be formed by electrochemical methods. Rather simple procedure of the electrochemical MIP manufacturing process and the ability to modify, and ameliorate characteristics of the MIP with dopants or by electrochemical parameters have attracted significant attention of researchers. However, the comprehensibility of the interaction peculiarities between the molecule of interest and imprinted cavity formed within the MIP is still relevant. Molecularly imprinted polymers (MIPs) are used in the recognition process because the way by which they operate can be described as synthetic analogs to the natural, biological antibody-antigen, or receptor-ligand-based systems. The process of MIP fabrication usually involves steps such as the polymerization of monomers in the presence

of a template molecule, extraction of the template molecules after polymerization, and afterward, MIP-based structures are ready for application in electrochemical MIP-based sensors [1–3]. During the polymerization, the template molecule forms an imprint within the polymer, which creates a cavity complementary to template molecule. Therefore, such cavities enables the selective recognition/binding of template molecules.

MIPs can be successfully designed for the recognition of various types of small molecular weight template molecules [1,4–7] imprinted within different polymers, including polypyrrole (Ppy) [4,5,8], polyaniline [8–10], and many others. These MIPs can be used in analytical systems based on different analytical techniques [4,11–13]. Some challenges and limitations of these MIPs are well discussed in several recently published review articles [2,3,14–18]. But among the different template molecules, the imprinting of macromolecules has some specific features [14,19,20]. Kan et al. [20] identified three limitations that are the most critical during protein imprinting. In particular, it is difficult to

remove the template protein from the bulk polymer matrix after the polymerization. Furthermore, organic solvents are often used in the formation of MIPs, although, they are unsuitable for the synthesis of protein-imprinted MIPs due to the poor solubility of the protein molecule in these solvents and possible denaturation of proteins in organic solvents. Due to this shortage, electrochemical polymerization is a better choice, because it can be performed in aqueous solutions. In this case, the environment is less polluted, therefore, it perfectly meets the principles of the green chemistry [21]. Finally, the size and structural complexity of the protein results in a more significant non-specific binding [20].

Some conducting polymers have been molecularly imprinted with various high molecular mass biomolecules including proteins [22–33], DNA [34,35], or even bacteria [36–38]. Polypyrrole has previously been molecularly imprinted by glycoproteins of virus [33], bovine hemoglobin [20,39,40], bovine serum albumin [41], prostate-specific antigen [42], cardiac troponin-I [43], and cardiac troponin T [44]. It is noteworthy to mention that cyclic voltammetry (CV) [20,41–44], differential pulse voltammetry (DPV) [20,39–41,43,44], and electrochemical impedance spectroscopy (EIS) [20,39–41,43] in presence of redox probe $[Fe(CN)_6]^{3-}/[Fe(CN)_6]^{4-}$ were the most frequently used electrochemical methods for the evaluation of the MIPs imprinted with proteins. The MIPs based on polypyrrole with bovine leukemia virus glycoproteins imprints [33] and SARS-CoV-2 spike glycoproteins [45] were evaluated by pulsed amperometric detection (PAD) method in the absence of ferrocyanide-ferricyanide system as a redox probe. According to the review of Faria et al. [46], such an analytical system should be classified as a type of non-faradaic sensor. In such case, charging and discharging of the double-layer capacitance are playing the most important role. At the same time, it is important to keep in mind that by changing the potential, the charging and the discharging of the conducting polymers occur. This effect was well discussed by Heinze et al. [47]. The electrochemical charging process of conducting polymers should be described by a sequence of discrete but overlapping redox steps. By changing the potential, there are more effects observed and the volume change is one of them. These effects are induced by the oxidation and the reduction of the polymer [48–50].

SARS-CoV-2 protein plays a key role in the cell receptor recognition/binding and penetration of the SARS-CoV-2 virus through the cell membrane. Aspects of electrochemical determination methods of proteins employing MIPs are especially interesting due to the recent widespread of the SARS-CoV-2 virus causing the COVID-19 disease. Recently some studies employing MIP-technology for SARS-CoV-2 spike glycoprotein were published [45,51–56]. The sensors mentioned in the literature differ in their primary system, composition, and preparation method, however, all of them are characterized by low cost, fast response, and real applicability [52,57,58]. The nucleocapsid, envelope, spike, and membrane proteins of the SARS-CoV-2 virus could be used as template macromolecules during the development of MIPs. Among the here-mentioned proteins, the spike protein SARS-CoV-2-S plays a key role in the cell receptor recognition/binding and the penetration of the SARS-CoV-2 virus through the cell membrane.

In this work, the polypyrrole-based MIP (MIP-Ppy) was developed and applied for the determination of the SARS-CoV-2-S spike glycoprotein to examine in detail complex and little-studied advantages/peculiarities of pulsed amperometric detection as the non-faradaic method. The novelty of the article was based on the application of total charge for the evaluation of the interaction between electrode and analyte. This total charge was calculated according to the integrated Cottrell equation and was plotted, as it was first demonstrated in articles of the F. C. Anson's research group for studies of reactants adsorption on the electrode [59–61]. In honor of this scientist nowadays, the plot of the total charge vs. square of time is called the Anson plot. So, the key idea of this work was based on the application of the Anson plots for elucidation of the interaction between SARS-CoV-2 spike glycoproteins and the molecularly imprinted polypyrrole.

2. Materials and methods

2.1. Chemicals and instrumentation

All chemicals were used as received without further purification. The chemicals were purchased as follows: pyrrole 98% – from *Alfa Aesar* (Germany), sulfuric acid (H$_2$SO$_4$; 96%) from *Lachner* (Czech Republic), nitric acid (HNO$_3$, 63%), sodium hydroxide (NaOH, 98%), and chloroplatinic acid (H$_2$PtCl$_6$, 40% Pt) from *Merck* (Germany), potassium phosphate (KH$_2$PO$_4$, 98%) from *Honeywell Riedel-de Haen* (Germany), sodium chloride (NaCl, 99,5%), potassium chloride (KCl, 99,5%), and disodium hydrogen phosphate (Na$_2$HPO$_4$, 99%) from *Carl Roth* (Germany). SARS-CoV-2 spike glycoproteins were purchased from UAB *Baltymas* (Lithuania).

The experiment was performed using potentiostat/galvanostat Metrohm-Autolab model μAutolabIII/FRA2 μ3AUT71079 controlled by NOVA 2.1.3 software (*EcoChemie*, The Netherlands). All measurements were done in a homemade cell. The total volume of the cell was 250 μL. Three-electrode system consisted of a working electrode (WE) – Pt disk with 1 mm diameter sealed in glass, reference electrode (RE) – Ag/AgCl, and counter electrode (CE) – Pt disk of 2 mm diameter.

2.2. Pretreatment of the working electrode

The working electrode was pretreated according to the procedure described in previous studies [33,62]. Solutions were degassed with a stream of nitrogen (N$_2$) before use. According to this procedure: 1) the Pt electrode was rinsed with concentrated HNO$_3$ solution in an ultrasonic bath for 10 min, 2) then rinsed with water, and 3) polished with alumina paste. Later on, 4) it was rinsed with water again and then 5) with 10 M of NaOH, thereafter – 6) with 5 M of H$_2$SO$_4$ in an ultrasonic bath for 5 min. 7) Electrochemical cleaning of the electrode was carried out in 0.5 M H$_2$SO$_4$ by cycling the potential 20 times in the range between -100 mV and $+1200$ mV vs. Ag/AgCl at a sweep rate of 100 mV s^{-1}. The bare electrode surface was indicated by a stable cyclic voltammogram. A layer of 'platinum black' was deposited over the working electrode to improve the adhesion of the Ppy layer to the electrode surface [62]. 'Platinum black' was deposited from a 5 mM solution of H$_2$PtCl$_6$, 0.1 M of KCl by 10 potential cycles in the range between $+500$ mV and -400 mV vs. Ag/AgCl at a sweep rate of 10 mV s^{-1}.

2.3. Electrochemical deposition of MIP and NIP layers. Sensor signal evaluation

The electrochemical deposition of the polypyrrole layer was performed in the same electrochemical cell. Non-imprinted polypyrrole (NIP-Ppy) was electrochemically deposited from the polymerization solution containing 0.5 M of pyrrole in PBS with 0.1 M of KCl, pH 7.4. Deposition of molecularly imprinted polypyrrole (MIP-Ppy) was carried out from the polymerization solution containing 0.5 M of pyrrole and 50 μg/mL of SARS-CoV-2 spike glycoprotein in the same PBS with 0.1 M of KCl, pH 7.4. The polymeric layers were formed by a sequence of 20 potential pulses of $+950$ mV vs. Ag/AgCl for 1 s, between these pulses 0 V vs. Ag/AgCl potential for 10 s was applied [33,62]. MIP-Ppy or NIP-Ppy modified electrodes were immersed in 0.05 M H$_2$SO$_4$ solution for 10 min and so the template molecules were extracted. MIP-Ppy or NIP-Ppy layers were incubated for 2 min in the PBS solution in the absence of SARS-CoV-2 spike glycoprotein or the presence of SARS-CoV-2 spike glycoprotein, in a concentration range from 0 μg/mL to 25 μg/mL. Next, MIP-Ppy and NIP-Ppy modified electrodes and interactions with SARS-CoV-2 spike glycoproteins were analyzed with the PAD method: the sequence of 10 potential pulses of $+600$ mV vs. Ag/AgCl for 2 s, between these pulses 0 V vs. Ag/AgCl was applied for 2 s (Fig. S1 and S2) [33].

3. Results and discussions

As it was described in the experimental part, the MIP-Ppy and NIP-Ppy modified electrodes were evaluated with the PAD method. The obtained amperograms are presented in Fig. 1.

The concentration of the SARS-CoV-2 spike glycoprotein varied from 0 μg/mL to 25 μg/mL. Fig. 1A and B demonstrate the dependence of the amperometric response of MIP-Ppy and NIP-Ppy modified Pt electrodes which were incubated in the SARS-CoV-2 spike glycoprotein containing PBS solution, pH 7.4. The change in the amperometric response is related to the adsorption of less conductive protein molecules on the MIP-Ppy or the NIP-Ppy layer. When SARS-CoV-2 spike glycoprotein concentration in solution increased, the registered amperometric response of both MIP-Ppy and NIP-Ppy-modified Pt electrodes decreased. Before the incubation of the electrode in the SARS-CoV-2 spike glycoprotein-containing solution, higher currents were registered. This effect is determined by the presence of water molecules and electrolyte ions in the places where molecular imprints were formed. After the incubation in the solution containing SARS-CoV-2 spike glycoprotein, the molecules of SARS-CoV-2 spike glycoprotein have replaced the ions of solvent and the electrolyte and thus the current at the potential of +600 mV was decreased. The amperometric response of the last pulses of +600 mV and 0 V from a 10 potential pulses-based sequence applied to MIP-Ppy and NIP-Ppy modified electrodes was selected for a more detailed evaluation (Fig. 2).

The relation of the cumulative charge passed and time in Ppy-based electrochemical sensors obeys the integrated Cottrell equation (1) [59, 63]:

$$Q = 2nFAC\sqrt{\frac{D}{\pi}}\sqrt{t} + Q_{d.l.} + Q_{ads.} = k\sqrt{t} + Q_{d.l.} + Q_{ads.} \quad (1)$$

where: Q – total charge (C); n – number of electrons; F – Faraday constant (96,485 C/mol); A – area of the electrode (cm^2); C – concentration (M); D – diffusion coefficient (cm^2/s); t – time (s); $Q_{d.\,l.}$ – the charge of the electrical double layer; $Q_{ads.}$ – charge induced by adsorbed ions.

The cumulative charge in the Cottrell equation corresponds to the charge passed associated with redox activity leading to Faradaic charges ($Q_{F.}$), charging, and discharging of electrode-electrolyte double-layer capacitive charges ($Q_{d.l.}$), and charge changes associated with the adsorbed species ($Q_{ads.}$) [64]. Hence, the plot of Q vs. $t^{1/2}$ has a linear correlation with the slope k and the intercept corresponding to $Q_{ads.}$ + $Q_{d.\,l.}$. As it was described previously, the absence of specific adsorption of analytes on the surface of the unmodified mercury electrode was indicated by two straight lines with equal slopes that intersect each other at

the $Q = 0$ axis [59]. Several studies are appointed to evaluate the adsorption process on the electrode. As stated in a previous study [61], the expected effect of the adsorbed analyte is inducing the increase of the intercept, although the slope remains unchanged. In the other two former articles [61,65], the adsorption process was evaluated by using mercury and the screen-printed electrodes (printed using a carbon-graphite ink). In these studies, it was demonstrated that the slope is proportional to the concentration and the intercept reflects the increasing adsorption. Confirmation that there is no analyte adsorbing on the electrode is based on the Q vs. $t^{1/2}$ plots, which were registered during potential pulses of different polarity, with equal (but with opposite signs) slopes and intercepts [60]. It was stated, that this might usually be taken as a good evidence for the absence of reactant (or product) adsorption. Another study was appointed to determine the type of adsorbate (reactant or product) on the electrode and the evidence of reactant or product adsorption was based on changes in slope and intercept [66].

The effect described in this study is more complex compared to those presented in literature [59,61,65]. In these studies, a plain electrode without any modification was used. Therefore, it is possible to describe the simplified reaction of the analyte on the electrode in several steps: diffusion of the analyte from the solution to the electrode, electrochemical oxidation-reduction reaction, and then diffusion of the reaction products from the electrode to the solution. Analysis of the slopes and intercepts in the Anson plot may be used for the identification of the adsorption either of the analytes or the reaction products on the electrode. In this study, the Pt electrode was modified with the conducting polymer Ppy that was further imprinted or non-imprinted with glycoprotein. It is noteworthy that by changing the potential, the Ppy layer itself can take part in charging and discharging during the electrochemical oxidation and reduction reaction [47]. On the other hand, the evaluation of charge carrier transfer mechanisms between glucose oxidase and organic semiconductors gives serious insights into the potential transfer of charge carriers (holes and electrons) [67]. These insights make the analysis of the amperograms complex but still possible to describe in the terms suggested by Anson.

The Anson plots are depicted (Fig. 3A and D, and Fig. S3) for the data from the amperograms in Fig. 2. The relationship of Q vs. $t^{1/2}$ was fitted by linear regression, and the parameters of the corresponding linear equations are listed in Table 1. The obtained R^2 values indicate that there is a linear correlation in the plot of Q vs. $t^{1/2}$ (Table 1). According to the experimental conditions, it was not expected that oxidation of SARS-CoV-2 spike glycoprotein can occur at the potential of +600 mV. However, the interaction of SARS-CoV-2 spike glycoprotein with
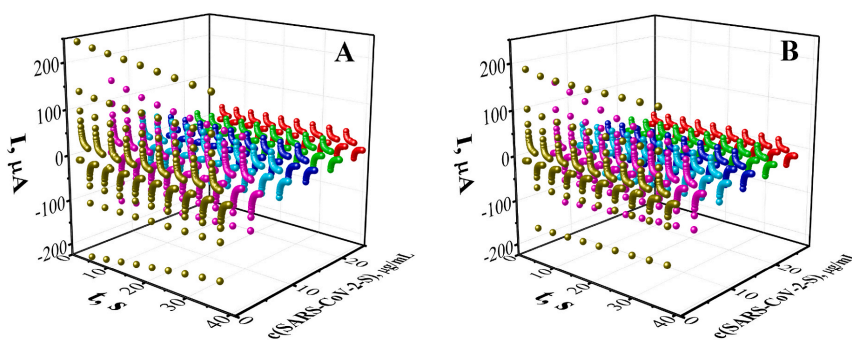

Fig. 1. Pulsed amperometry-based evaluation of MIP-Ppy and NIP-Ppy modified electrodes performed by the potential pulse sequence (+0.6 V and 0 V potentials), representing the incubation process of the SARS-CoV-2 spike glycoprotein. Amperograms were obtained at Pt electrode modified: **A)** with MIP-Ppy modified electrode and **B)** with NIP-Ppy modified electrode in PBS with 0.1 M of KCl, pH 7.4 in the absence of SARS-CoV-2 spike glycoprotein or the presence of SARS-CoV-2 spike glycoprotein concentrations from 5 μg/mL up to 25 μg/mL.
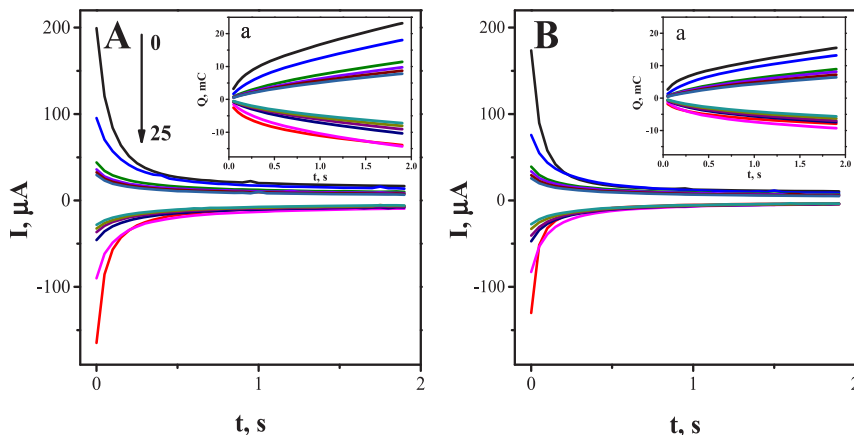
Fig. 2. Amperometric responses were registered during the last (10th) potential pulse of the applied potential pulse sequence (+0.6 V and 0 V potentials), for **A** – MIP-Ppy modified electrode and **B** – NIP-Ppy modified electrode in the absence of SARS-CoV-2 spike glycoprotein and in the presence of SARS-CoV-2 spike glycoprotein from 5 μg/mL up to 25 μg/mL in PBS with 0.1 M of KCl, pH 7.4. The insets (a) represent the change of charge (Q, mC vs. t, s) of the corresponding amperograms.

Table 1
Linear regression parameters of the Anson plot (Q, mC vs. $t^{1/2}$, $s^{1/2}$) (derived from on the MIP-Ppy and NIP-Ppy modified Pt electrodes for the last (10th) pulse of the potential pulse sequence.

y = ax + b C, μg/mL		MIP-Ppy modified electrode			NIP-Ppy modified electrode		
		a	b	R^2	a	b	R^2
0	+600 mV	16.35	0.46	0.99	10.26	1.22	0.99
	0 V	−8.09	−2.87	0.99	−4.17	−2.22	0.99
5	+600 mV	13.99	−1.39	0.99	9.70	−0.19	0.99
	0 V	−10.48	0.095	0.99	−5.56	−1.74	0.99
10	+600 mV	9.84	−2.27	0.99	7.37	−1.29	0.99
	0 V	−8.39	1.25	0.99	−5.10	−0.46	0.99
15	+600 mV	8.61	−2.22	0.99	6.83	−1.32	0.99
	0 V	−7.57	1.40	0.99	−4.97	−0.20	0.99
20	+600 mV	7.65	−1.91	0.99	6.12	−1.26	0.99
	0 V	−6.68	1.14	0.99	−4.61	0.03	0.99
25	+600 mV	6.85	−1.69	0.99	5.47	−1.13	0.99
	0 V	−5.98	1.05	0.99	−4.22	0.12	0.99

carboxyl, carbonyl, and hydroxyl groups, formed during partial over-oxidation of formed polypyrrole structure and complementary arranged in imprinted cavities was playing an important role in the recognition of SARS-CoV-2 spike glycoprotein and the formation of Ppy/SARS-CoV-2 spike glycoprotein complex, similarly, as it was described for the small molecular weight molecules [68,69]. Due to the replacement of water molecules by SARS-CoV-2 spike glycoprotein, changes in registered current are observed after the incubation of the MIP-Ppy modified electrode in SARS-CoV-2 spike glycoprotein-containing solutions.

Fig. 3A (for MIP-Ppy modified electrode) and Fig. 3D (for NIP-Ppy modified electrode) demonstrate the plots of Q vs. $t^{1/2}$ of +600 mV and 0 V pulses. The linear dependence of the slope on the concentration of SARS-CoV-2 spike glycoprotein is represented in Fig. 3B (for MIP-Ppy modified electrode) and Fig. 3E (for NIP-Ppy modified electrode). The plots represented in Fig. 3 illustrate that slope values are very different for MIP-Ppy and NIP-Ppy modified electrodes under the same experimental conditions. The linear dependence of the slope value on the concentration of the analyte for the MIP-Ppy modified electrode (−0.387 for +600 mV pulse and 0.1303 for 0 mV pulse (Fig. 3B)) is steeper than for the NIP-Ppy modified electrode (−0.2015 for +600 mV pulse and 0.0156 for 0 mV pulse (Fig. 3E)). This confirms that the

analyte tends to interact stronger with the MIP-Ppy than with the NIP-Ppy. A positive value of the intercept was calculated only in the case where MIP-Ppy and NIP-Ppy modified Pt electrodes were incubated in SARS-CoV-2 spike glycoprotein-free PBS solution (Table 1, Fig. 3C and F). When the concentration of SARS-CoV-2 spike glycoprotein in the solution was increased, all obtained intercept values became negative. A plausible explanation of the observed effect was given by Plausinaitis et al. [63]. The mentioned work describes the quartz crystal microbalance-based evaluation of the electrochemical formation of an aggregated polypyrrole layer. Concerning some other reports [70,71], it was assumed that the pyrrole oxidation process is occurring according to the principles described by heterogeneous kinetics. Here described study is based on the operating principles of the MIP. This means the formation of the complementary cavities in the polymer in the stage of polymerization and the attendance of these cavities in the specific interaction with the analyte during the evaluation step. Thus, molecules adsorbed on the Ppy surface hinder the heterogeneous pyrrole oxidation and reduction reaction.

Data presented in Fig. 3B and E illustrate that the slope *k* of the Anson equation, which was calculated according to equation (1), decreases by increasing the concentration of SARS-CoV-2 spike glycoprotein. At the electrode potential of +600 mV, this effect is much more distinct in comparison to that at 0 mV potential. The slope '*k*', which is indicated by equation (1), is related to (i) the equivalent number of electrons '*n*', which is transferred during the electrochemical reaction; (ii) electrochemically active area '*A*'; concentration of material '*C*' and diffusion coefficient '*D*'. In our case, this dependence of slope '*k*' on the concentration '*C*' of glycoprotein is related to the decrease of electrochemically active area '*A*'. This conclusion is based on the estimation that values of *n* and *D* parameters are constant at all here evaluated concentrations of SARS-CoV-2 spike glycoprotein because the concentration of all other components in the solution and, therefore, physicochemical characteristics (e.g., density and viscosity) are the same. It should be noted that in the case of the MIP-Ppy modified electrode, the dependence of '*k*' on the concentration of SARS-CoV-2 spike glycoprotein is more significantly expressed in comparison to that of the NIP-Ppy modified electrode. At the first glance, taking into account that the dependence of '*k*' on the concentration of SARS-CoV-2 spike glycoprotein '*C*' is linear, it was determined that the dependence of '*k*' value on C is 1.9 times more
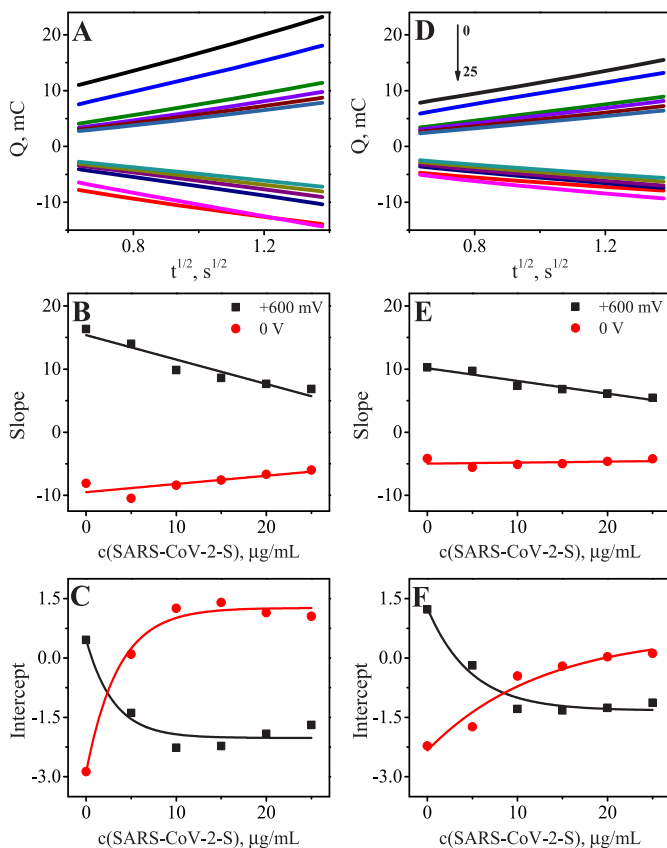
Fig. 3. A and **D** represent the Anson plots (Q, mC vs. $t^{1/2}$, $s^{1/2}$) derived from the amperometric response registered during the last (10th) potential pulse of the applied potential pulse sequence (+0.6 V and 0 V potentials), presented in Fig. 2 for **A** – MIP-Ppy modified electrode and **D** – NIP-Ppy modified electrode. **B** and **E** represent the slope values of the linear regression equation $y = ax + b$ (from) vs. the concentration of SARS-CoV-2 spike glycoprotein (concentration, μg/mL). **C** and **F** represent the intercept of the same linear regression values (from Table 1) vs. the concentration of SARS-CoV-2 spike glycoprotein (μg/mL).

strongly expressed in the case of MIP-Ppy modified electrode in comparison to that value of NIP-Ppy modified electrode at +600 mV. This fact enables us to conclude that according to the slope, the active area of MIP-Ppy ($A_{\text{MIP-Ppy}}$) is 1.9 times larger in comparison to that area of NIP-Ppy ($A_{\text{NIP-Ppy}}$).

A schematic representation of action, which represent results determined by chronoamperometry, is presented in Fig. 4. As it was discussed above, the decrease of surface charge at higher concentrations of SARS-CoV-2 spike glycoprotein is related to the blocking of MIP-Ppy surface by dielectric material – SARS-CoV-2 spike glycoprotein. All electrical charge passing during this chronoamperometric experiment is determined by adsorption/desorption of ions on MIP-Ppy or NIP-Ppy layers and by doping/dedoping of Ppy-based layers by anions such as PO_4^{3-}, HPO_4^{2-}, $H_2PO_4^-$ and Cl^-. Therefore, SARS-CoV-2 spike glycoprotein adsorbed on the Ppy surface forms a significant barrier for the adsorption/desorption of ions on the MIP-Ppy layer and by doping/dedoping of the MIP-Ppy layer by anions. Fig. 4A and C well represent results that could be determined by experiment when in solution and on the surface of modified electrode SARS-CoV-2 spike glycoprotein concentration is equal to 0 μg/mL. Therefore, in this case, the adsorption/desorption of ions on MIP-Ppy or NIP-Ppy layers and doping/dedoping of Ppy-based layers is more intensive in comparison to the MIP-Ppy layer. On the contrary, schematics represented in Fig. 4B and D

illustrate the interaction of Ppy-based layers with SARS-CoV-2 spike glycoprotein and, respectively, partial blocking of the Ppy surface.

In this context, according to the Anson plot-based evaluation, a SARS-CoV-2 spike glycoprotein molecule is an analyte that is interacting with MIP-Ppy and nonspecifically adsorbing on NIP-Ppy layers.

Fig. 5 represents the calibration plot based on ΔQ values vs. logarithm of the concentration of SARS-CoV-2 spike glycoprotein in PBS solution, pH 7.4. The calibration plot (Fig. 5) of the described system has a linear relationship.

$$y = Ax + B$$

The obtained functions of the linear relationships were as follows: y = 24.3599x-11.0234, with R^2 = 09497 (for MIP-Ppy modified electrode) and y = 14.3361x-8.4771 with R^2 = 0.9591 (for NIP-Ppy modified electrode). The linear relationship, in the PBS in absence of SARS-CoV-2 spike glycoprotein (c(SARS-CoV-2-S) = x = 0 μg/mL), represents the lowest change of charge (mC). The charge passed through MIP-Ppy at the initial point was higher than that through NIP-Ppy. This effect is explained by the complementary cavities in the polymer. The presence of the complementary cavities enables the faster charge transfer after extraction of the SARS-CoV-2 spike glycoprotein from the MIP-Ppy layer. After the MIP-Ppy and NIP-Ppy modified electrodes were re-incubated in the SARS-CoV-2 spike glycoprotein containing PBS, a
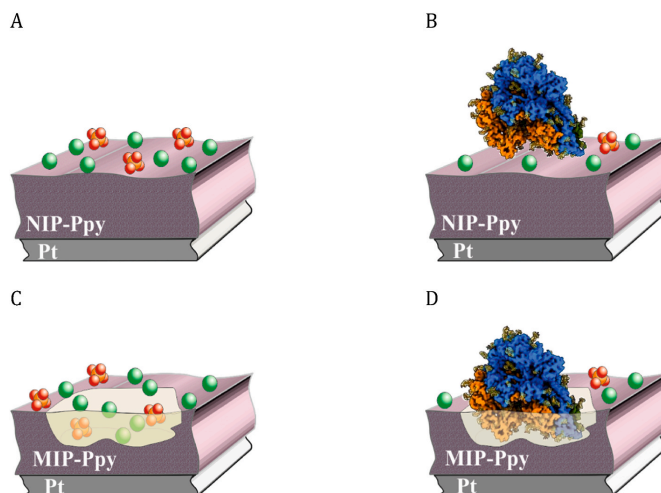
Fig. 4. Interaction of NIP-Ppy and MIP-Ppy with SARS-CoV-2 spike glycoprotein and anions (PO_4^{3-}, HPO_4^{2-}, or $H_2PO_4^-$ and Cl^-). **A** – NIP-Ppy in a solution containing 0 μg/mL of SARS-CoV-2 spike glycoprotein; **B** – NIP-Ppy in a s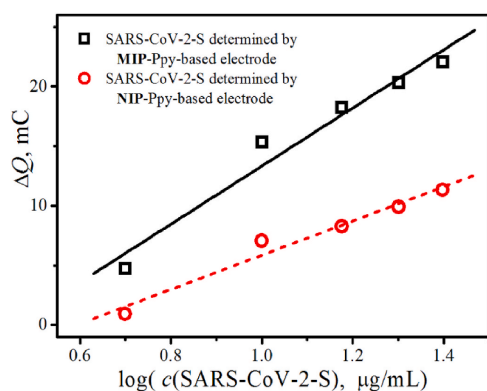olution containing >0 μg/mL of SARS-CoV-2 spike glycoprotein; **C** – MIP-Ppy in a solution containing 0 μg/mL of SARS-CoV-2 spike glycoprotein; **D** – MIP-Ppy in a solution containing >0 μg/mL of SARS-CoV-2 spike glycoprotein.

Fig. 5. Calibration curves of MIP-Ppy and NIP-Ppy modified electrodes presented as ΔQ vs. logarithm of the concentration of SARS-CoV-2 spike glycoprotein.

significant current drop was observed. The change of charge within the MIP-Ppy layer was observed higher than on the NIP-Ppy layer. This means that the MIP-Ppy modified electrode was more sensitive towards SARS-CoV-2 than the NIP-Ppy modified electrode. The registered charge variations of MIP-Ppy and NIP-Ppy modified electrodes at the highest concentrations of SARS-CoV-2 spike glycoprotein (c(SARS-CoV-2-S) = 25 μg/mL) were very similar. This should indicate that the protein covers the surface of both MIP-Ppy and NIP-Ppy layers, although differences between MIP-Ppy and NIP-Ppy layers were observed.

A comparison of some studies that were assessing the applicability of MIP-based sensors for the detection of SARS-CoV-2 proteins is demonstrated in Table 2.

The described method applied for the evaluation of the interaction between SARS-CoV-2 spike glycoproteins and the MIP-Ppy modified

electrode has significant advantages and the most important is that those insights about the interaction are concluded by the evaluation of PAD results. This means that the detection of SARS-CoV-2 spike glycoproteins can be performed by the assessment of Anson plot. Therefore, we believe, that the Anson plot is a simple and handy method for quick assessment the adsorption process on the electrode MIP-modified electrode.

4. Conclusions

After the MIP-Ppy and NIP-Ppy modified electrodes were incubated for the first time in the SARS-CoV-2 spike glycoprotein containing PBS, a significant current drop was observed. Based on the total charge vs. square of time plots (the Anson plots), the interaction between SARS-CoV-2 spike glycoproteins and the molecularly imprinted polypyrrole was assessed. Based on the dependence of the Anson plot's slope values on the concentration of the glycoproteins, we declare that glycoproteins adsorb more strongly on MIP-Ppy than on NIP-Ppy. Moreover, taking into the account the Anson plot-based evaluation it was concluded that, the SARS-CoV-2 spike glycoprotein molecule is an analyte, which is interacting with MIP-Ppy and at some extent non-specifically adsorbing on NIP-Ppy. Therefore, Anson plot-based calculations are valuable for determining the interaction between SARS-CoV-2 spike glycoproteins and molecularly imprinted polypyrrole (MIP-Ppy). Further, the calibration curve of current values was depicted for glycoprotein concentrations in the range from 0 μg/mL to 25 μg/mL. The calibration plot of the described system has a form of exponential decay. The current drop registered by the MIP-Ppy modified electrode was significantly higher than that determined by the NIP-Ppy modified electrode. This means that the MIP-Ppy modified electrode was more sensitive towards SARS-CoV-2 spike glycoprotein than the NIP-Ppy modified electrode. The current value observed in the calibration curve for the MIP-Ppy modified electrode at the initial point (glycoprotein concentration was 0 μg/mL) was 1.36 times higher in comparison with that of the NIP-Ppy modified electrode. This phenomenon occurred due to the presence of the complementary cavities in Ppy that were formed after the extraction of SARS-CoV-2 spike glycoprotein from MIP-Ppy. This observation can also

Table 2

MIP-based sensors used for the detection of SARS-CoV-2 proteins.

Electrode	Polymer	Analyte	Method of analysis	Comments	Ref.
Gold-based thin-film electrode	Poly(*m*-phenylenediamine)	SARS-CoV-2 nucleoprotein	DPV	Analyzed by using a redox probe; LOD 15 fM	[52]
macroporous gold screen-printed electrode	Poly(*o*-phenylenediamine)	SARS-CoV-2 receptor-binding domain	EIS	Analyzed by using a redox probe; LOD 0.7 pg mL^{-1}	[53]
Disposable thin-film metal electrode	Poly(3-aminophenylboronic acid)	SARS-CoV-2 spike protein subunit S1	SWV[a]	Analyzed by using a redox probe; LOD 15 fM	[54]
Gold SPRi chip	Poly(scopoletin)	SARS-CoV-2 receptor binding domain	SPRi[b]	Peptide epitope-imprinted polymer microarrays	[55]
Glassy carbon electrode	Polypyrrole-poly(3-aminophenyl boronic acid)	SARS-CoV-2 antigen	DPV, CA[c]	Graphene was added to the polymer composition; Analyzed by using a redox probe; LOD 0.326 fg mL^{-1}	[56]
Platinum electrode	Polypyrrole	SARS-CoV-2 Spike Glycoprotein	CA	No redox probe was used during CA.	[45]

[a] – square wave voltammetry.
[b] – surface plasmon resonance imaging.
[c] – chronoamperometry.

serve as the validation for the formation of MIP-Ppy. This technique can be applied to the development of a sensor for the diagnosis of a SARS-CoV-2 infection.

Declaration of competing interest

The authors declare that they have no known competing financial interests or personal relationships that could have appeared to influence the work reported in this paper.

Data availability

Data will be made available on request.

Appendix A. Supplementary data

Supplementary data to this article can be found online at https://doi.org/10.1016/j.talanta.2022.123981.

References

[1] V. Ratautaite, U. Samukaite-Bubniene, D. Plausinaitis, R. Boguzaite, D. Balciunas, A. Ramanaviciene, G. Neunert, A. Ramanavicius, Molecular imprinting technology for determination of uric acid, Int. J. Mol. Sci. 22 (2021) 5032, https://doi.org/10.3390/ijms22095032.

[2] S. Ramanavicius, A. Jagminas, A. Ramanavicius, Advances in molecularly imprinted polymers based affinity sensors (review), Polymers (Basel) 13 (2021) 974, https://doi.org/10.3390/polym13060974.

[3] S. Ramanavicius, A. Ramanavicius, Conducting polymers in the design of biosensors and biofuel cells, Polymers 13 (2021) 49, https://doi.org/10.3390/polym13010049.

[4] V. Ratautaite, S.D. Janssens, K. Haenen, M. Nesládek, A. Ramanaviciene, I. Baleviciute, A. Ramanavicius, Molecularly imprinted polypyrrole based impedimentric sensor for theophylline determination, Electrochim. Acta 130 (2014) 361–367, https://doi.org/10.1016/j.electacta.2014.03.035.

[5] V. Ratautaite, M. Nesladek, A. Ramanaviciene, I. Baleviciute, A. Ramanavicius, Evaluation of histamine imprinted polypyrrole deposited on boron doped nanocrystalline diamond, Electroanalysis 26 (2014) 2458–2464, https://doi.org/10.1002/elan.201400294.

[6] V. Ratautaite, D. Plausinaitis, I. Baleviciute, L. Mikoliunaite, A. Ramanaviciene, A. Ramanavicius, Characterization of caffeine-imprinted polypyrrole by a quartz crystal microbalance and electrochemical impedance spectroscopy, Sens. Actuat. B-Chem. 212 (2015) 63–71, https://doi.org/10.1016/j.snb.2015.01.109.

[7] M. Peeters, F.J. Troost, B. van Grinsven, F. Horemans, J. Alenus, M.S. Murib, D. Keszthelyi, A. Ethirajan, R. Thoelen, T.J. Cleij, P. Wagner, MIP-based biomimetic sensor for the electronic detection of serotonin in human blood plasma, Sens. Actuat. B-Chem. 171–172 (2012) 602–610, https://doi.org/10.1016/j.snb.2012.05.040.

[8] G. Bagdžiūnas, Theoretical design of molecularly imprinted polymers based on polyaniline and polypyrrole for detection of tryptophan, Mol. Syst. Des. Eng. 5 (2020) 1504–1512, https://doi.org/10.1039/D0ME00089B.

[9] A.K. Roy, N.V. S, C. Dhand, B.D. Malhotra, Molecularly imprinted polyaniline film for ascorbic acid detection, J. Mol. Recogn. 24 (2011) 700–706, https://doi.org/10.1002/jmr.1104.

[10] Y. Kong, J.H. Ni, W.C. Wang, Z.D. Chen, Enantioselective recognition of amino acids based on molecularly imprinted polyaniline electrode column, Electrochim. Acta 56 (2011) 4070–4074, https://doi.org/10.1016/j.electacta.2011.01.120.

[11] Z. Mazouz, S. Rahali, N. Fourati, C. Zerrouki, N. Aloui, M. Seydou, N. Yaakoubi, M. M. Chehimi, A. Othmane, R. Kalfat, Highly selective polypyrrole MIP-based gravimetric and electrochemical sensors for picomolar detection of glyphosate, Sensors (Basel) 17 (2017) 2586, https://doi.org/10.3390/s17112586.

[12] J.M. Kim, J.C. Yang, J.Y. Park, Quartz crystal microbalance (QCM) gravimetric sensing of theophylline via molecularly imprinted microporous polypyrrole copolymers, Sens. Actuat. B-Chem. 206 (2015) 50–55, https://doi.org/10.1016/j.snb.2014.09.047.

[13] D. Plausinaitis, L. Sinkevicius, U. Samukaite-Bubniene, V. Ratautaite, A. Ramanavicius, Evaluation of electrochemical quartz crystal microbalance based sensor modified by uric acid-imprinted polypyrrole, Talanta 220 (2020), 121414, https://doi.org/10.1016/j.talanta.2020.121414.

[14] R.D. Crapnell, N.C. Dempsey-Hibbert, M. Peeters, A. Tridente, C.E. Banks, Molecularly imprinted polymer based electrochemical biosensors: overcoming the challenges of detecting vital biomarkers and speeding up diagnosis, Talanta Open 2 (2020), 100018, https://doi.org/10.1016/j.talo.2020.100018.

[15] J.W. Lowdon, H. Diliën, P. Singla, M. Peeters, T.J. Cleij, B. van Grinsven, K. Eersels, MIPs for commercial application in low-cost sensors and assays – an overview of the current status quo, Sens. Actuat. B-Chem. 325 (2020) 128973, https://doi.org/10.1016/j.snb.2020.128973.

[16] A. Yarman, F.W. Scheller, How reliable is the electrochemical readout of MIP sensors? Sensors (Basel) 20 (2020) 2677, https://doi.org/10.3390/s20092677.

[17] E.N. Ndunda, Molecularly imprinted polymers—a closer look at the control polymer used in determining the imprinting effect: a mini review, J. Mol. Recogn. 33 (2020), e2855, https://doi.org/10.1002/jmr.2855.

7

[18] P.S. Sharma, A. Garcia-Cruz, M. Cieplak, K.R. Noworyta, W. Kutner, 'Gate effect' in molecularly imprinted polymers: the current state of understanding, Curr. Opin. Electrochem. 16 (2019) 50–56, https://doi.org/10.1016/j.coelec.2019.04.020.

[19] J. Erdőssy, V. Horváth, A. Yarman, F.W. Scheller, R.E. Gyurcsányi, Electrosynthesized molecularly imprinted polymers for protein recognition, TRAC-Trends Anal. Chem. 79 (2016) 179–190, https://doi.org/10.1016/j.trac.2015.12.018.

[20] X. Kan, Z. Xing, A. Zhu, Z. Zhao, G. Xu, C. Li, H. Zhou, Molecularly imprinted polymers based electrochemical sensor for bovine hemoglobin recognition, Sens. Actuat. B-Chem. 168 (2012) 395–401, https://doi.org/10.1016/j.snb.2012.04.043.

[21] R. Viveiros, S. Rebocho, T. Casimiro, Green strategies for molecularly imprinted polymer development, Polymers (Basel) 10 (2018) 306, https://doi.org/10.3390/polym10030306.

[22] Q. Zeng, X. Huang, M. Ma, A molecularly imprinted electrochemical sensor based on polypyrrole/carbon nanotubes composite for the detection of S-ovalbumin in egg white, Int. J. Electrochem. Sci. 12 (2017) 3965–3981, https://doi.org/10.20964/2017.05.61.

[23] Z. Stojanovic, J. Erdőssy, K. Keltai, F.W. Scheller, R.E. Gyurcsányi, Electrosynthesized molecularly imprinted polyscopoletin nanofilms for human serum albumin detection, Anal. Chim. Acta 977 (2017) 1–9, https://doi.org/10.1016/j.aca.2017.04.043.

[24] Y. Lai, C. Zhang, Y. Deng, G. Yang, S. Li, C. Tang, N. He, A novel α-fetoprotein-MIP immunosensor based on AuNPs/PTh modified glass carbon electrode, Chin. Chem. Lett. 30 (2019) 160–162, https://doi.org/10.1016/j.cclet.2018.07.011.

[25] A. Yarman, D. Dechtrirat, M. Bosserdt, K.J. Jetzschmann, N. Gajovic-Eichelmann, F.W. Scheller, Cytochrome c-derived hybrid systems based on molecularly imprinted polymers, Electroanalysis 27 (2015) 573–586, https://doi.org/10.1002/elan.201400592.

[26] L.-W. Qian, X.-L. Hu, P. Guan, B. Gao, D. Wang, C.-L. Wang, J. Li, C.-B. Du, W.-Q. Song, Thermal preparation of lysozyme-imprinted microspheres by using ionic liquid as a stabilizer, Anal. Bioanal. Chem. 406 (2014) 7221–7231, https://doi.org/10.1007/s00216-014-8133-9.

[27] S. Wu, W. Tan, H. Xu, Protein molecularly imprinted polyacrylamide membrane: for hemoglobin sensing, Analyst 135 (2010) 2523–2527, https://doi.org/10.1039/C0AN00191K.

[28] V.K. Tamboli, N. Bhalla, P. Jolly, C.R. Bowen, J.T. Taylor, J.L. Bowen, C. J. Allender, P. Estrela, Hybrid synthetic receptors for MOSFET devices for detection of prostate specific antigen in human plasma, Anal. Chem. 88 (2016) 11486–11490, https://doi.org/10.1021/acs.analchem.6b02619.

[29] P. Karami, H. Bagheri, M. Johari-Ahar, H. Khoshsafar, F. Arduini, A. Afkhami, Dual-modality impedimetric immunosensor for early detection of prostate-specific antigen and myoglobin markers based on antibody-molecularly imprinted polymer, Talanta 202 (2019) 111–122, https://doi.org/10.1016/j.talanta.2019.04.061.

[30] V.V. Shumyantseva, T.V. Bulko, L.V. Sigolaeva, A.V. Kuzikov, A.I. Archakov, Electrosynthesis and binding properties of molecularly imprinted poly-o-phenylenediamine for selective recognition and direct electrochemical detection of myoglobin, Biosens. Bioelectron. 86 (2016) 330–336, https://doi.org/10.1016/j.bios.2016.05.101.

[31] F.T.C. Moreira, S. Sharma, R.A.F. Dutra, J.P.C. Noronha, A.E.G. Cass, M.G.F. Sales, Protein-responsive polymers for point-of-care detection of cardiac biomarker, Sens. Actuat. B-Chem. 196 (2014) 123–132, https://doi.org/10.1016/j.snb.2014.01.038.

[32] F.T.C. Moreira, R.A.F. Dutra, J.P.C. Noronha, M.G.F. Sales, Electrochemical biosensor based on biomimetic material for myoglobin detection, Electrochim. Acta 107 (2013) 481–487, https://doi.org/10.1016/j.electacta.2013.06.061.

[33] A. Ramanaviciene, A. Ramanavicius, Molecularly imprinted polypyrrole-based synthetic receptor for direct detection of bovine leukemia virus glycoproteins, Biosens. Bioelectron. 20 (2004) 1076–1082, https://doi.org/10.1016/j.bios.2004.05.014.

[34] B. Babamiri, A. Salimi, R. Hallaj, A molecularly imprinted electrochemiluminescence sensor for ultrasensitive HIV-1 gene detection using EuS nanocrystals as luminophore, Biosens. Bioelectron. 117 (2018) 332–339, https://doi.org/10.1016/j.bios.2018.06.003.

[35] V. Ratautaite, S.N. Topkaya, L. Mikoliunaite, M. Ozsoz, Y. Oztekin, A. Ramanaviciene, A. Ramanavicius, Molecularly imprinted polypyrrole for DNA determination, Electroanalysis 25 (2013) 1169–1177, https://doi.org/10.1002/elan.201300063.

[36] A.A. Lahcen, F. Arduini, F. Lista, A. Amine, Label-free electrochemical sensor based on spore-imprinted polymer for Bacillus cereus spore detection, Sens. Actuat. B-Chem. 276 (2018) 114–120, https://doi.org/10.1016/j.snb.2018.08.031.

[37] S. Chen, X. Chen, L. Zhang, J. Gao, Q. Ma, Electrochemiluminescence detection of Escherichia coli O157:H7 based on a novel polydopamine surface imprinted polymer biosensor, ACS Appl. Mater. Interfaces 9 (2017) 5430–5436, https://doi.org/10.1021/acsami.6b12455.

[38] Z. Iskierko, P.S. Sharma, K. Bartold, A. Pietrzyk-Le, K. Noworyta, W. Kutner, Molecularly imprinted polymers for separating and sensing of macromolecular compounds and microorganisms, Biotechnol. Adv. 34 (2016) 30–46, https://doi.org/10.1016/j.biotechadv.2015.12.002.

[39] Z. Wang, F. Li, J. Xia, L. Xia, F. Zhang, S. Bi, G. Shi, Y. Xia, J. Liu, Y. Li, L. Xia, An ionic liquid-modified graphene based molecular imprinting electrochemical sensor for sensitive detection of bovine hemoglobin, Biosens. Bioelectron. 61 (2014) 391–396, https://doi.org/10.1016/j.bios.2014.05.043.

[40] L. Li, L. Yang, Z. Xing, X. Lu, X. Kan, Surface molecularly imprinted polymers-based electrochemical sensor for bovine hemoglobin recognition, Analyst 138 (2013) 6962–6968, https://doi.org/10.1039/C3AN01435E.

[41] H.-J. Chen, Z.-H. Zhang, L.-J. Luo, S.-Z. Yao, Surface-imprinted chitosan-coated magnetic nanoparticles modified multi-walled carbon nanotubes biosensor for detection of bovine serum albumin, Sens. Actuat. B-Chem. 163 (2012) 76–83, https://doi.org/10.1016/j.snb.2012.01.010.

[42] Z. Mazouz, M. Mokni, N. Fourati, C. Zerrouki, F. Barbault, M. Seydou, R. Kalfat, N. Yaakoubi, A. Omezzine, A. Bouslema, A. Othmane, Computational approach and electrochemical measurements for protein detection with MIP-based sensor, Biosens. Bioelectron. 151 (2020) 111978, https://doi.org/10.1016/j.bios.2019.111978.

[43] M.L. Yola, N. Atar, Development of cardiac troponin-I biosensor based on boron nitride quantum dots including molecularly imprinted polymer, Biosens. Bioelectron. 126 (2019) 418–424, https://doi.org/10.1016/j.bios.2018.11.016.

[44] B.V.M. Silva, B.A.G. Rodríguez, G.F. Sales, M.D.P.T. Sotomayor, R.F. Dutra, An ultrasensitive human cardiac troponin T graphene screen-printed electrode based on electropolymerized-molecularly imprinted conducting polymer, Biosens. Bioelectron. 77 (2016) 978–985, https://doi.org/10.1016/j.bios.2015.10.068.

[45] V. Ratautaite, R. Boguzaite, E. Brazys, A. Ramanaviciene, E. Ciplys, M. Juozapaitis, R. Slibinskas, M. Bechelany, A. Ramanavicius, Molecularly imprinted polypyrrole based sensor for the detection of SARS-CoV-2 spike glycoprotein, Electrochim. Acta 403 (2022) 139–581, https://doi.org/10.1016/j.electacta.2021.139581.

[46] R.A. Dorledo de Faria, L.G. Dias Heneine, T. Matencio, Y. Messaddeq, Faradaic and non-faradaic electrochemical impedance spectroscopy as transduction techniques for sensing applications, Int. J. Bios. Bioelectron 5 (2019) 29–31, https://doi.org/10.15406/ijbsbe.2019.05.00148.

[47] J. Heinze, B.A. Frontana-Uribe, S. Ludwigs, Electrochemistry of conducting polymers—persistent models and new concepts, Chem. Rev. 110 (2010) 4724–4771, https://doi.org/10.1021/cr900226k.

[48] M.F. Suárez, R.G. Compton, In situ atomic force microscopy study of polypyrrole synthesis and the volume changes induced by oxidation and reduction of the polymer, J. Electroanal. Chem. 462 (1999) 211–221, https://doi.org/10.1016/S0022-0728(98)00414-8.

[49] M.R. Gandhi, P. Murray, G.M. Spinks, G.G. Wallace, Mechanism of electromechanical actuation in polypyrrole, Synth. Met. 73 (1995) 247–256, https://doi.org/10.1016/0379-6779(95)80022-0.

[50] T.F. Otero, E. Angulo, Oxidation-reduction of polypyrrole films. Kinetics, structural model and applications, Solid State Ion 63–65 (1993) 803–809, https://doi.org/10.1016/0167-2738(93)90200-M.

[51] O.I. Parisi, M. Dattilo, F. Patitucci, R. Malivindi, V. Pezzi, I. Perrotta, M. Ruffo, F. Amone, F. Puoci, "Monoclonal-type" plastic antibodies for SARS-CoV-2 based on molecularly imprinted polymers, bioRxiv (2020), https://doi.org/10.1101/2020.05.28.120709, 2020.2005.2028.120709.

[52] A. Raziq, A. Kidakova, R. Boroznjak, J. Reut, A. Öpik, V. Syritski, Development of a portable MIP-based electrochemical sensor for detection of SARS-CoV-2 antigen, Biosens. Bioelectron. 178 (2021), 113029, https://doi.org/10.1016/j.bios.2021.113029.

[53] M.A. Tabrizi, J.P. Fernández-Blázquez, D.M. Medina, P. Acedo, An ultrasensitive molecularly imprinted polymer-based electrochemical sensor for the determination of SARS-CoV-2-RBD by using macroporous gold screen-printed electrode, Biosens. Bioelectron. 196 (2021), 113729, https://doi.org/10.1016/j.bios.2021.113729.

[54] A.G. Ayankojo, R. Boroznjak, J. Reut, A. Öpik, V. Syritski, Molecularly imprinted polymer based electrochemical sensor for quantitative detection of SARS-CoV-2 spike protein, Sens. Actuat. B-Chem. 353 (2022) 131160, https://doi.org/10.1016/j.snb.2021.131160.

[55] Z. Bognár, E. Supala, A. Yarman, X. Zhang, F.F. Bier, F. Scheller, R.E. Gyurcsányi, Peptide epitope-imprinted polymer microarrays for selective protein recognition. Application for SARS-CoV-2 RBD protein, Chem. Sci. 13 (2022) 1263–1269, https://doi.org/10.1039/D1SC04502D.

[56] S.A. Hashemi, S. Bahrani, S.M. Mousavi, N. Omidifar, N.G.G. Behbahan, M. Arjmand, S. Ramakrishna, K.B. Lankarani, M. Moghadami, M. Firoozsani, Graphene-based femtogram-level sensitive molecularly imprinted polymer of SARS-CoV-2, Adv. Mater. Interfaces 8 (2021), 2101466, https://doi.org/10.1002/admi.202101466.

[57] N. Cennamo, G. D'Agostino, C. Perri, F. Arcadio, G. Chiaretti, E.M. Parisio, G. Camarlinghi, C. Vettori, F. Di Marzo, R. Cennamo, G. Porto, L. Zeni, Proof of concept for a quick and highly sensitive on-site detection of SARS-CoV-2 by plasmonic optical fibers and molecularly imprinted polymers, Sensors 21 (2021) 1681, https://doi.org/10.3390/s21051681.

[58] G. Jamalipour Soufi, S. Iravani, R.S. Varma, Molecularly imprinted polymers for the detection of viruses: challenges and opportunities, Analyst 146 (2021) 3087–3100, https://doi.org/10.1039/D1AN00149C.

[59] F.C. Anson, Innovations in the study of adsorbed reactants by chronocoulometry, Anal. Chem. 38 (1966) 54–57, https://doi.org/10.1021/ac60233a014.

[60] F.C. Anson, R.A. Osteryoung, Chronocoulometry: a convenient, rapid and reliable technique for detection and determination of adsorbed reactants, J. Chem. Educ. 60 (1983) 293, https://doi.org/10.1021/ed060p293.

[61] F.C. Anson, J.H. Christie, R.A. Osteryoung, A study of the adsorption of cadmium (II) on mercury from thiocyanate solutions by double potential-step chronocoulometry, J. Electroanal. Chem. Interf. Electrochem. 13 (1967) 343–353, https://doi.org/10.1016/0022-0728(67)80037-8.

[62] A. Ramanavicius, Y. Oztekin, A. Ramanaviciene, Electrochemical formation of polypyrrole-based layer for immunosensor design, Sens. Actuat. B-Chem. 197 (2014) 237–243, https://doi.org/10.1016/j.snb.2014.02.072.

8

[63] D. Plausinaitis, V. Ratautaite, L. Mikoliunaite, L. Sinkevicius, A. Ramanaviciene, A. Ramanavicius, Quartz crystal microbalance-based evaluation of the electrochemical formation of an aggregated polypyrrole particle-based layer, Langmuir 31 (2015) 3186–3193, https://doi.org/10.1021/la504340u.

[64] K. Zhou, H. Wang, Y. Zhang, J. Liu, H. Yan, An advanced technique to evaluate the electrochromic performances of NiO films by multi-cycle double-step potential chronocoulometry, J. Electrochem. Soc. 163 (2016) H1033–H1040, https://doi.org/10.1149/2.1011610jes.

[65] A. García-Miranda Ferrari, C.W. Foster, P.J. Kelly, D.A.C. Brownson, C.E. Banks, Determination of the electrochemical area of screen-printed electrochemical sensing platforms, Biosensors (Basel) 8 (2018) 53, https://doi.org/10.3390/bios8020053.

[66] J. Puy, M. Pla, F. Mas, F. Sanz, Adsorption in double potential step chronocoulometry, J. Electroanal. Chem. Interf. Electrochem. 241 (1988) 89–104, https://doi.org/10.1016/0022-0728(88)85118-0.

[67] G. Bagdžiūnas, A. Ramanavicius, Towards direct enzyme wiring: a theoretical investigation of charge carrier transfer mechanisms between glucose oxidase and organic semiconductors, Phys. Chem. Chem. Phys. 21 (2019) 2968–2976, https://doi.org/10.1039/C8CP07233G.

[68] V. Syritski, J. Reut, A. Menaker, R.E. Gyurcsányi, A. Öpik, Electrosynthesized molecularly imprinted polypyrrole films for enantioselective recognition of l-aspartic acid, Electrochim. Acta 53 (2008) 2729–2736, https://doi.org/10.1016/j.electacta.2007.10.032.

[69] T.C. Tsai, H.Z. Han, C.C. Cheng, L.C. Chen, H.C. Chang, J.J.J. Chen, Modification of platinum microelectrode with molecularly imprinted over-oxidized polypyrrole for dopamine measurement in rat striatum, Sens. Actuat. B-Chem. 171–172 (2012) 93–101, https://doi.org/10.1016/j.snb.2011.07.052.

[70] J.H. Christie, G. Laurer, R.A. Osteryoung, Measurement of charge passed following application of a potential step-application to the study of electrode reactions and adsorption, J. Electroanal. Chem. 7 (1964) 60–72, https://doi.org/10.1016/0022-0728(64)80005-X.

[71] J.H. Christie, G. Lauer, R.A. Osteryoung, F.C. Anson, Determination of charge passed following application of potential step in study of electrode processes, Anal. Chem. 35 (1963), https://doi.org/10.1021/ac60205a003, 1979-1979.

Article

Towards Molecularly Imprinted Polypyrrole-Based Sensor for the Detection of Methylene Blue

Raimonda Boguzaite [1], **Greta Pilvenyte [1]**, **Vilma Ratautaite [1,*]**, **Ernestas Brazys [2]**, **Almira Ramanaviciene [3]** and **Arunas Ramanavicius [1,2,*]**

[1] Department of Nanotechnology, State Research Institute Center for Physical Sciences and Technology (FTMC), Sauletekio Av. 3, LT-10257 Vilnius, Lithuania

[2] Department of Physical Chemistry, Institute of Chemistry, Faculty of Chemistry and Geosciences, Vilnius University (VU), Naugarduko Str. 24, LT-03225 Vilnius, Lithuania

[3] NanoTechnas—Center of Nanotechnology and Materials Science, Institute of Chemistry, Faculty of Chemistry and Geosciences, Vilnius University (VU), Naugarduko Str. 24, LT-03225 Vilnius, Lithuania

* Correspondence: vilma.ratautaite@ftmc.lt (V.R.); arunas.ramanavicius@chf.vu.lt (A.R.)

Abstract: This study is dedicated to molecularly imprinted polymer-based sensor development for methylene blue detection. The sensor was designed by molecular imprinting of polypyrrole with phenothiazine derivative methylene blue (MB) as a template molecule. The molecularly imprinted polymer (MIP) was deposited directly on the surface of the indium tin oxide-coated glass electrode by potential cycling. Different deposition conditions, the layer's durability, and thickness impact were analysed. The working electrodes were coated with molecularly imprinted and non-imprinted polymer layers. Potential pulse chronoamperometry and cyclic voltammetry were used to study these layers. Scanning electron microscopy was used to determine the surface morphology of the polymer layers. The change in optical absorption was used as an analytical tool to evaluate the capability of the MIP layer to adsorb MB. Selectivity was monitored by tracking the optical absorption changes in the presence of Azure A. In the case of MB adsorption, linearity was observed at all evaluated calibration plots in the concentration range from 0.1 μM to 10 mM. The novelty of this article is based on the methodology in the fabrication process of the sensors for MB, where MB retains its native (non-polymerised) form during the deposition of the MIP composite.

Keywords: methylene blue (MB); polypyrrole (Ppy); conducting polymers (CPs); molecularly imprinted polymers (MIPs); phenothiazine derivatives; optical sensors; indium tin oxide (ITO) electrodes

1. Introduction

Molecular imprinting technology allows the formation of specific molecular recognition sites that operate on the principle of complementarity between the imprinted sites and the analyte, on the lock and key model. Therefore, molecularly imprinted polymers (MIPs) can selectively bind the analytes of interest, which were used as templates during the formation of these MIPs [1–3]. In previous studies, it was reported that various types of molecules (both low and high molecular weight) can be imprinted [4–11]. The MIP technique is extremely relevant even today when we are looking for better and more useful sensors and sensing systems for improved diagnosis, treatments, and assays [12–14]. Modern analytical chemistry has a range of sensitive and powerful equipment available to detect target molecules. However, many of these methods, such as immunoassays, capillary zone electrophoresis, and chromatography (e.g., high-performance liquid chromatography, ion chromatography, and micellar electro-kinetic capillary chromatography) require trained personnel for time-consuming sample preparation and analysis. MIP-based sensors offer an attractive alternative as they can provide sensitive and specific results using inexpensive materials. They also present advanced storage stability and enable quick analysis with point-of-care testing possibilities in complex sample matrices. Overall, MIP-based sensors

represent a promising technology for a wide range of analytical applications, including environmental monitoring, food safety, and biomedical diagnostics [15–17]. In MIP-based sensors, conducting polymers exhibit favourable properties, such as high electrical conductivity as well as the ability to adhere to electrically conductive surfaces and maintain mechanical stability [18]. Even though MIPs are studied by various research groups, there are still unanswered questions and unexplored possibilities. Although we can choose the template quite confidently, there are still challenges in analysing the interactions and choosing functional monomers, cross-linkers, initiators, and solvent compositions [19].

To create a complex between the template and the monomer, the template must have functional groups that interact with the monomer (or several monomers). Usually, a template–monomer molar ratio of 1:4 provides suitable stability to the complex, assuring the imprint effect [20]. Many different polymers can be used to form a MIP, including polypyrrole (Ppy), which can be very efficiently applied to the design of MIP-based sensors [4]. Ppy is a π-π conjugated polymer that is easily electropolymerisable [5]. Electrochemical methods like cyclic voltammetry (CV), differential pulse voltammetry, and electrochemical impedance spectroscopy were used for the detection of different molecules using the Ppy modified with molecular imprints [21–23].

As Ppy is one of the most frequently used polymers in MIP-based sensor design [18], several studies have concluded that combining phenothiazine derivatives with polymers like Ppy can help create coatings with improved characteristics, quicker response, and receptiveness to environmental changes [24,25]. Also, the long-term stability of the resulting polymer is the principal benefit of the electropolymerised phenothiazine derivative methylene blue (MB) [26]. MB can be used in different application areas. MB is an effective electron redox mediator, having a redox potential close to that of some biomolecules [27–30]. Moreover, MB is used in clinical medicine to increase vascular tone and myocardial function in patients with septic or anaphylactic shock [31]. However, MB has side effects, the main of which are nausea, diarrhoea, gastritis, severe headache, or mental confusion if it is inhaled or ingested [32]. Since MB is a cationic dye and is used in the textile industry, this leads to certain environmental issues. Despite some downsides and growing concerns about the environment, the usage of dyes is still growing in many countries through the textile industry and other colouring processes. Among the pollutants, dyes are particularly noted for their harmful effects on the environment and human health. Therefore, researchers have been led in both analytical and materials science to investigate appropriate methods for removing and/or monitoring various pollutants [13,33–35].

Since MB can cause unwanted or negative effects and diseases, it is important to identify and detect it. Various studies have been conducted to analyse the properties of MB as a polymerised layer. Kaplan et al. [26] study determined the oxidation and reduction peak positions. In that study, firstly, the potential of the working Au electrode was scanned from 0 V to −0.275 V, and a cathodic peak was observed at −0.235 V (Ag/AgCl$_{3M NaCl}$ as reference electrode). Next, the potential was reversed in the positive direction, and an oxidative peak was seen at −0.22 V. This pair of redox peaks corresponds to the reduction and oxidation of MB monomer species in the solution, respectively. In this case, when the potential of the working electrode was swiped at higher positive potentials, the current density quickly increased at about +0.800 V and this effect is linked to the oxidation of MB. In another study, the MB was electropolymerised in an aqueous solution [30]. This study demonstrates that the value of anodic switching potential was increased above +1.0 V (on a glassy carbon disk electrode, Ag/AgCl$_{1M KCl}$ as reference electrode). The results of this study indicate that there is an extra conjugated chain in the MB polymer compared to the monomer. Liu et al. [36] reported the electrochemical polymerisation of MB on a glassy carbon electrode by cyclic voltammetry. The observed anodic peak (at +0.15 V) and a cathodic peak (+0.09 V) belong to the redox peaks of the MB monomer. Moreover, at about +0.89 V potential, the anodic current increases quickly, and a broad anodic peak appears at +1.02 V, which is ascribed to the formation of the polymer (saturated calomel electrode as reference electrode). According to this study's reasoning, if the parent monomer

contains primary amino groups as ring substituents, cation radical species are produced during the electropolymerisation of phenoxazines or phenothiazines at a potential of +0.8 V. Mokhtari et al.'s [37] study describes a MIP preparation method in which MB was electrochemically polymerised to obtain MIP on the aptamer/cTnI/Nafion/ZnONPs/GCE surface for cardiac troponin I (cTnI) detection. During the electrochemical polymerisation of MB, a broad anodic peak emerged at about +1.2 V (Ag/AgCl as reference electrode). This anodic peak was related to the formation of MB cation radical and could be considered evidence for polymethylene blue formation. In the case of Ppy and MB polymerised on the indium tin oxide (ITO) coated glass electrode, polymerisation of MB at higher potentials was also observed [24,38]. One of the latest articles on MIP technology application for MB sensing was published by A. Sedelnikova et al. [39]. This study describes the design of magnetic MIPs with nylon-6 as a monomer (dissolved in 2,2,2-trifluoroethanol). The samples had good imprinting factors ranging from 4.2 to 5.4 and a high adsorption capacity between 20.0 and 34.8 mg/g.

The objective of the recent study is to explore the applicability of the Ppy layer in the phenothiazine derivative MB sensor design as a MIP with MB as a template molecule. From our previous study [24] and those of other groups [38,40–42], it is known that MB can be polymerised on the electrode at some specific potential values. Therefore, the difficulty and challenge of this study were to find out such electrochemical conditions at which the pyrrole (the monomer) was polymerised into a thin layer on the surface of the glass/ITO electrode and MB (the template molecule) was not. For this purpose, Ppy layers were deposited on the working glass/ITO electrode from the water-based polymerisation mixture containing MB and pyrrole. The following challenge was to extract the MB from the Ppy layer present on the electrode without damaging the polymer. The performance and stability of the electrode modified by the deposited MIP layers were investigated. The final task was to demonstrate that the resulting polymer is a MIP capable of recognising MB molecules. Considering the challenges, the novelty of this study is based on the methodology in the fabrication process of the Ppy-based MIP with MB templates, where MB retains its native (non-polymerised) form during the deposition of the MIP composite.

2. Materials and Methods

2.1. Chemicals and Instrumentation

Pyrrole CAS: 109-97-7 (Alfa Aesar, Kandel, Germany); methylene blue (MB) CAS: 122965-43-9 and Azure A CAS: 531-53-3 (Alfa Aesar, Kandel, Germany); heparin Lot nr.: 80020 (Rotexmedica, Trittau, Germany); sulfuric acid CAS: 7664-93-9 (Lach-Ner, Neratovice, Czech Republic); ammonia solution 30% CAS: 1336-21-6 (Carl Roth GmbH, Karlsruhe, Germany); hydrogen peroxide 35% CAS: 7722-84-1 (Alfa Aesar, Kandel, Germany); sodium hydroxide CAS: 1310-73-2 (StanLab, Lublin, Poland); boric acid CAS: 10043-35-3 (Alfa Aesar, Kandel, Germany); phosphoric acid CAS: 7664-38-2 (Alfa Aesar, Kandel, Germany); acetone CAS: 67-64-1 (Alfa Aesar, Kandel, Germany); potassium chloride CAS: 7447-40-7 (Carl Roth GmbH, Karlsruhe, Germany); redox probe ($K_3[Fe(CN)_6]/K_4[Fe(CN)_6]$): potassium hexacyanoferrate(III) CAS: 13746-66-2, (Carl Roth GmbH, Karlsruhe, Germany); and potassium hexacyanoferrate(II) (Reachim, Donetsk, Ukraine) were used in the experiments.

Galvanostat/potentiostat Metrohm DropSens (Llanera, Spain) equipped with DropView 8400 software, version 3.78, a spectrometer USB4000-FL equipped with SpectraSuite software (Ocean Optics, Largo, FL, USA), pH-meter Seven Compact Mettler-Toledo GmbH (Greifensee, Switzerland), and Hitachi tabletop scanning electron microscope (TM) PT4000Plus (Hitachi-naka, Japan) were used in the experiments.

Electrochemical polymerisation was performed using computer-controlled galvanostat–potentiostat Metrohm DropSens equipped with DropView 8400 software, version 3.78. A glass cuvette (high × depth × width = 32 mm × 18 mm × 30 mm) was used as an electro-chemical cell for synthesis.

The three-electrode system was the setup of an indium tin oxide (ITO) glass slide (Sigma-Aldrich, Steinheim, Germany) as a working electrode (WE), Ag/AgCl wire as a ref-

erence electrode (RE) (for electrochemical deposition of polymer layers) or Ag/AgCl$_{3M\ KCl}$ (for evaluation of the obtained polymer layers), and platinum wire (Alfa Aesar, Kandel, Germany) as a counter electrode (CE).

2.2. Pre-Treatment of the Working Electrode

Before the electrochemical deposition of polymer layers, the glass/ITO electrode was washed for 3 min in the solution consisting of 27% NH$_4$OH and 30% H$_2$O$_2$ mixed at a ratio of 3:1 and preheated up to 50 °C. Later, the electrode was cleaned at room temperature and, subsequently, in water, acetone, and water for 15 min in each liquid in an ultrasonic bath.

2.3. The Electrochemical Deposition of Ppy Layers

Polymer layers were electrochemically deposited by potential cycling in a potential range from −0.4 V to +1.0 V vs. Ag/AgCl, at a potential sweep rate of 50 mV/s, by 25, 20, 15, 10, 7, 5 and 3 cycles with a step lift of 2.44 mV. A polymerisation solution in water contains 10 mM MB, 50 mM pyrrole, and 5 µg/mL heparin. The rationale for using heparin in a polymerisation solution is based on our previous studies [24]. The inclusion of heparin in the polymerisation mixture improves the adhesion of the layer to the electrode surface. There are reports where MB in the polymerisation solution acts as the supporting electrolyte, as described by [25]. Therefore, MB in the polymerisation solution has two functions: it behaves as a template, as well as a supporting electrolyte.

2.4. Evaluation of Ppy Layers

The variation of optical absorbance (ΔA) was examined after each 3 min incubation of the electrode in water (wash procedure), and the stability of the layer was analysed. The potential pulse chronoamperometry was used and set to a total of 5 pulses, with a pulse profile based on a potential step of −0.8 V for 10 s followed by a potential step of +0.8 V. Simultaneously, the optical absorbance was monitored at 530 nm, 668 nm, and 750 nm. ΔA was calculated using the equation:

$$\Delta A = A_i - A_j \tag{1}$$

where ΔA—the variation of absorbance (a. u.); A$_i$—the absorbance during the +0.8 V pulse (a. u.); A$_j$—the absorbance during the −0.8 V pulse (a. u.).

Cyclic voltammograms were recorded without and with 5 mM of K$_3$[Fe(CN)$_6$]/K$_4$[Fe(CN)$_6$] in Britton-Robinson (BR) buffer solution weekly in the potential range from −0.2 V to +0.6 V vs. Ag/AgCl$_{3M\ KCl}$, at the scan rate of 50 mV/s and step lift of 2.44 mV, in total 3 potential cycles.

The electrochemical evaluation of polymer films was performed in BR buffer solutions. BR buffer solution consisted of 0.01 M boric acid, 0.01 M acetic acid, and 0.01 M phosphoric acid. The ionic strength of the BR was supported with 0.1 M KCl. The pH value of BR was adjusted (with 1 M sodium hydroxide) to 3.00—the pH was monitored using pH meter SevenCompact S220 (Mettler-Toledo GmbH, Greifensee, Switzerland).

3. Results

The three-electrode system was used during the electrochemical deposition of the Ppy-MB layer. Firstly, the Ppy layer with MB as the template is deposited on the glass/ITO electrode (glass/ITO/Ppy-MB). Further, the polymer layers were subjected to voltammetry and potential pulse chronoamperometry-based experiments to elucidate their properties.

The schematic representation of the study is shown in Figure 1A. This study aimed to create a molecularly imprinted Ppy with MB as a template molecule. Figure 1B represents an imprinted Ppy layer on a glass/ITO electrode. The influence of the varying thickness of the surface polymer on the durability and efficiency of the MIP properties was also analysed.
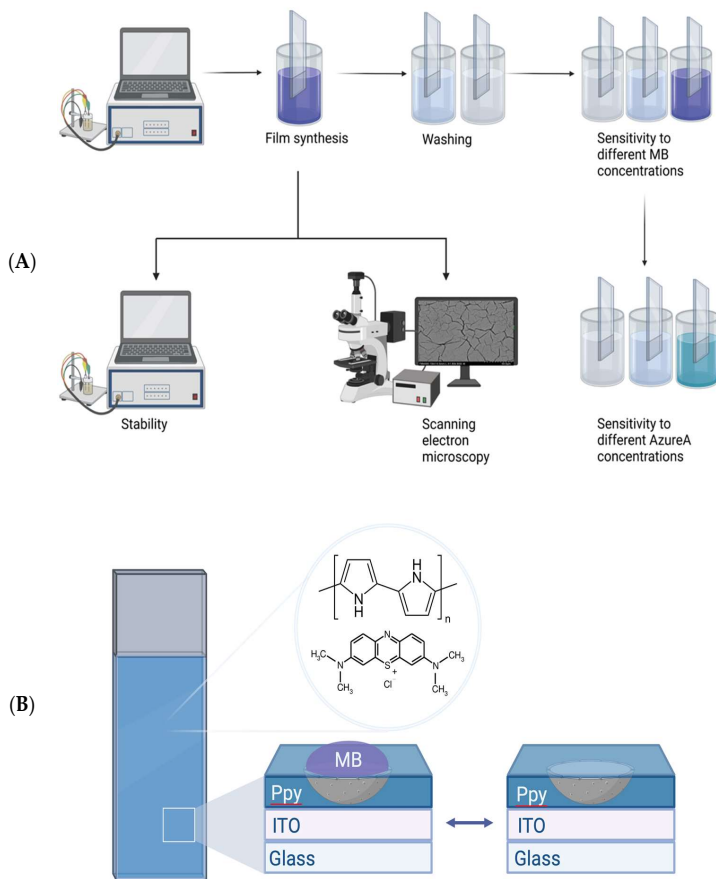
Figure 1. Schematic representation of the study. (**A**) A scheme of MB-based sensor evaluation steps. (**B**) Visualisation of an imprinted Ppy layer on an ITO electrode.

Polymer layers with entrapped MB as a template were electrochemically deposited according to the aforementioned conditions and by applying 3, 5, 7, 10, 15, 20, or 25 potential cycles. The successful polymerisation of pyrrole is visible from the cyclic voltammograms presented in Figure 2 and Figure S1. Furthermore, the increase in the width of the cyclic voltammograms corresponds to an increase in the thickness of the polymer layer. CV is the most widely used technique for acquiring qualitative information about electrochemical reactions. The power of CV is based on the ability to provide rapidly considerable information on the thermodynamics of the redox process, on the kinetics of heterogeneous electron transfer reactions, and on coupled chemical reactions or adsorption processes. In order to find better synthesis conditions to imprint MB into the Ppy layer, we evaluated several different potential ranges vs. Ag/AgCl: from −0.4 V to +1 V (1), from −0.5 V to +1.2 V (2) (as it was described in [24]), from −0.4 V to +0.8 V (3), and from −0.4 V to +0.6 V (4). The comparison of cyclic voltammograms (5th cycle) obtained during the electrochemical polymerisation of polymer layers is presented in Figure 2.
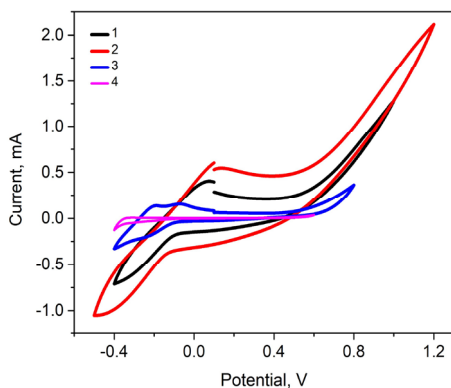
Figure 2. Electrochemical deposition of Ppy-MB during potential cycling at different conditions: (1) from −0.4 V to +1 V; (2) from −0.5 V to +1.2 V; (3) from −0.4 V to +0.8 V; (4) from −0.4 V to +0.6 V. Cyclic voltammograms at a scan rate of 50 mV/s, and a step potential of 2.44 mV. Number of potential cycles in total was 10. The 5th cycle is demonstrated for comparison. Electrochemical polymerisation was performed in a three-electrode system, in which glass/ITO was used as WE, Ag/AgCl as RE, and platinum wire as CE.

The pyrrole electropolymerisation on glass/ITO starts from +0.5 V [43], so, the electropolymerisation potential ranges in our study were selected between from −0.5 V to +1.2 V. In the ranges from −0.4 V to +0.6 V and from −0.4 V to +0.8 V, the voltammograms lack sufficient anodic peaks to investigate the pyrrole polymerisation. The anodic peak is enhanced, and the pyrrole polymerisation is identified in the cyclic voltammogram in the range from −0.4 V to +1.0 V. Considering the study of Kaplan et al. [26] to indicate the formation of the MB layer on the electrode surface, the current density should steadily decrease at −0.22 V and start increasing at about −0.05 V with the increase in scans. The range from −0.5 V to +1.2 V in our study showed the highest peaks at about −0.05 V towards the MB layer deposition. These results are quite similar to previously reported studies [24,26]. The aim of adjusting the electrochemical polymerisation conditions was to find the potential range in which MB would polymerise as little as possible while retaining Ppy layer growth. In that case, to efficiently deposit the Ppy layer and lower MB electropolymerisation, the potential range for further studies was chosen to be in the smaller potential window from −0.4 V to +1.0 V.

Scanning electron microscopy (SEM) was used to determine the surface morphology of the Ppy-MB layers. The influence of the applied potential cycles (25, 20, 15, 10, 7, 5, or 3) on the Ppy-MB polymer surface properties can be seen in the SEM images at a magnification of ×180 (Figure 3) and magnifications of ×800 and ×8000 (Figure S3). Folded structures and fairly even distributions are observed for the Ppy-MB layers obtained by 25 and 20 potential cycles (Figure 3A,B). Similar results were obtained when studying Ppy-MB layers in previous studies [24]. However, when applying other polymerisation conditions (different potential windows, as shown in Figure 2), it can be observed that layers of the same thickness had denser structures. It was observed that the thicker the layer, the larger and more visible the folds are, and the agglomerations are more noticeable (Figure 3A–C). The thinnest layers seem to be too thin to see clear structures (Figure 3G). A thinner and smoother layer showed better results. A thinner layer is less prone to mechanical damage and lasts longer on the electrode. However, a layer that was obtained by 3 potential cycles is too thin (Figure 3G). Based on the SEM study, it was also assumed that in the further part of this study, it is most functional to use the deposited layers obtained by 5 (Figure 3F), 7 (Figure 3E), and 10 (Figure 3D) potential cycles. (Different magnifications could be found

in the supporting material in Figure S3.) Those layers, hereinafter referred to as Ppy-MB-5, Ppy-MB-7, and Ppy-MB-10, were analysed further.
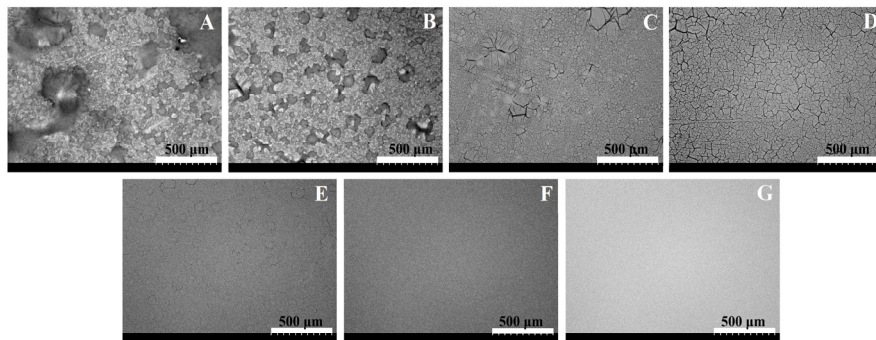

Figure 3. SEM images of Ppy-MB synthesised at different conditions ((**A–G**), Ppy-MB layers deposited by 25, 20, 15, 10, 7, 5, or 3 potential cycles, respectively). Magnification is ×180.

Figure 4 demonstrates the changes in optical absorbance (ΔA) that were measured immediately after deposition in BR buffer solution, pH 3. The potential pulse chronoamperometry was used and set to a total of 5 pulses, as described in the experimental part. Optical absorbance was followed at 530 nm, 668 nm, and 750 nm (conditions were chosen based on previous studies [24]). It is possible to see trends where the change in absorption increases with the layer thickness.
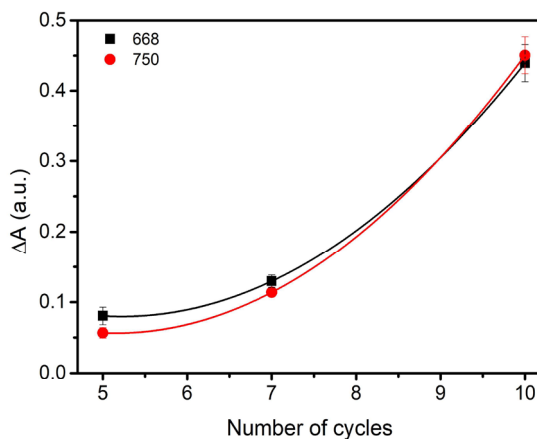
Figure 4. Changes of absorbance in different layers of Ppy-MB: Ppy-MB-5, Ppy-MB-7, Ppy-MB-10. Absorbance was measured at λ = 668 nm and λ = 750 nm.

The performance and stability (the ability to both remain mechanically on the electrode surface and the reproducibility of experiments using the same layer) of the electrode modified by the deposited MIP layer imprinted with MB were investigated. The following storage conditions were analysed: BR buffer solution in an acidic medium, water, and air. After a dozen days of conducting tests with such a layer, it was possible to see changes in the cyclic voltammograms (Figure S2). In both cases where voltammograms are obtained in BR buffer solution or water, oxidation peaks were observed at a potential of +0.5 V and

reduction peaks at −0.45 V. In the case of storage in air, during cycle 2, the oxidation peak is detected at +0.10 V; however, even two peaks are visible in the reduction region. The peak at −0.15 V can be attributed to the reduction process of the Ppy layer. As the potential changes further up to cycle 10, the oxidation peak shifts to +0.45 V, while the reduction peak remains at −0.15 V. Due to the risk of swelling of the layer in water and BR buffer solution, these storage conditions have been discarded. During the research, it was also noticed that the layer, which was stored in the air, remained attached to the electrode longer. Even with the naked eye, the long-term persistence of the layer on the surface of the electrode was visible when the tests were carried out. The previous study described the Ppy stability on the pencil graphite electrode [44]. The obtained results of our and previous studies prove that storage of the Ppy in the air is more convenient. Afterwards, it was chosen to study the layers that will be stored in the air for further parts of this study.

The further part of this study aimed to analyse the performance of the layer and the influence of the determination and washing procedures on the properties of the polymer layer. The stability of the layers Ppy-MB-5, Ppy-MB-7, and Ppy-MB-10 was checked by washing them in water. After each wash (3 min), the change in optical absorbance (ΔA) was observed. The potential pulse chronoamperometry was applied with 5 pulses, as described in the Experimental section. Simultaneously, the optical absorbance was monitored. A consistently decreasing trend is visible in Figure 5A. It was observed that the Ppy-MB-5 layer lost mechanical stability on the electrode after the third wash (or a similar number of washes), and absorption could not be recorded. Other layers were durable even after 10 washes. The Ppy-MB-7 and Ppy-MB-10 layers displayed the highest stability in this respect. Later, every few weeks, the layers were electrochemically tested, and CVs were recorded with and without a redox probe in the BR buffer solution (Figures S4 and S5), wherein clearly expressed oxidation–reduction peaks were visible. The width of the cyclic voltammograms has decreased over storage time.
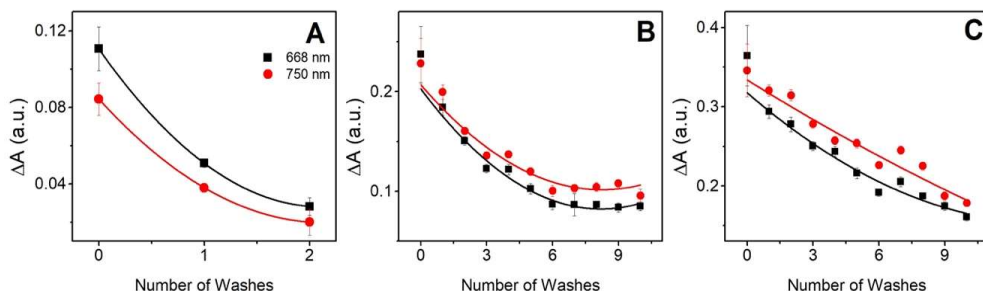

Figure 5. The dependence of change in absorption on the number of times the layer was washed in water. (**A**) Ppy-MB-5, (**B**) Ppy-MB-7, (**C**) Ppy-MB-10. Absorbance was measured at λ = 668 nm (black line) and λ = 750 nm (red line). Error bars represent the standard deviation of ΔA from N = 3.

To demonstrate that the resulting polymer is a MIP capable of interacting with MB molecules, the non-specific interaction of another phenothiazine, which in our particular case was Azure A (AA), was examined. A further experiment involved the analysis of the imprinted Ppy as an MB sensor. A non-imprinted polymer (NIP) that did not have MB was also produced to test the effectiveness of the imprinted layer. After evaluating the previous stages of this research, it was found that the most reliable and effective layer can be considered the one that was deposited using 7 potential cycles. It is less thick than Ppy-MB-10, so it stays longer on the surface of the electrode. Also, it is transparent and does not wash off after several detection/washing cycles. For these reasons, further investigation and verification of the sensor as an imprinted Ppy-MB was carried out precisely with this layer. The first task was to remove the imprinted MB from the created

layer. For this, 0.1 M sulfuric acid was used, in which the washing lasted for 5 min. The NIP was also washed to create the same experimental conditions. In the following part of the research, the formed MIP and NIP layers were evaluated by observing the change in optical absorption. The concentrations of MB varied from 0.1 μM to 10 mM. The results are presented in Figure 6.
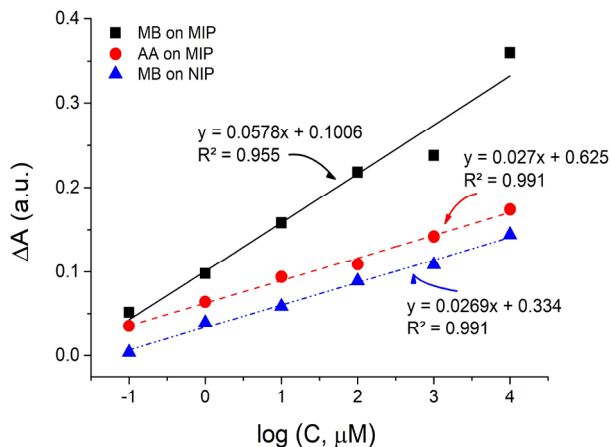

Figure 6. The calibration plots (ΔA vs. log[C, μM]) present the change in absorption on Ppy-MB-7 layers as MIP or NIP, in the presence of MB and Azure A adsorption, λ = 668 nm.

The calibration plots in Figure 6 demonstrate the change in absorption (ΔA) on MIP and NIP layers in the presence of MB or Azure A. Linearity was observed at all evaluated calibration graphs in the concentration range from 0.1 μM to 10 mM. It can be seen that R is greater than 0.9: MB on MIP is 0.955, AA on MIP, and MB on NIP is 0.991. The apparent imprinting factor when comparing MB interaction with MIP or NIP is about 2.15. The slope values for the calibration plots of AA on MIP and MB on NIP are roughly the same, while the slope for the calibration plot of MB on MIP is visibly steeper. The magnitude of slope values for calibration plots can be attributed to the strength of target molecule interactions with polymer layers. The slope for MB on MIP being larger than that of MB on NIP was anticipated, as there was no imprinting process during the fabrication of the sensor. Due to the presence of complementary cavities/imprints, MB interacted with MIP both specifically and non-specifically. On the other hand, MB interacted with NIP only non-specifically, thus resulting in smaller slope values. Furthermore, the slope values for MB on MIP and AA on MIP differ similarly, which indicates that MIP is selective for MB molecules. After taking the aforementioned observations into account, it can be concluded that the described procedures can be applied in the development of imprinted Ppy-based sensors for the detection of MB.

Table 1 compares other MB detection ways, but there is no identical one, applying the same methods and materials. A summary of the different detection methods for MB includes information about the sensing platform, evaluation method, and the limit of detection (LOD).

Table 1. Different detection methods for MB.

Sensing Platform	Evaluation	LOD	Ref.
QCM/Fe$_3$O$_4$NPs/MIP/Ppy	QCM-D	1.4 µg/L	[45]
Carbon paste/MIP/PMAA	DPV	36.4 µM	[46]
MIP/PAA	UV-Vis spectroscopy	-	[47]
AgNPs/GO/g-CN	Raman spectroscopy	0.001 nM	[48]
GCE/NH$_2$-*f*MWCNTs	SWV	0.21 nM	[49]
Red-emitting CDs	Fluorescence spectroscopy	10 nM	[50]
Au-glass/NiCo-layered double hydroxide	Surface plasmon resonance	0.005 ppm	[51]
ITO-glass/MIP/Ppy	Potential pulse chronoamperometry, cyclic voltammetry, UV-Vis spectroscopy	-	This work

QCM—quartz crystal microbalance; Fe$_3$O$_4$-NPs—Iron(ll,lll) oxide nanoparticles; QCM-D—quartz crystal microbalance with dissipation monitoring; PMAA—polymethacrylic acid; DPV—differential pulse voltammetry; PAA—polyacrylic acid; AgNPs/GO/g-CN—silver nanoparticles/graphene oxide nanosheets/graphitic carbon nitride; GCE/NH$_2$-*f*MWCNTs—glassy carbon electrode/amino-group functionalized multi-walled carbon nanotubes; SWV—square wave voltammetry; CDs—carbon dots; Au/glass—gold-coated thin glass; ITO—indium tin oxide; Ppy—polypyrrole.

In multiple studies, the detection of MB was successfully achieved using diverse sensing platforms that contained conducting [45] polymer (to form MIP around magnetic Fe$_3$O$_4$ nanoparticles) or non-conducting polymers [46,47] for molecular imprinting. In addition to polymers, different metal-based (silver nanoparticles [48], Fe$_3$O$_4$ nanoparticles [45], and carbon-based (graphene oxide nanosheets, graphitic carbon nitride [48], multi-walled carbon nanotubes [49]) modifications were used to enhance the sensitivity of detection. Each of these articles leveraged the specific evaluation method and modified materials in MB detection, contributing valuable insights into the field of MB sensing.

4. Conclusions

The electrochemical polymerisation of the Ppy layer was carried out by potential cycling. The performance and stability of the MIP-modified electrode were studied. By increasing the number of applied potential cycles during the deposition of the Ppy layers, some morphological differences are visible: the surface of the layer becomes rougher, more folds appear on the surface, and it becomes less transparent. Analyses of Ppy layers were carried out, assessing washability, stability over time, and storage conditions. The most reliable and effective layer can be considered the one that was deposited using seven potential cycles. Later, the analysis of the layers deposited using seven potential cycles as a MIP was conducted. The obtained slope values of the calibration plots display that MIP interacts specifically and is selective for MB in comparison to another phenothiazine derivative, Azure A. This research shows that the MIP with MB imprints can be applied in the development of imprinted Ppy-based sensors sensitive towards MB.

Supplementary Materials: The following supporting information can be downloaded at: https://www.mdpi.com/article/10.3390/chemosensors11110549/s1. Figure S1: Cyclic voltammograms of Ppy-MB during electrochemical deposition. Ppy-MB layers deposited by (**A–G**) 3, 5, 7, 10, 15, 20, 25 potential cycles, respectively; Figure S2: Electrode storage in different mediums (layer polymerized with 25 cycles), after 12 days, (**A**) 0,01 M BR buffer solution, pH 3; (**B**) in water; (**C**) in air; Figure S3: SEM images of Ppy-MB which were electropolymerized by: 25 potential cycles at magnification ×800 (**A**) and ×8000 (**B**), 20 potential cycles at magnification ×800 (**C**) and ×8000 (**D**), 15 potential cycles at magnification ×800 (**E**) and ×8000 (**F**), 10 potential cycles at magnification ×800 (**G**) and ×8000 (**H**), 7 potential cycles at magnification ×800 (**I**) and ×8000 (**J**), and 5 potential cycles at magnification ×800 (**K**) and ×8000 (**L**); Figure S4: Cyclic voltammograms of differently modified electrodes were recorded immediately after deposition in the BR buffer solution without (1) and with (2) K$_3$[Fe(CN)$_6$]/K$_4$[Fe(CN)$_6$] as a redox probe. (**A**) Ppy-MB-5, (**B**) Ppy-MB-7, (**C**) Ppy-MB-10 electrode; Figure S5: Cyclic voltammograms of differently modified electrodes were recorded six weeks after deposition in the BR buffer solution without (1) and with (2) K$_3$[Fe(CN)$_6$]/K$_4$[Fe(CN)$_6$] as a redox probe. (**A**) Ppy-MB-5, (**B**) Ppy-MB-7, (**C**) Ppy-MB-10 electrode.

References

1. Tretjakov, A.; Syritski, V.; Reut, J.; Boroznjak, R.; Öpik, A. Analytica Chimica Acta Molecularly Imprinted Polymer Film Interfaced with Surface Acoustic Wave Technology as a Sensing Platform for Label-Free Protein Detection. *Anal. Chim. Acta* **2016**, *902*, 182–188. [CrossRef]
2. Kidakova, A.; Boroznjak, R.; Reut, J.; Öpik, A.; Saarma, M.; Syritski, V. Molecularly Imprinted Polymer-Based SAW Sensor for Label-Free Detection of Cerebral Dopamine Neurotrophic Factor Protein. *Sens. Actuators B Chem.* **2020**, *308*, 127708. [CrossRef]
3. Lowdon, J.W.; Diliën, H.; Singla, P.; Peeters, M.; Cleij, T.J.; van Grinsven, B.; Eersels, K. MIPs for Commercial Application in Low-Cost Sensors and Assays—An Overview of the Current Status Quo. *Sens. Actuators B Chem.* **2020**, *325*, 128973. [CrossRef]
4. Ratautaite, V.; Janssens, S.D.; Haenen, K.; Nesládek, M.; Ramanaviciene, A.; Baleviciute, I.; Ramanavicius, A. Molecularly Imprinted Polypyrrole Based Impedimetric Sensor for Theophylline Determination. *Electrochim. Acta* **2014**, *130*, 361–367. [CrossRef]
5. Mazouz, Z.; Mokni, M.; Fourati, N.; Zerrouki, C.; Barbault, F.; Seydou, M.; Kalfat, R.; Yaakoubi, N.; Omezzine, A.; Bouslema, A.; et al. Biosensors and Bioelectronics Computational Approach and Electrochemical Measurements for Protein Detection with MIP-Based Sensor. *Biosens. Bioelectron.* **2020**, *151*, 111978. [CrossRef]
6. Ansari, S.; Masoum, S. Molecularly Imprinted Polymers for Capturing and Sensing Proteins: Current Progress and Future Implications. *TrAC—Trends Anal. Chem.* **2019**, *114*, 29–47. [CrossRef]
7. El-Sharif, H.F.; Stevenson, D.; Reddy, S.M. MIP-Based Protein Profiling: A Method for Interspecies Discrimination. *Sens. Actuators B Chem.* **2017**, *241*, 33–39. [CrossRef]
8. Dabrowski, M.; Lach, P.; Cieplak, M.; Kutner, W. Nanostructured Molecularly Imprinted Polymers for Protein Chemosensing. *Biosens. Bioelectron.* **2018**, *102*, 17–26. [CrossRef]
9. Shumyantseva, V.V.; Bulko, T.V.; Sigolaeva, L.V.; Kuzikov, A.V.; Archakov, A.I. Electrosynthesis and Binding Properties of Molecularly Imprinted Poly-*o*-Phenylenediamine for Selective Recognition and Direct Electrochemical Detection of Myoglobin. *Biosens. Bioelectron.* **2016**, *86*, 330–336. [CrossRef]
10. Tlili, A.; Attia, G.; Khaoulani, S.; Mazouz, Z.; Zerrouki, C.; Yaakoubi, N.; Othmane, A.; Fourati, N. Contribution to the Understanding of the Interaction between a Polydopamine Molecular Imprint and a Protein Model: Ionic Strength and pH Effect Investigation. *Sensors* **2021**, *21*, 619. [CrossRef]
11. Erdőssy, J.; Horváth, V.; Yarman, A.; Scheller, F.W.; Gyurcsányi, R.E. Electrosynthesized Molecularly Imprinted Polymers for Protein Recognition. *TrAC—Trends Anal. Chem.* **2016**, *79*, 179–190. [CrossRef]
12. Piletsky, S.A.; Alcock, S.; Turner, A.P.F. Molecular Imprinting: At the Edge of the Third Millennium. *Trends Biotechnol.* **2001**, *19*, 9–12. [CrossRef]
13. Vasapollo, G.; Sole, R.D.; Mergola, L.; Lazzoi, M.R.; Scardino, A.; Scorrano, S.; Mele, G. Molecularly Imprinted Polymers: Present and Future Prospective. *Int. J. Mol. Sci.* **2011**, *12*, 5908–5945. [CrossRef]
14. Ding, S.; Lyu, Z.; Li, S.; Ruan, X.; Fei, M.; Zhou, Y.; Niu, X.; Zhu, W.; Du, D.; Lin, Y. Molecularly Imprinted Polypyrrole Nanotubes Based Electrochemical Sensor for Glyphosate Detection. *Biosens. Bioelectron.* **2021**, *191*, 113434. [CrossRef]

15. Xing, X.; Liu, S.; Yu, J.; Lian, W.; Huang, J. Electrochemical Sensor Based on Molecularly Imprinted Film at Polypyrrole-Sulfonated Graphene/Hyaluronic Acid-Multiwalled Carbon Nanotubes Modified Electrode for Determination of Tryptamine. *Biosens. Bioelectron.* **2012**, *31*, 277–283. [CrossRef]

16. Uzun, L.; Turner, A.P.F. Molecularly-Imprinted Polymer Sensors: Realising Their Potential. *Biosens. Bioelectron.* **2016**, *76*, 131–144. [CrossRef]

17. Haupt, K. Molecularly Imprinted Polymers in Analytical Chemistry. *Analyst* **2001**, *126*, 747–756. [CrossRef]

18. Ramanavicius, S.; Jagminas, A.; Ramanavicius, A. Advances in Molecularly Imprinted Polymers Based Affinity Sensors (Review). *Polymers* **2021**, *13*, 974. [CrossRef]

19. El-Schich, Z.; Zhang, Y.; Feith, M.; Beyer, S.; Sternbæk, L.; Ohlsson, L.; Stollenwerk, M.; Wingren, A.G. Molecularly Imprinted Polymers in Biological Applications. *Biotechniques* **2020**, *69*, 407–420. [CrossRef]

20. Turiel, E.; Esteban, A.M. *Molecularly Imprinted Polymers*; Elsevier Inc.: Amsterdam, The Netherlands, 2019; ISBN 9780128169063. [CrossRef]

21. Kan, X.; Xing, Z.; Zhu, A.; Zhao, Z.; Xu, G.; Li, C.; Zhou, H. Molecularly Imprinted Polymers Based Electrochemical Sensor for Bovine Hemoglobin Recognition. *Sens. Actuators B Chem.* **2012**, *168*, 395–401. [CrossRef]

22. Yola, M.L.; Atar, N. Development of Cardiac Troponin-I Biosensor Based on Boron Nitride Quantum Dots Including Molecularly Imprinted Polymer. *Biosens. Bioelectron.* **2019**, *126*, 418–424. [CrossRef] [PubMed]

23. Silva, B.V.M.; Rodríguez, B.A.G.; Sales, G.F.; Sotomayor, M.D.P.T.; Dutra, R.F. An Ultrasensitive Human Cardiac Troponin T Graphene Screen-Printed Electrode Based on Electropolymerized-Molecularly Imprinted Conducting Polymer. *Biosens. Bioelectron.* **2016**, *77*, 978–985. [CrossRef] [PubMed]

24. Ratautaite, V.; Boguzaite, R.; Mickeviciute, M.B.; Mikoliunaite, L.; Samukaite-bubniene, U.; Ramanavicius, A.; Ramanaviciene, A. Evaluation of Electrochromic Properties of Polypyrrole/Poly(Methylene Blue) Layer Doped by Polysaccharides. *Sensors* **2022**, *22*, 232. [CrossRef] [PubMed]

25. Ion, R.M.; Scarlat, F.; Scarlat, F.; Niculescu, V.I.R. Methylene—Blue Modified Polypyrrole Film Electrode for Optoelectronic Applications. *J. Optoelectron. Adv. Mater.* **2003**, *5*, 109–115.

26. Kaplan, I.H.; Dağci, K.; Alanyalioğlu, M. Nucleation and Growth Mechanism of Electropolymerization of Methylene Blue: The Effect of Preparation Potential on Poly(Methylene Blue) Structure. *Electroanalysis* **2010**, *22*, 2694–2701. [CrossRef]

27. Erdem, A.; Kerman, K.; Meric, B.; Akarca, U.S.; Ozsoz, M. Novel Hybridization Indicator Methylene Blue for the Electrochemical Detection of Short DNA Sequences Related to the Hepatitis B Virus. *Anal. Chim. Acta* **2000**, *422*, 139–149. [CrossRef]

28. Pfaffen, V.; Ortiz, P.I.; Córdoba de Torresi, S.I.; Torresi, R.M. On the pH Dependence of Electroactivity of Poly(Methylene Blue) Films. *Electrochim. Acta* **2010**, *55*, 1766–1771. [CrossRef]

29. Brett, C.M.A.; Inzelt, G.; Kertesz, V. Poly(Methylene Blue) Modified Electrode Sensor for Haemoglobin. *Anal. Chim. Acta* **1999**, *385*, 119–123. [CrossRef]

30. Karyakin, A.A.; Strakhova, A.K.; Karyakina, E.E.; Varfolomeyev, S.D.; Yatsimirsky, A.K. The Electrochemical Polymerization of Methylene Blue and Bioelectrochemical Activity of the Resulting Film. *Synth. Met.* **1993**, *60*, 289–292. [CrossRef]

31. Clifton, J.; Leikin, J.B. Methylene Blue. *Am. J. Ther.* **2003**, *10*, 289–291. [CrossRef]

32. Tonlé, I.K.; Ngameni, E.; Tcheumi, H.L.; Tchiéda, V.; Carteret, C.; Walcarius, A. Sorption of Methylene Blue on an Organoclay Bearing Thiol Groups and Application to Electrochemical Sensing of the Dye. *Talanta* **2008**, *74*, 489–497. [CrossRef] [PubMed]

33. Guo, S.; Huang, Y.; Wei, T.; Zhang, W.; Wang, W.; Lin, D.; Zhang, X.; Kumar, A.; Du, Q.; Xing, J. Amphiphilic and Biodegradable Methoxy Polyethylene Glycol-Block-(Polycaprolactone-Graft-Poly(2-(Dimethylamino)Ethyl Methacrylate) as an Effective Gene Carrier. *Biomaterials* **2011**, *32*, 879–889. [CrossRef] [PubMed]

34. Asman, S.; Yusof, N.A.; Abdullah, A.H.; Haron, M.J. Synthesis and Characterization of a Molecularly Imprinted Polymer for Methylene Blue. *Asian J. Chem.* **2011**, *23*, 4786–4794.

35. Houas, A.; Lachheb, H.; Ksibi, M.; Elaloui, E.; Guillard, C.; Herrmann, J.M. Photocatalytic Degradation Pathway of Methylene Blue in Water. *Appl. Catal. B* **2001**, *31*, 145–157. [CrossRef]

36. Liu, B.; Cang, H.; Cui, L.; Zhang, H. Electrochemical Polymerization of Methylene Blue on Glassy Carbon Electrode. *Int. J. Electrochem. Sci.* **2017**, *12*, 9907–9913. [CrossRef]

37. Mokhtari, Z.; Khajehsharifi, H.; Hashemnia, S.; Solati, Z.; Azimpanah, R.; Shahrokhian, S. Evaluation of Molecular Imprinted Polymerized Methylene Blue/Aptamer as a Novel Hybrid Receptor for Cardiac Troponin I (CTnI) Detection at Glassy Carbon Electrodes Modified with New Biosynthesized ZnONPs. *Sens. Actuators B Chem.* **2020**, *320*, 128316. [CrossRef]

38. El Fazdoune, M.; Bahend, K.; Ben Jadi, S.; Oubella, M.; García-García, F.J.; Bazzaoui, E.A.; Asserghine, A.; Bazzaoui, M. Different Electrochemical Techniques for the Electrosynthesis of Poly Methylene Blue in Sodium Saccharin Aqueous Medium. *J. Solid. State Electrochem.* **2023**, *27*, 667–678. [CrossRef]

39. Sedelnikova, A.; Poletaeva, Y.; Golyshev, V.; Chubarov, A.; Dmitrienko, E. Preparation of Magnetic Molecularly Imprinted Polymer for Methylene Blue Capture. *Magnetochemistry* **2023**, *9*, 196. [CrossRef]

40. Sun, W.; Wang, Y.; Zhang, Y.; Ju, X.; Li, G.; Sun, Z. Poly(Methylene Blue) Functionalized Graphene Modified Carbon Ionic Liquid Electrode for the Electrochemical Detection of Dopamine. *Anal. Chim. Acta* **2012**, *751*, 59–65. [CrossRef]

41. Barsan, M.M.; Pinto, E.M.; Brett, C.M.A. Methylene Blue and Neutral Red Electropolymerisation on AuQCM and on Modified AuQCM Electrodes: An Electrochemical and Gravimetric Study. *Phys. Chem. Chem. Phys.* **2011**, *13*, 5462–5471. [CrossRef]

42. Phonklam, K.; Wannapob, R.; Sriwimol, W.; Thavarungkul, P.; Phairatana, T. A Novel Molecularly Imprinted Polymer PMB/MWCNTs Sensor for Highly-Sensitive Cardiac Troponin T Detection. *Sens. Actuators B Chem.* **2020**, *308*, 127630. [CrossRef]

43. Kim, S.; Jang, L.K.; Park, H.S.; Lee, J.Y. Electrochemical Deposition of Conductive and Adhesive Polypyrrole-Dopamine Films. *Sci. Rep.* **2016**, *6*, 30475. [CrossRef] [PubMed]

44. Samukaite-Bubniene, U.; Valiūnienė, A.; Bucinskas, V.; Genys, P.; Ratautaite, V.; Ramanaviciene, A.; Aksun, E.; Tereshchenko, A.; Zeybek, B.; Ramanavicius, A. Towards Supercapacitors: Cyclic Voltammetry and Fast Fourier Transform Electrochemical Impedance Spectroscopy Based Evaluation of Polypyrrole Electrochemically Deposited on the Pencil Graphite Electrode. *Colloids Surf. A Physicochem. Eng. Asp.* **2021**, *610*, 125750. [CrossRef]

45. Hu, Y.; Xing, H.; Li, G.; Wu, M. Magnetic Imprinted Polymer-Based Quartz Crystal Microbalance Sensor for Sensitive Label-Free Detection of Methylene Blue in Groundwater. *Sensors* **2020**, *20*, 5506. [CrossRef] [PubMed]

46. Soysal, M.; Muti, M.; Esen, C.; Gençdağ, K.; Aslan, A.; Erdem, A.; Karagözler, A.E. A Novel and Selective Methylene Blue Imprinted Polymer Modified Carbon Paste Electrode. *Electroanalysis* **2013**, *25*, 1278–1285. [CrossRef]

47. Wang, N.; Xiao, S.J.; Su, C.W. Preparation of Molecularly Imprinted Polymer for Methylene Blue and Study on Its Molecular Recognition Mechanism. *Colloid. Polym. Sci.* **2016**, *294*, 1305–1314. [CrossRef]

48. Santhoshkumar, S.; Murugan, E. Rationally Designed SERS AgNPs/GO/g-CN Nanohybrids to Detect Methylene Blue and Hg2+ Ions in Aqueous Solution. *Appl. Surf. Sci.* **2021**, *553*, 149544. [CrossRef]

49. Hayat, M.; Shah, A.; Nisar, J.; Shah, I.; Haleem, A.; Ashiq, M.N. A Novel Electrochemical Sensing Platform for the Sensitive Detection and Degradation Monitoring of Methylene Blue. *Catalysts* **2022**, *12*, 306. [CrossRef]

50. Zhao, D.; Liu, X.; Wei, C.; Qu, Y.; Xiao, X.; Cheng, H. One-Step Synthesis of Red-Emitting Carbon Dots: Via a Solvothermal Method and Its Application in the Detection of Methylene Blue. *RSC Adv.* **2019**, *9*, 29533–29540. [CrossRef]

51. Sadrolhosseini, A.R.; Ghasemi, E.; Pirkarimi, A.; Hamidi, S.M.; Taheri Ghahrizjani, R. Highly Sensitive Surface Plasmon Resonance Sensor for Detection of Methylene Blue and Methylene Orange Dyes Using NiCo-Layered Double Hydroxide. *Opt. Commun.* **2023**, *529*, 129057. [CrossRef]

NOTES

NOTES